Imperial College London

Electrospun Scaffolds for Tissue Engineering

by

Farina Muhamad

A thesis submitted to Imperial College

for the award of PhD and the

Diploma of Imperial College

Department of Materials

Imperial College London

September 2012

London, England

To my parents

ABSTRACT

A critical challenge in designing materials for tissue engineering (TE) is to provide essential cues that can control cellular behaviour and promote tissue regeneration. TE with fibrous scaffolds by using electrospinning is emerging as a major research area in the field of regenerative medicine. This thesis presents the development of novel electrospun fibrous acrylate scaffolds for bone TE.

Acrylate fibrous scaffolds were developed by electrospinning photocrosslinkable and low molecular weight acrylate monomers, methyl acrylate (MA) and diethylene-glycol dimethacrylate (DEGMA). Photocrosslinked fibres were successfully produced by electrospinning different MA and DEGMA compositions and post-UV crosslinking. The ability to produce topologically and mechanically diverse fibrous scaffold materials was demonstrated. Varying MA and DEGMA composition affected overall fibre morphology, swelling and mechanics of the fibrous scaffold. An assessment of biological activity of the acrylate fibrous scaffold was performed to evaluate the effect of varying ratios of MA/DEGMA of the fibrous scaffold on the viability of two different cell types, osteosarcoma-derived osteoblastic cells (Saos-2) and mesenchymal stromal cells (hMSCs). The potential of MA/DEGMA fibrous scaffolds to support Saos-2 cell viability and proliferation was demonstrated. However, the considerable increase in apoptosis of hMSCs cultured on both fibrous and flat samples suggested a lower potential of the MA/DEGMA scaffolds to support hMSCs cell attachment and viability.

The fibrous scaffolds were immobilized with synthetic peptides utilizing cysteine-functionalized RGD or DGEA peptide sequences in combination with MA/DEGMA monomers and by employing a photoinitiated mixed-mode thiol-acrylate polymerization mechanism. Cysteine-functionalized DGEA and RGD peptides were incorporated efficiently in the synthesized acrylate scaffold. The peptide-conjugated fibrous scaffolds showed increased hMSCs adhesion and viability. Through cell adhesion and soluble peptide competition assays, the bioactivity and specificity of each peptide conjugated to the scaffold was confirmed. Finally, hMSCs cultured on DGEA conjugated scaffolds exhibited the activation of osteogenic differentiation markers, alkaline phosphatase (ALP) and osteocalcin (OCN). The results presented in this thesis strongly suggest the potential of the acrylate fibrous scaffold for bone TE.

PREFACE

Author's Declaration

This thesis is a record of the work by me in the Department of Materials and Department of Biomedical Engineering at Imperial College London except where explicitly stated.

This work was funded by University Malaya and Ministry of Higher Education, Malaysia.

Some of the work presented in this thesis has been presented in various conferences.

Conference contributions

F. Muhamad, Y. X. Dong, J.H.G. Steinke, M.M. Stevens. *Electrospinning Photocrosslinkable Acrylate Monomers for Tissue Engineering.* Poster presentation, MACRO2010, The 43rd IUPAC World Polymer Congress, 11th-16th July 2010, Glasgow, Scotland.

F. Muhamad, Y. X. Dong, J.H.G. Steinke, M.M. Stevens. *Electrospinning Photocrosslinkable Acrylate Monomers for Tissue Engineering.* Oral presentation, 4th International Conference on Tissue Engineering, Aegean Conferences, 31st May- 5th June, Crete, Greece.

N.C. Bell, F. Muhamad, S. Fearn, J.L.S. Lee, D.S. McPhail, A.G. Shard and M.M. Stevens. *The peptide functionalization of tissue engineering scaffolds investigated by ToF-SIMS.* Oral presentation, SIMS XVIII, 18th International Conference on Secondary Ion Mass Spectrometry, 18th-23rd September 2011, Riva del Garda, Italy.

ACKNOWLEDGEMENTS

First and foremost, I would like to thank the Malaysian Government and University Malaya for the generous financial support. Without the scholarship that was given to me I would not be here pursuing my PhD.

I would like to thank my supervisors, Prof. Molly Stevens and Dr. Joachim Steinke for their academic guidance and support throughout the PhD. It has been a privilege and honour working under the supervision of both of them. Both of them have always given me a lot of encouragement and enthusiasm throughout my PhD. Molly, thank you for accepting me into this fantastic group!

I would like to also thank a group of people that have helped me throughout my project. Dr Yixiang Dong for introducing me to the lab and helping me during the first year of the PhD, Dr Cristina Gentillini and Dr Luis Rojo for all the polymer chemistry help and NMR, Dr Seth McCullen and Dr Helene Autefage for help in the cell lab, Dr Heiko Anderson for help with peptide synthesis and Ms Nia Bell for her help with ToF-SIMS. I would also like to thank Dr Maria Azevedo for support and advice throughout the PhD. AdditionaIly, I would also like to thank Ms Sabrina Skeete for all the excellent administrative support. Also, many other group members have contributed scientific advice or help at some point.

Next, I would like to thank current and past Steven's Group members. Thank you for creating such a great working environment. Thank you for the support, advice and encouragement, it has been great experience to be part of the group.

I would especially like to thank members that have become friends that are special to me, Maria, Elsie, Nasrin, Mathew, Stuart, Pelin, Ben and Sangwon. Your kindness, company and support have really made my time here in Imperial and London special.

I am exceptionally fortunate in having an incredibly supportive family. My parents gave never ending support and encouragement throughout my academic pursuits. Specifically, my father for inspiring me to always do my best in whatever I do and pursuing my PhD. Pa, you have always been the rock in my life. My mother for her unconditional love, patience and advice. Without your support and love Ma, I would not be the person I am today. My brothers, Dax and Boboi, thank you for all of the encouragement and support and making me happy. Boi, thank you for the help and support!

Last and foremost, my husband Farouk. You are truly my best friend and thank you for always being there for me. Thank you for dropping everything in KL and deciding to accompany me here. Our experience in London has been great and it will definitely be in our memories forever. Thank you for always reminding me to savour and enjoy life!

TABLE OF CONTENTS

LIST OF FIGURES

LIST OF TABLES

ABBREVIATIONS

3D	Three dimensional
AIBN	Azobisisobutyronitrile
ALP	Alkaline phosphotase
ATR-FTIR	Attenuated Total Internal Reflectance-Fourier Transform Infrared Spectroscopy
BTMSB	1,4-(bistrimethylsilyl) benzene
CGRGD	Cysteine-arginine-glycine-aspartic acid
CGDGEA	Cysteine-Aspartic acid-Glycine-Glutamine-Alanine
DAPI	4’,6-Diamidino-2-phenylindole dihydrochloride
DEGMA	Diethylene glycol dimethacrylate
DGEA	Aspartic acid-Glycine-Glutamine-Alanine
DMF	Dimethylformamide
ECM	Extracellular matrix
ERK	Extracellular signal related kinase
Etoh	Ethanol
FAK	Focal adhesion kinase
FBS	Fetal Bovine Serum
FDA	U.S. Food and Drug Administration
GAG	Glycosaminoglycan
HA	Hyaluronic acid
hMSCs	Human mesenchymal stem cell
H-NMR	Proton nuclear magnetic resonance
HEMA	2-hydroxyethyl methacrylate
HFIP	Hexafluoroisopropanol
Irgacure 2959	2-hydroxy-4′-(2-hydroxyethoxy)-2-methylpropiophenone
MA	Methyl acrylate
MAPK	Mitogen-activated protein kinase signal
MMA	Methyl methacrylate

MTS	3-(4,5-dimethylthiazol-2-yl)-5-(3-carboxymethoxyphenyl)-2-(4-sulfophenyl)-2H- tetrazolium
OCN	Osteocalcin
OPA	*o*-phtalaldehyde
PBS	Phosphate buffer saline
PCL	Poly(caprolactone)
PEG	Polyethylene glycol
PEG-DA	Poly (ethylene glycol) -diacrylate
PEO	Poly (ethylene oxide)
PGA	Poly(glycolic-acid)
PLA	Poly(lactic acid)
PLGA	Poly (D,L-lactic-co-glycolic acid)
PVA	Poly-vinyl alcohol
RGD	Arginine-glycine-aspartic acid
S.D	Standard Deviation
SEM	Scanning Electron Microscope
SFF	Solid freeform fabrication
TCP	Tissue culture plastic
THF	Tetrahydrofuran
ToF-SIMS	Time of Flight-Secondary Ion Mass Spectrometry
TE	Tissue Engineering
UV	Ultraviolet

CHAPTER 1

Scope of Thesis

Bone is a highly vascularised tissue that rapidly remodels during the life span of an individual [1]. However, large bone defects do not heal naturally and requires medical intervention [1]. Furthermore, with the increasing aging population there is an increasing prevalence of osteoporosis and bone fractures and the existing therapies used to repair bone defects have many drawbacks [2]. The development of biomaterials in the area of orthopedics to replace autografts is consequently an imperative medical goal. Currently, researchers are focused on the design of bioactive materials that can mimic the natural healing process by integrating biological molecules and cells to regenerate tissues [3]. Tissue Engineering (TE) scaffolds are no longer regarded simply as passive cell carriers but rather as instructive devices with the potential to have information that can be sensed and interpreted by transplanted or host cells [4].

The extracellular matrix (ECM) plays an essential role in directing cellular behaviour [5, 6]. Biomaterial scaffolds can be developed to interact with cells by mimicking essential molecular events of the ECM [7]. A critical challenge in designing materials for TE is to provide essential cues that can control cellular behaviour and promote tissue regeneration. For cells adhering on a material, the characteristics of its surface, for example topography, stiffness, wettability and specific cell-surface interactions are key to control cellular activity [7-9]. Material-based control of cellular response is a potentially powerful approach for regulating the behaviour of different cell types, including stem cells that are cells with the potential to differentiate into many tissue types.

Electrospinning has been widely used to create biodegradable scaffolds for the engineering of several tissues, particularly those of the skeletal system [10-12]. As discussed in chapter 2, to fabricate electrospun fibrous scaffolds, a polymer solution are electrically charged until charge repulsion overrides the surface tension of the droplet at the spinneret tip and a polymer jet is generated [10, 13, 14]. Subsequently, as the polymer liquid jet travels and solvent evaporates, a fibrous strand is produced and collected onto a grounded collector [10]. The fibrous scaffolds mimic the size and structure of the natural ECM which can lead to enhanced cellular interactions [10, 15].

Photopolymerization with acrylate and methacrylate monomers have been shown to have a controlled nature of photoinitiated polymerization with a choice of non-cytotoxic photoinitiators and degradation products. The spatial and temporal control afforded during photoinitiation is a pivotal advantage which has motivated its wide application in the field of TE [16, 17]. Acrylates are ubiquitously used in the synthesis of hydrogel networks due to the active double bonds [18-21]. In addition, there are a number of commercially available monomers which can be photocrosslinked rapidly using a photoinitiator [9]. The photopolymerization of acrylate and methacrylates has been used in biomedical research and has become an essential approach for *in situ* delivery of resins in the area of dentistry [22-25] and as bone-replacement materials [17]. Anderson and colleagues

demonstrated the ability of acrylates and methacrylate photocrosslinked networks to support cell attachment, viability and proliferation [9]. Moreover, using an acrylate/methacrylate microarray library, they were able to identify specific monomers that support human embryonic stem cells. Hence, based on the 'hit' polymer microarrays which have demonstrated monomers that support cell growth, diethylene-glycol dimethacrylate (DEGMA) and methyl acrylate (MA) have been chosen to be utilized in the electrospinning system here.

ECM comprises of many biomacromolecules such as collagens, proteoglycans, laminins and fibronectin and it is mainly this biological information that leads to its bioactivity [7, 26]. Interaction of integrins which are receptors on the cell surface with specific ECM molecules can activate signalling pathways leading ultimately to gene expression [27, 28]. The variety of ECM proteins presented to cells in a specific tissue is pivotal in regulating how cells function within that tissue type [7]. One approach to include sites of integrin binding in biomaterials is to incorporate purified ECM proteins for example fibrin and collagen [7]. However, supplementing full proteins to scaffolds can be challenging to execute as proteins are susceptible to denaturation and degradation [29]. For this reason, a frequently used technique to enhance cell adhesion is to integrate short peptide motifs or analogues derived from binding regions of ECM components [7]. While they may have a fraction of the activity of the complete protein, they can be incorporated at very high concentration and increase the overall activity of the peptide [7]. Moreover, peptides are easy to synthesize and functionalize. Hence, bioactive peptides offer a synthetic and scalable alternative to complex ECM proteins [30].

The widely used Arg-Gly-Asp (RGD) peptide sequence present in various ECM proteins, including fibronectin, laminin, collagen I, fibrinogen and vitronectin was studied as a mode of enhancing cell adhesion by inducing focal adhesion through integrin interaction on biomaterial surfaces as early as the 1980's [31, 32]. Since then RGD has been functionalized into an extensive range of surfaces, scaffolds and hydrogels (reviewed in [33], [34] and [35]).

DGEA (Asp-Gly-Glu-Ala) is a collagen type 1 peptide sequence and has displayed specific binding affinity for osteoblasts via the $\alpha_2\beta_1$ integrin. In addition, DGEA has been shown to induce osteogenic differentiation [36-38]. Therefore, DGEA could be used to promote cell adhesion and stimulate differentiation [38]. Nevertheless, the cellular response of collagen-derived peptides has been relatively less studied compared to other ECM peptides, while full collagen has been mostly applied for making scaffolds [39-41]. Moreover, it has been revealed that collagen I interacts with different integrin receptors than that of fibronectin and the integrin/collagen I binding is RGD-independent [42].

This thesis focuses on the development of scaffolds which can actively support bone tissue repair. Chapter 2 of the thesis provides a review of the fields on TE specifically bone, summary of

functions of ECM and the use of peptides in TE applications, overview of electrospinning, as well as summary of UV light polymerization and their use in TE. Chapters 3-6 describe and discuss the main experimental results of this PhD project. The final conclusions, general overview and suggestions for future work are presented in Chapter 7.

This project was divided into four main parts. **Chapter 3** consists of the development of fibrous acrylate scaffolds. **Chapter 4** consists of the biological response of the acrylate scaffolds. **Chapter 5** consists of the incorporation of bioactive peptides on the fibrous acrylate scaffolds. Lastly, **Chapter 6** consists of the biological assessment of the peptide conjugated scaffolds.

Chapter 3. Development of electrospun fibrous acylate scaffolds

The feasibility of electrospinning photocrosslinkable and low molecular weight acrylate monomers was investigated. MA and DEGMA were the monomer and crosslinker of choice respectively with the aid of PEO as a polymer carrier and viscosity modifier. Photocrosslinked fibres were developed by electrospinning different MA and DEGMA compositions and post-UV crosslinking. The effects of various processing parameters of electrospinning were investigated, including carrier polymer concentration, accelerating voltage, rate of delivery and monomer/PEO ratios. The determination of the optimal range of parameters required to produce uniform and bead-free electrospun MA/DEGMA fibrous scaffolds were determined. The overall UV-reaction of the post-crosslinking was investigated. PEO (carrier polymer) was extracted with thorough washing with water and changes in fibre morphology were monitored. In addition, the PEO extraction from the fibres was characterized. Next, the MA and DEGMA ratio (mol%) was varied to evaluate the effects of increasing the crosslinker (DEGMA) concentration on fibre morphology, swelling and mechanics of the fibrous scaffolds.

Chapter 4. Biological evaluation of acrylate fibrous scaffolds with Saos-2 and hMSC cells

The biological response of Saos-2 (osteosarcoma-derived osteoblastic cells) and human MSC cells to varying ratios of MA/DEGMA electrospun fibers and flat surfaces with similar chemistry were assessed and discussed. These studies were intended to evaluate the effect of varying ratios of MA:DEGMA of the fibrous scaffold on the viability of two different cell types, Saos-2 and hMSCs. Several techniques were used to evaluate the effect of MA/DEGMA electrospun fibers on cell viability. Lastly, the effect of the fibrous scaffolds and flat surfaces on protein adsorption was investigated.

Chapter 5. Functionalization of acrylate scaffolds with cell adhesive peptides -DGEA and RGD

The development of electrospun acrylate scaffolds conjugated with biologically active peptides, RGD and DGEA were described. The synthesis of the functionalized scaffolds utilizes cysteine-functionalized RGD or DGEA peptide sequences in combination with MA/DEGMA monomers and employs a photoinitiated mixed-mode thiol-acrylate polymerization mechanism. Firstly, immobilization of DGEA and RGD peptides on the acrylate fibrous scaffold was analyzed by varying cysteine-conjugated DGEA and RGD concentrations. Measurement of peptide incorporation was determined by measuring the amount of free primary amine. The amount of free amine measured was compared to the initial concentration of free amine prior to UV crosslinking. The measurement of peptide incorporation was further confirmed by quantifying free sulfhydryl groups in solution. Next, the morphology, swelling, mechanical and degradation behaviour of the functionalized acrylate scaffold was investigated. Subsequently, the presentation of peptides on the surface of the scaffold was studied using ToF-SIMS. Lastly, the effects of varying the number of glycine amino acid spacer residues on overall peptide incorporation were assessed.

Chapter 6. Assessment of effect of DGEA- and RGD-functionalized electrospun fibers on hMSC adhesion and differentiation

The biological response of hMSCs on the peptide immobilized fibrous scaffolds were investigated by evaluating the initial cell adhesion, viability and osteogenic differentiation. First, the effect of CGDGEA and CGRGD peptides with different concentrations on hMSCs initial cell attachment was evaluated. Next, the difference between the two peptides of CGDGEA and CGRGD on hMSCs adhesion and viability was assessed. Then, the effect of varying the length of DGEA and RGD comprising sequences with the use of glycine was analyzed by looking at hMSCs adhesion and viability. Next, the integrin specificity of hMSCs adhesion to the two peptides using competitive adhesion assays was evaluated. Finally, the ability of the peptide conjugated scaffolds to stimulate osteogenic differentiation of hMSCs was investigated.

CHAPTER 2

Literature Review

2.1 TISSUE ENGINEERING

Cost-effective replacement of the function of injured tissues or failed organs with man-made substitutes represents one of the major achievements of biomedical research in the second half of the 20th century [43]. Substitute medicine, as it was labelled by Pierre Galletti [44], started in 1955 with the development of artificial hips, blood oxygenators (artificial lungs), hemodialysis, and pacemakers [43]. However, even with numerous achievements, contemporary technico-medical strategies are restricted and rely on organometallic materials, which are inherently non-biocompatible and inert materials that do not grow or "heal" themselves. Furthermore, therapies can be invasive and implants can only be sustained in the body for short periods of time, often less than the life of the patient [43]. Hence, with these limitations, scientists have progressed to a new paradigm of biological man-made replacements, specifically termed Tissue Engineering (TE). This new field of research aims to engineer biologically inspired scaffolds that not only integrate with native tissue but also induce the human body's repair mechanism to regenerate damaged tissue and restore function [45].

Living tissues often have an innate capacity for regeneration even without intervention [1]. A remarkable example of this is the human liver, which can regrow to its initial size even after more than half of its mass is removed [7, 46]. Other tissues, such as bone and skin, can also self-repair and regenerate to fill injuries below a critical size, facilitated by resident or recruited stem cells to the damaged site [7]. However, self-healing is restricted in tissues with low regenerative potential, as is the case of cartilage, in older patients, or when the damaged site is larger than the critical defect size. Hence, in these instances, or when the original tissue is completely nonviable, therapeutic intervention is required for the patient [7]. The use of stem cell therapy is seen as a possible popular treatment option; however, it is highly limited by the control of cell fate. Benign tumours from selected mature tissues, for example teeth, hair and gut epithelium, have been demonstrated to form when stem cells are injected into an immunocompromised mouse [7, 47]. Thus, such simple therapeutic approaches do not offer a complete resolution for regeneration; biomaterials are required as carriers of either the stem cells to the injury site or of specific signalling molecules that can direct the cell function.

Significant challenges have been involved in early commercialization of TE products due to problems related to scale-up, shelf-life, quality control and distribution [7]. In addition, early commercialization suffered from withdrawal of corporate finance and from unsuitable business models in the early millennium, after rapid growth in the early 1990s through 2001 [7, 43, 48]. However, despite these challenges, the field of TE has recovered and matured, which is shown by the resurgence of development-stage companies and return of investments for TE corporations [49]. Currently, sales of TE products exceed USD 240 million per annum [49].

Although the initial concept of TE was maintained, during the last decade the philosophy of the field has changed tremendously due to accumulation of knowledge and experience. The initial grand objectives of engineering entire organs have become more specific, achievable goals because of the overall complexity of recreating tissues [7]. In addition, the TE community has also realized the importance of basic developmental research. Trying to recreate the complexity of organs or tissues at a macroscopic level is not enough; TE strategies should aim at stimulating the essential steps of tissue development or natural repair at a microscopic and molecular level [7, 50].

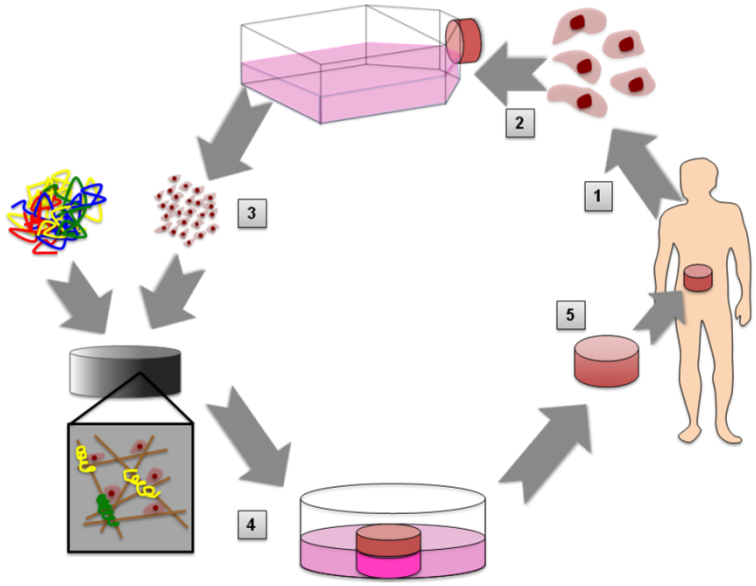

Figure 2.1 Tissue Engineering (TE) common approaches. (1) Cells are harvested from the patient; (2) cells are expanded *in vitro*; (3) cells are seeded in a scaffold with specific cues; (4) cells are cultured in the scaffold *in vitro*; (5) scaffold containing cultured cells is implanted in the patient's body. (Figure adapted from [51])

TE aims to utilize materials to promote new tissue formations and involves interaction of cells with the material. The most common approach for TE is to culture cells into a scaffold; a structural component which classifies the shape or configuration of the specific tissue and offers specific signals which induce tissue regeneration (Figure 2.1) [7, 44]. In traditional TE, for the use of cell-seeded scaffolds, an *in vitro* maturation step is included before the scaffold is implanted into the patient, to allow cells to attach to the scaffold, differentiate, and deposit functional ECM. These processes can be further induced by adding growth factors or, in the case of scaffolds expected to have load-bearing role, such as cartilage or heart valve replacements, mechanical conditioning [52, 53]. Alternatively, for an *in vivo* TE approach, the scaffold is implanted directly into the patient

with cells [54, 55]. In this case, the body can be used as a bioreactor. Hence, if the body supplies the appropriate stimuli, formation of new tissue does not need to take place before implantation. In addition, the scaffold material can be implanted without the presence of cells or growth-factor administration [7]. Such implantation was demonstrated by Stevens *et al.*, by injecting calcium-crosslinked alginate or modified HA hydrogels into an artificially-created space between the tibia and the periosteum [48]. The gels induced bone and cartilage formation from native progenitor cells present in the periosteum [7, 48].

2.1.1 Bone TE

Bone is a highly vascularised tissue that rapidly remodels during the life span of an individual [1]. It contributes in movement, supports and protects delicate organs in the body, and provides a frame for adequate load-bearing capacity. Apart from these mechanical functions, bone also mediates metabolic activity of the body such as homeostasis through its reserves of Ca^{2+} and phosphate ions and by controlling the level of electrolytes in the blood [1]. The highly regenerative nature of bone means that most fractures will repair without the need for medical intervention [1, 7]. However, large bone defects do not heal naturally and require medical intervention [1]. Furthermore, with the increasingly aging population, osteoporosis and bone fractures have become more recurrent, and the existing therapies used to repair bone defects cannot tackle this problem completely [2]. Current practice for bone repair at the injury site is to graft autologous bone from the iliac crest, however supply of bone tissue are insufficient [56]. Moreover, pain caused at the donor site affects 18-31% of patients post-operatively, and the surgical treatment could also cause blood loss, infection, haematoma, nerve injuries and scarring [57]. The development of biomaterials in the area of orthopaedics to replace autografts is, consequently, an imperative medical goal and TE scaffolds are beginning to show potential.

Due to the crucial clinical need, the market for TE-based scaffolds in bone repair is expanding at an accelerated rate [1]. Some commercially available scaffold products in orthopaedics are shown in Table 2.1. Currently, researchers are focused on the design of bioactive materials that mimic the natural healing process by integrating biological molecules, cells and regenerate tissues [3]. For bone TE, materials should be osteoinductive (able to induce differentiation of progenitor cells down to osteoblastic lineage), osteoconductive (encourage bone growth) and capable of osteointegration (integrate into area around the bone) [1].

Table 2.1 Examples of current commercial bone TE scaffold products

Name	Description Of Technology	Cell Seeding	Material	Regulatory status
INFUSE® Bone Graft by Medtronic	Bovine type I collagen sponges soaked in rhBMP-2 in LT-CAGE Lumbar Tapered Fusion Device	No	Synthetic	Commercially available (FDA approved in 2002)
OP-1 Implant by Stryker	Combination of recombinant human BMP-7 (rhBMP-7) and purified Type I bovine collagen, which is utilized as a carrier.	No	Natural from bovine collagen	Commercially available in 2001
Pura Matrix by 3DM	A nanofibrous hydrogel that is composed of 16 amino acid residues that will self-assemble in aqueous solution due to hydrophobic and ionic bonding of the 16 amino acids.	No	Natural	Commercially available 2010
FortrOss™ by Pioneer Biologics	Scaffold construct made of nanocrystalline hydroxyapatite	No	Synthetic	Commercially available (FDA Approved in 2008)
Vitoss Scaffold FOAM by Orthovita/ Stryker	Porous scaffold comprising β-TCP and bovine type I collagen	No	Synthetic	Commercially available (FDA Approved in 2008)
Regenafil, Regeneration Technologies by Exatech	Human mineralised bone matrix in porcine gelatine carrier	No	Natural	Commercially available (FDA Approved in 2010)

2.1.2 Cranial bone defects

The use of bone TE biomaterial for non-load-bearing injury sites for application in oral and maxillofacial surgery has shown increased interest [58]. Bony defects in the craniomaxillofacial skeleton can occur due to congenital defects (for example, in 2001, 37,732 children required surgery to repair birth defects) or acquired injuries (for example, in 2001, 24,298 patients required maxillofacial surgery for injuries to the face and jaw) [58].

Bony defects in the craniomaxillofacial skeleton are functionally debilitating, socially incapacitating, and economically burdensome. The war on terrorism has brought numerous new challenges to surgeons: combat-associated craniomaxillofacial injuries [58]. Increased survival because of body armor and advanced battlefield medicine, as well as the increased use of explosive devices, has contributed to the increased incidence of craniomaxillofacial combat injuries [58]. This unique

patient population ultimately requires reconstruction of the cranial skeleton for protection of the brain as well as aesthetic and functional restoration of the calvaria or the bones of the face.

Thus, a variety of materials and methods have been proposed to restore such defects including autogenous bone grafts and allogeneic banked bone, demineralized matrix pastes, ceramic scaffolds, and even synthetic materials and bone substitutes such as calcium ceramics [58, 59]. The multitude of methods reflects both the inadequacy of each technique, as well as the pressing need to adequately reconstruct the skeleton. While each method may achieve craniofacial reconstruction, each possesses inherent limitations, such as donor-site morbidity, an obligatory graft resorption phase, contour irregularities, insufficient autogenous resources, disease transmission, graft-versus-host disease, immunosuppression, structural failure, and foreign body Infection [58]. These limitations preclude most large defects from being repaired with these materials. Therefore, the need for new and improved treatment options is imperative.

To overcome these issues in this area, we would focus on developing a fibrous electrospun scaffold which will be inserted with cells to the site of injury in the craniomaxillofacial bone. The potential of the fibrous scaffold for application in repairing non-load-bearing bone defects will be described in the thesis.

2.1.3 Principles of bone TE

The key requirement of a scaffold is biocompatibility; a scaffold should integrate with native tissue without inducing a high immune response. In addition, the scaffold should be porous to permit cell attachment and vascular in-growth, besides transport of nutrients *in vitro* and *in vivo* [61]. In addition, the scaffold should be able to mimic the natural bone mechanical strength to withstand the biological stimuli *in vivo*. Moreover, the scaffold has to be biodegradable so additional surgery is not needed to remove the scaffold. A list of characteristics of an ideal TE scaffold for bone applications is listed in Table 2.2.

Table 2.2 Basic characteristics of a tissue scaffold, adapted from [62]

Characteristics	General remarks
Biodegradable	The rate of degradation must perfectly match the rate of bone tissue regeneration and the degraded product(s) should not harm living tissues
Nontoxic	Should not evoke toxicity to tissues
Nonimmunogenic	Should not evoke immunogenic response to tissues
Porosity with interconnected pores	To maximize the space for cellular adhesion, growth, extracellular matrix secretion, revascularization, adequate nutrition and oxygen supply without compromising mechanical strength
3D structure	To assist cellular in-growth and transport of nutrients and oxygen
High surface area to volume	To accommodate high-density osteoblast cells
Surface modifiable	To functionalize chemical or bimolecular groups to improve cell adhesion for example, TGF-β and BMPs
Adequate mechanical strength and structure for bone application	To withstand load bearing mechanical of bone. Mechanical/structural strength will be dependent on the rate of degradation and type of bone.

2.1.4 Tissue engineering scaffolds for Bone

There is a variety of structures for TE scaffolds for bone applications based on different materials and processing to form scaffolds, most of which can be classified as either fibrous, solid or hydrogel (Figure 2.2) [29]. Materials for TE scaffolds can be compose of natural polymers, such as fibrin, collagen, hyaluronic acid (HA) or alginate, or synthetic polymers, such as polyethylene glycol (PEG), dextran, acrylates, or polyvinyl alcohol [29, 45]. Fibrous scaffolds can be produced by a few processing methods, including phase separation and electrospinning. Electrospinning will be described in detail in Section 2.3. Hydrogels are composed of hydrated insoluble networks of crosslinked polymers, and have been used for applications such as bone tissue regeneration [63]. Hydrogels can be produced from synthetic or natural polymers and crosslinked using a variety of methods, including self-assembly (non-covalent), ionic crosslinking (non-covalent) and radical polymerizations (covalent) [45, 64].

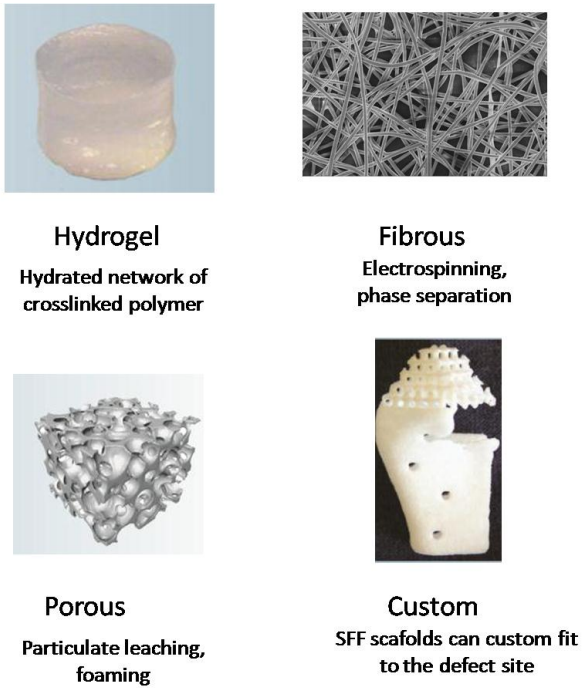

Figure 2.2 Examples of TE scaffolds for bone. Hydrogel, fibrous and porous scaffolds are commonly used in TE applications. Custom scaffolds can be designed using solid freeform fabrication methods. Custom and porous scaffolds are from [65] and [66].

Macroporous solid implants can be produced from polymers, ceramics or metals by a variety of engineering processes. They are resistant to mechanical forces and can incorporate pores to promote cell infiltration and mass transport of nutrients [29] which can useful for bone applications. Porous solid scaffold production methods include particulate leaching, foaming by chemical methods or by CO_2 expansion, microsphere sintering and phase separation [29, 67-70]. Recently, another technologically advanced approach to fabricate solid scaffolds was introduced; it consists of using the solid freeform fabrication (SFF) technique. These scaffolds are produced by using computer-aided systems whereby layer-by-layer deposition of materials, including potentially, cells, into a pre-specified 3D shape, is achieved either by printing or extrusion of a polymer melt [29, 71, 72]. Also, laser beams can be used to solidify polymers into complex shapes by photopolymerization or sintering as the laser is guided over polymer liquids or layers of powder [65, 73]. These novel technologies provide precise control over scaffold architectures, and when used concurrently with medical imaging techniques can produce solid bone TE scaffolds fitted to the shape and dimensions of the damaged site in the patient [29].

2.1.5 Cell source(s) for Bone TE

The role of osteogenic cells is to contribute to bone remodelling and in fracture repair. After specific stimulation in culture, these cells should express osteogenic markers such as alkaline phosphatase (ALP) or osteocalcin (OCN) and produce calcified nodules [2, 74]. At present, the most suitable osteogenic cells for bone TE have not been identified [2]. Critical requirements for cells in clinical use are isolation efficiency, stability of the osteoblastic phenotype *in vitro*, bone induction capability and long-term safety [2]. Our research group have demonstrated the higher potential of hMSCs and osteoblasts to produce material similar to native bone in comparison to embryonic stem cells [75].

MSCs play an important role in bone regeneration because these cells are recruited from the bone marrow and are known to migrate into sites of bone injury, where they differentiate into the osteoblastic lineage, and produce an osteoid matrix which is consequently mineralized and remodelled to bone [76-80]. The use of MSCs to induce tissue regeneration has been extensively investigated [81-83]. These cells have been seeded into the scaffold and implanted into the body either directly or a few weeks later, after *in vitro* differentiation [81]. Successful bone and cartilage defect repair has been demonstrated [84].

Osteoblasts reside at the surface of the bone where new matrix is formed and contribute to bone development [2, 85]. These cells synthesize osteoids and then mature to osteocytes, which are found in the calcified matrix [2]. *In vitro* osteoblasts exhibit osteogenic differentiation and *in vivo* they stimulate the formation of bone in many types of surfaces [86]. The majority of the cell lines currently utilized is acquired from bone tumours or immortalized osteogenic cells [2, 87]. While the easy availability and optimum *in vitro* characterization make these cells attractive for TE investigations, however, safety concerns prevent osteoblasts from being utilized in applied TE [2].

2.2 EXTRACELLULAR MATRIX

Biomaterials can be engineered to interact with cells by mimicking key events of the ECM [7]. ECM is composed of several distinct types of nanometer-scale fibrous networks of proteoglycans, glycosaminoglycans, collagens, non-collagenous glycoproteins and growth factors [26]. These fibrous structures exhibit cellular instructive cues to control cell-matrix interactions by presenting biochemical ligands that interact exclusively with cellular integrins to activate cascading cellular signals [26]. Figure 2.3 describes the different functions of the ECM. Specifically, in addition to anchoring cells to mediate cell adhesion and providing tissue organization, integrins convey intracellular signals that regulate cell migration, cell cycle progression and differentiation [88-90].

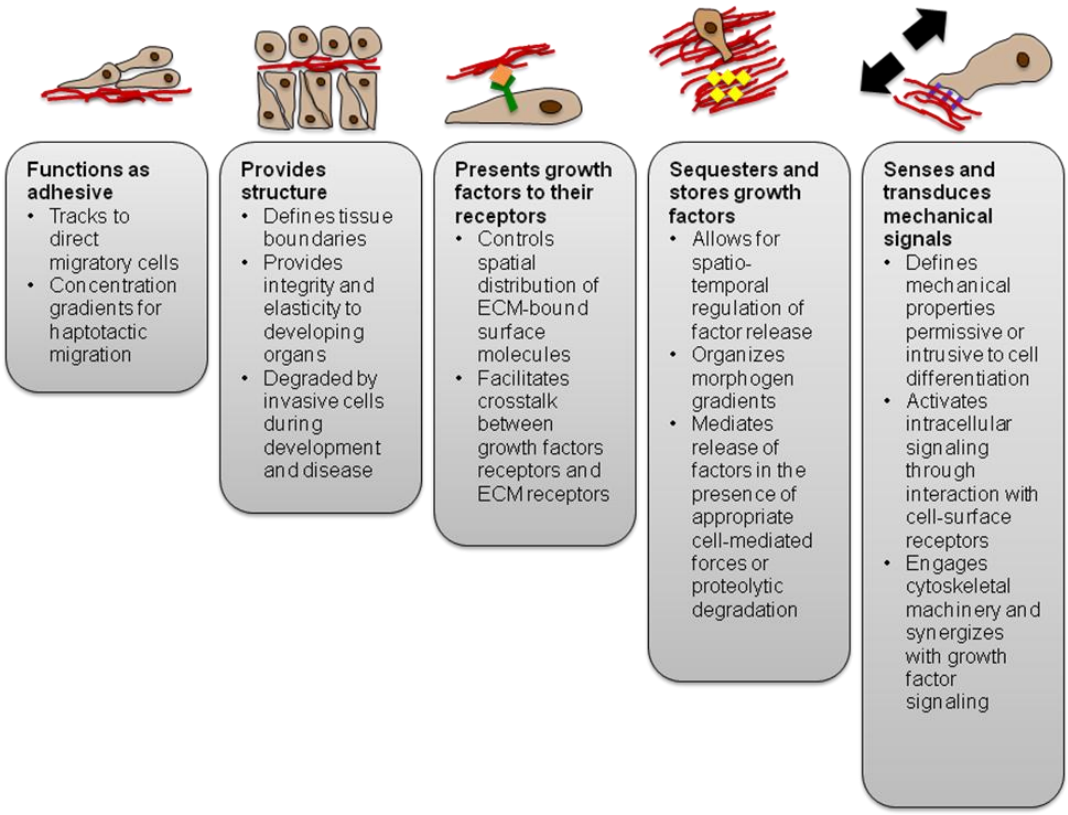

Figure 2.3 Summary of ECM functions. Simultaneously, the ECM can influence multiple biochemical and mechanical functions. (Figure adapted from [26])

Glycosaminoglycans (GAGs) are linear unbranched networks of repeating disaccharides made of hexoseamine and uronic acid [26]. Apart from hyaluronan, all GAGs are covalently bound to proteins, forming proteoglycans [26]. ECM glycoproteins are composed of collagens and a varied range of non-collagenous proteins, for example laminins, tenascins and fibronectin [26].

Collagens are the most abundant protein in ECM, representing approximately 25% of total protein content in mammals [91, 92]. A triple helical organization of pro-α-chain components defines the

collagens and plays a part in the remarkable physical properties of the ECM [26]. Currently, there are 28 known types of collagen [26, 93] and the most abundant category of collagens is fibrillar collagens (type I, II and III), which form the basic scaffolds for connective tissue, while other collagens form network-like structures (type IV and VIII) as part of the basement membrane, and are critical for epithelial cell organization [26, 92]. The overall organization of fibrils and collagen networks vary with different tissue types and the scale of forces to which a specific tissue is usually exposed [26]. Even though collagens' supramolecular architectures and specialized roles within the ECM differ widely, all collagen molecules have a similar basic structure; they are composed of three identical or similar strands with the repeating sequence Gly-X-Y. In this triplet sequence, X is frequently proline and Y is hydroxyproline [93]. Depending on the type of collagen, the α-chains construct trimeric molecules, which are woven collectively into a triple helix in at least one region [93]. The stable triple helical domains are formed through interchain hydrogen bonds, resulting from glycine being used every third residue which allows the three collagen strands to pack closely and form a stable triple helix [92, 93].

Non-collagenous glycoproteins are comprised of different types of proteins such as laminin, fibronectin, and vitronectin [94]. Laminin is ubiquitous in the basal lamina, a tough, thin, sheetlike substratum, which is essential for cell adhesion, differentiation and tissue remodelling. Fibronectin is an abundant, multi domain dimeric glycoprotein with binding sites for a selection of other ECM molecules, such as collagen, heparins A and B, fibrin, and chondroitin sulphate [26, 94]. Each fibronectin subunit has a sequence of reiterating modules of type I, II and III repeating units: 12 type I modules, two type II, and 15 to 17 (depending on splicing) type III, as shown in Figure 2.4 [95]. For stabilization of the folded structure, two intramolecular disulfide bonds form within each type I and type II modules, whereas type III modules are seven-stranded β-barrel structures that do not have disulfides [95]. Modules are structured with binding sites for collagen, integrins, heparin and other ECM proteins [95].

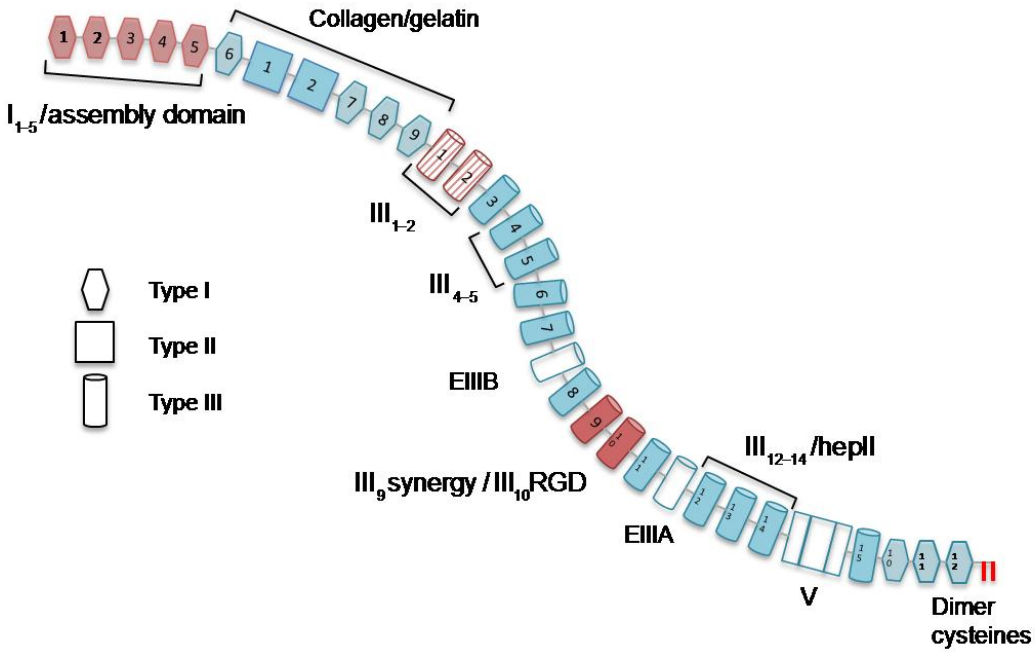

Figure 2.4 Schematic of a fibronectin subunit. Each subunit consist of three types of subunits, type I, type II and type III. (Adapted from [95])

Collectively, these different groups of ECM molecules present vast functional complexity. Hence, the ECM can be known to contain “morphogenetic language and code” that is understood and interpreted by cells that come in contact with it [26]. The ECM has embedded information that is “sensed” by receptors at the surface of the cell has which has immense influence on the cell behaviour by affecting cell attachment, motility and other intracellular cues which control cell fate [26].

2.2.1 Role of integrins

The name “integrin” was chosen to highlight the significance of these receptors in preserving the integrity of the cytoskeletal-ECM bond [96, 97]. The interaction between integrins with the ECM is though their specific extracellular domains, and with the constituents of the cytoskeleton, through their intracellular domains [98]. Integrins comprise of two transmembrane glycoprotein subunits that are non-covalently bound, the α chain and the β chain [99]. The extracellular segment of the α and β subunits interacts with each other, producing a heterodimer Figure 2.5. Both subunits have disulfide bridges that protect them from proteolysis [26, 99]. Many combinations of subunits can be achieved, and each combination has the capability to interact with one or more ligands [99]. In humans, the family is comprised of 18 α subunits and 8 β subunits, which can generate 24 different heterodimers [100]. Table 2.3 shows a variety of known combinations of integrin subunits and their protein ligands.

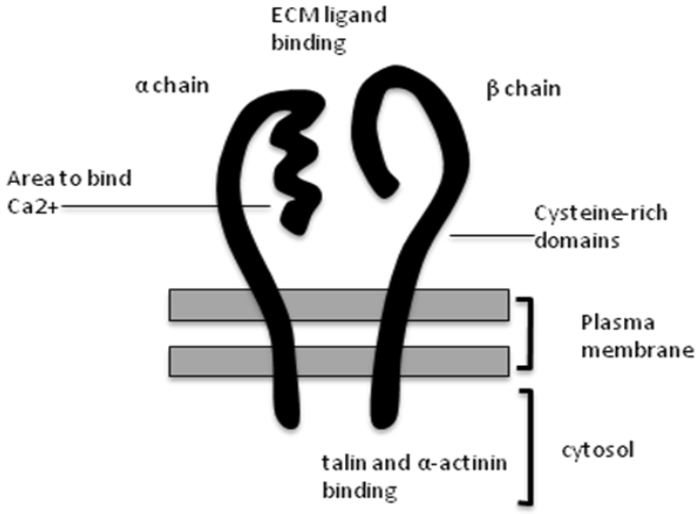

Figure 2.5 Schematic structure of the subunit structure of a cell-surface integrin. Figure adapted from [99])

Table 2.3 Possible combinations of integrin subunits and their protein ligands. (Adapted from [79])

	Subunits	Ligands
β1	α1	Collagens, Laminins
	α2	Collagens, Laminins
	α3	Laminins, Fibronectin, Thrombospondin
	α4	Fibronectin, VCAM
	α5	Fibronectin
	α6	Laminins
	α7	Laminins
	α8	Fibronectin, Tenascin
	α9	Tenascin
	α10	Collagens
	α11	Collagens
	αv	Fibronectin, Vitronectin
β2	αL	ICAMs
	αM	Fibrinogen, ICAMs, iC3b
	αX	Fibrinogen, ic3B
	αD	VCAM, ICAMs
β3	αIib	Collagens, Fibronectin, Vitronectin, Fibrinogen, Thrombospondin
	αv	Fibronectin, Vitronectin, Fibrinogen, Thrombospondin
β4	α6	Laminins
β5	αv	Vitronectin
β6	αv	Fibronectin, Tenascin
β7	α4	Fibronectin, VCAM, MAdCAM
	αE	E-cadherin
β8	αv	Collagens, Laminins, Fibronectin

After binding to ligands, integrins would cluster simultaneously together into focal contacts, a region of close contact between a cell and the ECM, comprising of cytoskeletal proteins, adapter molecules and kinases [99, 101, 102]. Following to the activation of the clustering, the “outside-in signalling” will be triggered with cytoskeletal and signalling molecules recruited and activated. The signalling cascade inside the cell involves the interaction of quite a few proteins, such as focal adhesion kinase (FAK), Src and cytoskeletal proteins [99]. The early stage begins with the autophosphorylation of FAK, which leads to tyrosine phosphorylation and the engagement of other protein molecules [27, 79, 99, 103, 104]. In addition to the interaction of signalling molecules, integrin binding also triggers alterations in the regulation of the cytoskeleton, consequently influencing cell adhesion and migration [99]. Moreover, integrins are bidirectional signalling receptors [96, 105]. The inside-out signalling is used to bring the integrin into the active conformation, by which signalling pathways in the cell itself can control the ligand-binding of the integrins on the cell surface [106].

Furthermore, the interaction of integrins with ECM proteins has been shown to affect signal transduction and the expression of transcription factors and osteoblast-specific genes in osteoblasts [103, 107]. The ECM-integrin-activated interaction induces osteoblastic differentiation through the stimulation of the mitogen-activated protein kinase signal (MAPK) transduction pathway [77, 108]. Production of ECM osteogenic proteins is due to the aggregation of the α2β1 [37, 109, 110] and αvβ3 [41] integrins ,which induces intracellular signalling pathways, leading to the phosphorylation of the osteoblast-specific transcription factor, Runx2/Cbfa-1 [110-112].

The main regulator of osteogenic differentiation and matrix production is influenced by the transcriptional activity of Runx2/Cbfa-1 [113]. Post-translational modification and protein interactions contribute a central role in controlling Runx2/Cbfa-1 [113, 114]. FAK distributes integrin signals by assembling complexes with signalling proteins rich in SH2 domains [113, 115].

2.2.2 Peptides

Many attempts have been carried out to emulate the natural microenvironment by using synthetic ECM-mimetic macromolecules to mimic the ECM’s biological, chemical and mechanical properties [116-119]. One approach to offer sites of integrin attachment to scaffolds is to immobilize purified ECM proteins, such as collagen or fibrin, on the scaffold [7, 120, 121]. However, immobilization of full proteins to scaffolds can be difficult, as the proteins are susceptible to denaturation and degradation. Consequently, a widely used method to improve bioactivity of the scaffold is to incorporate short peptide motifs/analogues derived from the binding regions of ECM components

[7]. Peptides have been demonstrated to be adequate molecules for protein-binding-site mimics, since peptides can be produced as protein fragments, allowing comprehensive investigation of the interaction at the level of individual amino acid residues [122]. Compared to full proteins, peptides are more resistant to denaturation due to variations in pH and heat [123]. In addition, while peptides may have a fraction of the activity of the complete protein, they can still be immobilized at high concentrations to increase overall effect and they are easy to synthesize and functionalize. Hence, biologically active peptides allow a synthetic, scalable substitute to ECM proteins [30].

Essentially, peptides that influence and induce cell adhesion are derived from sequences found in ECM molecules. The amino sequence Arg-Gly-Asp (RGD) (Figure 2.6), is found in the tenth type III repeat of fibronectin, can be used to enhance cell adhesion by inducing focal adhesion through integrin binding to surfaces, which was known as far back as the late 1980s [31, 32]. A number of ECM components, for example, collagen type 1, thrombospondin, osteopontin, vitronectin and fibronectin, contain one or more RGD sequences, which are essential for interacting with many types of integrins and function as cell attachment signals [26]. Nevertheless, RGD sequences located in ECM molecules do not necessarily have to be active and functional [26, 123].

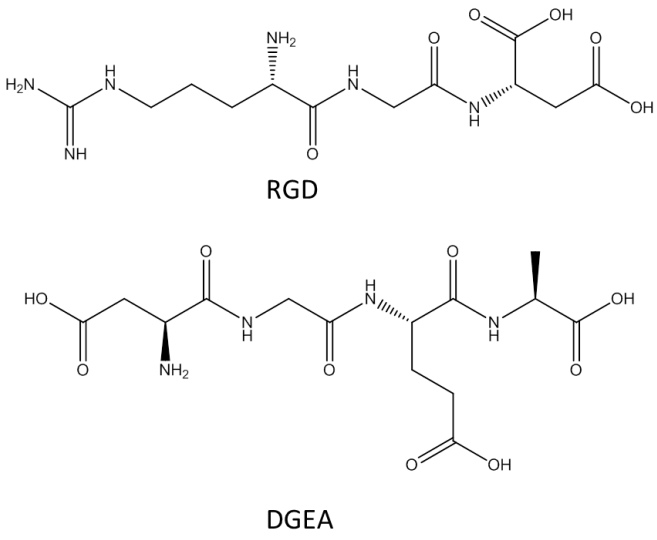

Figure 2.6 Peptide sequences of RGD and DGEA

Apart from RGD peptides, which have been extensively investigated, other adhesion peptide motifs have also been studied. These include IKLLI, IKVAV, LRE, PDSGR and YIGSR from laminin, DGEA from collagen I and GEFYFDLRLKGDK from collagen IV [29, 116, 124, 125]. DGEA (Asp-Gly-Glu-Ala), also shown in Figure 2.6, is a collagen type 1 peptide motif and exhibits specific binding for osteoblast via α2β1 integrin. In addition, there is growing literature to suggest that activation of a collagen-selective integrin, $\alpha_2\beta_1$ integrin induces osteoblast differentiation

mediated by collagen-$\alpha_2\beta_1$ integrin interaction [36-38, 42]. Therefore, DGEA could serve as both a cell adhesion and a differentiation factor [42]. It has been demonstrated that collagen I binds to a different integrin receptor than fibronectin and the integrin/collagen I interaction is reported to be RGD independent [42]. Collagen-derived peptides have been relatively less investigated for their cellular response compared to other ECM peptides, while full collagen has been mostly used for making scaffolds [39-41].

Engagement of the $\alpha_2\beta_1$ integrin is associated with the activation of the osteoblast-specific factor Runx-2/Cbfa-1, a transcription factor that mediates osteogenic differentiation, specifically the osteoblastic phenotype [107, 110, 112, 126, 127]. Moreover, the collagen-$\alpha_2\beta_1$ integrin interaction has been shown to induce the osteoblastic phenotype in MSCs [36, 37]. Integrin $\alpha_2\beta_1$ regulated interaction to collagen type 1 induces tyrosine phosphorylation of FAK and consequently promotes the stimulation of ERK, a mitogen activated protein kinase (MAPK) which has been demonstrated in regulating osteoblast-specific gene expression and matrix mineralization [109, 111, 126, 128, 129].

2.2.3 Influence of peptide presentation on biological response

There are numerous approaches by which peptide sequences can be presented to cells with respect to the choice of peptide length, sequence arrangement, as well as concentration [35]. For example, a biphasic cell response was demonstrated with varying RGD concentrations and maximum cell migration was shown at intermediate peptide densities, because low amount of adhesion sites fail to sufficiently support contractile force, whereas high concentrations overwhelm the cells' ability to detach from the substrate [130]. Massia *et al.* showed that an average distance of 440nm between the RGD peptides was necessary for fibroblast adhesion and migration, but an interpeptide distance of 140nm was needed for focal contact formation and cytoskeletal reorganization into stress fibres [7, 35, 131].

In addition, the varying affinities of peptides for integrins are greatly affected by ligand sequence, conformation and accessibility to integrins [35]. The binding specificity of the peptide to a cell-surface integrin receptor can be enhanced by ligand conformation [33, 132]. The enhancement of cell adhesion can only be achieved if the ligands are spatially accessible to the cell-surface integrins [35]. The distance between biomaterial and peptide can be regulated with the use of additional amino acid residues in the peptide sequence, by the integration of a spacer arm [35]. Varying the length of the spacer arms is essential for cell-scaffold interactions as it has been shown to regulate adhesion and spreading of certain cell types [133].

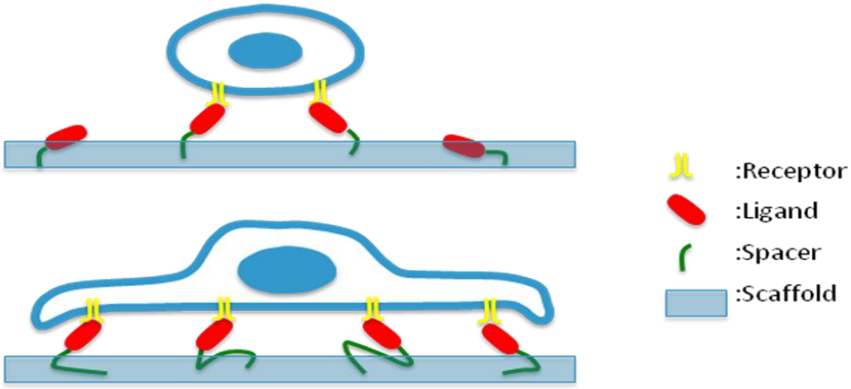

Figure 2.7 Schematic of cellular adhesion onto peptide-modified scaffold with different spacer-arm lengths. Providing a distance between the peptides and the biomaterial will present better access for integrin-ligand binding. (Figure adapted from [133]).

The enhancement of integrin-ligand interactions can be achieved by providing a distance between the peptide and the biomaterial as shown in Figure 2.7 [133]. Studies conducted by Lee *et al.* have also shown the influence of glycine spacer arms on cell adhesion and viability on RGD sequence immobilized on alginate gels [133]. They found that a minimum number of four glycine residues were essential for enhanced cell adhesion and viability. This difference could be substrate specific, since the gap that the peptide is needed to be from the material relies on the physical properties of the bulk material [35].

Furthermore, a few groups have shown that PEG-diacrylate (PEG-DA) based hydrogels need a long spacer arm between the hydrogel and the peptide to enhance cell adhesion and viability [18, 134, 135], because PEG-DA hydrogels have two acrylate groups and produce a highly cross-linked network with long chains extending from the backbone [35].

2.2.4 Conjugation of peptides onto TE scaffolds

There are two approaches of presenting peptides towards cells on scaffolds, physical and chemical methods [35]. Physical methods involve deposition, adsorption or precipitation onto or into the material; hence, the peptides are not covalently linked to the scaffold [35]. Physical adsorption is a relatively weak force, which may therefore not be suitable for TE scaffolds as prolonged signalling is needed [136]. In contrast, chemical methods of peptide-conjugation involve the formation of covalent bonds between the functionalized-peptide and the material [35]. The conjugation can be done as the scaffold is being produced/synthesized or by immobilization onto the prepared solid [35]. It is possible to either incorporate the peptides on the surface of the scaffold or bulk modification throughout the scaffold. Surface modification on electrospun fibres using covalent immobilization of peptides has been accomplished by surface etching [137] and

plasma/gamma-ray [138] treatment, which induces the cleavage of a polymer backbone to form carboxyl (-COOH) groups or radicals. Hence, these functional groups could react with bioactive peptides on the surface of various scaffolds including PLLA, PCL and PLA [45, 139].

Peptides can be incorporated into the scaffold by including a reactive group in the peptide sequence and copolymerizing it with other monomers [35]. The polymerization can be activated by an initiator induced by the use of heat, UV light or chemical reaction. The use of UV radiation will be described in detail in Section 2.4. The final concentration of the peptide in the scaffold could be regulated by varying the ratio of peptide and/or the other co-monomers before UV-crosslinking [35]. A significant amount of research using this bulk modification has been performed in the area of hydrogels. For example, the incorporation of RGD peptides into PEG-DA hydrogels was demonstrated by Hern and Hubbell [134]. In addition, several studies have utilized mixed-mode thiol-acrylate polymerization specifically for the synthesis of hydrogels. Specifically, during UV radiation, the reaction mechanism consist of two steps, acrylate homopolymerization and thiol-acrylate step-growth reaction [140, 141]. Rydholm *et al.* described the formation of degradable thiol-acrylate networks under exposure to UV light with or without the presence of a photoinitiator [142, 143]. This method of peptide conjugation will be described in detail in Chapter 5.

2.3 ELECTROSPINNING

Although there are many other techniques of producing nanofibrous scaffolds, such as phase separation and self-assembly, these approaches cannot match electrospinning in terms of its versatility, cost-effectiveness, flexibility and ability to scale-up [144]. In terms of flexibility, electrospinning allows the fabrication of nanofibres from a range of materials, such as polymers, composites, semiconductors and ceramics [144, 145]. This technique is capable of generating fibres with adjustable dimensions ranging from diameters of several micrometers down to a few nanometers. Based on the literature published, it is evident that by using electrospinning most polymers are relatively easy to electrospin compared to other methods [146]. Fibres can be produced by regulating electrospinning parameters, such as accelerating voltage, flow rate of solution and polymer solution parameters like viscosity and conductivity [146].

In 1934, the first patent that explained the technique of electrospinning emerged, when Formhals described an apparatus for creating polymer filaments by using electrostatic repulsions between surface charges [147]. The technique was known as *electrostatic spinning* up until 1939 and only a few papers were published about the production of thin fibres [14]. In the early 1990s several research groups, in particular, the Reneker group revived interest in the technique by showing the production of fibres from a selection of organic polymers and the term *electrospinning* was coined [14, 148].

Electrospinning has been applied ubiquitously in engineering fibrous scaffolds for TE applications. The technique is able to produce scaffolds composed of fibres, which creates high surface area to volume ratio; excellent conditions to induce cell growth and infiltration [145]. Furthermore, the morphological resemblances between the nanofibrous scaffold and the ECM are shown to increase biological response and biocompatibility [15, 61]. The large surface area encourages cellular adhesion, as well as formation of multiple focal adhesion points because of the nanosized diameters of the fibres [61].

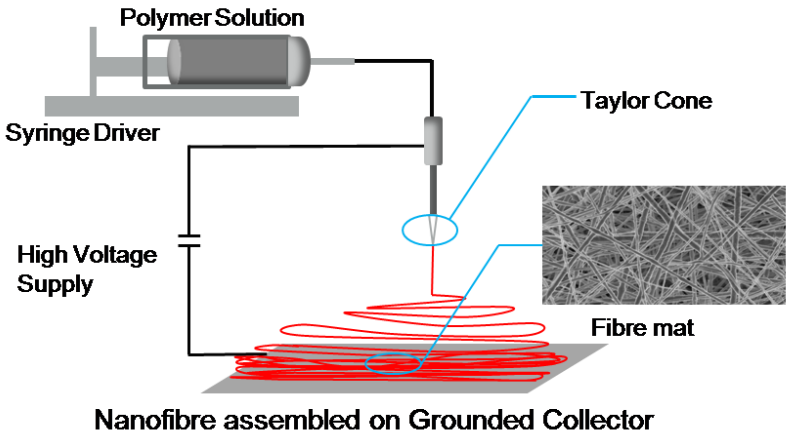

Figure 2.8 Schematic of an electrospinning system. The insets illustrate the Taylor cone and an SEM image of electrospun fibres accumulated on the collector.

The essential configuration of an electrospinning system is illustrated in Figure 2.8. It consists of a spinneret (a metallic needle), a fibre collector and high voltage power system. The spinneret is connected to the syringe and the polymer solution is provided through the spinneret using a syringe pump at a constant and regulated flow rate [62]. The spinneret serves as an electrode to which the voltage is applied [62, 149]. In addition, the target collector is placed right below the spinneret with a suitable space in between [62].

2.3.1 Electrospinning process and mechanism

The stable electrospinning jet was illustrated by Reneker *et al.*; as the polymer solution is injected at a constant rate, a droplet begins to form at the end of the needle [13, 14]. When a high voltage is employed, the pendant drop of the polymer solution at the tip of the spinneret will become highly electrically charged and the induced charges will be dispersed over the surface [14]. Consequently, the polymer solution at the tip of the needle is subjected to two different types of electrostatic forces: the electrostatic repulsion of the surface charges and the Coulombic forces put forth by the external field [13, 14]. Hence, due to these interactions, the drop will form into a cone shape, identified as the Taylor cone. Once the charge accumulated exceeds the surface tension of the solution, an electrified liquid jet is ejected from the tip of the needle [13, 14]. As the liquid jet travels towards the counter-electrode, this electrified jet becomes elongated and the solvent rapidly evaporates. A phenomenon called “splaying” occurs, the different polymer strands in the jet gets separated because of the mutual repulsion of the charges [62]. The diameter of the filaments will greatly reduce from hundreds of micrometers to as small as tens of nanometers [14, 148]. As a result, these filaments assemble in a non-woven fashion on the grounded collector. The diameter

of the fibres formed on the collector depends on how many splays are produced during electrospinning [150].

Even though the setup for electrospinning is extremely simple, the mechanism of electrospinning process is more complex [14]. It has been demonstrated with high speed photography that the jet formed which seems to splay is really in fact a single, rapidly whipping and thinning jet [61, 150, 151]. Under high electric fields, the jet becomes unstable and whips at a high rate and causes bending and stretching, mainly due to the bending instability of the electrified jet [61, 151]. Conventional photography was unable to capture the high frequency of whipping, presenting the notion that the original jets splits into multiple branches when it travels towards the collector [61]. Rutledge and colleagues modelled the behaviour of the jet by describing three different instabilities; Rayleigh instability and two conducting modes [61, 151]. The axisymmetric Rayleigh instability is greatly influenced by surface tension and is opposed at high electric fields, whereas the two conducting modes, one axisymmetric and the other non-axisymmetric (whipping/bending instability), are independent of surface tension and are influenced by electric forces [61, 150, 151].

2.3.2 Parameters of electrospinning process

2.3.2.1 Processing parameters

There are three important processing parameters that can influence fibre morphology [152]. These parameters that can control the production of bead defects during electrospinning are: applied voltage, polymer flow rate and tip-collector distance [152].

Applied voltage

One of the parameters most studied in literature for electrospinning is applied electric field or voltage. Deitzel *et al.* studied a polyethylene oxide (PEO)/water electrospinning system, which showed that changes in the electric field alters the shape of the Taylor cone and consequently affects the fibre jet [152, 153]. When the electric field is sufficient to dominate the surface tension, at specific voltage conditions, the drop is suspended at the tip of the spinneret and a jet will form from the Taylor cone creating bead-free electrospinning [61, 153]. However, more beading can be produced when the applied voltage is increased because the overall volume of the drop decreases, which will trigger the Taylor cone to diminish, thus the jet will originate from the liquid surface within the tip [61, 153]. Furthermore, even more beading is produced when the voltage is further amplified, the jet will shift around to the side of the tip; no Taylor cone is formed [61, 153].

It has also been shown by Meechaisue *et al.* that, when the solution concentration or viscosity and flow rate is constant, an increase in the applied voltage leads to an increase in the jet velocity. As a

result of the increase, more solution is being removed from the tip of the droplet. For this reason, fibres spun at higher voltage exhibit larger average diameter and causes production of several jets [154]. Based on the work of the groups above and others, it is clearly demonstrated that there is an optimum range of applied voltage for a specific polymer/solvent electrospinning system, as a suboptimal field strength (too high or low) can produce bead defects in the electrospun fibres [152].

Flow rate

Many research groups have studied the effects of polymer flow rate on fibre morphology and size. It has been demonstrated that decreased flow rates form fibres with smaller diameters [61]. For example, Megeski and co-workers investigated the relationship of flow rate on the fibre morphology of polystyrene/tetrahydrofuran (THF) solution [61, 155]. They showed that increasing flow rate produces higher fibre diameter and pore size [155]. In addition, significant amounts of beading were produced when flow rates were too high due to the inability of fibres to dry prior to contacting the grounded collector [152, 155-157].

Tip-collector distance

Another method to regulate fibre diameter and morphology is changing the distance between the tip and the collector [61]. Most importantly, this distance can influence whether electrospinning or electrospraying occurs. There is a requirement of a minimum distance to facilitate solvent evaporation for fibres to dry or elongation of the jet, which leads to further thinning of the fibres before reaching the collector [158]. Hence, beaded electrospraying will occur if the tip-collector distance is too short. However, it is critical to not exceed the distance between tip and other surrounding structures such as the wall of the electrospinning container [158]. This is due to the charged polymer deposition, which will try to obtain the path of least resistance as the fibres will be accumulated on other substrates in closer proximity than the collector in spite of it being the only object of high conductivity [158]. Investigations performed by Doshi and Reneker concluded that the fibre diameter decreased with increasing tip-collector distances [148, 152].

2.3.2.2 Solution parameters

A number of solution parameters also take part in a critical role in fibre production and morphology. Listed in order of relative importance to the electrospinning process, the variables include polymer concentration, solvent volatility and solvent conductivity [152].

Polymer concentration

Solution concentration or its corresponding viscosity has been established to be one of the critical variables that control fibre size and morphology. Moreover, it determines the capability of a polymer solution to electrospin, namely whether fibre or droplets form or not. The solution must have sufficient polymer concentration for chain entanglement to occur [152]. However it is important to note that the polymer also needs sufficient molecular weight for chain entanglement to take place. Concentration is important because it controls both the viscosity and the surface tension of the electrospinning solution. At low concentrations, the polymer fibre will break up into droplets before reaching the collector due to the effect of surface tension, which will produce beading and droplets formation [152]. Nevertheless, if the concentration of the polymer solution is too high, which makes it difficult to regulate the flow rate through the needle, consequently, the fibres cannot be produced. Hence, there is an optimal window of solution concentration to fibre formation when all other variables are constant. In many studies it has been demonstrated that when electrospinning is conducted in the optimum range of polymer solution concentration, larger fibre diameter forms with increasing polymer concentration [61, 148, 153, 155].

Solvent volatility

The selection of solvent is essential to determine if fibres can be produced during the electrospinning process, as well as influence fibre porosity. The volatility of the solvent will permit the fibres to dry in before their deposition on the target collector [158]. The volatility of the solvent influences the phase separation which happens when the fibre jet travels through the atmosphere [152]. Megelski *et al.* showed that high volatile solvent (100% THF) yielded higher porosity for the fibres, which increased surface area by as much as 20-40%, depending on fibre diameter [155]. On the other hand, a less volatile solvent (100% DMF) produced decreased pore density and almost complete loss of microtexture [152, 155].

Solution conductivity

Solution conductivity has also been found to influence fibre size, and this dependence can be utilized for the electrospinning process. A solution with higher conductivity will have a larger charge-carrying capacity compared to a solution with low conductivity [152]. Consequently, in the presence of an electric field, the fibre jet with highly conductive solutions will to undergo a higher tensile force in comparison to a solution with low conductivity [152]. Zhang *et al*. studied the effect of varying concentrations of ions to PVA/water solution on the diameters of fibres [159]. It was shown that by increasing concentrations of NaCl from 0.05 to 0.2% (w/v), the fibre diameter

decreased from 214 ± 19nm to 159 ± 21nm [159]. They found that the decrease in fibre diameter is caused by the increase of net charge density attributed to the addition of NaCl, which increases the voltage applied on the jet [152, 159]. A number of general relationships between processing/solution parameters discussed above are summarized in Table 2.4.

.

Table 2.4 Effect of changes in the electrospinning process parameters on the resultant fibre morphology. Adapted from [61, 152].

Parameter	Effect on Fibre Morphology
Viscosity/Concentration	Fibre diameters increase with increasing concentration/viscosity (within optimal range)
Conductivity/Solution charge density	Increasing the conductivity encourage the production of uniform bead-free fibres In general, increasing conductivity produces smaller fibres
Polymer molecular weight	At constant viscosity, increasing molecular weight reduces the number of beads and droplets
Flow Rate	Lower flow rates produce fibres with smaller diameters.
Field strength/Voltage	At too high voltage, beading will be observed At increased flow rates, fibre diameter decreases
Distance between tip and collector	A minimum distance is required to obtain dry fibres At distances either too close or too far, beading can be observed.

2.3.3 Polymers for electrospinning

Natural biopolymers have been electrospun to generate fibrous scaffolds for TE such as polysaccharides; hyaluronic acid (HA), cellulose, chitosan and proteins; silk, fibrinogen, collagen, gelatin [146]. The advantage of using these natural polymers for TE is they provide many instructive cues needed for high cell attachment and proliferation, however, unlike synthetic polymers, these natural polymers may have the problem of batch-to-batch variation [146]. Many research groups have reported combination or blends of synthetic and natural polymers that could combine both the biofunctionalities of natural polymers with the capability of properties modification of synthetic polymers [146, 160-162].

Synthetic polymers which are degradable or hydrolysable under physiological conditions, for example aliphatic polyesters, polyanhydrides, and polyphosphazenes, are essential for producing electrospun nanofibrous scaffolds for TE [29]. Poly(lactic acid) (PLA), an aliphatic polyester, is one of the quintessential biodegradable polymers used for electrospinning [15, 149]. Poly(glycolic-acid) (PGA) has also been electrospun but to a limited extent, because of its low solubility in organic solvents except for hexafluoroisopropanol (HFIP), whereas poly(ϵ-caprolactone) (PCL) and copolymers of PCL, which are soluble in many types of solvents, have been used extensively in

electrospinning for scaffolds [149]. Because of their biocompatibility, slow degradation rate and ease of electrospinning, these electrospun synthetic polymers are capable of supporting a wide variety of cell types [61].

Electrospinning has been demonstrated to have immense potential in the engineering of many tissues including: bone [163-165] and cartilage [162, 166]. In bone TE, electrospun PCL seeded with MSCs has been shown to provide an environment that promotes mineralization and tissue formation [167]. Yoshimoto *et al.* cultured rat MSCs on electrospun PCL and incubated the scaffold in a dynamic bioreactor [61, 167]. After four weeks, the scaffold showed matrix mineralization and collagen type 1 deposition. Furthermore, a similar scaffold was cultured *in vivo* in the omenta of rats and displayed bonelike appearance with osteocyte-like cells in the mineralized matrix [168]. In addition, Cai *et al.* utilized an electrospun PLLA scaffold with the addition of a porous collagen membrane [169, 170]. After three weeks, using a rabbit tibia model, defects implanted with the dual-layer scaffolds showed 91% bone formation in contrast to 64% and 32% for nanofibrous and collagen membrane alone [170].

2.4 POLYMER PHOTOCHEMISTRY

The past couple of decades have seen many studies of photoinitiated materials used in exploring strategies to design a biomaterial for TE especially for cardiovascular materials [22, 23], drug delivery systems and biological adhesives [17, 171]. Photochemistry is a process in which chemical reactions are induced by light radiation [17, 172]. The light energy utilized is frequently ultraviolet (200-400nm) or visible light (400-800nm), but sometimes it is infrared light (800-2500nm) [17]. Photoinitiated reactions are attractive in the fabrication of biomaterials because they have a controlled initiation and termination, and they yield spatial control [17]. Also, photochemical reactions can be performed under a wide range of conditions, and may include variations in monomer structures, the amount of reactive functional group, temperature, atmosphere, irradiation time and photoinitiator type [173]. There are two steps that describe photoinitiation: the absorption of light of a photosensitive molecule and the resulting photoreaction of this is the excited molecule [17, 174].

Molecules or macromolecules utilized as photopolymerizable monomers or macromers have a general characteristic: a photopolymerizable residue is positioned at one or both ends of the molecule [175]. Commonly used monomers in these light-induced systems are acrylates and methacrylates because of their high reactivity during photoreactions [173, 175]. Acrylic and di(methacrylic) derivatives of poly(ethylene glycol) (PEG) are widely used for TE applications due to their active double bond group for photocrosslinking [19, 21, 176-181].

A selection of photoinitiators, each with its specific adsorption spectrum, is commercially available in the current market. Photoinitiators are molecules that are responsible for initiating the photoreaction by producing reactive species when activated by UV light [175]. Critical aspects that need to be considered when choosing a suitable photoinitiator include peak absorption wavelength of the initiator, reactivity of the initiator towards other species, kinetics of the initiator and, most importantly, the biocompatibility of the photoinitiator and its decomposition products towards cells and the human body [17]. One of the most commonly used photoinitiators are ketones which are associated to acetophenone (Ph-CO-CH_3), which has been shown to have a strong absorbance band at 280 nm and weaker one at 330nm [17, 172]. The commonly employed 2,2-dimethoxy-2-phenylacetophenone increases the rate of radical polymerization due to its additional electron donating groups, which enhances its ability to absorb light and become excited [17, 174, 182]. On the other hand, the production of high-energy radical species have been shown to cause damage to cell membranes, nucleic acids and proteins, which causes cell death [183-185].

2.4.1 Photopolymerization with acrylates/methacrylates for TE

The photopolymerization of acrylates has been used for several decades in biomedical research and has become an essential approach for *in situ* delivery of resins in the area of dentistry [22-25] and as bone-replacement materials [17]. Recently, a variety of photocrosslinkable and degradable acrylate polymers have been utilized for a range of applications such as drug delivery vehicles, TE scaffolds and in the fabrication of microdevices [17, 171]. The spatial and temporal control during photoinitiation is a pivotal advantage which has motivated its wide application in the field of TE [16, 17]. For example, photocrosslinkable acrylate hydrogels are synthesized for the delivery of cells to injured tissues [21, 178, 180, 181] and for the encapsulation of biological molecules for controlled delivery [171, 176, 179]. These applications are achievable because of the controlled nature of the photoinitiated polymerization with a choice of non-cytotoxic photoinitiators (and their degradation products) [171].

Acrylates are ubiquitously used in the synthesis of hydrogel networks due to the active double bonds [18-21]. In addition, there are a number of commercially available monomers which can be photocrosslinked rapidly using a photoinitiator [9]. The bulk properties of the network can be easily altered by simple adjustments during synthesis (e.g. amount of crosslinker), thus rendering the system tunable with respect to mechanical properties and morphology [177]. When formed as films, the acrylate polymers show a wide range of physical properties, such as mechanical properties and swelling rates [10, 171]. Anderson and colleagues demonstrated the ability of acrylates and methacrylate photocrosslinked networks to support cell attachment, viability and proliferation [9]. Moreover, using an acrylate/methacrylate microarray library, they were able to identify specific monomers that support growth of human embryonic stem cells [9]. Hence, based on the 'hit' polymer microarrays, which identified specific monomers that increased and sustained cell growth, diethylene glycol dimethacrylate (DEGMA) and methyl acrylate (MA) were chosen to be employed in the electrospinning system described in this thesis.

There are only few studies in the literature on electrospinning of acrylate monomers. Kim and colleagues introduced a novel method of reactive electrospinning whereby 2-hydroxyl methacrylate, methacrylic acid, ethylene glycol dimethacrylate, AIBN and a photoinitiator were prepolymerized and subsequently photochemically crosslinked during electrospinning [186]. However, no cell culture studies were reported in their work. The first study found in literature which developed electrospun fibres from monomers and investigated cellular response on the fibres was reported by Tan *et al*. [10]. The authors successfully electrospun photocrosslinked macromers from a library of multifunctional poly(β-amino-ester)s, but preliminary cell studies using bovine MSCs have shown limited cell adhesion to the fibers, contrary to the results shown in our study [10]. Sundararaghavan and his co-workers created multiscale porous scaffolds, utilizing

photopatterning and electrospining methacrylated hyaluronic acid, to enhance cellular infiltration of hMSCs. However, cell viability was demonstrated to be significantly low [187]. The low cell adhesion observed in their investigation could either be due to cytotoxic effects of the macromer itself or to the presence of PEO. Failure of PEO extraction would cause PEO to block protein adhesion, which would consequently affect cell adhesion. Subsequently, the same research group increased the viability and proliferation of hMSCs by using photocrosslinkable acrylate-poly(glycerol sebacate) and co-electrospinning with gelatin instead of PEO [177].

The pore size and overall porosity of scaffolds are essential for cell infiltration and diffusion of nutrients and waste, and the design of optimal vascular structures has been a major hurdle for TE. However, one of the main disadvantages of electrospun scaffolds is the limitation of cell infiltration and vascular construction due to the small pore sizes. Cell infiltration is limited in electrospun fibres because of dense fibre packing during the electrospinning process. To address this issue, by utilizing the UV system and the use of a UV mask on top of the scaffold during photocrosslinking could be investigated to increase porosity of the scaffold. Subsequently, uncrosslinked monomers could be leached out during washing and this could produce pores to improve infiltration throughout the fibrous scaffold. Alternatively, pores could be introduced by introducing salt particles which can then be leached out by thorough washing with water.

2.4.2 Network formation and degradation

One of the advantages of using free radical polymerization (i.e., photoreaction, thermal, redox) is the possibility to introduce specific properties in the polymer networks, such as mechanical strength, wettability, biodegradability, surface topology or cell adhesiveness, which can be achieved simply by selecting specific monomers or additional molecules (crosslinkers) during the design of the biomaterial formulation specific for the TE application [9, 16], for example, a hydrophilic monomer could be chosen to be introduced into the network to increase the hydrophlicity of the crosslinked network. In addition, mechanical strength of the network can be tuned by varying the amount of crosslinker. However, photopolymerization adds another advantage of spatial and temporal control during polymerization.

The reaction mechanism for free radical polymerization, initiation, propagation and termination is illustrated in Figure 2.9 [16, 173]. This mechanism was described in detail by Ifkovits *et al*., and Andzejewska *et al.,* [16, 173]. Briefly, the radical polymerization begins with irradiation of an initiator. The rate of initiation (R_i) is influenced by efficiency and concentration of the photoinitiator and intensity of UV light [173]. This induced initiator divides into two radicals that attack a monomer, producing two radical species [17]. Subsequently, the radicals proliferate through unreacted double bonds to produce long kinetic chains [16]. The growth ceases with chain transfer

or radical termination. The degree of termination (R_t) is a bimolecular reaction and is highly dependent on the concentration of radicals in the reaction, while the rate of polymerization (R_p) is proportional to the degree at which double bonds are reacted [16, 173]. This reaction happens in the propagation step; hence, R_p could be estimated as a reaction which is dependent on the double-bond concentration and the radical concentration [16]. In addition, if assumption of a pseudo-state of radical concentration (R_i=R_t) is made, R_p becomes proportional to R_i, the monomer concentration [M], the propagation (k_p) and termination (k_t) kinetic constants [16, 172]. Hence, although the reaction mechanism is simple, the polymerization behaviour is more intricate, as k_p and k_t are highly influential on the conversion and organization of the network structure [16].

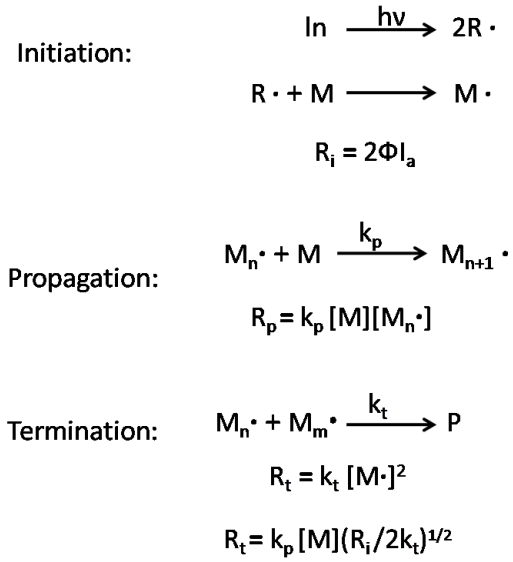

Figure 2.9 Reaction mechanism for photoinitiated polymerizations.I_a is dependent on the initiating light intensity, initiator concentration and molar absorptivity coefficient. The polymerization rate equation assumes pseudo-state conditions. (R_i) = rate of initiation, (R_t) = rate of termination, (R_p) = rate of polymerization, [M] = monomer concentration, (k_p) = propagation kinetic constants and (k_t) = termination kinetic constants. Adapted from [16].

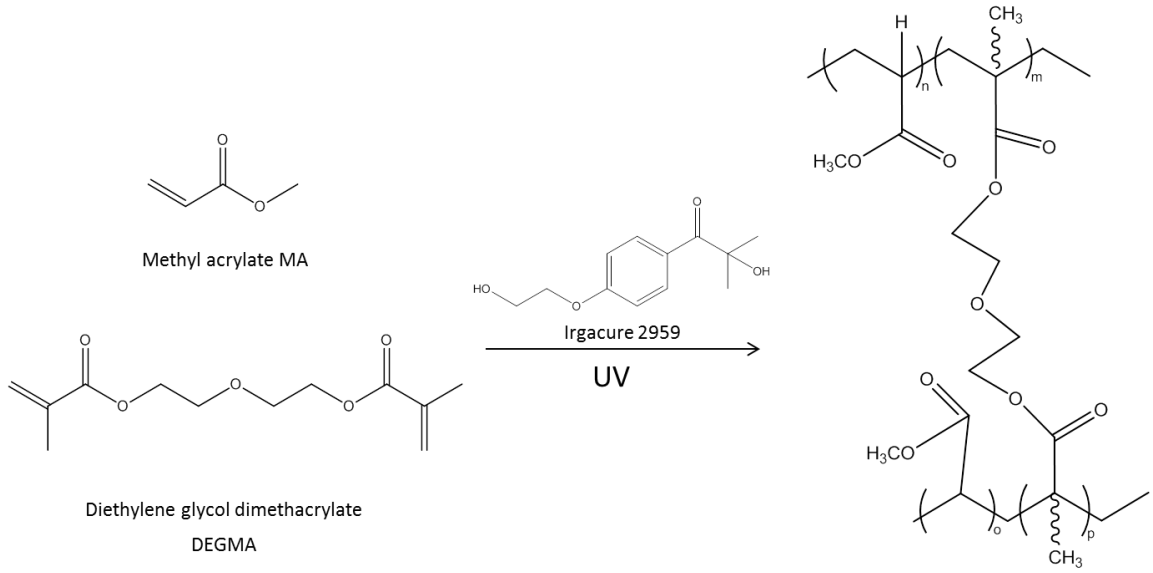

Figure 2.10 Reaction scheme of network for photocrosslinking of MA and DEGMA after UV radiation with the use of a photoinitiator, Irgacure 2959.

An example of crosslinking between monomer and crosslinker is shown in Figure 2.10 using methyl acrylate (MA) and diethylene glycol dimethacrylate (DEGMA). These monomers will be used in the current thesis; their use will be described in detail in Chapter 3.

Central to the TE approach is the degradation of the scaffold over time, to become completely replaced by the natural ECM in the bone tissue. Hence, the objective is to implant the scaffold that will remain in a robust state for structural/mechanical integrity in the site of injury for long enough to allow for the formation of native tissue, but which will in the end degrade and become replaced by newly synthesized matrix [29]. The acrylate scaffolds undergo bulk degradation mostly through hydrolysis of the ester bonds [16]. In the presence of an aqueous environment, the hydrolytically degradable units are cleaved which results in the end products of the degradable units and kinetic chains formed during photocrosslinking (usually an alcohol and an oligomer polymer backbone) (Figure 2.11). Hence when the hydrolytically degradable units are degraded, the poly-acrylic backbone, depending on its molecular weight, can be excreted through the glomerular filtration [175]. The molecular weight of the degraded poly-acrylic backbone is an important factor in the ultimate excretion.

A vast majority of biodegradable polymers studied belongs to the polyester family, which includes polyglycolides and polylactides. One of the disadvantages of these polymers in TE applications are their loss of mechanical properties very early during degradation [188]. The degradation mechanism involves both hydrolytically and enzymatically [188]. Hence, *in vivo* the polyester based scaffolds would undergo bulk erosion and quick mass loss after implantation which is detrimental to native tissue (due to the high amount of acidic degradation products) and also loss

of structural integrity of the scaffold [188, 189]. To overcome this issue, the use of acrylate scaffolds offers a more stable degradation profile due to the slower degradation rate through hydrolysis of the ester bonds [190, 191]. This will be described in detail in Chapter 5 (Section 5.4.5).

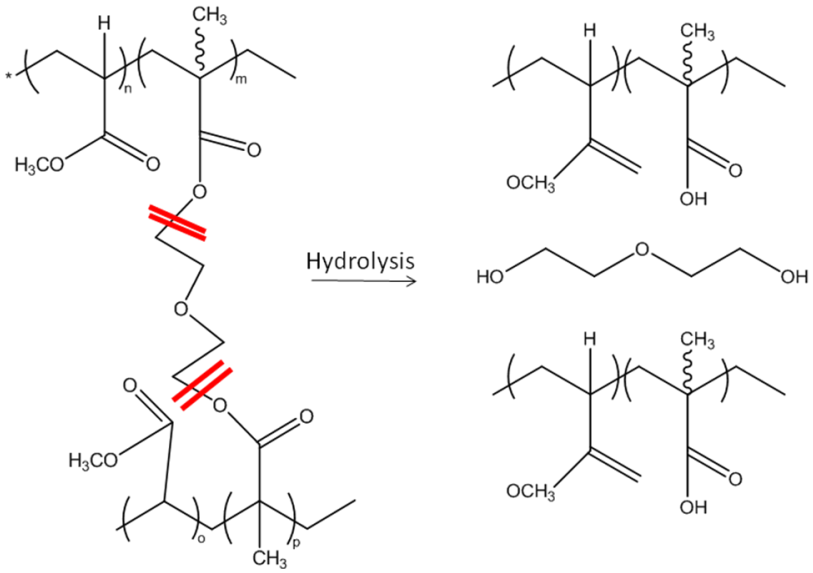

Figure 2.11 Schematic of degradation for the MA:DEGMA scaffolds after hydrolysis of ester bonds.

2.4.3 Modifications of electrospun fibres using photocrosslinking

Post-crosslinking of electrospun fibres was also studied to improve the stiffness and strength of the scaffold, all of which are particularly crucial when the fibres have to degrade slowly in the body. Recently, crosslinked electrospun polybutadiene (BR) fibres were produced using UV irradiation for crosslinking after electrospinning [192]. The crosslinked electrospun fibres retained the fibre morphology and did not dissolve in solvent. The same technique of post-photocrosslinking was employed by Liu *et al.,* which produced water resistant poly(vinyl alcohol) (PVA) fibres by crosslinking the PVA backbones [193]. In addition, Kim *et al.,* introduced a novel method of reactive electrospinning whereby 2-hydroxyl methacrylate, methacrylic acid, ethylene glycol dimethacrylate, azobisisobutyronitrile (AIBN) and a photoinitiator were prepolymerized into a hyperbranched polymer solution and subsequently photochemically crosslinked during electrospinning by completing the crosslinking reaction [186]. However, the electrospinning process is becoming more technically complex. Recently, Wang and colleagues demonstrated the same method of *in situ* electrospinning with UV photopolymerization of polyurethane with polymerizable groups and poly(ethylene glycol) methacrylate (PEGMA) [194] for use in TE applications.

This thesis will focus on the development of fibrous acrylate scaffolds for bone TE applications specifically for injuries in the craniomaxillofacial skeleton using both electrospinning and UV post-crosslinking. The feasibility of electrospinning photocrosslinkable and low molecular weight acrylate monomers, MA and DEGMA was investigated in Chapter 3. The biological response of Saos-2 and human MSC cells cultured on the acrylate scaffolds were assessed in Chapter 4. The development of the acrylate scaffolds conjugated with biologically active peptides of DGEA and RGD were described in Chapter 5. Lastly, in Chapter 6 the biological response of DGEA- and RGD-functionalized acrylate scaffolds were assessed.

CHAPTER 3

Synthesis and characterization of fibrous acrylate scaffolds

3.1 INTRODUCTION

Electrospinning has been widely used to create biodegradable scaffolds for the engineering of several tissues, particularly those of the skeletal system [10-12]. As discussed in Chapter 2, to fabricate electrospun fibrous scaffolds, a polymer solution is electrically charged until charge repulsion overrides the surface tension of the droplet at the spinneret tip and a polymer jet is generated [10, 13, 14]. Subsequently, as the polymer liquid jet travels and solvent evaporates, a fibrous strand is produced and collected onto a grounded collector [10]. The fibrous scaffolds mimic the size and structure of the natural ECM, which can lead to enhanced cellular interactions [10, 15].

A number of synthetic polymers such as polyesters, polyanhydrides, and polyurethanes, as well as natural polymers, such as collagen, silk, and fibrinogen have been used in electrospinning to produce scaffolds for TE [10, 15]. Each of these polymers has distinctive mechanical and degradation properties, which can be translated into a range of scaffold properties that can be tuned [10]. By selecting the specific polymer, the mechanical properties and degradation of the electrospun scaffold can be controlled [195]. Nevertheless, the capacity to modify the scaffold, for example to immobilize peptides or biomolecules on these polymers is limited and requires the interaction of synthesis and processing steps. Hence, it may be advantageous to further expand the existing polymers used for electrospinning fibrous scaffolds to enhance cellular interactions for TE applications [10].

To achieve this, the use of photopolymerizable acrylate monomers can be utilized. Photopolymerization with acrylates has been shown to have a controlled nature of the photoinitiated polymerization with a choice of non-cytotoxic photoinitiators and degradation products. Acrylates are ubiquitously used in the synthesis of hydrogel networks due to the active double bonds [18-21]. In addition, there are a number of commercially available monomers which can be photocrosslinked rapidly using a photoinitiator [9]. The bulk properties of the network can be easily altered by simple adjustments during synthesis (e.g. amount of crosslinker), thus rendering the system tunable with respect to mechanical properties and morphology [177]. When formed as films, the acrylate polymers show a wide range of physical properties, such as mechanical properties and swelling rates [10, 171]. Anderson and colleagues demonstrated the ability of acrylates and methacrylate photocrosslinked networks to support cell attachment, viability and proliferation [9]. Moreover, using an acrylate/methacrylate microarray library, they were able to identify specific monomers that support growth of human embryonic stem cells [9]. Hence, based on the ‘hit’ polymer microarrays, which identified specific monomers that increased and sustained cell growth, diethylene glycol dimethacrylate (DEGMA) and methyl acrylate (MA) were chosen to be employed in the electrospinning system described here.

The photopolymerization of acrylates has been used for several decades in biomedical research and has become an essential approach for *in situ* delivery of resins in the area of dentistry [22-25] and as bone-replacement materials [17]. Recently, a variety of photocrosslinkable and degradable acrylate polymers have been utilized for a range of applications such as drug delivery vehicles, TE scaffolds and in the fabrication of microdevices [17, 171]. The spatial and temporal control during photoinitiation is a pivotal advantage which has motivated its wide application in the field of TE [16, 17]. For example, photocrosslinkable acrylate hydrogels are synthesized for the delivery of cells to injured tissues [21, 178, 180, 181] and for the encapsulation of biological molecules for controlled delivery [171, 176, 179]. These applications are achievable because of the controlled nature of the photoinitiated polymerization with a choice of non-cytotoxic photoinitiators (and their degradation products) [171].

In this chapter, the feasibility of electrospinning photocrosslinkable and low molecular weight acrylate monomers is investigated. Methyl acrylate (MA) and diethylene glycol dimethacrylate (DEGMA) (Figure 3.1) were selected as the monomer and crosslinker of choice, respectively, with the aid of PEO as a polymer carrier and viscosity modifier. The use of monomers enables the tailoring of the scaffold properties by selecting specific monomers that will produce topological and functionally diverse fibre scaffold materials.

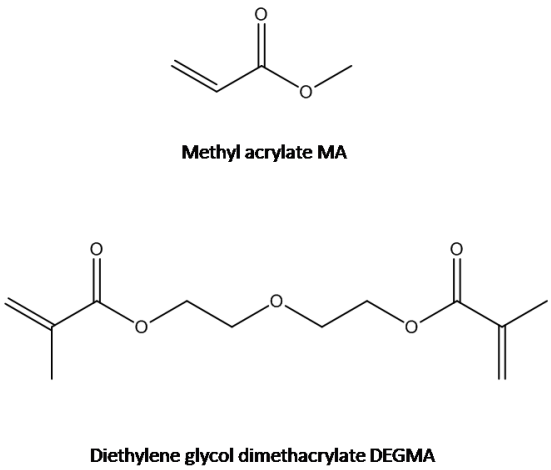

Figure 3.1 Chemical structure of methyl acrylate (MA) and diethylene glycol dimethacrylate (DEGMA).

3.2 MATERIALS

Aluminium Scanning Electron Microscopy (SEM) pin stubs and adhesives carbon tape were purchased from Agar Scientific (UK). Ten ml Becton Dickinson plastic syringes and 27G Becton Dickinson disposable needles were from Cole Palmer (UK). The high voltage supply was from Glassman High Voltage Inc. (UK), the UVB lamp (Transilluminator 2000) from Biorad (UK) and single-syringe infusion pump (230 VAC) and static fibre collector (labarotory jiff-jacks) from Cole-Parmer (UK). Methyl acrylate (MA) (99%), diethylene glycol dimethacrylate (95%) (DEGMA), poly(ethylene oxide) (PEO) (200 kDa) (95.5%) and 2-hydroxy-4′-(2-hydroxyethoxy)-2-methylpropiophenone (Irgacure 2959) (98%), were obtained from Sigma Aldrich (Poole, England). All chemicals were used as received and stored in a dry and dark environment.

3.3 METHODS

3.3.1 Electrospinning setup

The electrospinning system used is shown in Figure 3.2 and Figure 3.3. The simple setup consists of a syringe pump, spinneret (27G disposable needle), static fibre collector and high voltage power system. The spinneret was connected to the syringe [62] and the polymer solution was fed through the spinneret by using a syringe pump at a constant and controlled feed rate. A high voltage and low current voltage system was needed for the conversion of the polymer solution to a charged jet [62]. The spinneret serves as an electrode to which the voltage was applied [149]. The static fibre grounded collector was placed right below the spinneret with distance of 10 cm. Parametric optimization studies on the electrospinning parameters was investigated and described in Section 3.3.2.

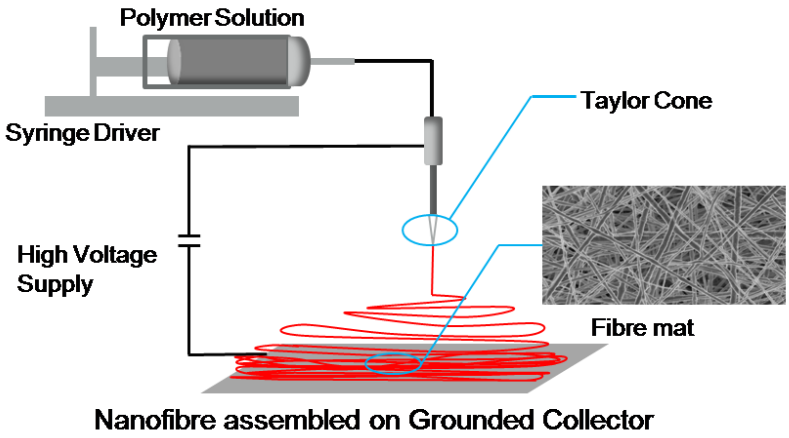

Figure 3.2 Schematic of the electrospinning setup. A polymer solution was supplied through a needle. At a critical voltage, charge imbalance starts to override the surface tension of the polymer producing an electrically charged jet [61]. This electrified jet becomes elongated and the solvent rapidly evaporates which generates fibres.

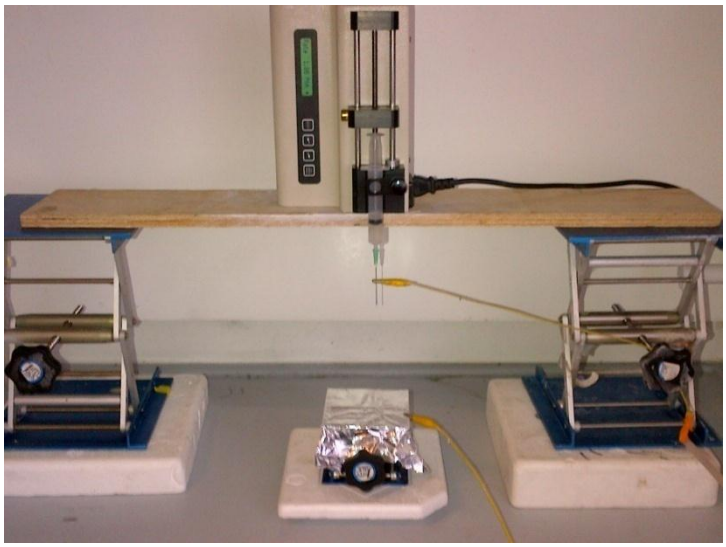

Figure 3.3 The electrospinning setup used in the lab. Polymer solution is supplied at a constant rate which is controlled by the syringe pump situated on top. The high voltage supply creates the electric field difference required for electrospinning. The entire system is set up in the fume hood.

3.3.2 Parametric study of electrospinnning

3.3.2.1 Preparation of solution and PEO concentration

Solutions of 2.5, 5, 10, 12.5 and 15% (w/v) solution of PEO were prepared by dissolution in 90% ethanol in water and magnetically stirred until a homogenous solution has been formed. The polymer solutions were electrospun for 10 minutes at constant voltage of 10 kV over 10 cm distance and collected on a static grounded plate. The spinneret was a 27-gauge blunt-ended needle and the rate of polymer solution delivery was set to 0.5ml/hr. The electrospun fibres were analyzed with scanning electron microscopy (Section 3.3.5).

3.3.2.2 Accelerating Voltage

A range of high voltages was applied to the tip of the needle and controlled by the voltage supply to generate the polymer jet. The voltages used were 2.5, 5, 7.5, 10, and 15 kV. The lower limit of the accelerating voltage parameter was set at 2.5 kV as this was found in this investigation to be the voltage at which the initiation of the polymer jet occurred. A voltage of 20kV was chosen as the upper limit because above this voltage, static discharge occurred around the grounding wires. When examining the effects of accelerating voltage at each polymer concentration, the rate of polymer solution delivery was set to 0.5ml/hr and target distance of 10cm.

3.3.2.3 Flow rate

Two ml of the polymer solution of 10% (w/v) PEO concentration in ethanol was fed into a syringe which was controlled by a syringe pump at constant flow rates of 0.2, 0.3, 0.4, 0.5, and 1.0ml/hr. When investigating the effects of flow rate at each polymer concentration, the parameters were set constant at target distance of 10cm and accelerating voltage of 10kV.

3.3.3 Preparation of photocrosslinked acrylate fibrous scaffold

The monomer mixtures were prepared by varying ratios of MA and DEGMA with the aid of PEO as a high molecular weight carrier polymer. Table 3.1 lists the compositions of monomer and crosslinker. Refer to section 3.4.1 for the final optimal electrospinning compositions and parameters, which were investigated and described in the results section and listed in Table 3.2 (page 81). Briefly, MA and DEGMA monomer solutions were added together according to specific concentrations in a 5ml glass vial. Next, 0.1 mol% 2-Hydroxy-4′-(2-hydroxyethoxy)-2-methylpropiophenone (Irgacure 2959) was added to the solution. Then, 10% (w/v) PEO concentration in ethanol mixture was added to the solution and mixed thoroughly for 30 minutes with help of a magnetic stirrer. The electrospinning solution was added into a syringe with a 27-gauge blunt-ended needle. Next, electrospinning was carried out in the set-up described previously in section 3.3.1. The fibres were immediately exposed to UV light for 10 minutes using a UVB (302nm) lamp in an oxygen free environment. After photocrosslinking, PEO from the scaffold was extracted from the scaffold by repeated washing with water for 5 days. The process of producing the photocrosslinked fibrous scaffold is shown in the schematic below (Figure 3.4).

Table 3.1. Compositions of the monomer (MA) and crosslinker (DEGMA) used in mol percentages for producing the photocrosslinked acrylate fibrous scaffold.

MA concentration (mol%)	DEGMA concentration (mol%)
90	10
70	30
50	50
30	70

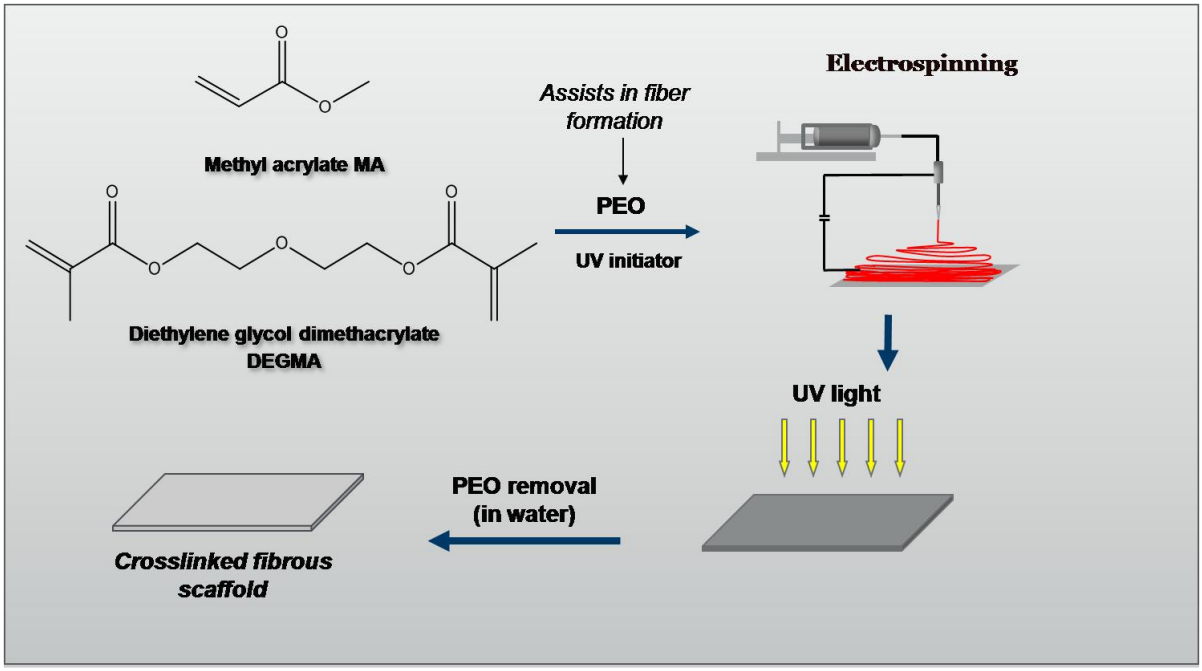

Figure 3.4 Schematic of photocrosslinked fibrous scaffold production. MA and DEGMA monomer solutions were added together according to specific concentrations in a 5 ml glass vial. Next, 0.1 mol% 2-Hydroxy-4′-(2-hydroxyethoxy)-2-methylpropiophenone (Irgacure 2959) was added to the solution. Then, 10% (w/v) PEO concentration in ethanol mixture was added to the solution and mixed thoroughly for 30 minutes. Subsequently, the fibres were photocrosslinked by exposure to UVB light for 10 minutes followed by extraction of PEO through repeated washing with water for 5 days.

3.3.3.1 Optimization of (MA:DEGMA): PEO electrospinning formulations

After the optimal range of parameters of PEO solution concentration, accelerating voltage and flow rate were established, the composition of the acrylate components with PEO were varied using the optimized electrospinning parameters. The solution flow rate was constant 0.5ml/hr. Solutions were electrospun at 10 kV and collected for 120 min on a stationary plate.

3.3.4 Evaluation of varying the monomer/crosslinker concentration on fibre morphology

MA and DEGMA monomer ratios were varied to evaluate the effects of increasing crosslinker (DEGMA) concentration on fibre morphology. Mats were electrospun at various ratios of 90:10, 70:30, 50:50, 30:70 ratio (mol%) of MA to DEGMA solutions with PEO and post-crosslinked with UVB light (302nm) prior to visualization under SEM. The monomer: PEO mass ratios were kept constant at 50:50.

3.3.5 Morphology analysis using SEM

Fibres produced by electrospinning were examined using scanning electron microscopy (SEM) to determine fibre morphology and approximate fibre diameter. Samples of approximately 1.5cm^2 were placed on an adhesive carbon tape and attached to aluminium SEM pin stubs. The samples were sputter coated with chromium. The LEO 1525 Gemini SEM was operated at an accelerating voltage of 5kV.

3.3.6 Water resistance of crosslinked acrylate fibres

Water resistance of the crosslinked MA:DEGMA fibres was tested with the incubation of the fibres in deionised water. The fibres were incubated with deionised water for 5 days (with gentle shaking on orbital shaker) and washed to remove PEO. After washing, the fibres were left to dry at room temperature overnight. Fibre morphology was determined using SEM.

3.3.7 Evaluation of photo-reaction using Attenuated Total Internal Reflectance-Fourier Transform Infrared Spectroscopy (ATR-FTIR)

The extent of photoreactions was evaluated using the ATR-FTIR (Nicolet 6700, Thermo Fisher Scientific). The disappearance of acrylate double bond band at 1640cm^{-1} was used to indicate double bond conversion. The change of the peak maximum was monitored. For each measurement, 128 spectra were accumulated at a resolution of 4 cm^{-1}.

3.3.8 Mass loss analysis of fibres during PEO extractions

The water solubility of the photocrosslinked electrospun fibres during PEO extraction was studied by mass loss analysis. The electrospun membranes were cut into rectangular shapes with dimensions of 10 x 3 cm^2. The fibre samples were immersed in distilled water and incubated to obtain time points of 6 hours, 1, 2, 3, 4 and 5 days. All samples placed under vacuum overnight at room temperature for drying before measuring mass loss. Weight of the degraded samples (gd) was measured and from it the mass loss was calculated according to:

Mass loss percentage = (gd – g0)/ g0 x 100

g0 = initial mass before incubation

This experiment was performed four times and quantitative data was presented as mean ± S.D.

3.3.9 Quantitative ^{1}H-NMR analysis of PEO

The individual supernatants from the mass loss analysis (see Section 3.3.8) were collected, lyophilized and mixed with DMSO-d6 in the NMR tube for ^{1}H-NMR spectroscopy. NMR spectra were recorded on a Bruker DRX 400 MHz (operating at 400MHz) using DMSO-d6 as deuterated solvent. The quantification of ^{1}H-NMR was carried out using an internal standard, 1,4-(bistrimethylsilyl) benzene (BTMSB). NMR calibration curves using the unique peaks at 0.2, 3.6 and 7.5 ppm for each component were calculated relatively to BTMSB integration values using the Mestrenova software version 1.8 (Mestrelab Research, US).

3.3.10 Swelling test

The swelling test was conducted as described in [191]. Briefly, the electrospun samples from which PEO had been extracted (refer to section 3.3.8) were cut into rectangular shapes with dimensions of 10 x 3 cm^2 (n= 5). The fibres were immersed in distilled water and incubated for 6 hours. The wet weight of each sample was measured every hour prior to placing each of the samples in the vacuum oven at 60°C overnight. The dry weight of the samples was determined.

Swelling ratio (percentage) = (wet weight/dry weight) x 100%.

3.3.11 Mechanical testing of fibrous scaffolds

The electrospun samples were cut into rectangular shapes with dimensions of 10 x 3 cm^2 (n= 10). Uniaxial tensile testing was performed using an Instron Model 5540 with a 50N load cell with a constant deformation (5mm/min) on untreated samples (uncrosslinked) and on samples that were crosslinked with UV light. Additionally, PEO extracted samples, dry and hydrated (after incubation in deionised water for one hour) were evaluated mechanically. Tensile extension and reactive forces were recorded using the Bluehill 2 software, and the Young's modulus (E) was calculated from the linear region of the stress-strain curves.

3.3.12 Wettability measurements

The wettability of flat acrylate surfaces was analyzed using an EasyDrop instrument (Kruss, Germany). The sessile drop technique was used in contact angle measurement. The polymer samples prepared and were placed in the chamber and 1 µL water droplet was introduced onto the polymer surface through a microsyringe. The photographic pictures of droplets on the surfaces captured by the camera, and the value of their contact angles were calculated from the drop

profiles by using Drop Shape analysis software. All samples were analyzed at five different positions on flat polymer surface surface (n= 5).

3.3.13 Statistical analysis

All experimental data shown are expressed as mean ± standard Deviation (SD) and were obtained from experiments performed in triplicates at least. All data analysis was performed in Excel. Statistical analyses were performed with a one-way analysis of variance (ANOVA) using multiple comparisons (Bonferonni test) and significance was determined by $p<0.05$. This analysis was performed with GraphPad InStat software (GraphPad Software, US).

3.4 RESULTS AND DISCUSSION

3.4.1 Parametric study of electrospinning

In order to optimize the electrospinning system to aim for smooth and uniform fibre morphology, the processing and solution parameters during electospinning were characterized. The effects of these parameters on fibre morphology are discussed in Sections 3.4.1.1 to 3.4.1.4 below.

3.4.1.1 Effects of PEO concentration in solvent on fibre formation

Poly(ethylene oxide)(PEO, 200 kDa) was selected as a carrier polymer to assist in fibre formation during electrospinning [10]. Ethanol was chosen as solvent due to its low toxicity in comparison to other harsh solvents and because it has been shown to enhance the formation of fibres during electrospinning [196].

Firstly, the optimization of PEO concentrations with the chosen solvent, ethanol was performed without the presence of the acrylate monomers. This optimization step is essential because polymer concentration is one of most important parameters of the electrospinning solution for controlling fibre morphology. The variation of fibre morphology is shown in Figure 3.5. Beaded fibres were obtained from 5% (w/v) PEO concentration (Figure 3.5B), whereas 2.5% (w/v) only yielded electrospraying droplets (Figure 3.5A). Fibre formation was obtained in 10% (w/v) with only slight beading and smooth fibres, without beads, were produced from electrospinning of 10-12.5% (w/v) PEO concentrations; an average diameter size of 890 ± 65nm was obtained for 12.5% (w/v) (Figure 3.5D). Furthermore, fibre diameter increased to 1550 ± 55nm as PEO concentration increased to 15% (w/v) (Figure 3.5E). The ease in fibre formation by increasing polymer concentration is due to the effect on the solution viscosity. Consequently, as the viscosity of the PEO solution increases, the beads becomes larger, the average distance between beads smaller, the fibre diameter bigger and the shape of the beads is altered from spherical to spindle-like [197].

The transition observed between the production of electrospraying droplets to the formation of uniform fibres with increasing polymer concentration was due to the function of chain entanglement with the increase in polymer concentration [152, 198]. Chain entanglements have been illustrated as the physical overlapping in polymers, consequently causing the interlocking of chains [158, 198]. At a fixed polymer concentration, the number of chain entanglements increases with the molecular weight of the polymer [158]. On the other hand, the equivalent number of entanglements can be attained at a specific molecular weight by increasing the polymer concentration [158, 198]. In the electrospinning process, adequate chain entanglements are necessary to override the surface tension for the formation of fibres [158, 196, 199, 200]. For the production of a stabilised electrospinning jet, it has been shown that more than 2.5 entanglements per chain are needed

[158, 198]. Based on the formation of smooth fibre morphology, 10-12.5% (w/v) PEO concentration was chosen to be optimal concentration for our electrospinning system.

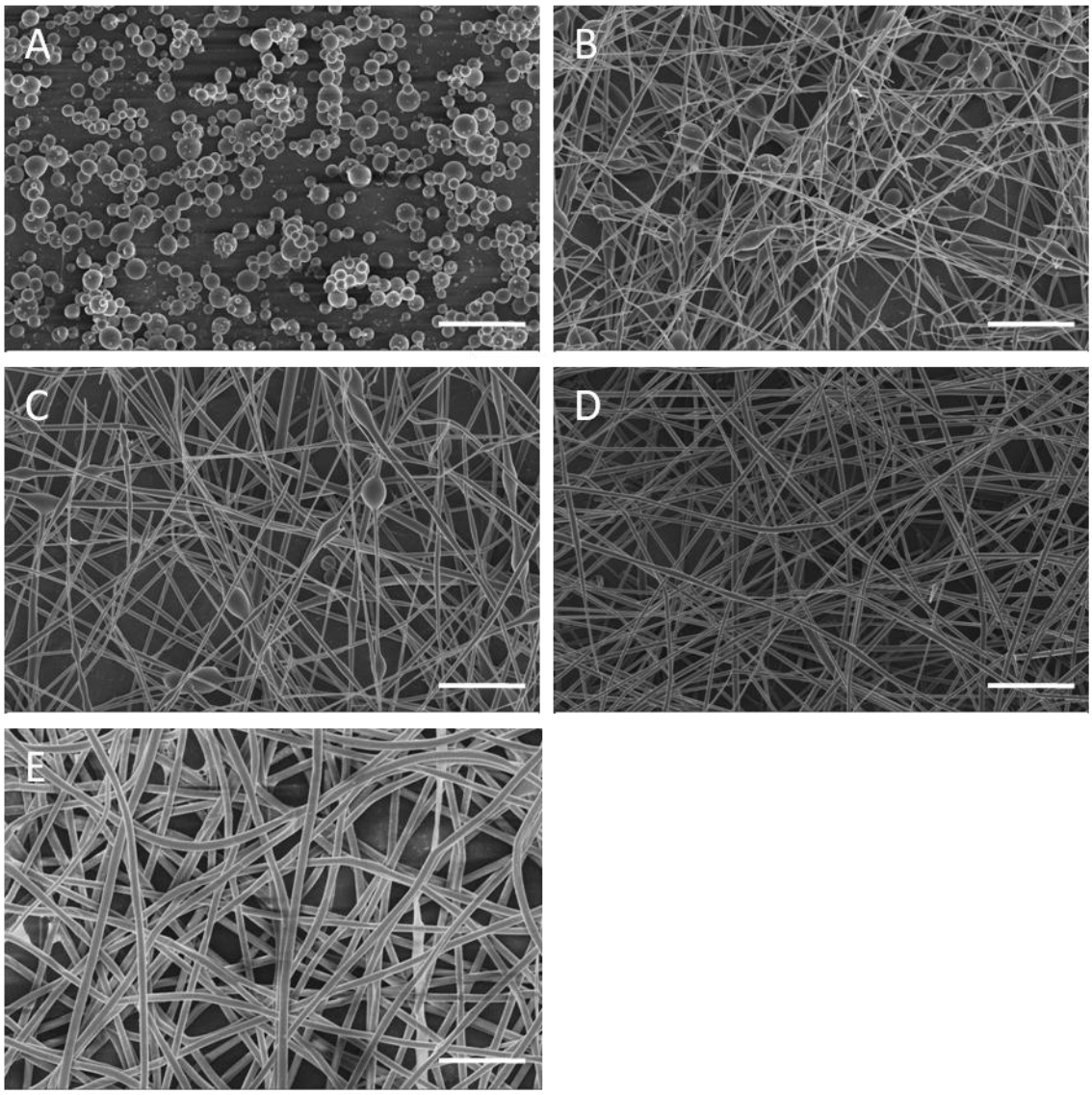

Figure 3.5 SEM images of electrospun fibres with varying PEO concentrations in ethanol. A) 2.5%; B) 5%; C) 10%; D) 12.5%; E) 15% PEO concentrations in ethanol. During electrospinning, the accelerating voltage was kept constant at 10 kV over 10 cm distance and collected on a stationary plate. Scale bar: 10µm.

3.4.1.2 Effect of accelerating voltage on fibre formation

The effect of varying accelerating voltage at a constant 10% (w/v) PEO concentration was assessed and it is shown in Figure 3.6. When investigating the effects of accelerating voltage at each polymer concentration, the rate of polymer solution delivery was set to a constant rate of 0.5ml/hr. This flow rate for the polymer solution was chosen as it was identified to be the initial flow

rate where the droplet at the tip of the needle could be maintained during electrospinning. At a rate lower than 0.5ml/hr, the removal of polymer solution by electrospinning surpasses the flow rate to the needle tip and the droplet was shown to reduce into the needle tip. This was demonstrated by other groups [153, 158, 201] and confirmed further in the next section.

In Figure 3.6 (A and B), SEM images revealed that accelerating voltages of 2.5kV and 5kV only produced electrospraying droplets. The transition between droplets and beaded fibres can be seen in Figure 3.6C with accelerating voltage of voltage of 7kV. Electrospinning with accelerating voltage of 10kV produced smooth fibres with an average diameter of 915 ± 40nm (Figure 3.6D). Furthermore, increasing accelerating voltage to 15kV caused fibre diameter to increase to 2100 ± 153nm (Figure 3.6E).

The accelerating voltage is a critical aspect for the initiation of the electrospinning process [158]. A high voltage source is needed to initiate the required self-repulsive charges in the solution and to create an external electric field to overcome the surface tension of the polymer solution [61, 158, 197]. It has been demonstrated that an accelerating voltage of approximately 7kV is required for the production of a Taylor Cone and jet initiation during electrospinning [153, 200].

In this investigation, the initiation of electrospinning jets was shown at a similar accelerating voltage of 7kV. The increase in fibre diameter when the accelerating voltage was increased from 10 kV to 15kV may be explained due to increase of the coulomb repulsive forces at the surface of the initial electrospinning solution, resulting in more polymer solution being displaced in the electrospinning jet, causing an increase in jet diameter [158, 202].

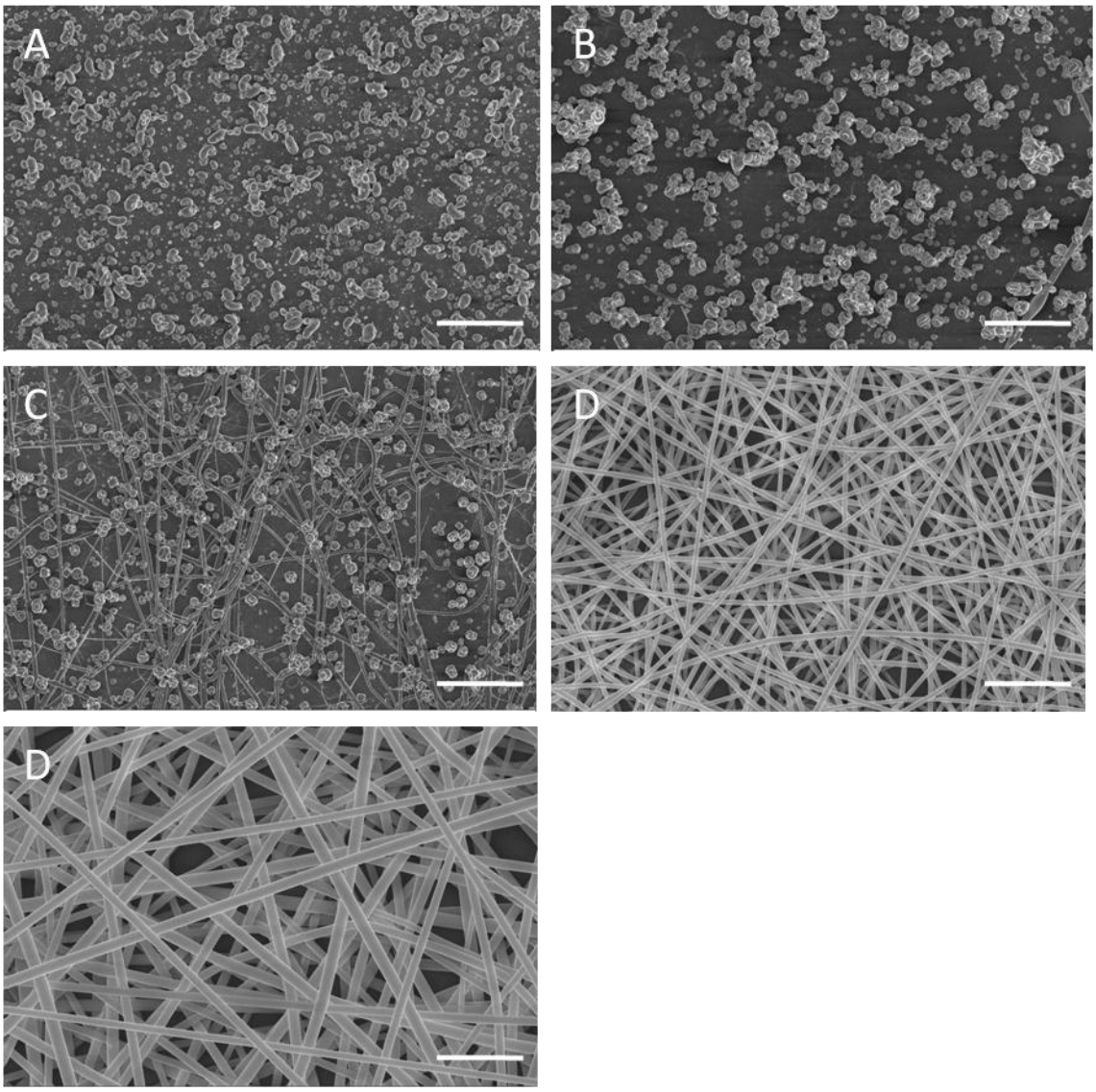

Figure 3.6 SEM images of electrospun fibres of PEO with varying accelerating voltage at a constant 10% (w/v) PEO concentration. A) 2.5kV; B) 4kV; C) 7kV; D) 10kV; E) 15kV accelerating voltages. Scale bar: 10µm.

3.4.1.3 Effect of the flow rate of the polymer solution on fibre formation

The effect of the flow rate of PEO solution is demonstrated in Figure 3.7. At a constant PEO concentration of 10% (w/w) and accelerating voltage of 10kV, smooth fibre formation can only be obtained for electrospinning at the rate delivery of 0.5ml/hr (Figure 3.7D). Electrospraying droplets are produced at a flow rate of less than 0.4ml/hr in Figure 3.7 (A and B). Formation of beaded fibres can be seen when electrospinning at the flow rate of 0.4ml/hr. However, the flow rate of 1ml/hr produced larger diameter fibres, from 883 ± 84nm (flow rate of 0.5ml/hr) to 1512 ± 135nm.

The flow rate of the polymer solution regulates the amount of solution available to sustain the Taylor Cone during electrospinning, and hence it controls the formation of fibres. The balance between the delivery of polymer solution to the tip of the needle and the displacement of polymer solution during electrospinning is required for the formation of uniform fibres [158]. At a constant accelerating voltage, an increase in the flow rate during the electrospinning process would cause an increase in the amount of polymer solution accumulated on the collector [158]. As a result of this, there may be an increase in fibre diameter and bead formation [156-158, 201]. In fact this is evident in Figure 3.7E in our system. However, some research groups have demonstrated that flow rate plays a less significant role in controlling the final fibre size and morphology in comparison to other parameters such as polymer and solvent concentration [199].

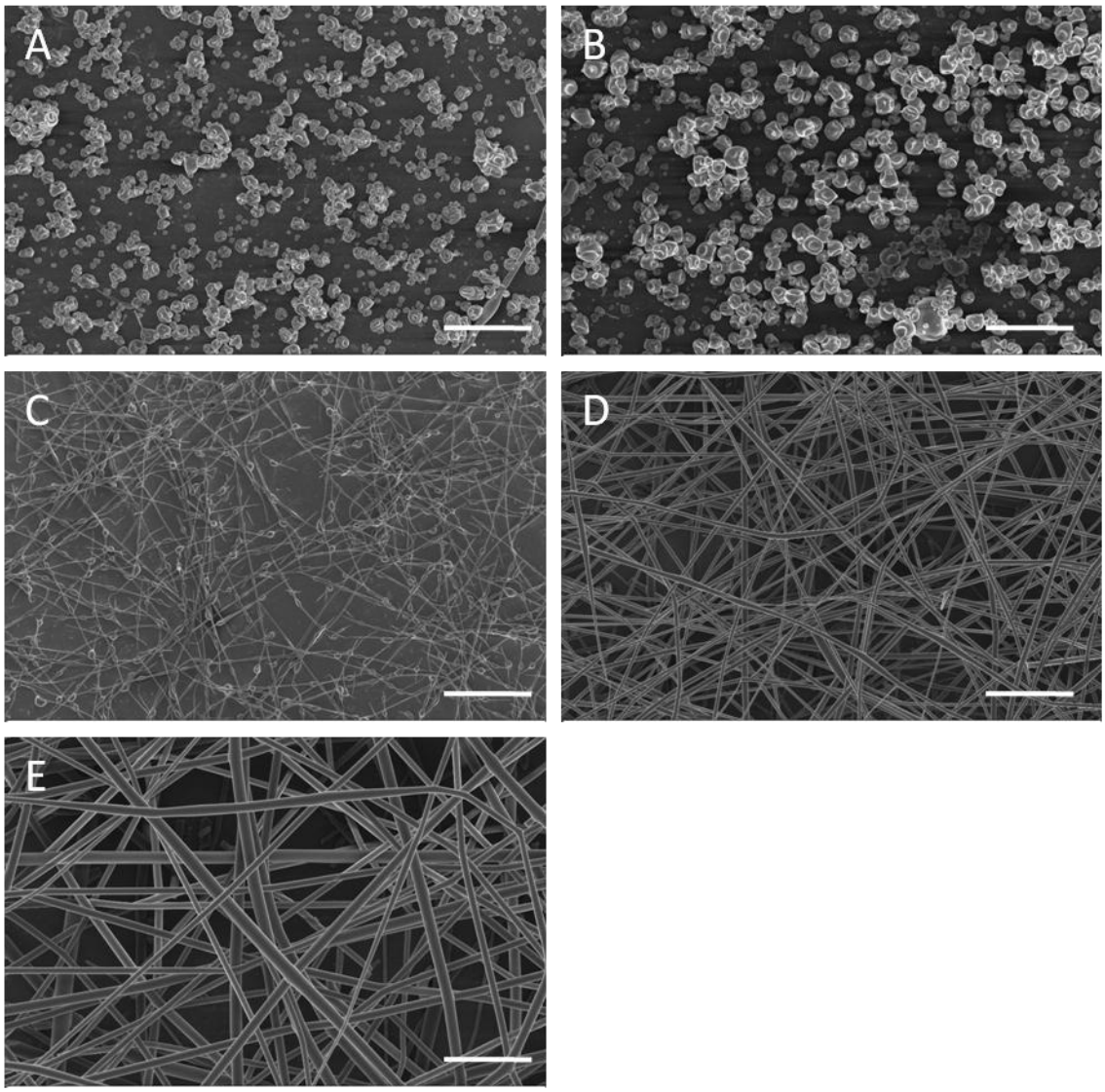

Figure 3.7 SEM images of electrospun fibres of PEO with varying flow rate of 10% (w/w) of PEO solution in ethanol. A) 0.2ml/hr; B) 0.3ml/hr; C) 0.4ml/hr; D) 0.5ml/hr; E) 1ml/hr. At a constant PEO concentration of 10% (w/v) and accelerating voltage of 10kV. Scale bar: 10μm.

3.4.1.4 Optimization of (MA-DEGMA): PEO electrospinning concentration

Since the effects of electrospinning PEO solution on fibre production have been performed and an optimal range of parameters established, the optimization of electrospinning the acrylate components with PEO has also been conducted. This is essential as both acrylate components and PEO would be co-electrospun to produce the electrospun scaffold. Initial attempts to electrospin acrylate monomers alone resulted in electrospraying, likely due to its low molecular weight (results not shown). Consequently, PEO was chosen as a high molecular weight carrier to help induce fibre formation. The process of utilizing PEO to ease fibre formation during electrospinning for low molecular weight polymers has been previously reported by several groups [10, 160, 187]. They revealed the importance of the ratio of reactive acrylate components to carrier polymer in the blend in determining the resulting smooth and uniform fibre morphology. Even though PEO would be eluted and extracted out after post UV-crosslinking, it is essential to promote even and smooth formation of fibres during electrospinning to produce a homogenous fibrous scaffold.

The MA-DEGMA:PEO blend solutions with different mass ratio from 70:30 to 20:80 were electrospun and morphology of the fibres was examined using SEM. The fibre morphology of the fibres before and after PEO extraction is shown in Figure 3.8. The monomer (MA:DEGMA) concentration ratios were kept constant at 90:10 mol%.

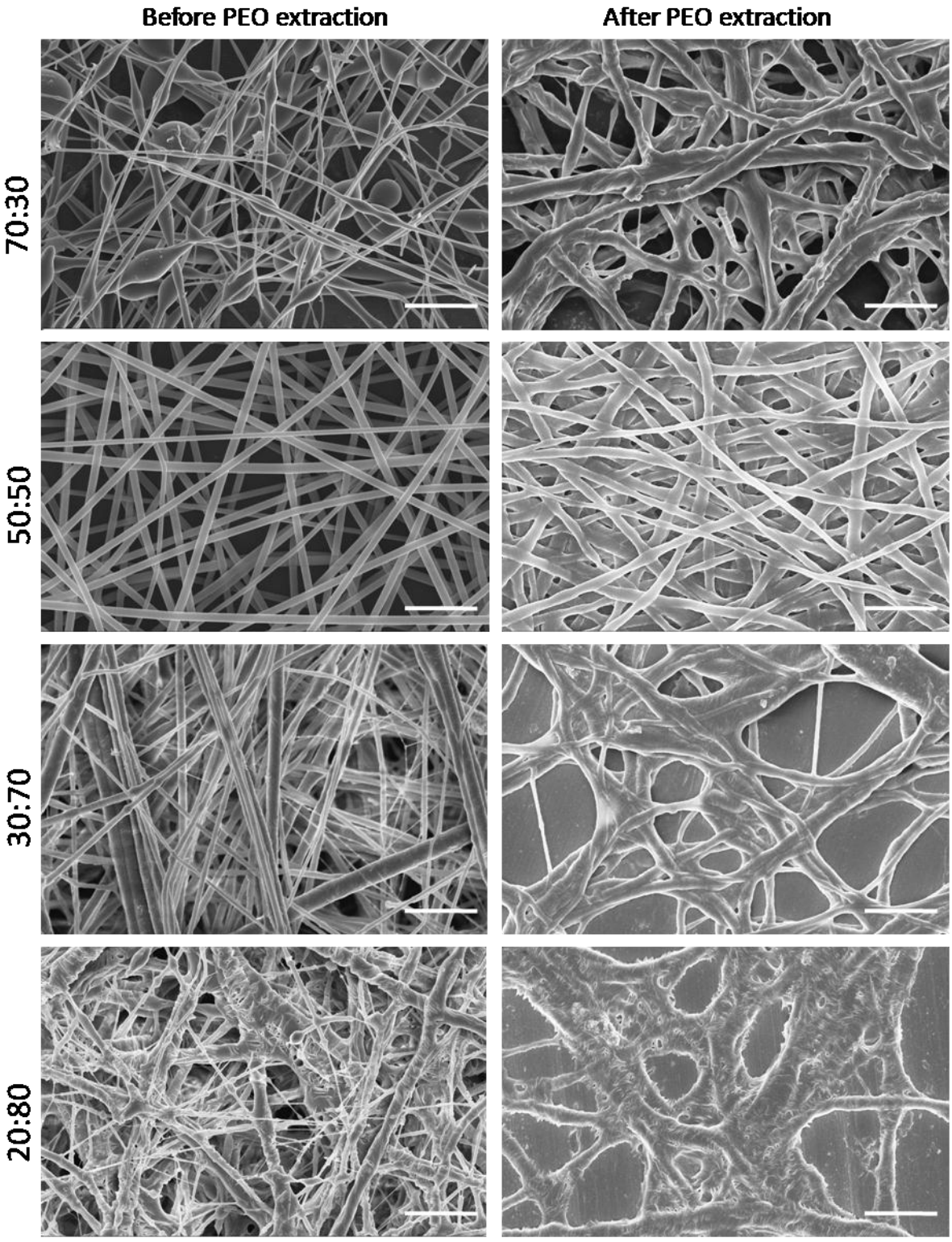

Figure 3.8 SEM images of monomer:PEO ratios. Electrospinning at an accelerating voltage of 10kV and target distance of 10cm. Electrospun fibres of monomers (MA:DEGMA) and PEO at various mass ratios (monomers:PEO (see labels)) before and after PEO extraction. The mol ratio of monomers (MA:DEGMA) was kept constant at 90:10 mol%. Scale bar: 5µm.

For unwashed fibrous scaffolds, slight beading can be observed for 70:30 (monomers:PEO) ratio due to the decrease of the PEO content reducing the viscosity of the electrospinning solution (Figure 3.8). However, distinct smooth fibres are produced with average fibre diameter of 1020 ± 64nm for a 50:50 (monomer:PEO) ratio. Inhomogeneous and fragmented larger fibres were displayed for the 30:70 and 20:80 (monomer:PEO) ratios and increased webbing could be seen between the fibres. Higher PEO concentration increases viscosity, which causes difficulty in the control of the solution flow rate through the needle and prevents homogenous fibre formation even though larger diameter fibres were formed. Hence, there is an optimal window of monomer:PEO solution concentration to facilitate fibre formation when all other parameters are constant.

In addition, in Figure 3.8 the SEM images of MA-DEGMA photocrosslinked fibres after PEO extraction are also shown. The crosslinked fibres were washed repeatedly and soaked with deionized water for one day. Noncrosslinked fibres completely disappeared after being immersed in water, whereas photocrosslinked fibres could endure the water treatment and maintained a fibrous structure but swelled to a certain degree. In the case of high PEO concentration fibres for 30:70 and 20:80 (monomer:PEO ratio), the starting fibre structure collapsed and adhered together after PEO extraction. When the fibres are immersed in water, PEO is mobilized from the fibres thus MA and DEGMA components of the fibres melt together resulting in welding of the fibres. Fibres with a 50:50 (monomer:PEO) ratio produced a scaffold with distinct uniform fibres of 1124 ± 94 nm. However, the diameter of the fibres for other ratios could not be quantified due to inconsistency of fibre diameter formation after PEO was extracted. From these SEM characterizations, 50:50 (monomer:PEO) ratio was chosen based on its ability to preserve fibre form and limit junction formation after PEO extraction.

From the parametric studies described above, the optimal range of parameters required to produce uniform and bead-free electrospun acrylate fibrous scaffold was determined and listed is in Table 3.2. With the use of the electrospinner set-up and UV-crosslinking system, operated at the optimal range of parameters determined, a fibrous electrospun acrylate scaffold can be fabricated and these parameters will be used for further studies in this thesis.

Table 3.2 Optimal electrospinning parameters determined for the fabrication of MA:DEGMA fibrous scaffolds. This set of parameters form the key processing parameters in the production of the acrylate fibrous scaffold for subsequent part of this chapter and this thesis

Type of solvent and ratio	Ethanol: water, 90:10
PEO concentration in solvent	10% (w/v)
Target distance	10 cm
Flow rate	0.5-1.0ml/hr
Accelerating voltage	10kV
(Acrylate monomer:PEO) ratio	50:50

3.4.2 Effect of varying the monomer/crosslinker ratio on fibre morphology

After the optimization of MA-DEGMA (monomer) to PEO ratio was conducted and optimal electrospinning conditions have been identified, the MA and DEGMA ratio (mol%) was varied to evaluate the effects of increasing the crosslinker (DEGMA) concentration on fibre morphology. Mats were electrospun at ratios of 90:10, 70:30, 50:50, 30:70 (MA:DEGMA) mol% solutions with PEO and post-crosslinked through photoinitiation of radical polymerisation prior to visualization under SEM (Figure 3.9). The four MA:DEGMA ratios were selected because they provided an overall range of varying concentrations of monomer and crosslinker for screening and identifying the optimal concentration for fibrous scaffold production.

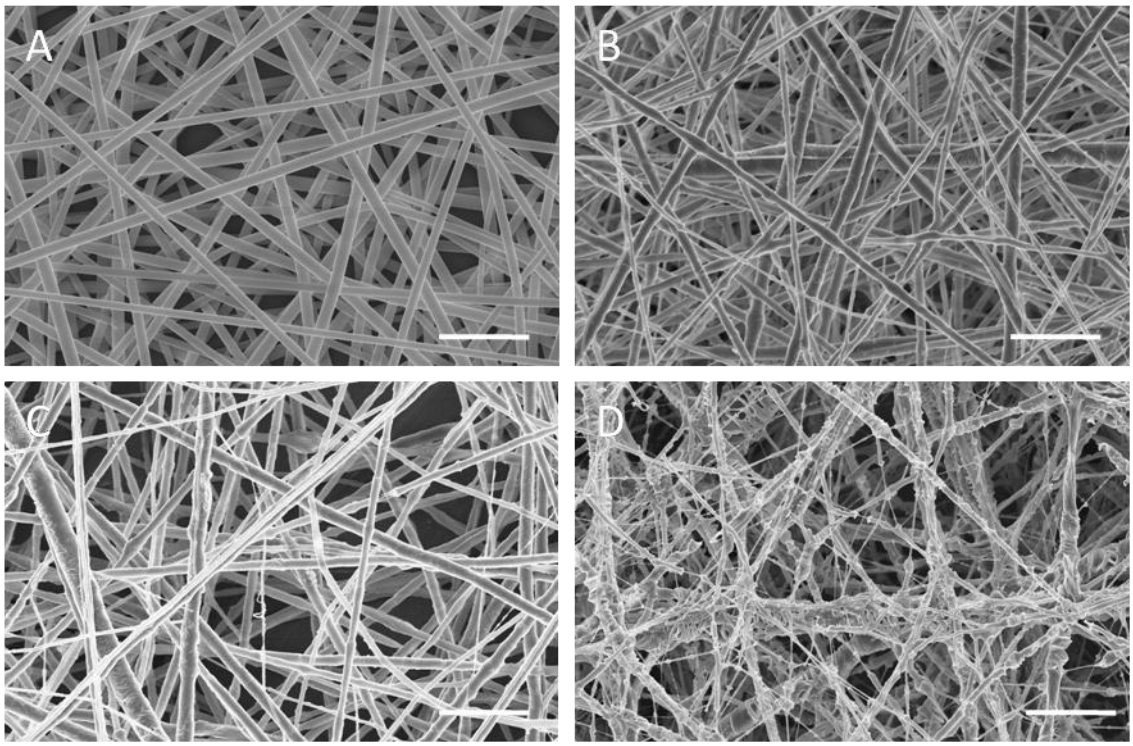

Figure 3.9 SEM micrographs of PEO/ MA:DEGMA unwashed fibres with varying ratio (mol%) of MA:DEGMA: A) 90:10; B) 70:30; C) 50:50; D) 30:70. Scale bar: 5µm.

Fibres can be seen forming at low crosslinker concentrations (Figure 3.9A) with an average diameter of approximately 900 ± 56nm. However, increased DEGMA concentrations caused poor fibre formation with inconsistent fibre sizes in the scaffold (Figure 3.9D). The fibre diameters ranged from 800 to 2000nm. The microheterogeneity observed within the fibres could affect the overall mechanical properties of the fibres. The increase in DEGMA concentration may have affected the overall electrospinnability of the monomer/PEO solution. Specifically, varying the ratios may have caused some parameters such as conductivity and viscosity to change, which affects the electrospinning process. However, the change in conductivity and viscosity of the electrospinning solution was not studied in this investigation.

To discern their stability and morphology in water, PEO was extracted by immersing the fibres in deionized water overnight. The photocrosslinked fibres were resistant to water and maintained a fibrous structure but swelled to a certain degree (Figure 3.10). The rate of bulk swelling was described in detail in Section 3.4.6. Analysis of diameter size quantification could not be performed precisely due inconsistency of fibre diameter formation but fibres with MA:DEGMA ratio of 90:10 were 925 ± 95nm. Specifically, the fibre diameter increased and more welding was observed with increasing DEGMA content. However, the diameter of the fibres for other ratios could not be quantified due to inconsistency of fibre diameter formation after PEO was extracted. The welding and swelling of the crosslinked fibres after water incubation and PEO dissolution into the solution

have been reported by a few groups [10, 11]. The crosslinker which Ji and co-workers utilized was poly(ethylene glycol) diacrylate (PEG-DA) in a hyaluronic acid scaffold, whereas Tan and colleagues used a macromer from library of poly (β-amino esters) to produce fibrous scaffolds [10, 11]. It was observed that the welding extent depends on the concentration of DEGMA; increasing the crosslinker agent somehow increases the extent of the welding. In this case it could be due to increased hydrophilicity of the crosslinked fibres, as increasing DEGMA concentrations causes the fibres to swell and merge in polar solvents, including water and buffer. Furthermore, the increase in DEGMA concentration may have affected the overall electrospinnability of the monomer/PEO solution, which was reflected in the morphology of the fibres before PEO extraction. Hence it might also have affected the morphology of the fibres after incubation in water.

Accordingly, due to the non-fibrous morphology of the 30:70 MA:DEGMA scaffold, further experiments will not include this composition.

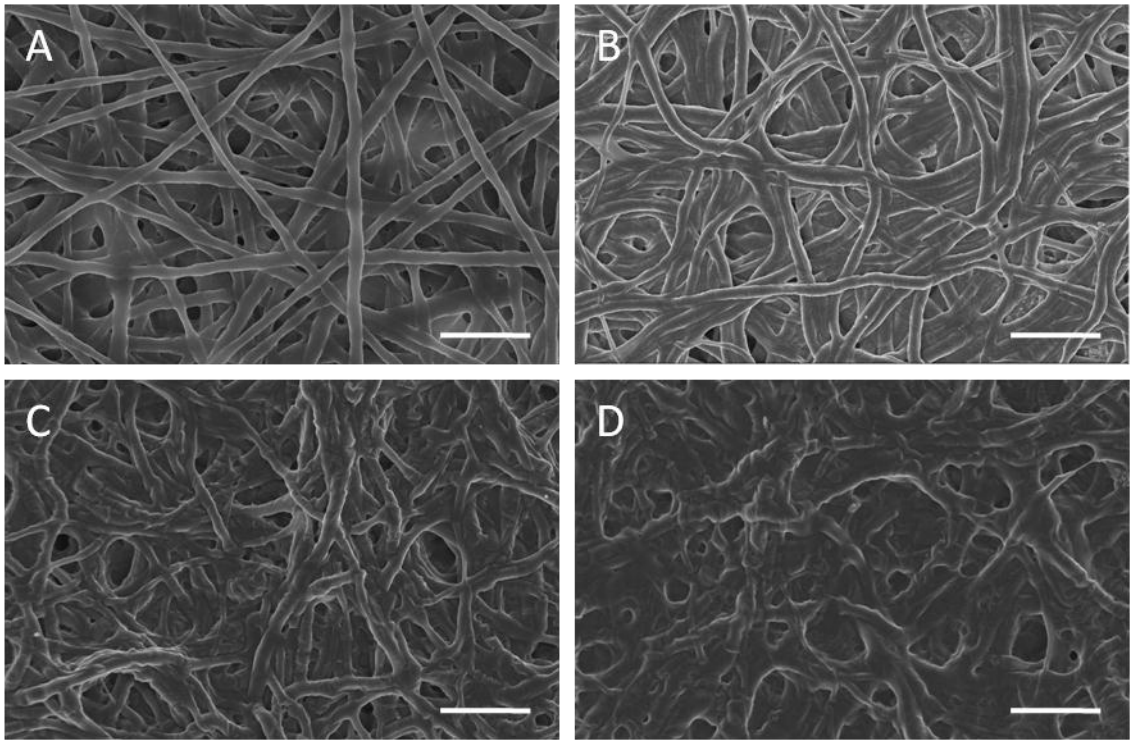

Figure 3.10 SEM micrographs of MA:DEGMA fibres that were washed and incubated overnight with varying ratios of MA:DEGMA: A) 90:10; B) 70:30; C) 50:50; D) 30:70. The acrylate: PEO concentration percentages were kept constant at a 50:50 ratio. Scale bar: 5µm.

3.4.3 Reaction characterization of UV-post crosslinking

After electrospinning, the crosslinking of the 90:10 (MA:DEGMA) fibres initiated by UV light employing a photoinitiator - Irgacure 2959 - was evaluated through the absorption of the reactive acrylate peak at approximately 1635cm^{-1} before and after 10 minutes UV radiation (Figure 3.11). Irgacure 2959 was selected for the UV electrospinning system because it has been shown to have minimal toxicity over a broad range of mammalian cell types and species [203]. The intensity of the absorption increased for the photocrosslinked fibres, which indicates the decrease of acrylate peak during photocrosslinking. These results demonstrate the successful crosslinking of the acrylate monomers during UV radiation. The reaction scheme of network for photocrosslinking of MA and DEGMA after UV radiation is illustrated in Figure 2.10 in Chapter 2 (page 60).

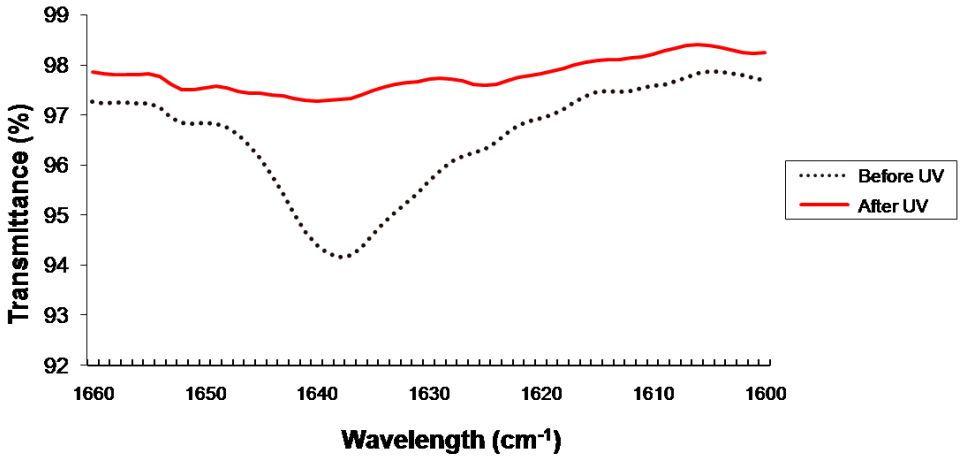

Figure 3.11 ATR-FTIR spectra of 90:10 MA-DEGMA photocrosslinkable fibres before and after UV radiation for 10 mins showing successful crosslinking of the electrospun fibres.

In addition, the morphology of the fibres was monitored before and after UV-radiation and the result is shown in the SEM images below (Figure 3.12). It was observed that photocrosslinking had no effect on the overall morphology of the fibres. Specifically, upon hydration and after PEO elution, the fibres become less smooth, less homogeneous and thicker but the morphology of the fibres remains intact (Figure 3.12C).

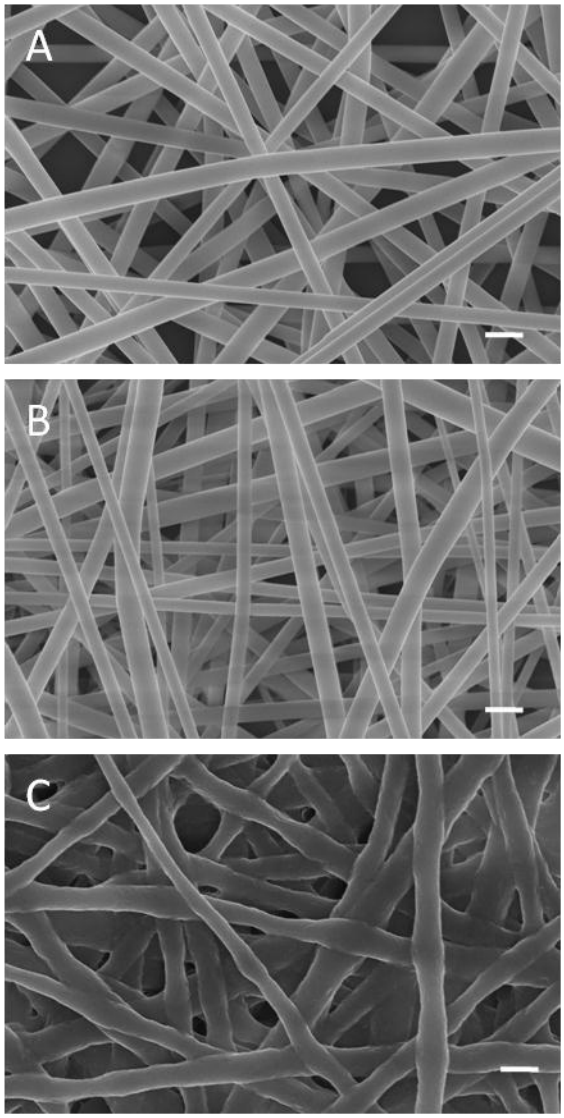

Figure 3.12 SEM micrographs of PEO/MA:DEGMA fibres that were washed and incubated overnight with 90:10 MA:DEGMA. A) Before UV-radiation; B) After UV-radiation; C) After UV and PEO extraction. Scale bar:1µm.

3.4.4 Characterization after PEO extraction

The characterization of the PEO extraction was assessed by monitoring the mass loss and NMR analysis of extracted products from the photocrosslinked fibres was performed. The mass loss monitoring for three photocrosslinked samples with the different ratios of 90:10, 70:30, and 50:50 (MA:DEGMA) after incubation in water showed a rapid loss of mass within the first day, followed by a more gradual release for the next 5 days, finally reaching a plateau (Figure 3.13). As described before in Section 3.3.6, due to the non-fibrous morphology of the 30:70 (MA:DEGMA) scaffold, further experiments did not include this composition. Non-crosslinked fibres were soluble in water; therefore the fibres were not analyzed. The 50:50 (MA:DEGMA) ratio fibres showed the highest mass loss approximately 75% mass loss followed by the 70:30 (MA:DEGMA) fibres (70%) and the 90:10 (MA:DEGMA) fibres (65%), all after 5 days. The rapid mass loss of these fibres was

because of the extraction of PEO from the fibres. This assumption was confirmed by employing ^{1}H-NMR for a quantitative analysis as shown below (Figure 3.14).

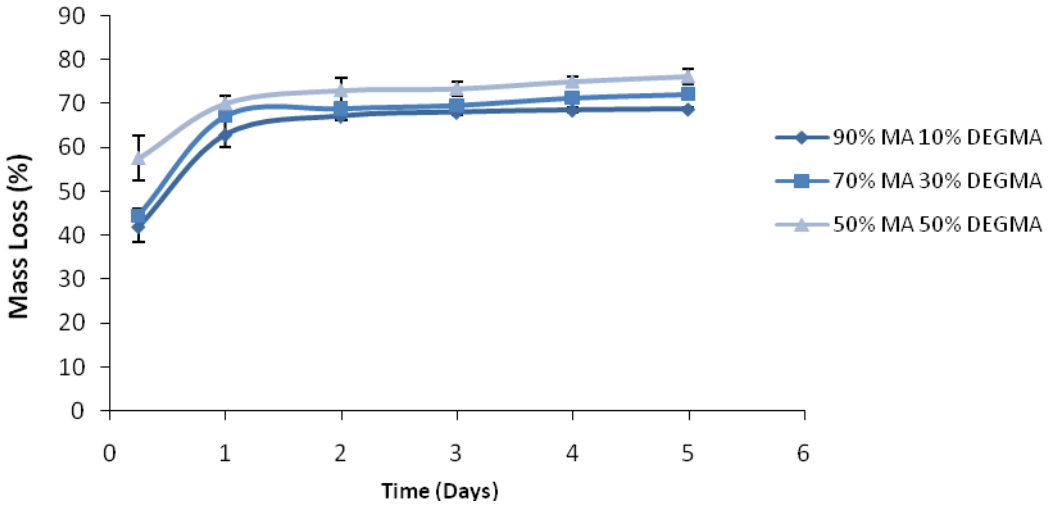

Figure 3.13 Mass loss for electrospun and crosslinked fibres. MA:DEGMA fibres that were washed and incubated overnight with varying ratios of MA:DEGMA of 90:10, 70:30 and 50:50. Mass loss after incubation in water for up to 5 days (n =5 per time point) for PEO extraction after photopolymerization.

The sol fraction from the fibres after PEO extraction was analyzed using ^{1}H-NMR. In Figure 3.14, the spectrum of the aqueous solution after incubation of the 90:10 MA:DEGMA fibres for 6 hours showed high intensity peaks at 3.6 ppm attributed to PEO. The absence of MA and DEGMA peaks detected relatively to the PEO concentrations in the solution, suggests that most of the monomers and crosslinkers have successfully reacted during photocrosslinking of the fibres. However, the absence of MA and DEGMA could also be due to rapid evaporation of unreacted MA and DEGMA during preparation of NMR samples (lyophilisation) because of the high levels of volatility. The visual analysis of the NMR spectrum showed a high PEO peak that decreased significantly over time and disappeared after 5 days (Figure 3.14B). This is consistent with the plateau reached by mass loss at the same time point (Figure 3.13).

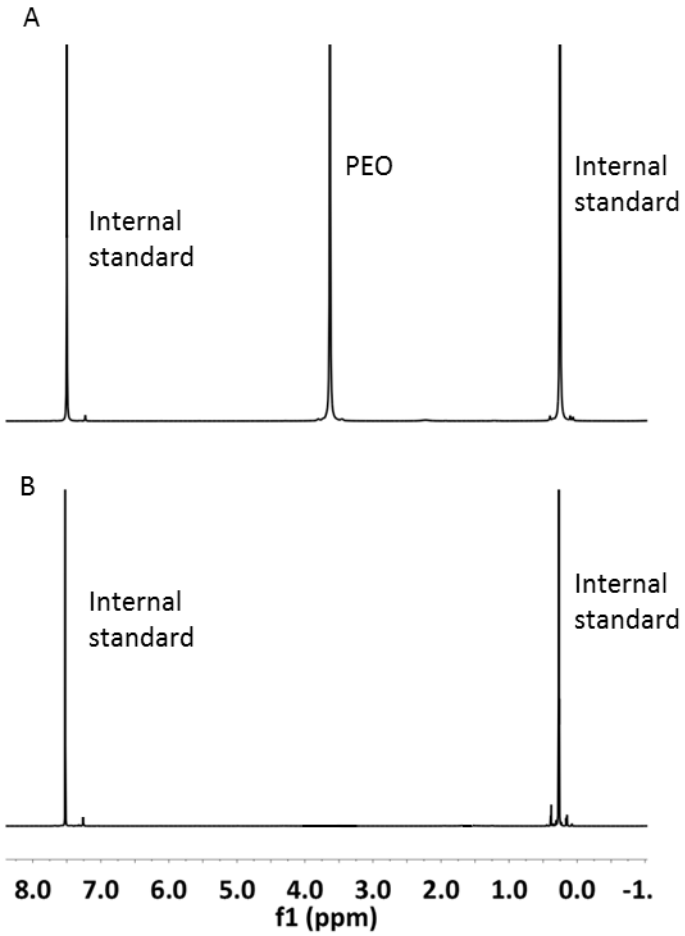

Figure 3.14 ^{1}H-NMR spectra of the release products from the 90:10 (MA:DEGMA) fibres after PEO extraction in water. (A) a representative spectrum of the collected electrospun solution of MA-DEGMA and PEO; B) a representative spectrum of the release products after five days.

In addition, mass loss for each component of the photocrosslinked fibres of 90:10 MA:DEGMA elutants was calculated using NMR integration normalized to an internal standard (Figure 3.15). In Figure 3.15, A and B correspond to 6 hours and 5 day time points, for which the ^{1}H-NMR spectra are shown in Figure 3.14. The quantification demonstrates that the primary component to be released from the fibres to the water is PEO. The rapid increase of PEO on the first day, which appears to plateau after 4 days, indicate that most of the PEO in the crosslinked fibres has been eluted out. It is important to note that due to the hygroscopic nature of PEO, we have confirmed by lyophilisation that the PEO product used adsorbs 4.5% water. This may have cause 4.5% less PEO being used during production of the scaffold. However this does not affect the overall determination of PEO extraction from the scaffolds since the level of hygroscopy is low. The overall ~ 65% mass loss of the photocrosslinkable fibres is consistent with the mass loss calculations determined by weight and shown in Figure 3.13. This proves that all of the PEO was eluted out of the scaffold.

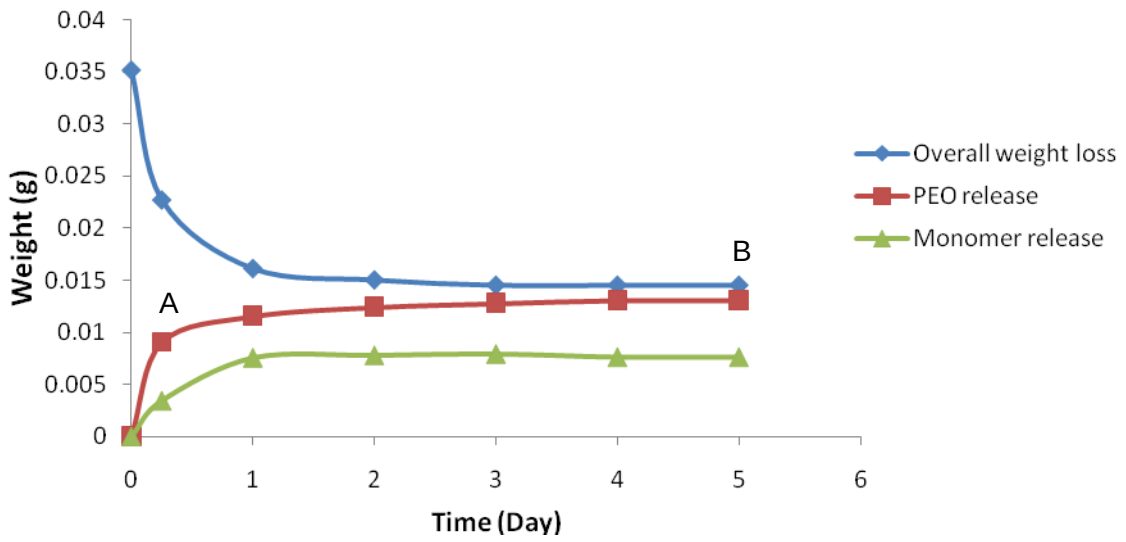

Figure 3.15 Mass loss for each component in the 90:10 MA:DEGMA photocrosslinked fibres calculated using NMR integration (n = 1). A and B denote the time points reflected in ^{1}H-NMR analysis in Figure 3.14.

3.4.5 Effect of varying the monomer/crosslinker concentrations on the mechanical properties of the fibrous scaffolds

Besides surface chemistry and topography, mechanical properties such as modulus are critical for the stability and support of implants/scaffolds in the body, and furthermore certain narrow ranges of stiffness have been shown in modulating cellular functions such as cell attachment, motility and differentiation [4, 204]. Cells are likely to mimic their *in vivo* behaviour more when they are cultured on scaffolds which rigidity matches that of the cell type's native tissue matrix [205]. Hence, it is essential to characterize the mechanical properties of the fibrous acrylate scaffolds and investigate the effect of varying the monomer/crosslinker concentrations. The mechanical properties of the formed scaffolds with varying MA:DEGMA ratios were determined under four different conditions: before and after photocrosslinking and in dry and hydrated states (after PEO extraction), using an uniaxial tensile test to failure (Figure 3.16). Tensile extension and reactive forces were recorded using the Bluehill 2 software, and the modulus (E) was calculated from the linear region of the stress-strain curves. The mechanical testing studies showed that the crosslinked samples had a higher tensile modulus than the uncrosslinked scaffolds. Moduli of 3.0 ± 0.14, 3.5 ± 0.17 and 2.9 ± 0.2 MPa were determined for the uncrosslinked samples with the 90:10, 70:30 and 50:50 (MA:DEGMA) concentrations, respectively, while the crosslinked counter parts with the referred chemical compositions had a modulus of 14.7± 0.24, 12.1± 0.21 and 10.6± 0.18 MPa, respectively.

The increase in tensile modulus of the fibres after UV radiation was expected mainly due to the photocrosslinking of the acrylate monomers. Such an effect has been previously reported in studies by Tan and co-workers [10]. Though the modulus reported in their work was much lower with values of 1.5 MPa after photocrosslinking of macromer from a poly(β-amino ester) library. For the crosslinked fibres (before PEO extraction), a lower tensile modulus was measured as DEGMA concentration increased. The reduction of the tensile modulus could be explained by the changes of the scaffold morphology (shown in Figure 3.9). Increasing DEGMA concentrations caused poor fibre formation with inconsistent fibre sizes in the scaffold. The microheterogeneity observed within the fibres possibly affected the overall mechanical properties of the fibres.

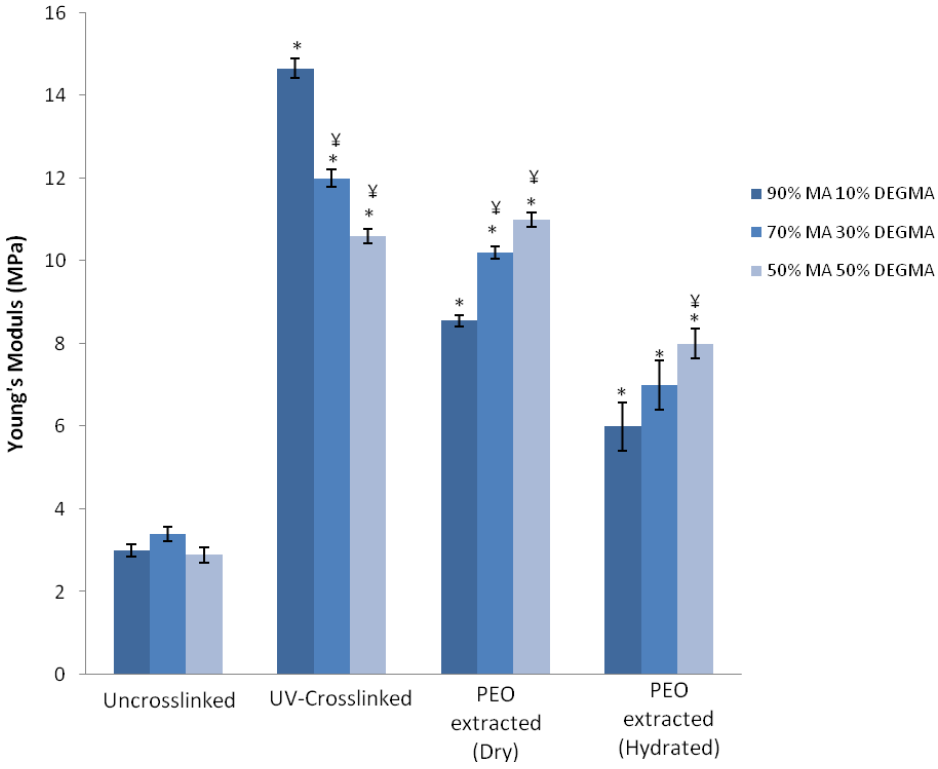

Figure 3.16 Mechanical properties: Young's modulus values of fibrous scaffolds with varied monomer/crosslinker ratio. (*) indicates that the difference between the marked bar and the uncrosslinked condition with the same chemical composition is statistically significant (p<0.05). (¥) indicates the difference between the marked bar and the 90:10 (MA:DEGMA) sample treated in the same condition is statistically significant (p<0.05).

After PEO extraction, for all chemical compositions, the fibrous scaffolds exhibited the lowest tensile modulus when compared with initial constructs. This effect is due to the reduction in overall mass as PEO was dissolved out from the scaffolds. This linear relationship between PEO content removed and overall scaffold properties was also demonstrated by Baker and colleagues with co-electrospinning PEO with poly-ε caprolactone (PCL) [206]. In contrast, the degree of crosslinking

appears to have more influence over the mechanics of the scaffold after PEO extraction. Increase in DEGMA (crosslinker) concentration lead to higher tensile modulus, which suggests an increase of crosslinking of acrylate within the network. Furthermore, the fibre diameter increased and more welding is found when increasing DEGMA content, which could have affected the stiffness of the overall structure. This effect of increase in modulus by increasing concentration of DEGMA as a crosslinker was also shown by Smith *et al*. but with photocrosslinking monomers of 2-hydroxyethyl methacrylate (HEMA) and DEGMA with varying ratios into polymer discs for bone implants from a range of 10 to 600MPa as DEGMA concentration increased [205]. They reported higher modulus values for their scaffolds because of difference in scaffold bulk properties since polymer discs were produced instead of porous electrospun scaffolds.

In order to investigate the mechanical properties under more physiologically relevant conditions, (i.e. *in vivo)* the fibrous scaffolds were tested following incubation in water. Hydrated scaffolds displayed decreased tensile moduli in comparison with the respective dry scaffolds. The difference between the dry and hydrated scaffolds is because of water absorption and swelling, which reduces the tensile modulus values. However, a similar trend was displayed whereby an increase in DEGMA (crosslinker) concentration leads to higher tensile moduli.

It has been shown by other research groups that the crosslinking density can be increased by the addition of a crosslinker agent, which increased mechanical strength of the networks [207-210]. This is relevant in the hydrated state of the fibrous scaffolds because it means that the material strength in swollen state can be increased by increasing the concentration of crosslinker agents [208].

Recently, Wang *et al*. demonstrated the development of photocrosslinked electrospun fibres with polyurethane (PU) and poly (ethylene glycol) methacrylate (PEGMA) by *in-situ* UV photopolymerization [194]. The PU/PEGMA fibres exhibited lower tensile modulus in the range of ~ 3 MPa compared to the MA:DEGMA fibres. Another research group, Tan *et al.* also produced fibres with a lower tensile modulus of ~ 5MPa after photocrosslinking a macromer from a poly(β-amino ester) library [10]. Furthermore, photocrosslinked hydrogels using acrylated hyaluronic acid and acrylated poly(glycerol sebacate) demonstrated even lower modulus of ~ 20kPa [211] and ~1MPa [212] respectively.

Even though the acrylate fibrous scaffolds exhibits higher tensile modulus than most photocrosslinked hydrogels and electrospun fibres described above, the major challenge of engineering TE applications for connective tissue, particularly bone is to provide adequate mechanical strength prior to cellular deposition of natural ECM [213]. The tensile moduli of 6.5-8 MPa was displayed for the acrylate fibrous scaffolds in the hydrated state. The tensile modulus is comparable to PCL that have been reported to have tensile modulus from a range of 5-15 MPa, a

commonly investigated polymer for electrospinning used for bone TE applications [206, 214]. This scaffold could potentially be suitable for regeneration of non-loading areas of bones such as craniomaxillofacial bone defects. Work by Motherway and colleagues have shown that cranial human exhibiting average moduli of 150 MPa [215]. Though the acylate scaffold has much lower moduli, some studies suggests that the overall mechanical strength of a scaffold increases after cellular infiltration [213 181].

However, based on its mechanical properties, this fibrous scaffold may not be strong enough to support large defects of load-bearing bone. Studies have shown mineralized cortical and trabecular human bone exhibiting average moduli of 9905 and 365 MPa respectively [205].

3.4.6 Effect of varying the monomer/crosslinker ratio on swelling properties of electrospun fibres

A unique characteristic of the fibrous scaffold was swelling could be observed when the scaffold is immersed in aqueous conditions. This hydrated state of the scaffolds is also more physiologically relevant, following incubation in water. The swelling can be seen in the bulk morphology of the scaffold shown in Figure 3.17. To understand the influence of the MA and DEGMA ratios on the swelling behaviour, swelling ratio of the different acrylate scaffolds was investigated.

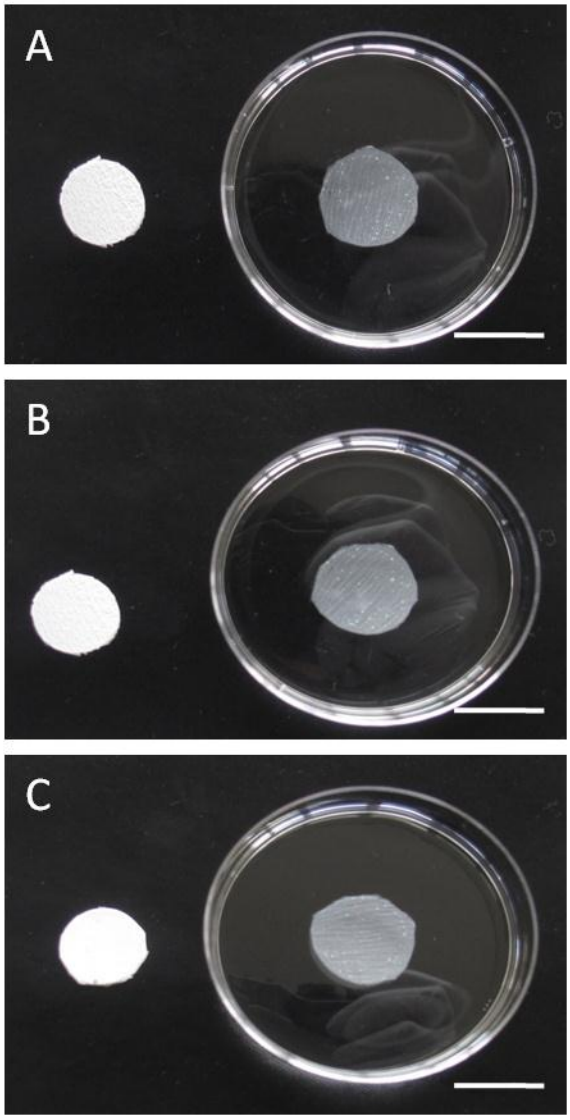

Figure 3.17 Images of the bulk morphology changes of the fibrous samples with varying ratios of MA:DEGMA (A) 90:10; B) 70:30; C) 50:50 before and after immersion in water. Scale bar: 5cm.

All MA:DEGMA fibres with varying monomer and crosslinker compositions showed similar swelling behaviour which are typical swelling curves for crosslinked polymers including hydrogels. An initial and short (10-30 mins) rapid swelling phase was followed by a slowing down of the penetrant uptakes (30-60 mins) and, eventually, the fibres reaches its maximum swollen state (Figure 3.18). Swelling reaches asymptotically to a limit which is the balance between the attractive interactions between water and the scaffold surface and then increasing conformational strain which is being generated (due to the reduction of conformational entropy) which counteracts this effect. The ultimate level of swelling is a compromise of these two effects. Hence, this gives a good indication for the degree of crosslinking. Swelling significantly increases with decreasing crosslinker concentration, with the 90:10 ratio scaffolds displayed the highest degree of swelling (~160%), followed by 70:30 (~140%) and 50:50 (~120%) percentage MA:DEGMA compositions. This behaviour demonstrates the increase in water uptake caused by lower levels of crosslinking in the

network [216]. In addition, SEM images also show the increase in welding which could affect the swelling behaviour (Figure 3.10).

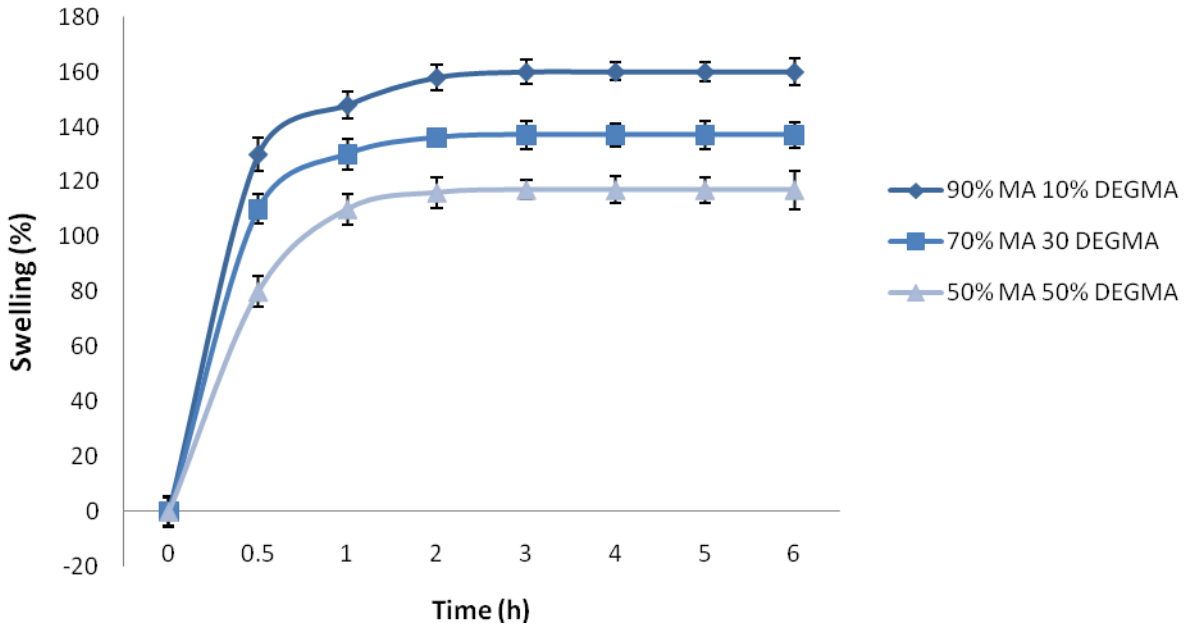

Figure 3.18 Swelling ratios (percentages) of electrospun fibres with different MA:DEGMA ratios. (n=5 per time point).

The evaluation of both mechanical and swelling properties demonstrated that the increase in swelling ratio is always accompanied by a corresponding decrease in tensile modulus (Figure 3.16). This is simply due to the increase in the volume of water uptake by the scaffold. Hence, the degree of swelling is correlated to the material strength. Typically, increasing the crosslinking density reduces the degree of swelling of the material and thus improves its mechanical properties [208]. The effects of swelling on tensile modulus is reported by Buyonov *et al*. for polyacrylamide gels crosslinked with N,N-methylene-bisacrylamide by demonstrating that when the degree of swelling increases, the tensile modulus decreases dramatically [208, 217].

Based on the morphology and the mechanical and swelling properties, the 90:10 MA:DEGMA composition was considered to have the best overall properties as a tissue engineering scaffold among all the fibrous scaffolds synthesized, as it develops the highest swelling ratio yet maintaining mechanical integrity. Furthermore, SEM images demonstrated that the 90:10 MA:DEGMA fibres preserved the fibrous morphology of the scaffold in water incubation.

3.4.7 Effect of varying the monomer/crosslinker ratio on wettability properties of flat surfaces of MA and DEGMA

To understand the influence of surface chemistry on wettability, contact angle values of different acrylate flat surfaces of MA:DEGMA were investigated. Contact angle measurements of the electrospun fibres could not be assessed due to the irregular and rough surface topography of the scaffold. The contact angle values for different flat surfaces of MA:DEGMA were shown in Figure 3.19. Depending on the concentration of MA and DEGMA, the hydrophobicity of the surfaces were expected to change as the crosslinker:monomer ratio was varied.

It is evident that the 50:50 MA:DEGMA surface showed the lowest contact angle (39 ± 4.2°) while 90:10 MA:DEGMA presented the highest (85 ± 2.66°) and followed by 70:30 MA:DEGMA (55 ± 3.5°). This is due to DEGMA being a more hydrophilic monomer because of the presence of oxygen atoms which is in contrast to MA. Hence, by varying the ratios of both MA and DEGMA, the hydrophilicity of the flat surfaces changed.

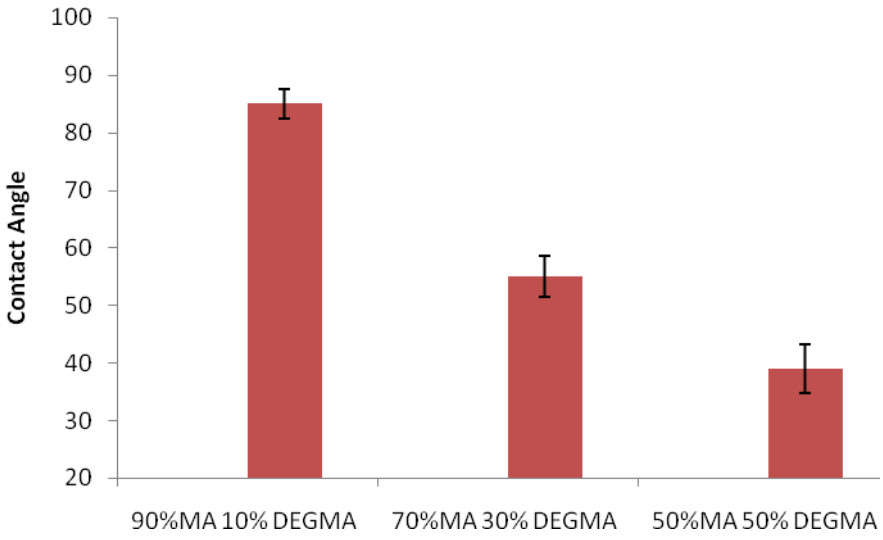

Figure 3.19 Contact angle measurements of varying MA:DEGMA ratios of acrylate flat surfaces. (n=5 per sample).

CONCLUSIONS

In this chapter, the electrospinning of photocrosslinkable and low molecular weight monomers is described. The ability to produce topologically and mechanically diverse fibrous scaffold materials was demonstrated. Photocrosslinked fibres were successfully developed by electrospinning different MA and DEGMA compositions and post-UV crosslinking. The effects of various processing parameters of electrospinning were investigated, including carrier polymer concentration, accelerating voltage, rate of delivery and monomer/carrier polymer ratios. With the use of high molecular weight PEO, all parameters were observed to have a profound effect on the electrospun fibres morphology. The analysis of this study lead to the determination of the optimal range of parameters required to produce uniform and bead-free electrospun MA:DEGMA fibrous scaffold. When exposed to UV light in the presence of a photoinitiator, the crosslinked network was produced by conversion of the double bonds and an increase in tensile moduli was observed. PEO was extracted with thorough washing with water, and scaffolds swelled after incubation in water. Most importantly, varying MA and DEGMA composition affected overall fibre morphology, swelling and mechanics of the fibrous scaffold.

The 90:10 (MA:DEGMA) composition was chosen as the best fibrous scaffold for bone tissue engineering purposes among the different compositions analysed, as it developed the highest swelling properties while maintaining its mechanical and morphological integrity.

CHAPTER 4

Biological evaluation of acrylate fibrous scaffolds with Saos-2 and hMSC cells

4.1 INTRODUCTION

The extracellular microenvironment plays an essential role in directing cellular behaviour [5, 6, 9]. For cells growing on a material, the properties of its surface, such as topography, stiffness, wettability and specific cell-surface interactions are key to control cellular activity [7-9]. A critical challenge in designing materials for TE is to provide essential cues that can control cellular behaviour and promote tissue regeneration. Material-based control of cellular response is a potentially powerful way for regulating the behaviour of different cell types, including stem cells, cells with the potential to differentiate into many tissue types. Anderson and colleagues demonstrated the ability of acrylates and methacrylate photocrosslinked networks to support cell attachment, viability and proliferation [9]. Moreover, using an acrylate/methacrylate microarray library, they were able to identify specific monomers that support human embryonic stem cells.

As previously discussed in Chapter 2, the electrospinning technique is able to create ECM-analogue scaffolds composed of nanoscale fibres. Such scaffolds have high surface area to volume ratio, which supports cell growth and infiltration. Moreover, the morphological resemblance between the fibrous scaffold and the ECM are shown to enhance cellular response [15]. The high surface area permits increased levels of cellular adhesion, and the occurrence of multiple focal adhesion points [15, 61].

Upon implantation of biomaterials in bone, MSCs have been demonstrated to be recruited from the bone marrow to the injury location, where they attach to the biomaterial and subsequently differentiate into osteoblasts [79, 218]. MSCs are uncommitted, cells that are characterized by their capability to differentiate after stimulation of appropriate cues [82, 84]. Their potential for differentiation (or plasticity), and the simplicity with which they can be isolated and cultured *in vitro* without phenotypic alterations before differentiation [76], make MSCs a suitable candidate for TE applications [84]. The use of MSCs to induce tissue regeneration has been extensively investigated [81-83]. These cells have been seeded into scaffolds and implanted into the body either directly or a few weeks later, after *in vitro* differentiation [81]. Successful bone and sub-optimal cartilage defect repair have been achieved [84]. However, the optimal conditions to promote MSC growth and differentiation towards a specific lineage have not been defined yet. Thus, investigations targeted at defining the optimal environment for MSC attachment and proliferation using a scaffold are therefore necessary.

In Chapter 3, the successful development of photocrosslinked fibres by electrospinning different MA and DEGMA compositions and post-UV crosslinking was described. The investigation of the material characteristics revealed that varying MA and DEGMA concentrations affected overall fibre morphology, swelling and mechanics of the fibrous scaffold. In the present chapter, the biological response of Saos-2 (osteosarcoma-derived osteoblastic cells) and human MSC cells to different

compositions of MA/DEGMA electrospun fibers and flat surfaces with similar chemistry is discussed. Additionally, the effect of the fibrous scaffolds and flat surfaces on protein adsorption is also investigated.

4.2 MATERIALS

Roswell Park Memorial Institute 1640 medium (RPMI 1640), Fetal Bovine Serum (FBS), L-Glutamine, penicillin/streptomycin, Phosphate buffered saline (PBS) and trypsin/ethylenediamine tetra-acetic acid (trypsin/EDTA), AlamarBlue® assay, Alexa-Fluor 568 Phallaoidin stain, Total DNA assay and the LIVE/DEAD® viability assay were purchased from Invitrogen GIBCO Corporation (UK). Caspase-glo®3/7 Assay was purchased from Promega (UK). The human osteosarcoma cell line Saos-2 was purchased from ECACC (UK) and human mesenchymal stem cells (hMSCs) growth media were purchased from Promocell (UK). BCA Protein assay kit was purchased from Thermo Fisher Scientific (UK).

4.3 METHODS

4.3.1 Cell culture

Saos-2 cells (an osteosarcoma-derived cell line) were expanded in RPMI 1640 with 10% (v/v) fetal bovine serum (FBS), 1% (v/v) L-glutamine and 1% (v/v) penicillin/streptomycin. Low passage (p3-p4) hMSCs were cultured using growth medium and supplements (Promocell). The hMSCs were obtained commercially from two different patients (48 and 56 years old) (Promocell). Initial culture for both cell types was performed in 75cm^2 flasks at 37°C, in a humidified atmosphere of 95% air with 5% CO_2, and supplied with fresh medium every 2-3 days. At 90% confluence, cells were detached using trypsin-EDTA and cell count was determined in a haemocytometer. Cells were resuspended to achieve the appropriate concentration for seeding in complete medium.

4.3.2 Preparation of electrospun scaffolds and flat surfaces

The aluminium foil of the collecting surface of the mandrel was plasma-treated before electrospinning. Fibrous membranes were deposited by electrospinning the PEO acrylate solution with the specifications mentioned in Chapter 3 (Section 3.3.3). The fibres were exposed to UV light for 10 minutes. Fifteen millimetre diameter scaffolds were excised using a biopsy puncher and PEO was extracted from the fibres for five days. Subsequently, the scaffolds were air-dried overnight and incubated in deionized water also overnight, before placed in 24-well plates previously coated with 1% (w/v) agarose gel (to prevent cell adhesion at the bottom of the plate).

Flat surfaces with the same chemical composition of the fibres, used as control, were fabricated by photocrosslinking. The MA:DEGMA solutions were photocrosslinked in 24-well plates under nitrogen purge with UVB light for 10 minutes. The flat surfaces were then washed in acetone and

ethanol for 5 days, to extract unreacted monomers thoroughly, before cell culture experiments. The sol fraction products from the flat surfaces were analyzed using ^{1}H-NMR to ensure no monomers and photoinitiator were present. Before cell culture, the flat surfaces were washed with water and PBS. For sterilization, samples in the 24-well plates were incubated with ethanol for one hour, soaked in PBS overnight and repeatedly rinsed with PBS and media before cell seeding. Saos-2 and hMSC cells were seeded on the electrospun fibres and flat surfaces prepared at a density of 1 x 10^4 cells/per cm^2 and incubated at 37°C overnight to allow cell adhesion. The cell culture medium was replaced every 2-3 days.

4.3.3 AlamarBlue® assay

The alamarBlue® assay was performed to assess the viability of cells on the fibrous scaffolds. The mechanism of detection of this assay is the conversion of its active product, resazurin, by cells into the fluorescent molecule, resorufin, which produces red fluorescence. Viable cells continuously convert resazurin into resorufin, due to their reduction potential. Hence, fluorescence can be used as a quantitative indicator of cell viability; the total of fluorescence produced is then directly proportional to the amount of living cells. The alamarBlue® assay was performed as specified by the manufacturer. Briefly, Saos-2 and hMSCs were seeded in 24-well plates (cell density, 1 x 10^4 cells/cm^2). At specific time points (1, 5, 10 days), cell-culture media were removed from the well plates and the wells were washed with 400 µL of PBS. 300µL of 10% (v/v) alamarBlue® in phenol red-free cell culture media were added per well (including one with no cells to be used as blank) and the well plates were incubated for 3 hours at 37°C. 100 µL of the reaction product was then transferred to a black 96-well plate and fluorescence was measured at an excitation wavelength of 540 nm and an emission wavelength of 590 nm using a microplate reader (SpectraMax M5, Molecular Devices).

4.3.4 Total DNA assay

DNA concentration was measured using the Hoechst 33258 dye fluorescent assay. This assay is based on the enhanced fluorescence and shift in the emission wavelength of the fluorochrome Benzamide (Hoescht) when bound to DNA. Briefly, after 1, 5, and 10 days, cell-culture medium was removed from the well plates and cells were washed with PBS. 400 µL of water were added per well and cells were lysed by freeze-thaw cycles (30 minutes at -80°C and 20 min at 37°C, repeated 3 times). 50 µL of the cell lysates were added to 50 µL of Hoescht dye diluted to the working concentration (20 µg/mL) and allowed to react for 5 minutes before measurement. Fluorescence was measured using an excitation wavelength of 360 nm and an emission

wavelength of 460 nm in a microplate reader (SpectraMax M5, Molecular Devices). In addition, DNA concentrations were calculated using a standard curve prepared using calf thymus DNA at concentrations between 0-100 µg/mL.

4.3.5 Caspase-glo®3/7 Assay

The Caspase-glo®3/7 assay is a luminescent apoptosis assay that measures caspase-3 and -7 activities, two members of the protease (caspase) family participate in critical effector roles in apoptosis in cells. The assay uses a luminogenic substrate DEVD sequence that has been shown to be specific to both caspase-3 and -7. The Caspase-glo®3/7 assay was performed as indicated by the manufacturer. Briefly, cell culture medium was removed and 300 µL of Caspase-glo®3/7 reagent were added to each well. The plates were gently mixed by using a plate shaker for 30 seconds and incubated in room temperature for one hour. Luminescence was measured using a microplate reader (SpectraMax M5, Molecular Devices). As positive control for caspase activation, cells were exposed to 0.1% (w/v) staurosporine overnight, a known inducer of apoptosis.

4.3.6 LIVE-DEAD® viability assay

The LIVE-DEAD® assay simultaneously detects live and dead cells, based on intracellular esterase activity and plasma membrane integrity. Live cells are detected by intracellular esterase activity, affected by the enzymatic conversion of the non-fluorescent cell-permeant calcein AM to the fluorescent calcein. Whereas Ethidium homodimer (ethD-1) penetrate cells with damaged membranes and produces red fluorescence upon interaction with nucleic acids for dead cells. Firstly, 1.5µl Calcein AM and 3µl of Eth-D were mixed with 6ml of PBS to make up the working solution. After rinsing the samples with PBS, 500 µl of working solution were added to each well and the cells were incubated for 20 minutes at room temperature. The labelled cells were viewed and photographed under the fluorescence Olympus IX51 inverted microscope.

4.3.7 SEM for cell attachment

Samples were washed with PBS twice and fixed with 2.5% (v/v) glutaraldehyde in PBS. Then samples were rinsed with PBS twice and dehydrated with a graded series (increasing concentration of 25%, 50%, 70%, 90% and 100%) of ethanol for 5 minutes/each concentration. After samples were dry, the samples were sputtered with gold and observed using SEM (LEO 1525, Gemini 1525 FEGSEM) at 10 kV.

4.3.8 Actin Immunostaining

The distribution/organization of actin fibres were observed by staining the cells with Alexa Fluor Phalloidin 488/568. Nuclei were stained with Diamidino-2-phenylindole (DAPI) staining. Firstly, the electrospun samples were washed twice with pre-warmed PBS and fixed with 4% (w/v) paraformaldehdye solution for 15 minutes at room temperature. After washing the samples twice with PBS, the cells were permeablized with 0.1% (v/v) Triton X-100 solution for 5 minutes at room temperature. After further washing, the samples were incubated with Alexa Fluor Phalloidin solution in 1% (w/v) BSA for 20 minutes at room temperature. The samples were then washed with BSA and PBS twice, repeatedly and, finally, Vectashield mounting medium with DAPI staining solution was added to samples and incubated for 5 minutes. Samples were rinsed with PBS twice and viewed with a fluorescence microscope (Olympus IX51 inverted microscope).

4.3.9 Protein adsorption

Fibrous scaffolds and thin films of identical composition were placed in a 24-well plate, sterilized with 70% ethanol for an hour, washed thoroughly and incubated overnight with PBS. All samples were incubated with 1ml of 25% (w/v) FBS for 4 hours at 37°C. The samples were then removed from the protein solution and washed with 600µl of PBS under gentle agitation. The free and loosely adsorbed proteins were removed by repeated washing. Proteins adsorbed on the surface of the samples were recovered by incubations in 200µl of 1% (w/v) sodium dodecyl sulphate (SDS) for 1 hour. The retrieved protein concentration was assessed, using BCA Protein assay kit. A microplate reader (SpectraMax M5, Molecular Devices) was used for the measurement and the result was normalized to surface area.

4.3.10 Statistical analysis

All experimental data shown were expressed as mean ± SD and were obtained from experiments performed in triplicate, at least. All data analysis was performed in Excel. Statistical analysis was performed with one-way analysis of variance (ANOVA) using multiple comparisons (Bonferonni test) and significance was determined by $p<0.05$. This analysis was performed with Graphpad InStat (Prism) software.

4.4 RESULTS AND DISCUSSION

The previous chapter describes the development of MA:DEGMA photocrosslinked fibrous scaffolds by electrospinning different MA and DEGMA compositions and post-UV crosslinking. Varying the MA:DEGMA composition was shown to affect overall fibre morphology, swelling and mechanics of the fibrous scaffold. Nevertheless, the biological response of cells to the fibrous scaffolds should be investigated. Hence, the Saos-2 cell line, an osteosarcoma cell line commonly used in our laboratory, was chosen to model osteoblastic behaviour and to assess the biological activity of the MA:DEGMA scaffolds. Saos-2 cells have been ubiquitously utilized as model systems for elucidating osteogenic cell behaviour on biomaterials [87, 218, 219]. Compared to other osteosarcoma cell lines, MG-63 and U-2 OS, Saos-2 cells exhibited the most mature osteoblastic phenotype with positive results for ALP, OCN, BSP, decorin and collagen I and III [220, 221]. Hence, rendering these cells as a good candidate for an *in vitro* model of osseointegration. To further investigate the biological effects of the fibrous scaffolds, the response of hMSCs was also evaluated. Their potential for differentiation (or plasticity), and the efficiency with which they can be isolated and cultured *in vitro* without phenotypic alterations before differentiation [76], make MSCs a suitable candidate for TE applications [84]

This chapter was divided into three main sections. Firstly, the Saos-2 cells response to different MA:DEGMA compositions and a comparison with flat surfaces with the same monomer concentrations will be described. Secondly, a similar study using hMSCs will be presented and finally, the protein adsorption studies on the scaffolds will be demonstrated.

4.4.1 Determination of the effect of varying MA:DEGMA compositions on Saos-2 cells behaviour (comparison to 2D surfaces)

Total DNA assay was performed to ensure the fibrous scaffolds were not cytotoxic. This assay is commonly used to assess cell number or cell viability. The various MA:DEGMA fibrous scaffolds used in the present study did not significantly affect Saos-2 cells viability (Figure 4.1). Total DNA content of the Saos-2 cells grown in the fibrous scaffolds was not significantly reduced in comparison with those grown in TCP, after both 1 and 2 days in culture. Increased cell number was observed for all MA:DEGMA fibres after 2 days, except for 50:50 MA:DEGMA ratio, which showed significant lower cell viability in comparison to TCP.

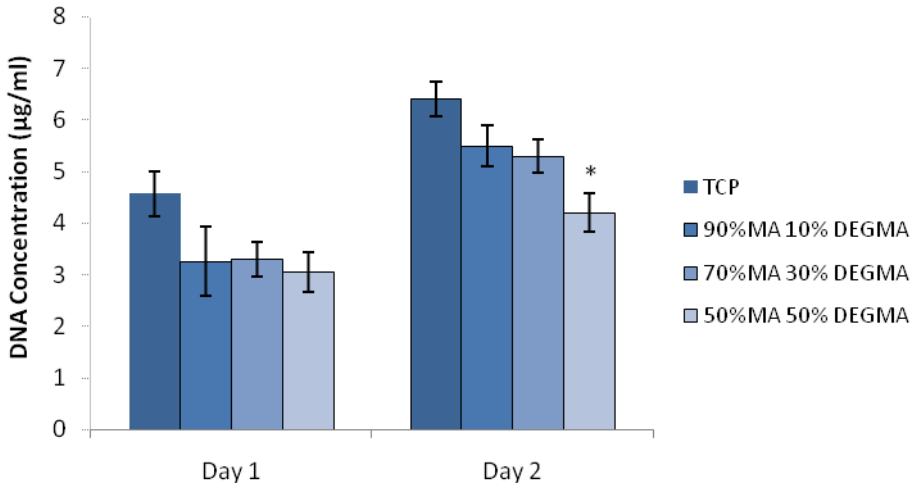

Figure 4.1 Effect of varying the MA:DEGMA ratio of the fibrous scaffolds on Saos-2 cell viability, determined using total DNA assay. Mean ± SD, n = 3. (*) indicates the difference between the marked bar and the control (TCP) of the same time period is statistically significant ($p<0.05$).

Saos-2 cell viability and proliferation on the photocrosslinked fibres was evaluated at days 1, 5 and 10, using the AlamarBlue® assay (Figure 4.2), an assay that measures enzymatic activity by assessing the cytoplasmic reduction potential of metabolically active cells. During the first 24 hours, no significant differences in cell viability between all samples were observed. However, the flat surfaces of photocrosslinked polymers presented slightly higher cell viability in comparison to the fibrous scaffolds. After 5 days in culture, this trend changed. The 90:10 (MA:DEGMA) fibres significantly enhanced Saos-2 cellular activity and the 70:30 and 50:50 (MA:DEGMA) fibres followed the trend in this specific order. At this time-point, cell viability was significantly lower for the MA:DEGMA flat surfaces in comparison to the fibrous scaffolds with equivalent chemistry. The concentration-dependent trend of MA:DEGMA continued to rise up to 10 days in culture. The 90:10 (MA:DEGMA) fibres supported the highest level of cell viability, followed by the 70:30 and 50:50 (MA:DEGMA) fibres. The flat surfaces with same chemical composition maintained a significantly lower cell viability when compared with their corresponding fibrous scaffold of the same chemistry. Interestingly, flat surfaces displayed the opposite trend of effect on cell viability. The 50:50 ratio (MA:DEGMA) showed the highest cell viability for flat surfaces, followed by the 70:30 and finally the 90:10 ratios (MA:DEGMA).

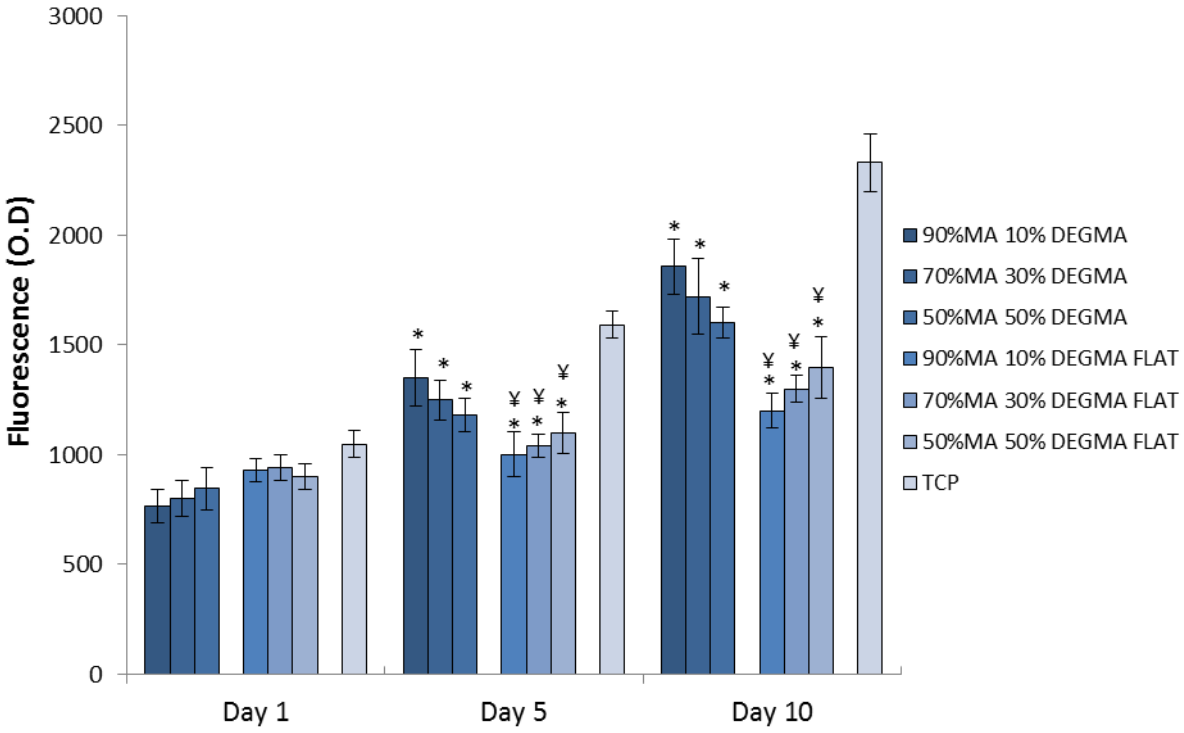

Figure 4.2 Effect of the photocrosslinked fibrous scaffolds on Saos-2 cell viability, determined using AlamarBlue® assay. Comparison of the effect of the photocrosslinked fibrous scaffolds with the flat surfaces with equivalent chemical compositions. Mean ± SD, n = 3. (*) indicates the difference between the marked bar and the control (TCP) of the same time period is statistically significant. (¥) indicates that the difference between the marked bar and flat surface with same chemical composition of the same time period is statistically significant (p<0.05).

The AlamarBlue® results were confirmed using a LIVE-DEAD® viability assay, shown in Figure 4.3, Figure 4.4, and Figure 4.5. The LIVE-DEAD® staining results demonstrated the Saos-2 cells seeded on the fibrous scaffolds remained largely viable. After 24 hours in culture, the cells seeded onto the photocrosslinked fibrous scaffolds and flat surfaces were green fluorescent, indicating viability was maintained after seeding into the scaffold. As observed with the AlamarBlue® assay (Figure 4.2), at this time-point, the cells grown in the flat surfaces presented higher viability compared to those grown in the fibrous scaffolds. After 5 days in culture, a significant increase in cell number was observed for Saos-2 cells grown in the 90:10 ratio (MA:DEGMA) fibrous scaffolds; growth that continued up to day 10 (Figure 4.5). This increase in cell viability was followed by Saos-2 cells growing in the 70:30 and 50:50 (MA:DEGMA) fibrous scaffolds, respectively. Only a small number of cells was found to be apoptotic (red fluorescent). Confluency was reached at day 10. On the flat surfaces, however, such enhancement of cell viability was not observed. A small increase in cell proliferation was only detected for cells seeded in the flat surfaces from day 5 to day 10. The cells on TCP showed larger size compared to cells on fibres and flat surfaces due to

the differences in magnification. The thickness of the fibres and flat surfaces samples in the 24-well plates caused differences in magnification with control cells cultured directly on the 24-well plate.

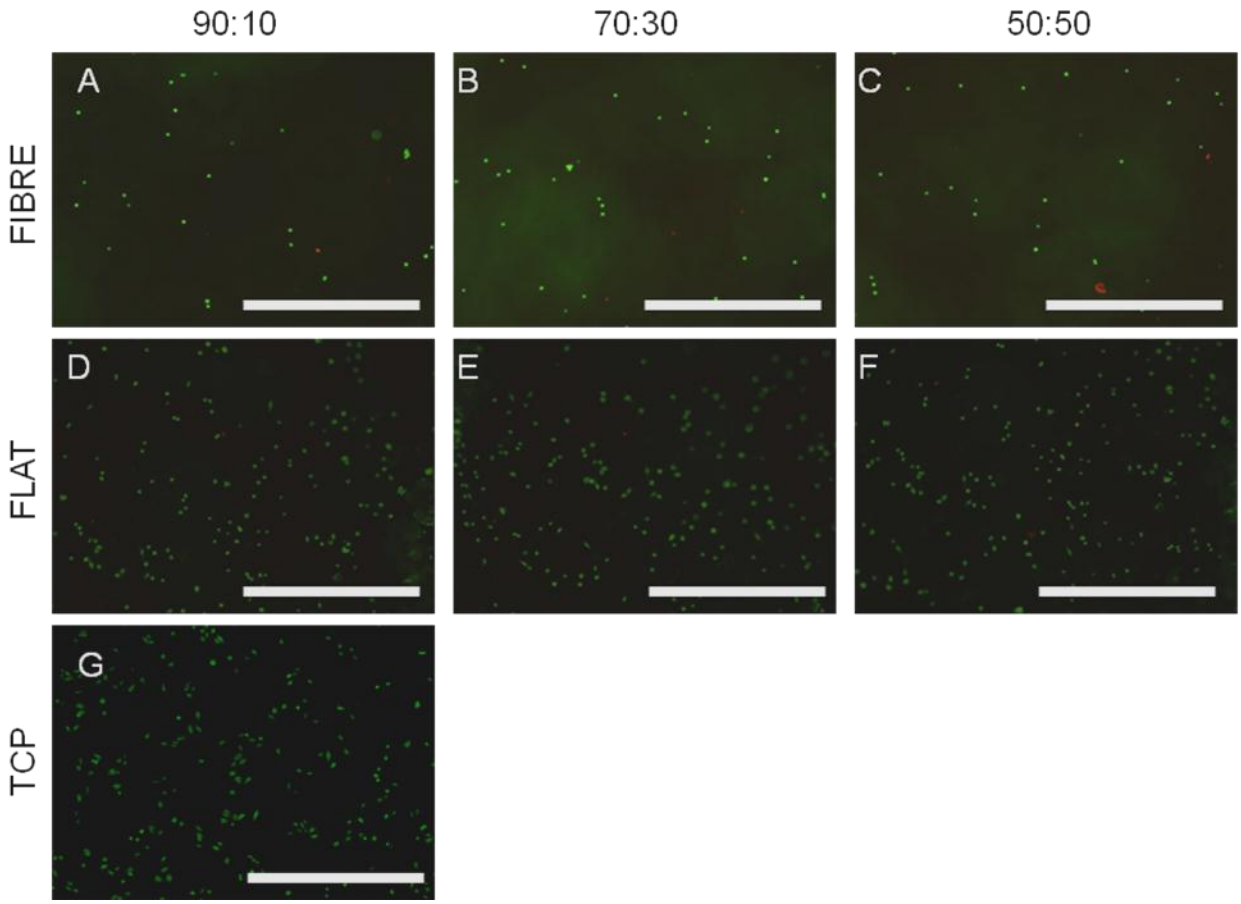

Figure 4.3 LIVE-DEAD® viability assay of Saos-2 cells cultured on MA-DEGMA photocrosslinked fibrous scaffolds, flat surfaces and TCP after 24 hours. The green fluorescence represented live cells whereas the red fluorescence, represented dead cells. Scale bar: 1.0 mm.

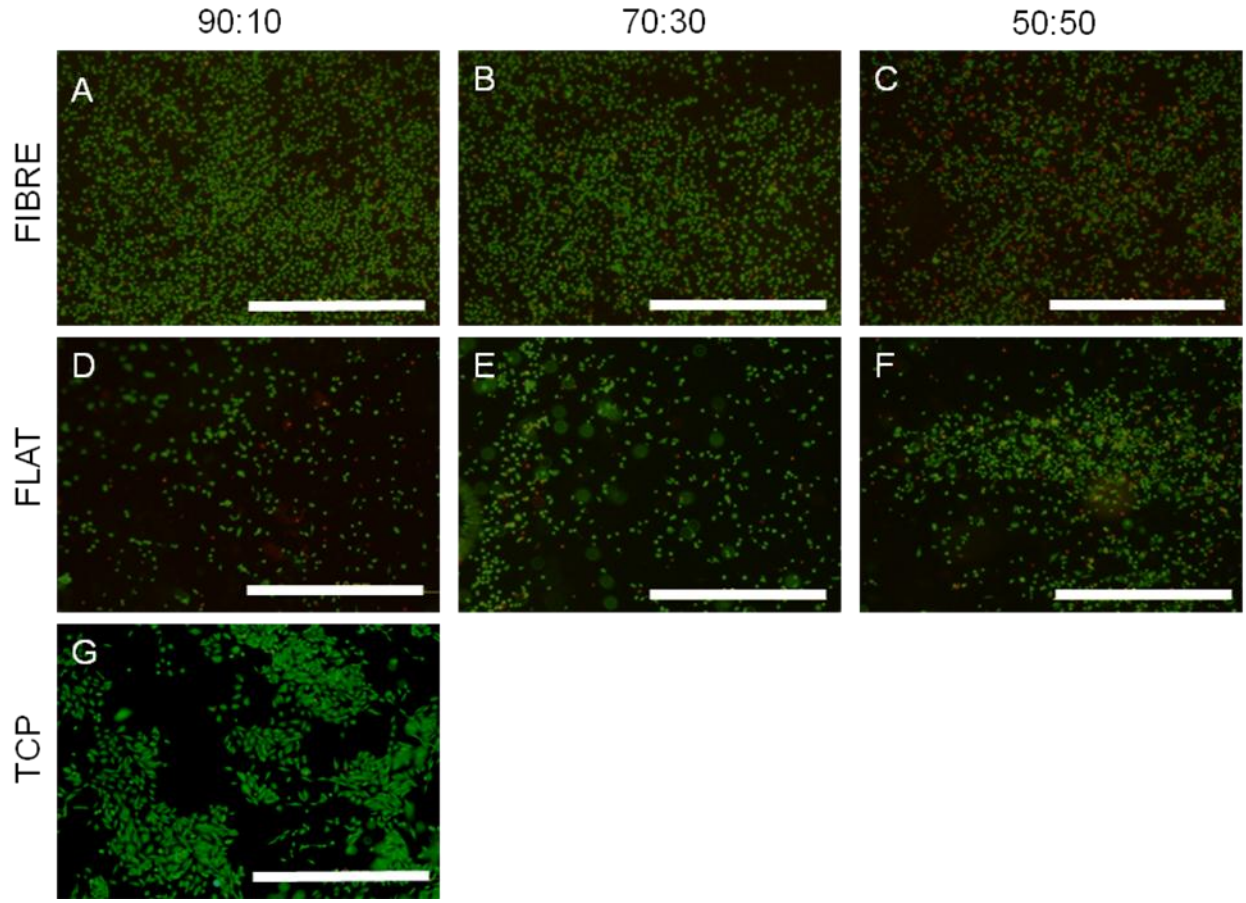

Figure 4.4 LIVE-DEAD® viability assay of Saos-2 cells cultured on MA-DEGMA photocrosslinked fibrous scaffolds, flat surfaces and TCP after 5 days. The green fluorescence represented live cells whereas the red fluorescence, represented dead cells. Scale bar: 1.0 mm.

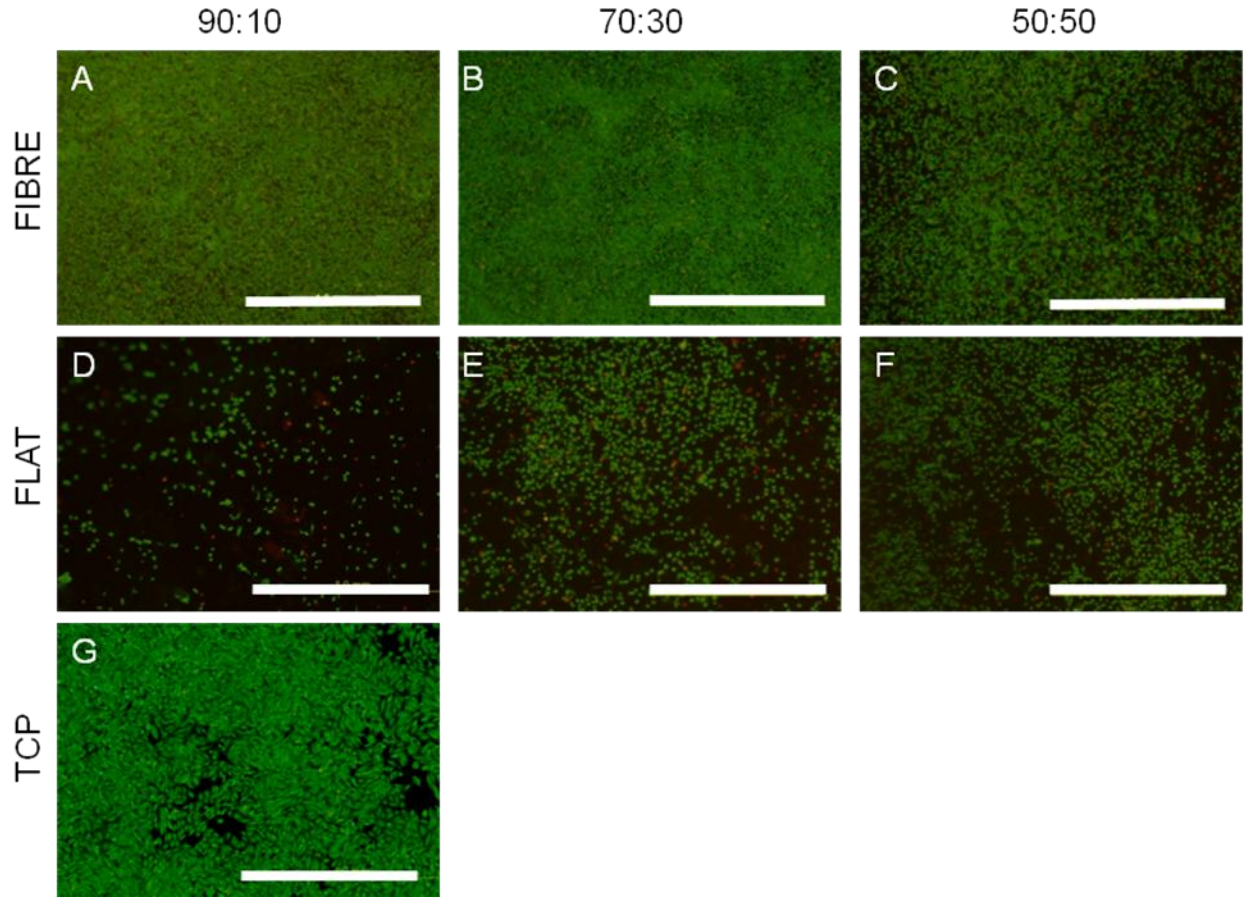

Figure 4.5 LIVE-DEAD® viability assay of Saos-2 cells cultured on MA-DEGMA photocrosslinked fibrous scaffolds, flat surfaces and TCP after 10 days. The green fluorescence represented live cells whereas the red fluorescence, represented dead cells. Scale bar: 1.0 mm.

To further confirm the viability of the cells on the different scaffolds, actin and nuclei (DAPI) immunostaining were performed (Figure 4.6). The increase in cell number in the 90:10 (MA:DEGMA) fibrous scaffolds over 10 days in culture demonstrated in the AlamarBlue® and the LIVE-DEAD® assays was also observed here, clearly confirming the scaffolds synthesized support cell growth. In addition, to examine the morphological shape of the cells on the MA:DEGMA fibres, actin and nuclei (DAPI) higher magnification images were shown (Figure 4.7). At day 10, the spindle shape cells on the fibres displayed organized actin filaments indicating cell spreading and cells were healthy.

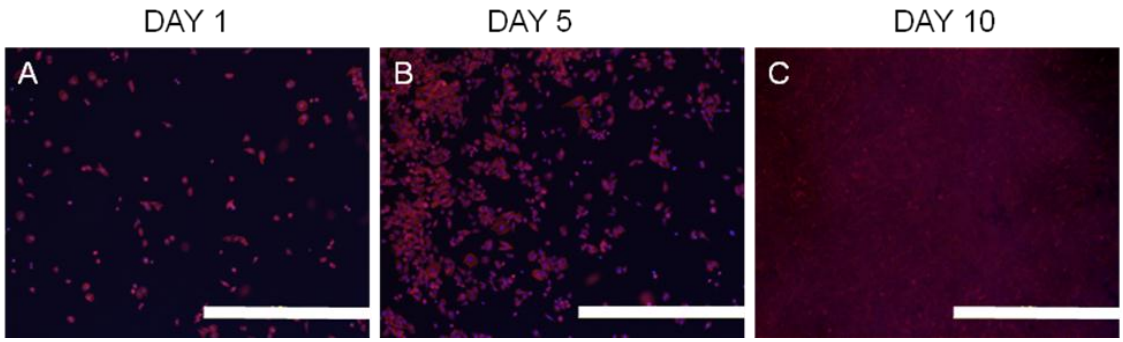

Figure 4.6 Actin and DAPI immunostaining of Saos-2 cells cultured on the 90:10 (MA:DEGMA) photocrosslinked fibrous scaffolds, at day 1,5 and 10. Actin filaments are labelled with Alexa-phalloidin 568, and appear in red and nuclei are labelled with DAPI, appearing in blue. Scale bar: 1.0mm.

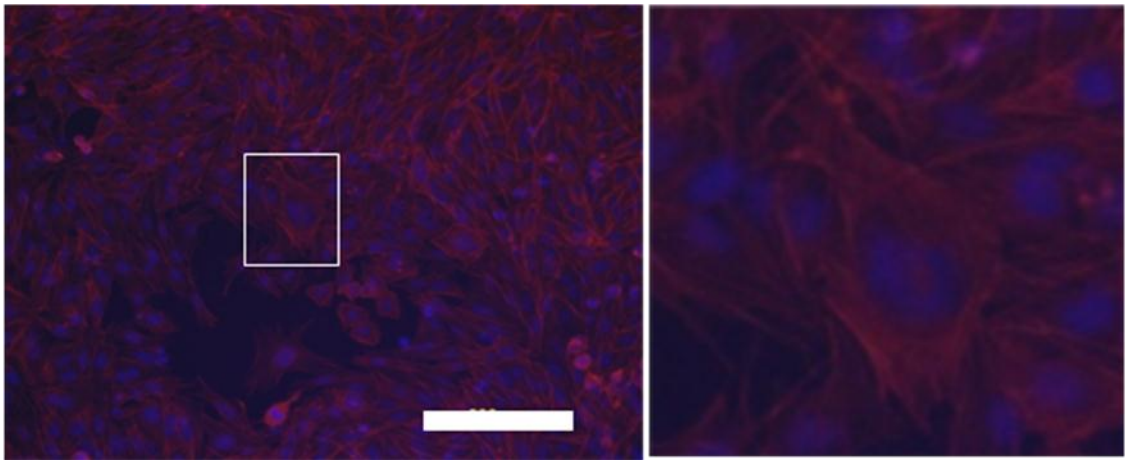

Figure 4.7 Higher magnification of actin and DAPI immunostaining of Saos-2 cells cultured on 90:10 (MA:DEGMA) photocrosslinked fibrous scaffolds at day 10. Actin filaments are labelled with Alexa -phalloidin 568, appearing in red, and nuclei are labelled with DAPI, appearing in blue. White box indicates higher magnification showed in the right image. Scale bar: 200µm.

The results presented here strongly demonstrate the potential of MA:DEGMA fibrous scaffolds to support Saos-2 cell viability and proliferation. The fibrous scaffolds were significantly better in promoting cell growth when compared with their equivalent flat surfaces. Amongst the fibrous scaffolds, however, the 90:10 (MA:DEGMA) fibres were the ones that presented the highest cellular activity. Both cell viability and cell number were significantly higher in the 90:10 scaffolds when compared to the other fibrous scaffolds tested. This could be correlated with the most uniform fibrous morphology (typical characteristic of electrospun fibres) of the 90:10 scaffolds in comparison to other scaffolds, as described in Chapter 3. Badami *et al.* revealed that MC3T-E1 cells adhere better in fibres in comparison to smooth flat surfaces [222], which is in agreement with our results that show that scaffolds with fibrous features were preferred by Saos-2 cells compared

to smooth surfaces. The fibrous architecture can alter the mode of cell anchorage and filopodia of the cells [223]. Elements of the fibrous architecture allow filopodia to anchor more tightly, and such mode of anchorage could also contribute to enhance the adhesion strength to the fibrous scaffold [223]. Interestingly, cell viability and proliferation reduced as fibre diameter size increased due to the welding of the fibres with high DEGMA concentrations after PEO extraction. The effect of surface topology on cell response will be discussed in detail in Section 4.4.2 using hMSCs.

To confirm the orientation and penetration of cells with respect to the fibres, Figure 4.8 shows a SEM image of Saos-2 cells cultured on 90:10 (MA:DEGMA) photocrosslinked fibrous scaffolds at day 5. The Saos-2 cells do not penetrate into the fibrous scaffold due to the small pore sizes of the fibrous scaffold in comparison to the size of the cells. In addition, the cells do not orientate themselves to the surface of the fibres. Moreover, Figure 4.12 also shows the lack of hMSCs penetration into the scaffold. Hence, one of the major limitations of the acrylate fibrous scaffolds is the lack of cell infiltration. The improvement of cell infiltration throughout the scaffold was discussed in page 55.

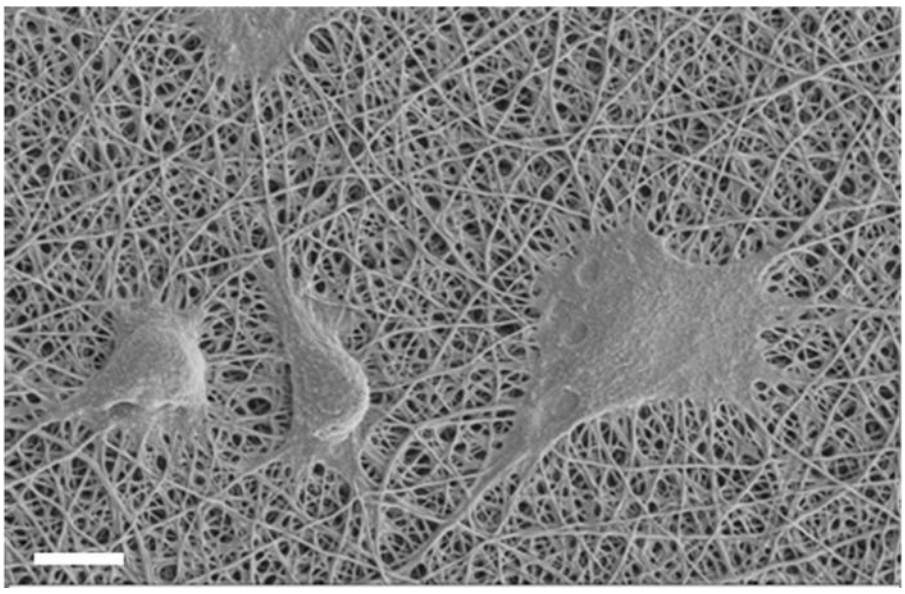

Figure 4.8 SEM image of of Saos-2 cells cultured on 90:10 (MA:DEGMA) photocrosslinked fibrous scaffolds at day 5. Scale bar: 30μm.

Contradicting results have been shown in the cytotoxic effects of MA based dental resins, Engel [224] and Tao [225] research groups presented positive results in cell proliferation on MA based matrices while Kojima [226], Nocca [227] and Chang [228] groups showed MA has cytotoxic effects on cell viability. The cytotoxic effects are probably due to unreacted monomers leaching out from the network rather than the polymer itself. There is a possibility that photocrosslinking of resins produces varying levels of crosslinking due to uneven UV light intensity throughout the

volume of the sample which may cause some unreacted monomers to be produced and leach out *in vitro*. Cytotoxic effects of free MA monomers were demonstrated by Eiichi Yoshii [229]. Investigations by About *et al.* showed decreasing amounts of unreacted acrylate monomers improved cell viability and differentiation of human pulp cells into odontoblasts [230, 231].

Consequently, it is critical that no monomers are leaching out from the fibrous scaffolds and flat surfaces investigated in this study. To ensure this, the flat surfaces were washed in acetone and ethanol for 5 days. The unreacted monomers were then thoroughly extracted before cell culture experiments and the elutant products were collected for ^{1}H-NMR studies. No monomers or photoinitiator were detected in the ^{1}H-NMR (results not shown), which ensures the biological response was not affected by monomer leaching. Also, ^{1}H-NMR studies described in the previous chapter showed no monomers and photoinitiator were present in the fibrous scaffold. It is possible that, during the PEO extraction process, unreacted monomers leached out. However, this effect of monomers leaching is probably less seen in fibrous scaffolds because the UV light intensity throughout the fibres is more uniform/constant due to a decreased overall mass and the topology of the scaffolds. Moreover, it might be more difficult to extract the unreacted monomers from the resin compared to the fibres.

The type of acrylate monomers used for crosslinking also plays a pivotal role. A study by Imazato *et al*. showed hydroxyethyl methacrylate (HEMA) decreased MC3T3-E1 viability and osteogenic differentiation in contrast to the same concentration of triethylene glycol dimethacrylate (TEGMA) and methyl methacrylate (MMA) monomers which did not affect growth and differentiation [232]. In contrast, another study demonstrated increased cell viability of MG63 osteoblast cells on HEMA hydrogels [205].

A range of photoinitiators, each with its unique adsorption spectrum, is currently available or being developed. Nonetheless, the production of high-energy radicals generates a potential for oxidative damage to the cells [185]. The free radicals can cause cell death by damaging cell membranes, nucleic acids and proteins [183, 184]. Irgacure 2959 was selected for the UV electrospinning system because it has been shown to have minimal toxicity over a broad range of mammalian cell types and species [203]. Bryant *et al.* investigated the toxicity profile of multiple photoinititors on NIH/3T3 fibroblast cell line and demonstrated that Irgacure 2959 had negligible effects on these cells viability [233]. Currently, Irgacure 2959 is used ubiquitously in many UV hydrogel systems [21, 178, 179, 216, 234].

The effect of chemistry on Saos-2 viability was also assessed. However, surface morphology took precedence in the effect on cell viability when assessed on fibrous scaffolds. The fibres morphology was what most significantly affected cell viability. Flat surfaces displayed a different trend of increase of cellular viability. The cells growing on the 50:50 ratio (MA:DEGMA) surfaces

showed the highest cell viability on flat surfaces, followed by the cells grown in the 70:30 surfaces and finally those grown on the 90:10 surfaces. The increase in hydrophilicity of the surface, due to increased DEGMA concentration, enhanced the overall cell viability. This result directly contrasts the trends of wettability for cell adhesion/behaviour, suggesting the role of other properties of the scaffold should be considered.

4.4.2 Determination of the effect of varying MA:DEGMA compositions on hMSCs (comparison between fibrous scaffolds and 2D surfaces)

To further investigate the biological potential of the fibrous scaffolds, their ability to sustain viability of hMSCs was evaluated. MSCs are uncommitted cells that are characterized by their ability to differentiate in response to specific cues [82, 84]. Many research groups are investigating the development of scaffolds for three dimensional MSCs culture. Thus, similarly to what was described in the previous section, the effect of varying concentrations of MA:DEGMA fibres and flat surfaces on hMSC cell viability was evaluated using total DNA and AlamarBlue® assays.

Firstly, total DNA assay was performed to evaluate the effect of varying MA:DEGMA ratios on hMSCs viability cultured in the fibrous scaffold (Figure 4.9). At day 1, the cell activity of hMSCs was clearly reduced by the MA:DEGMA fibrous scaffolds. Total DNA content significantly decreased for all MA:DEGMA concentrations in comparison to the control. A slight increase in cell viability was observed at day 2 but, similarly to what was seen at day 1, hMSCs viability in the fibrous scaffolds was significantly lower when compared to hMSCs cultured in TCP.

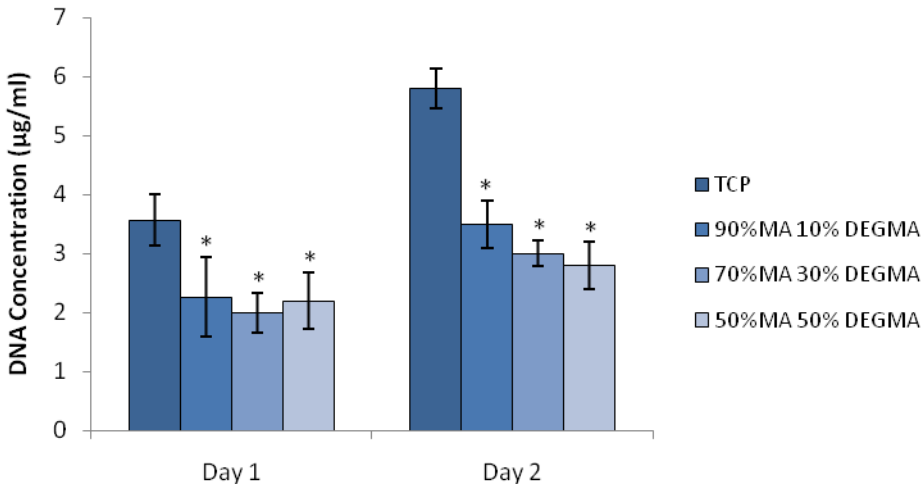

Figure 4.9 Effect of varying ratios of MA:DEGMA fibrous scaffolds on hMSCs cell viability using total DNA assay. Mean ± SD, n = 3. (*) indicates the difference between the marked bar and the control (TCP) of the same time period is statistically significant (p<0.05).

At day 1, the AlamarBlue® results (Figure 4.10) showed a significant reduction of cell viability when hMSCs were cultured on both MA:DEGMA fibrous scaffolds and flat surfaces in comparison to the control (TCP). Similarly, this trend was observed at days 5 and 10. At day 5, the 50:50 (MA:DEGMA) flat surface displayed significantly lower cell viability in comparison to the fibrous scaffold with the same chemistry. Interestingly, a concentration-dependent trend was observed. MSCs cultured in the 90:10 (MA:DEGMA) fibrous scaffolds showed the highest level of cell activity, followed by the 70:30 and finally the 50:50 (MA:DEGMA) scaffolds. This concentration-dependent trend was also observed at day 10, both for fibrous scaffolds and flat surfaces. Moreover, hMSCs cultured on flat surfaces presented a significantly lower cellular activity when compared to cells grown in fibrous scaffolds with an equivalent chemical composition.

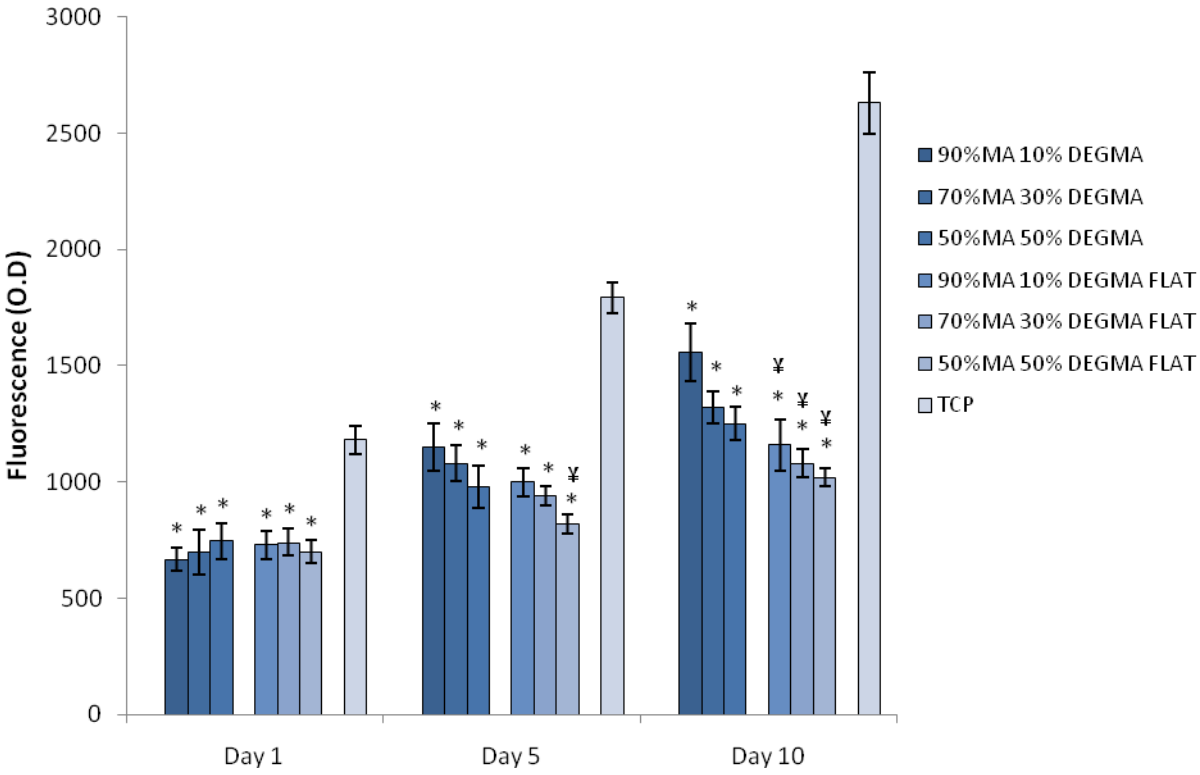

Figure 4.10 Viability of hMSC cultured on MA-DEGMA photocrosslinked fibrous scaffolds, flat surfaces with equivalent compositions and TCP assessed by AlamarBlue® assay. Mean ± SD, n = 3. (*) indicates the difference between the marked bar and the control (TCP) of the same time period is statistically significant. (¥) indicates that the difference between the marked bar and flat surface with same chemical composition of the same time period is statistically significant (p<0.05).

To further investigate the biological potential of the fibrous scaffolds, their ability to sustain cell viability over a longer period was conducted (Figure 4.11). The results obtained displayed no significant increase in cell viability at early time-points (1, 5 and 10 days) for all fibrous scaffolds.

However, from day 15 onwards, a significant enhancement of hMSC viability was observed for cells cultured in the 90:10 (MA:DEGMA) constructs. This enhancement in cell growth was not shown for other compositions. Hence, it indicates that, in the long term, the 90:10 ratio (MA:DEGMA) scaffolds support hMSCs viability better than the other scaffolds produced.

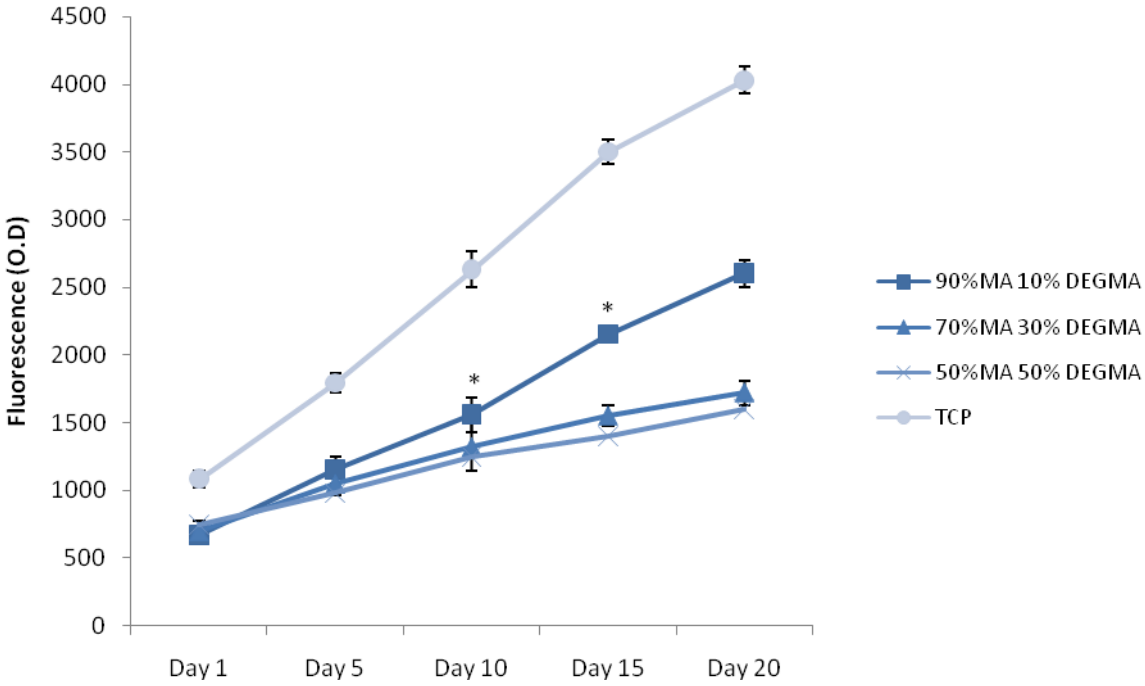

Figure 4.11 Long-term viability of hMSCs cultured on MA-DEGMA photocrosslinked fibrous scaffolds with varying MA:DEGMA ratios, using the AlamarBlue® assay. Mean ± SD, n = 3. (*) indicates the difference between the marked bar and the control (TCP) of the same time period is statistically significant (p<0.05).

The attachment and cell morphology of hMSCs cultured on the fibrous scaffolds are shown in the high magnification SEM images (Figure 4.12). A reduction in cell number was observed in a concentration-dependent manner following MA:DEGMA concentration. The highest cell number was observed on the 90:10 (MA:DEGMA) fibrous scaffolds, followed by the 70:30 and finally the 50:50 (MA:DEGMA) constructs. Clear differences in cell morphology were observed in all MA:DEGMA constructs when compared to TCP. The hMSCs cultured on the 90:10 (MA:DEGMA) scaffolds exhibited a more spread out morphology, more comparable to the cells grown on TCP. However, as DEGMA concentration was increased in the scaffolds, the hMSCs displayed a spindle-like morphology. This was especially seen for cells cultured on the 50:50 (MA:DEGMA) fibres. Similar results on cell attachment and morphology for the fibres can be seen in the immunostaining images in Figure 4.13.

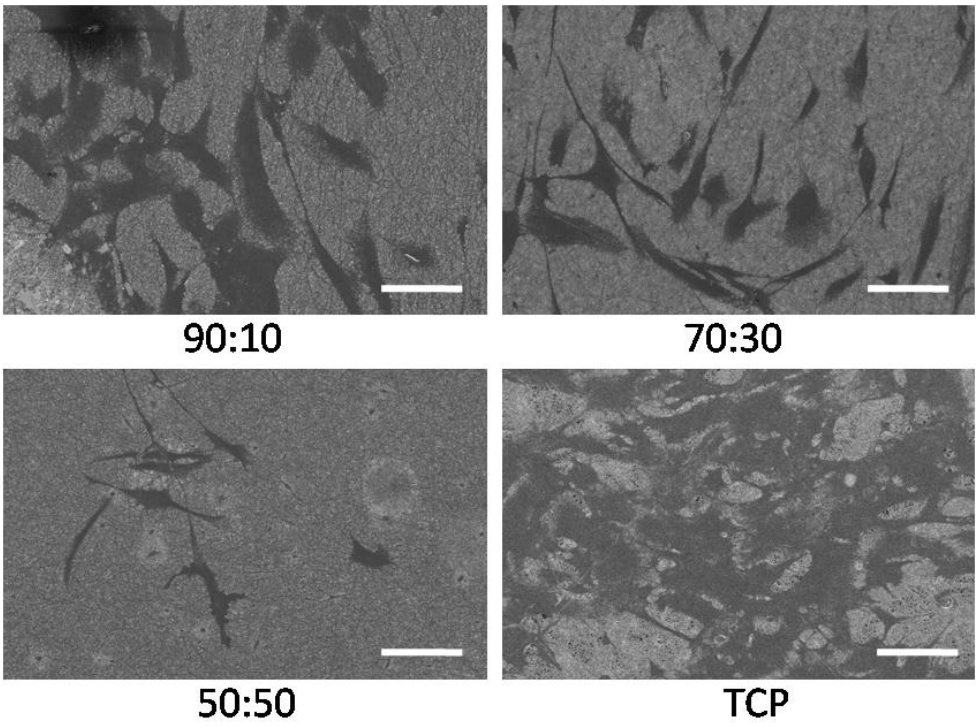

Figure 4.12 SEM images of hMSC cultured on fibrous scaffolds with varying ratios of MA:DEGMA for 10 days. Scale bar: 100µm

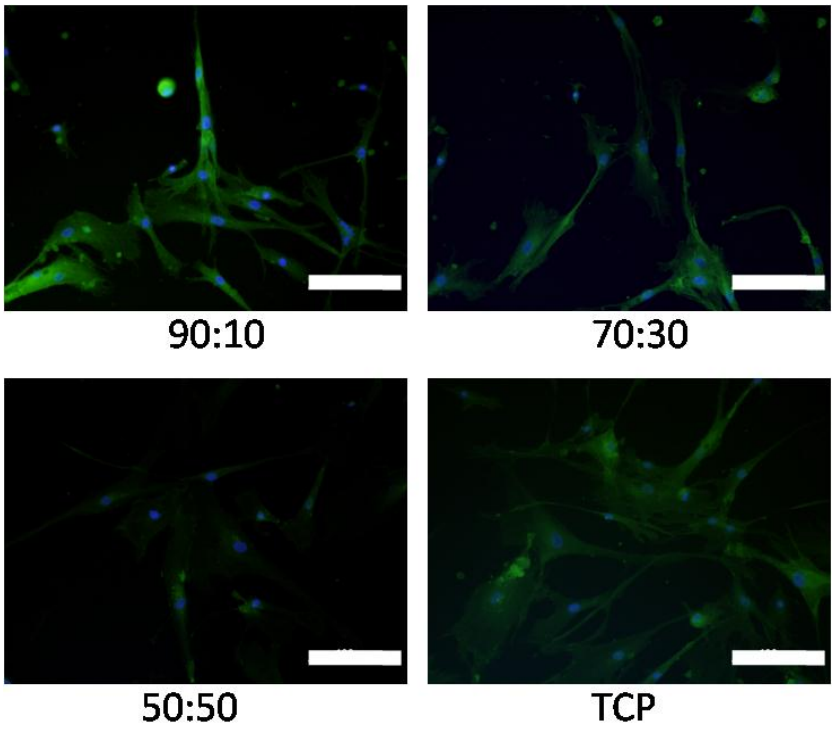

Figure 4.13 Actin and nuclei (DAPI) immunostaining of hMSC cells cultured on fibrous scaffolds with varying ratios of MA:DEGMA at day 10. Actin filaments were labelled with Alexa-phalloidin 488, appearing in green. Nuclei were labeled with DAPI, appearing in blue. Scale bar: 100µm.

To determine whether varying ratios of MA:DEGMA and the architecture of the scaffold affects hMSCs death, the level of apoptosis was evaluated using the Caspase-glo® assay that measures the activity of caspases-3 and -7 (Figure 4.14). Confirming the results obtained with the AlamarBlue® assay discussed previously, a significant increase in apoptosis was observed for

hMSCs cultured in the MA:DEGMA fibrous scaffolds when compared to the control (TCP). Furthermore, at day 5, the MA:DEGMA flat surfaces presented significant higher levels of apoptosis if compared to the fibrous scaffolds. This increase in apoptosis levels was more evident at day 10, which reflects the decrease in cell viability on flat surfaces in contrast to fibrous scaffolds. At day 5, the effect of chemistry on programmed cell death was also observed. As DEGMA concentration was increased, for 70:30 and 50:50 (MA:DEGMA) scaffolds, caspases-3 and -7 activities also increased for both fibrous scaffolds and flat surfaces.

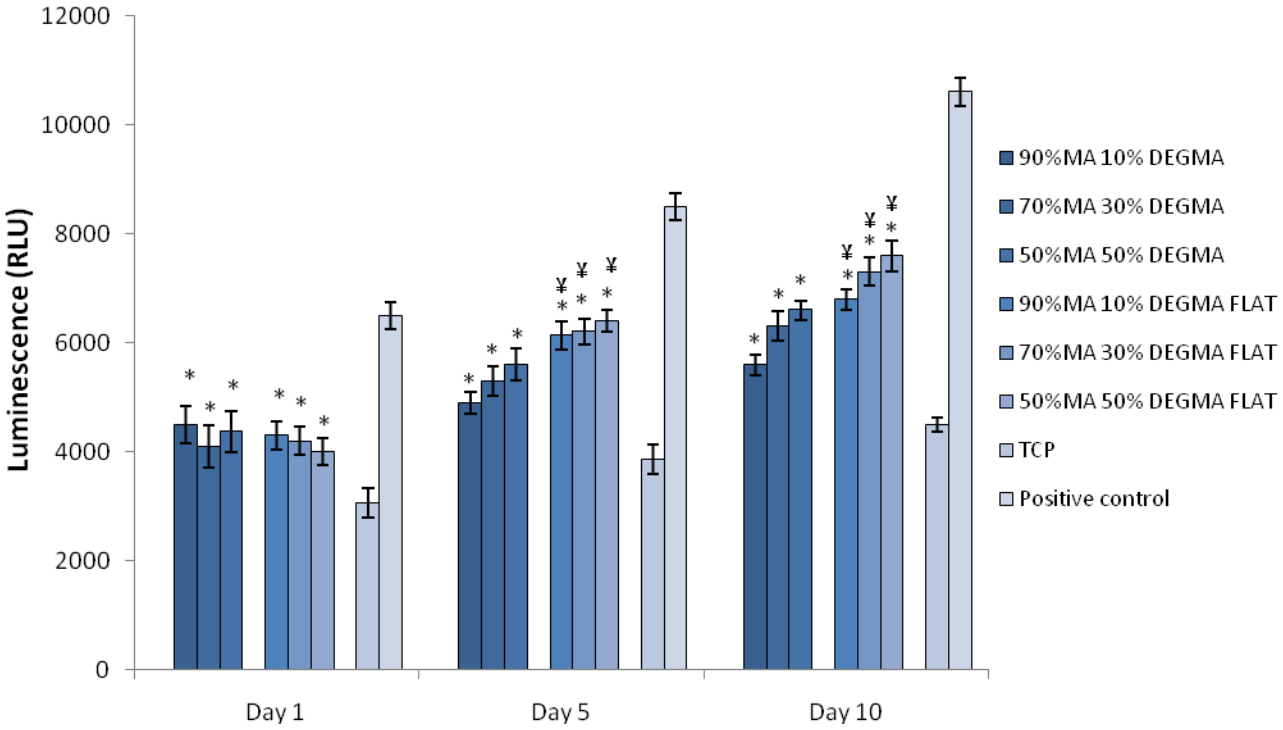

Figure 4.14 Caspase-glo® assay of hMSCs cultured on MA-DEGMA photocrosslinked fibrous scaffolds, flat surfaces and TCP. Cells treated with Staurosporine for 6 hours was used the positive control. Mean ± SD, n = 3. (*) indicates the difference between the marked bar and the control (TCP) of the same time period is statistically significant. (¥) indicates that the difference between the marked bar and flat surface with same chemical composition of the same time period is statistically significant (p<0.05).

The increase in apoptosis when hMSCS were cultured on the fibrous scaffolds or the flat surfaces demonstrated the lower potential of the MA/DEGMA scaffold to support hMSCs attachment and viability. This was also evident in the total DNA and AlamarBlue® results, which showed decreased hMSCs viability in comparison to TCP. Human MSCs behaviour is markedly different from the Saos-2 cells. The MA:DEGMA fibrous scaffolds were able to support viability of Saos-2 cells. This difference in overall cell viability could be due to the fact that Saos-2 cells are an immortalized cell line and they have the ability to grow for an indefinite number of passages. In addition, a study by

Kilpadi and colleagues has shown that Saos-2 and MSCs use different integrins when adhering to serum-coated surfaces and that these cells also display a different preference for selected ECM biomolecules [218, 235]. Furthermore, Saos-2 cells and MSCs utilize different mechanisms during cell attachment, exhibiting different adhesive behaviours and integrin expression profiles [218]. Thus, although the osteoscarcoma cells represent a suitable model for studying osteoblastic differentiation on scaffolds, these cells do not mimic the behaviour of MSCs during the stages of cellular adhesion to a biomaterial [218]. It is recognized in literature that the attainment of a transformed phenotype effects aberrant expression and/or activity of integrin receptors [218, 236-238].

There are only few studies in the literature on electrospinning of monomers. Kim and colleagues introduced a novel method of reactive electrospinning whereby 2-hydroxyl methacrylate, methacrylic acid, ethylene glycol dimethacrylate, AIBN and a photoinitiator were prepolymerized and subsequently photochemically crosslinked during electrospinning [186]. However, no cell culture studies were reported in their work. The first study found in literature which developed electrospun fibres from monomers and investigated cellular response on the fibres was reported by Tan *et al*. [10]. The authors successfully electrospun photocrosslinked macromers from a library of multifunctional poly(β-amino-ester)s, but preliminary cell studies using bovine MSCs have shown limited cell adhesion to the fibers, contrary to the results shown in our study [10]. Sundararaghavan and his co-workers created multiscale porous scaffolds, utilizing photopatterning and electrospining methacrylated hyaluronic acid, to enhance cellular infiltration of hMSCs. However, cell viability was demonstrated to be significantly low [187]. The low cell adhesion observed in their investigation could either be due to cytotoxic effects of the macromer itself or to the presence of PEO. Failure of PEO extraction would cause PEO to block protein adhesion, which would consequently affect cell adhesion. Such effect was not shown in the present investigation. Subsequently, the same research group increased the viability and proliferation of hMSCs by using photocrosslinkable acrylate-poly(glycerol sebacate) and co-electrospinning with gelatin instead of PEO [177].

The data presented here showed that surface architecture of the scaffold significantly affected viability and apoptosis of both Saos-2 and hMSC cells. Specifically, the 90:10 (MA:DEGMA) fibrous scaffolds were shown to better enhance cell activity, followed by the 70:30 and finally the 50:50 (MA:DEGMA) scaffolds. The fibrous morphology was preferred by both Saos-2 and hMSC cells when compared to flat surfaces. Furthermore, as fibre diameter size increased due to the welding and swelling of the fibres with high DEGMA concentrations after PEO extraction¸ cell viability and proliferation decreased considerably. It is well known that cells respond differently to various topographic substrates and to the geometry of the surfaces [239-242]. *In vivo*, cells are enveloped by nanostructures, formed by biomolecules organized in different arrangements, when

interacting with other cells or with the ECM [242]. Numerous studies have shown topography influences cell adhesion and proliferation [222, 224, 239, 243, 244]. Surface architecture can alter the mode of cell anchorage and filopodia of the cells have been reported to direct certain structures [223]. Elements of the surface architecture allow filopodia to anchor more tightly, and such mode of anchorage could also contribute to enhance the adhesion strength to the fibrous scaffold [223]. Thus, the role of scaffolds is more than that of offering mechanical support but also act as surfaces providing topographical cues to influence cell adhesion, spreading, proliferation and even differentiation [241, 242]. Engel and colleagues have shown that microstructured poly (methyl-methacylate) promoted rat MSC adhesion and induced osteogenic differentiation in comparison to flat surfaces [224]. Hence, the results presented in this chapter are in agreement with these studies.

The effect of surface chemistry on hMSC cellular activity was observed for all fibrous scaffolds produced. However, surface morphology (the presence of fibrous surfaces) took precedence in affecting cell viability, as it was described above. A trend of enhanced cell proliferation was observed with increased scaffold hydrophobicity, as MA concentration was increased for both fibrous and flat surfaces. The increase in hydrophobicity with increasing MA content on flat surfaces was investigated and described in Section 3.4.7 (page 94). This is in agreement with the work of Metter *et al.,* that showed that hMSCs activity was dependent on chemistry, using a library of photopolymerizable poly (β-amino ester)s [245]. This is likely to be because of differences in protein adsorption on the surfaces, which regulates adhesion to the scaffold [245]. It is established that protein adsorption is higher on hydrophobic surfaces and decreases on hydrophilic surfaces [246, 247] [245]. This has been further confirmed with protein absorption studies conducted and described in the next section.

4.4.3 Determining the effect of varying MA:DEGMA compositions on protein adsorption (comparison between fibrous scaffolds and 2D surfaces)

Protein adsorption is the first step that occurs when a foreign surface is placed in contact with blood [94]. Therefore, understanding the mechanism of protein adsorption is pivotal for the design of biomaterials surfaces. Protein adsorption to all fibrous scaffolds and flat surfaces synthesized was assessed. For this purpose, fibrous samples were incubated in 25% (w/v) FBS for four hours and the adsorbed proteins were later extracted with 1% (w/v) sodium dodecyl sulphate (SDS) and assessed using the BCA assay. Both fibrous scaffolds and flat surfaces displayed significantly lower protein adsorption compared to TCP (Figure 4.15). However, the fibrous scaffolds adsorbed higher amounts of serum proteins than the flat surfaces. This was most evident for the 90:10 (MA:DEGMA) ratio constructs, whereby the protein adsorption of the flat surface decreased to half

when compared to the fibrous scaffold. This interesting data gives evidence that the fibrous architecture can alter protein adsorption.

In addition, the 50:50 (MA:DEGMA) ratio exhibited lowest protein adsorption compared to different chemical concentrations for both fibrous and flat samples. Such low protein adsorption could be due to decreased hydrophobicity of the samples as DEGMA concentration is increased. The changes in hydrophobicity of flat surfaces were observed as DEGMA concentration was increased. This was investigated and described in Section 3.4.7 (page 94). In general, hydrophobic surfaces tend to adsorb larger amounts of proteins than hydrophilic surfaces [94, 246]. This is explained by the fact that high water levels within the surface of the materials encourage a low interfacial energy and reduce both protein adsorption and cell adhesion on the polymeric surface [94].

Exposure of a biomaterial to a biological environment causes immediate adsorption of proteins to its surface [248, 249]. It has been demonstrated that the material surface characteristics governs the type, amount and conformation of the adsorbed proteins and moreover the cell-mediated protein turnover [118, 246, 250, 251]. Hence, a critical feature in influencing the response of cells with the material surface and to its performance *in vitro* and *in vivo* is the composition and conformation of the adsorbed proteins [246].

Therefore, protein adsorption results could also explain the higher cell viability of both Saos-2 cells and hMSCs on fibrous scaffolds observed in the total DNA and Alamarblue® assays. Most cells are anchorage-dependent and need attachment to the substrate for maintenance of viability and growth [252]. In consequence, the early occurrences that happen when a cell contacts a surface are critical [253]. It is established that cell adhesion and successive cellular events are regulated by proteins adsorbed onto biomaterial surfaces [94, 252]. Therefore, this suggests that the electrospun scaffolds offer a more favourable environment for cells due to their fibrous features. The fibrous morphology of the scaffolds can increase cell adhesion to the fibrous scaffolds through enhanced protein adsorption [223, 253]. The improvement of protein adsorption for scaffolds with fibrous architecture was demonstrated by Woo and co-workers [253]. The author demonstrated that PLLA nanofibrous scaffolds adsorbed four times more proteins than scaffolds with solid walls [253], which could be due to higher surface-to-volume ratio of fibrous scaffolds.

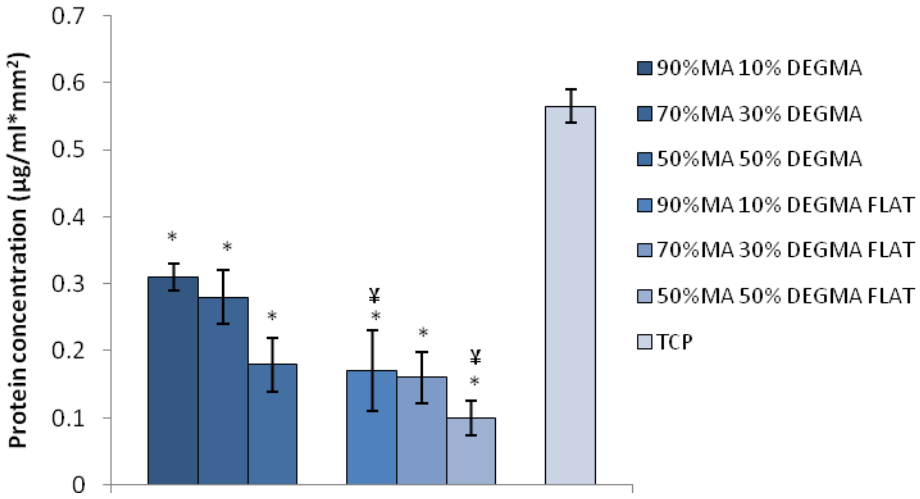

Figure 4.15 Protein adsorption studies on MA:DEGMA photocrosslinked fibrous scaffolds, flat surfaces and TCP. Mean ± SD, n = 3. (*) indicates the difference between the marked bar and the control (TCP) of the same time period is statistically significant. (¥) indicates that the difference between the marked bar and flat surface with same chemical composition of the same time period is statistically significant (p<0.05).

CONCLUSION

The present chapter describes cell studies performed with the acrylate fibrous scaffold developed and described in the previous chapter. These studies were intended to evaluate the effect of varying ratios of MA:DEGMA of the fibrous scaffold on the viability of two different cell types, namely Saos-2 and hMSCs. Additionally, the effect of surface morphology on cellular activity was assessed by comparing the fibrous scaffolds to flat surfaces with equivalent chemical compositions. Lastly, the response of protein adsorption to all fibrous scaffolds and flat surfaces was evaluated.

The results presented here strongly demonstrated the potential of MA:DEGMA fibrous scaffolds to support Saos-2 cell viability and proliferation. In agreement with literature, the MA:DEGMA photocrosslinked fibres increased the viability of Saos-2 cells in comparison to flat surfaces with similar chemistry. However, the considerable increase in apoptosis of hMSCS cultured on both fibrous and flat samples suggested a lower potential of the MA:DEGMA scaffold to support hMSCs cell attachment and viability. This was also evident in cell activity results, which showed decreased hMSCs viability in both the fibrous scaffolds and the flat surfaces when compared to TCP. On the other hand, to further investigate the biological potential of the fibrous scaffolds, their ability to sustain cell viability over a longer period of time was evaluated. From day 15 onwards, a significant increase in cell viability was observed for hMSCs cultured on the 90:10 (MA:DEGMA) fibres. Such a result was not observed for the other fibre compositions. Hence, this gives evidence that the 90:10 (MA:DEGMA) fibrous scaffolds could potentially support hMSCs viability better than the other scaffolds produced.

Furthermore, amongst the fibrous scaffolds and flat surfaces, the 90:10 (MA:DEGMA) fibres presented the highest cellular activity for both Saos-2 and hMSCs, which could be correlated to them displaying the best fibrous morphology compared to all the scaffolds (shown in Chapter 3). Hence, as it has shown the highest cell response, uniform fibrous morphology and capability of maintaining mechanical integrity, the 90:10 (MA:DEGMA) composition was chosen as the best fibrous scaffold for bone tissue engineering purposes among the different compositions analysed. For this reason, the studies described in following chapters were performed using this specific MA:DEGMA composition.

CHAPTER 5

Functionalization of acrylate scaffolds with cell adhesive peptides - DGEA and RGD

5.1 INTRODUCTION

Biomaterial scaffolds can be designed and developed to interact with cells by mimicking key molecular events of the ECM [7]. ECM is comprised of many bio-macromolecules such as collagens, proteoglycans, laminins and fibronectin and it is mainly this biological information which is responsible for ECM bioactivity [7, 26]. Interaction of integrins which are receptors on the cell surface with specific ECM molecules can activate signalling pathways leading ultimately to gene expression [27, 28]. The variety of ECM proteins presented to cells in a specific tissue is pivotal in regulating how cells function within that tissue type [7].

One approach to include sites of integrin binding in biomaterials is to incorporate purified ECM proteins for example fibrin and collagen [7]. However, supplementing full proteins to scaffolds can be challenging to execute as proteins are susceptible to denaturation and degradation [29]. For this reason, a frequently used technique to enhance cell adhesion is to integrate short peptide motifs or analogues derived from binding regions of ECM components [7]. While they may only have a fraction of the activity of the complete protein, they can be incorporated at very high concentration and increase the overall activity of the peptide. Moreover, peptides are easy to synthesize and functionalize. Hence, bioactive peptides offer a synthetic and scalable alternative to complex ECM proteins [30].

The widely used Arg-Gly-Asp (RGD) peptide sequence present in various ECM proteins, including fibronectin, laminin, collagen I, fibrinogen and vitronectin was studied as a mode of enhancing cell adhesion by inducing focal adhesion through integrin interaction on biomaterial surfaces as early as the 1980's [31, 32]. Since then RGD has been functionalized into an extensive range of surfaces, scaffolds and hydrogels (reviewed in [33], [34] and [35]). The binding specificity of the peptide to cell surface integrins receptor can be enhanced by flanking peptides, peptide conformation and immobilisation strategies [33, 35, 132]. Higher affinities for integrins can be improved by flanking the key peptide sequence with extra amino acids such as glycine [35]. For example, GRGDS is the most commonly used RGD sequence [254].

DGEA (Asp-Gly-Glu-Ala) is a collagen type 1 peptide sequence and has displayed specific binding affinity for osteoblasts via the $\alpha_2\beta_1$ integrin. In addition, DGEA has been shown to induce osteogenic differentiation [36-38]. Therefore, DGEA could be used to promote cell adhesion and control differentiation [38]. Nevertheless, the cellular response of collagen-derived peptides has been relatively less studied compared to other ECM peptides, while full collagen has been mostly applied for making scaffolds [39-41]. Moreover, it has been revealed that collagen I interacts with different integrin receptors than that of fibronectin and the integrin/collagen I binding is RGD-independent [42].

There are numerous strategies for immobilising peptide sequences on materials. One of the key advantages of the UV electrospinning system investigated here (electrospinning of acrylate monomers and post-crosslinking (refer to section 3.3.3)) is the capability of conjugating peptides in a simple yet elegant and potentially efficient “one pot synthesis” manner. In this chapter, the research will focus on using cysteine-functionalized RGD or DGEA peptide sequences in combination with MA/DEGMA monomers and employing a photoinitiated mixed-mode polymerization mechanism. Specifically, the acrylate monomers/crosslinkers are mixed with the cysteine-conjugated RGD or DGEA peptides and electrospun. During UV radiation, the reaction mechanism consists of two reactions, acrylate homopolymerization and the thiol-acrylate step growth reaction widely known as thiol-ene reaction [140, 141]. The reaction sequences are summarized below:

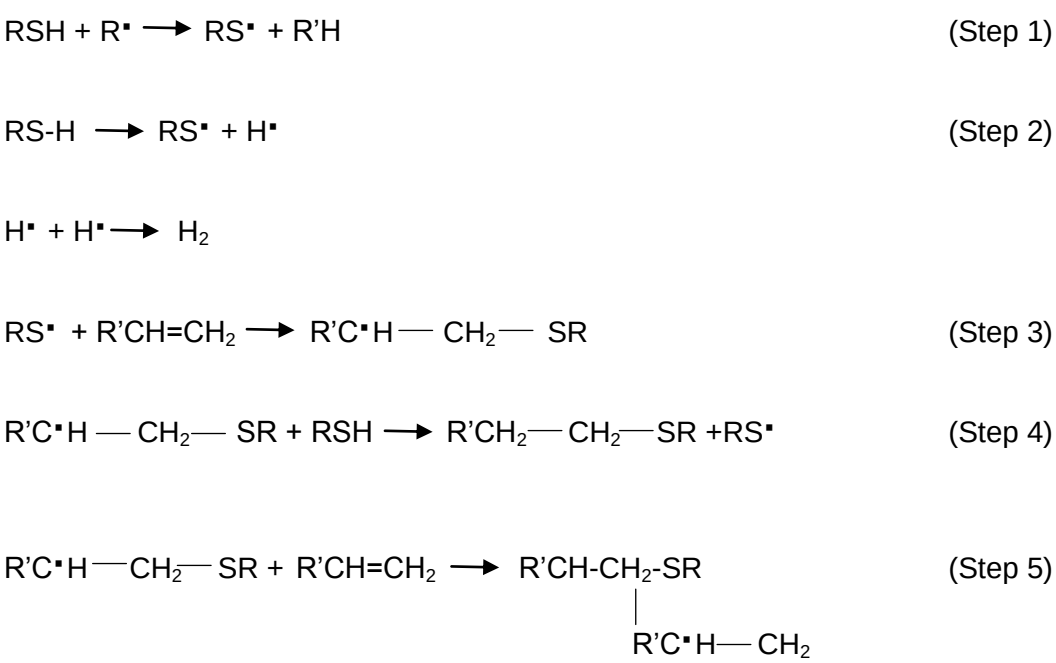

The polymerization is initiated photochemically and progresses through the reactions outlined above. The radical can be generated by radical abstraction from the photoinitiator and also simultaneously by photochemical S-H bond cleavage (steps 1 and 2), this is followed concurrently by step growth reactions (steps 3 and 4), the thiol-acrylate or more generally thiol-ene reaction. Next, this is followed by the acrylate homopolymerization (step 5) [140, 141, 255].

As previously described in Chapters 3 and 4, photocrosslinked fibres were successfully developed by electrospinning different MA and DEGMA compositions and post-UV crosslinking. Varying MA and DEGMA concentrations affected the overall fibre morphology, swelling and the mechanical properties of the fibrous scaffold. In addition, studies described in the same chapter determined the

optimal range of parameters required to produce uniform and bead-free electrospun MA/DEGMA fibrous scaffolds. Moreover, the results presented in Chapter 4 provided strong evidence that MA/DEGMA fibrous scaffolds can support Saos-2 cell viability and proliferation. However, the considerable increase in apoptosis of hMSCs for all fibrous scaffolds and flat samples demonstrates lower potential of the MA/DEGMA scaffolds to support hMSCs attachment and viability. Hence, to increase the overall bioactivity of the scaffold, conjugation of signalling peptides onto the scaffold was investigated. In this chapter, the development of electrospun polyacrylate scaffolds conjugated with biological active peptides, RGD and DGEA, will be described.

5.2 MATERIALS

Aluminium Scanning Electron Microscopy (SEM) pin stubs and adhesive carbon tape were purchased from Agar Scientific (UK). Ten ml Becton Dickinson plastic syringes and 27G Becton Dickinson disposable needles were from Cole Palmer (UK). Ellman's and OPA assays were purchased from Thermo Scientific (UK). The high voltage supply was acquired from Glassman High Voltage Inc. (UK), the UVB lamp (Transilluminator 2000) from Biorad (UK) and single-syringe infusion pump (230 VAC) and static fibre collector (labarotory jiff-jacks) from Cole-Parmer (UK). Amino acids were purchased from AGTC Bioproducts (UK) or Novabiochem, (UK). Ninhydrin assay, poly(ethylene oxide) (PEO)(200kDa) (95.5%), methyl acrylate (MA) (99%), diethylene glycol dimethacrylate (DEGMA)(95%), 2-hydroxy-4′-(2-hydroxyethoxy)-2-methylpropiophenone (Irgacure 2959) (98%), trifluoroacetic acid (TFA) (≥99%), diethyl-ether (DEE) (≥99%) were obtained from Sigma Aldrich (Poole, England). All chemicals were used as received and stored in a dry and dark environment to maintain photoreactivity.

5.3 METHODS

5.3.1 Synthesis of Peptides

The peptides, CGDGEA (cysteine-glycine-aspartic acid-glycine-glutamine-alanine, N-terminus to C-terminus) and CGRGD (cysteine-glycine-arginine-glycine-aspartic acid, N-terminus to C-terminus) were synthesized using a Solid Phase Peptide Synthesis (SPPS) [256] using Fmoc-protected amino acid monomers and HOBt/HBTU activation on a peptide synthesiser 433A (Applied Biosystems, UK). In each coupling step, a 10-fold excess of amino acids was used. After, the peptide sequences were cleaved from the resin and deprotected using trifluoroacetic acid (TFA), phenol and diethyl ether (DEE) before they were desiccated for 2 days. The dried product was redissolved in dH_2O and lyophilized. Molecular weight and purity of the peptide were determined by high performance liquid chromatography (HPLC) system model GX-271 (Gilson, Sweden) and matrix-assisted laser desorption/ionization (MALDI) mass spectrometry courtesy of the Chemistry Department, Imperial College London, using a MALDI micro MX (Micromass, UK). HPLC analysis showed that the purity of the peptides was ≥95% and MALDI-ToF mass spectral analysis confirmed the molecular weight of the peptides (please refer to Appendix).

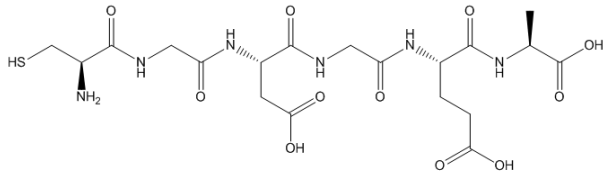

CGDGEA

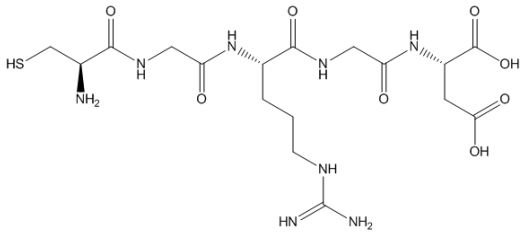

CGRGD

Figure 5.1 Chemical structure of the peptides used in this study, CGDGEA and CGRGD.

5.3.2 Preparation of peptide conjugated electrospun fibres

The preparation of the acrylate scaffold was illustrated in Chapter 3 (Section 3.3.3) however in this chapter with the addition of cysteine-conjugated peptides (Figure 5.1). One refers to Table 3.2 in Chapter 3 (page 81) for details on electrospinning solution and parameters. The conditions identified for the (90:10) mol% MA:DEGMA concentration was used for all the scaffolds in this chapter. The peptides were added at different concentrations (0.5, 1, 2 and 5 mol%) to the MA:DEGMA composition.

Briefly, the monomer mixtures were prepared by mixing (90:10) mol% of methyl acrylate (MA) and diethylene glycol diacrylate (DEGMA) and varying concentrations of peptides (0.5, 1, 2 and 5 mol%). Next, 0.1 mol% 2-Hydroxy-4′-(2-hydroxyethoxy)-2-methylpropiophenone (Irgacure 2959) was added to the solution. Then, 10% (w/v) PEO concentration in ethanol mixture was added to the solution and mixed thoroughly for 30 minutes with help of a magnetic stirrer. The electrospinning solution was added into a syringe with a 27-gauge blunt-ended needle. Next, electrospinning was carried out in the set-up described previously in Section 3.3.3. The fibres were immediately exposed to UV light for 10 minutes using a UVB (302nm) lamp in an oxygen free environment. After photocrosslinking, PEO from the scaffold is extracted from the scaffold by repeated washing with water for 5 days. The process of producing the photocrosslinked peptide immobilized fibrous scaffolds with *in situ* peptide conjugation is shown in the schematic below (Figure 5.2).

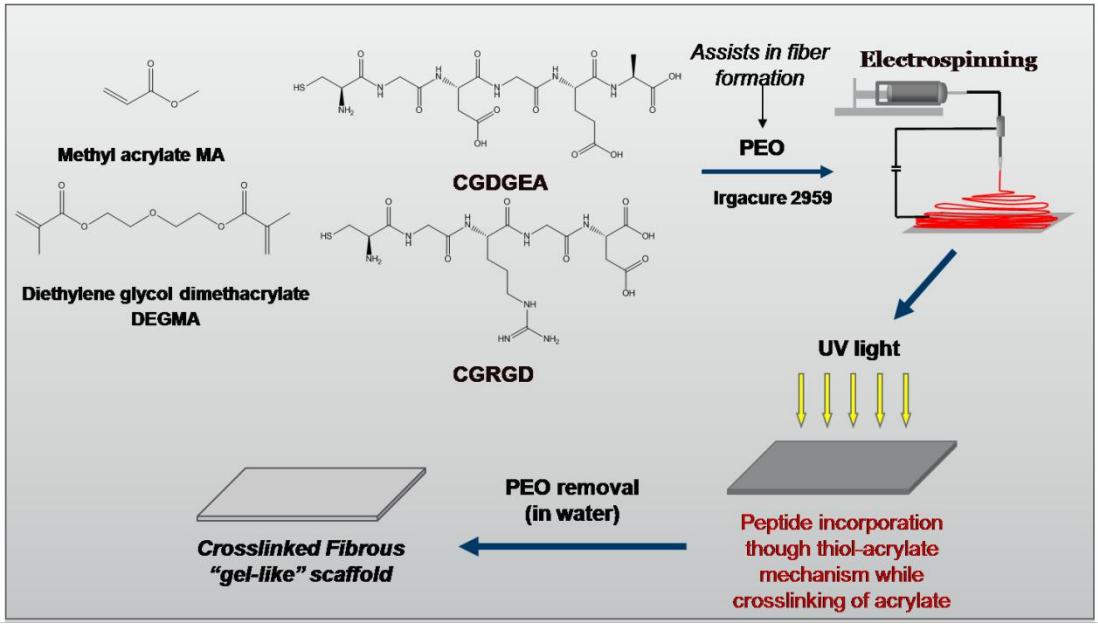

Figure 5.2 Schematic of the preparation of a photocrosslinked fibrous scaffold with *in situ* peptide conjugation. The fibrous scaffolds were produced by electrospinning monomer mixtures prepared by mixing (90:10) mol% of methyl acrylate (MA) and diethylene glycol diacrylate (DEGMA) and varying concentrations of peptides (0.5, 1, 2 and 5 mol%). Next, 2-Hydroxy-4′-(2-hydroxyethoxy)-2-methylpropiophenone (Irgacure 2959) was added to the solution. Then, 10% (w/v) PEO concentration in ethanol mixture was added to the solution and mixed thoroughly for 30 minutes with help of a magnetic stirrer. Subsequently, the fibres were photocrosslinked by exposure to UVB, which induces a photoinitiated mixed-mode polymerization mechanism to conjugate the peptides. Finally, PEO was extracted by repeated washing with water.

5.3.3 Ninhydrin assay

Ninhydrin (2,2-dihydroxyindane-1,3-dione) is a chemical used to specifically determine the presence of primary amine groups. The reaction of ninhydrin with primary amine groups produces a dark blue (Rheumann's Blue) colour. The assay was performed as previously described [117, 257] to quantitatively detect the amount of amine groups on scaffolds. Briefly, the scaffolds and controls were immersed in 1M ninhydrin solution for 6 hours in glass vials. The vials were then incubated at room temperature for 4 hours, placed on an orbital shaker, to ensure the reaction occurred between ninhydrin and the amine groups on the scaffolds. The scaffolds were then removed and the absorbance of the solution was measured at 570nm, on a microplate reader (Spectramax M5, Molecular devices). A calibration curve was obtained using glycine standards (please refer to Appendix for protocol). The amount of free amine measured was compared to the initial concentration of free amine in the soluble fraction solution prior to UV crosslinking to determine the percentage of peptide incorporation.

5.3.4 Fluoraldehyde (OPA) assay

OPA (*o*-phtalaldehyde) reagent is a primary-amine fluorescent detection reagent. When OPA interacts with primary amines in the presence of mercaptoethanol, OPA produces an intense blue colour fluorescent that has an excitation wavelength of 340nm and emission at 455nm [258, 259]. The assay was performed accordingly to the manufacturer's instructions. The scaffolds and controls were immersed in OPA solution for 1 hour in glass vials, in a dark room. The scaffolds were then removed and the fluorescence of the solution was measured at excitation at 330-390nm and emission at 436-475nm, on a microplate reader (Spectramax M5, Molecular devices). A calibration curve was obtained using glycine standards (please refer to Appendix for protocol). The amount of free amine measured was compared to the initial concentration of free amine in the soluble fraction prior to UV crosslinking to determine the percentage of peptide incorporation.

5.3.5 Ellman's assay

The Ellman's reagent [260], which contains 5-5'-dithio-bis(2-nitrobenzoic acid) and is also known as DNTB, is a chemical used for measuring free sulfhydryl groups in solution. A solution of DNTB yields a yellow-colour sample when it interacts with sulfhydryls. DNTB reacts with free sulfhydryl molecules to produce a mixed disulfide and 2-nitro-5-thiobenzoic acid (TNB) product. The amount of sulfydryl groups in a sample can be calculated by using a standard curve comprised of known concentrations of a sulfhydryl solution, such as cysteine. The assay was performed as indicated by the manufacturer. Briefly, the scaffolds and controls were immersed in the Ellman's reagent solution, which contained Ellman's reagent and reaction buffer solution, for 3 hours in glass vials, at room temperature and placed on an orbital shaker. The scaffolds were then removed and the absorbance was measured at 412nm, on a microplate reader (Spectramax M5, Molecular devices). A calibration curve was obtained using cysteine standards (please refer to Appendix for protocol).The amount of sulfydryl groups measured was compared to the initial concentration of free thiols prior to UV crosslinking to determine thiol conversion.

5.3.6 Surface analysis of CRGD conjugated scaffolds using Time of Flight-Secondary Ion Mass Spectrometry (ToF-SiMS)

The ToF-SIMS investigation on the surface of the RGD-conjugated scaffolds was analyzed by Nia Bell, another Ph.D. student from Prof. Stevens's group. Samples were prepared by electrospinning cysteine-conjugated peptide and acrylate monomer mixtures as described in the previous section

(Section 5.3.2). Importantly, samples were electrospun as thinly as possible, 10 – 20 µm on aluminium foil. After UV post-crosslinking and PEO extraction, the samples were sectioned into 1x 1 cm^2 dimensions and mounted on silicon wafer chips and the samples were stored under nitrogen. The samples were analyzed within 24 hours. ToF-SIMS analysis was carried out on an IonTOF V instrument (IONToF, Germany) using a 25 keV Bi_3^+ primary ion from a liquid metal ion gun (LMIG). Positive ion mass spectra from 100µm x 100µm were collected in the high current bunched mode (HCBM) with a typical mass resolution of 7,000 for the $C_2H_5O^+$ ions at m/z 45. All spectra were mass calibrated using the peaks: CH^+, CH_2^+ , CH_3^+ , $C_2H_5^+$, $C_3H_7^+$ and $C_4H_9^+$. Chemical maps were acquired in burst alignment mode (BAM). The fibres were imaged over 50 µm x 50 µm with 256 x 256 pixels with 20 shots per pixel. All spectra were normalised to CHO^+, an intense polymer derived ion peak. It also normalised for the variable fibre coverage in each analysis area. To display the main findings of the imaging experiment, RGB plots were produced in the IonToF software. A polymer, a peptide and a substrate derived ion were normalised and allocated to the red, green and blue channels respectively. Triplicates of each sample were prepared and high resolution spectra from twelve areas across these were used to investigate the effect of peptide concentration on the peptide derived ion intensities. The areas under the peaks of interest, including those corresponding to the CH_4N^+ and $C_4H_8N^+$ ions, were normalised to that of CHO^+, averaged and recorded along with their associated standard error as a function of peptide concentration.

5.3.7 Morphology analysis of SEM

Fibres produced by electrospinning were examined using scanning electron microscopy (SEM) to analyse fibre morphology and determine approximate fibre diameter. Samples of approximately 1.5cm^2 were placed on adhesive carbon tape and attached to aluminium SEM pin stubs. The samples were sputter coated with chromium. The LEO 1525 Gemini SEM was operated at an accelerating voltage of 5kV.

5.3.8 Mechanical testing of fibrous scaffolds

The electrospun membranes where cut into rectangular shape with dimensions of 10 x 3 cm^2 (n= 10). Uniaxial tensile testing was performed using an Instron Model 5540 with a 50N load cell with constant deformation (5mm/min) on the PEO extracted samples, dried and hydrated (after incubation in deionised water for one hour). Tensile extension and reactive forces were recorded using the Bluehill 2 software, and Young's modulus (E) was calculated from the linear region of the stress-strain curves.

5.3.9 Swelling test

The swelling test was conducted as described in [191] and in Chapter 3 (Section 3.3.10). Briefly, PEO extracted electrospun samples were cut into rectangular shape with dimensions of 10 x 3 cm^2 (n= 5). The fibres were immersed in distilled water and incubated for 6 hours. The wet weight of each sample was measured every hour prior to placing the samples in the vacuum oven at 60°C overnight and weighed again. The dry weight of the samples was determined.

Mass swelling percentage = (wet weight/dry weight) x 100%.

5.3.10 *In vitro* degradation of scaffolds

The *in vitro* degradation study was performed as described in [177] but with longer experimental duration. Five mol% CGDGEA and unfunctionalized scaffolds were used in this study. Briefly, PEO extracted electrospun membrane samples were cut into a rectangular shape with dimensions of 10 x 3 cm^2 (n = 5). The dry scaffolds were weighed before incubating the scaffolds in 150mM NaCl PBS and placed on an orbital shaker at 37°C. The buffer was changed every week to maintain the accelerated degradation conditions. At each time point (2, 4, 8, 12 and 16 weeks) samples were removed and dried in a vacuum oven at 60°C overnight and weighed afterwards. The dry weight of the samples was determined.

Mass loss (%) = ((gd – g0)/ g0) x 100

g0 = initial mass before incubation

5.3.11 Statistical analysis

All experimental data shown were expressed as mean ± SD and were obtained from experiments performed in at least in triplicates. All data analysis was performed in Excel. Statistical analysis was performed with one-way analysis of variance (ANOVA) using multiple comparisons (Bonferonni test) and significance was determined by $p<0.05$. This analysis was performed with Graph Pad InStat software.

5.4 RESULTS AND DISCUSSION

Chapters 3 and 4 described the development of MA/DEGMA photocrosslinked fibrous scaffolds by electrospinning different MA and DEGMA ratio compositions and post-UV crosslinking. The photocrosslinked scaffolds produced were characterized and the cellular response to the fibres was investigated. The results obtained provide strong evidence for the potential of MA/DEGMA fibrous scaffolds to support Saos-2 viability and proliferation. However, the considerable increase in apoptosis of hMSCS grown in all fibrous scaffolds and flat samples demonstrates the rather poor ability of the MA/DEGMA scaffold to support hMSCs attachment and viability. This was also evident in the cell activity assays, which showed decreased hMSCs metabolic activity assessed by Alamarblue® assay in comparison to the negative control, TCP. Hence, to increase the overall bioactivity of the scaffold, the effect of conjugating CGDGEA and CGRGD peptides onto the acrylate scaffolds was investigated.

This chapter is divided into four main sections. Firstly, immobilization of DGEA and RGD peptides on the acrylate fibrous scaffolds by mixed-mode thiol-acrylate photopolymerization was analyzed by varying cysteine-conjugated DGEA and RGD concentrations. Next, the morphology, swelling, mechanical and degradation behaviour of the functionalized acrylate scaffolds was investigated. Subsequently, the presentation of peptides on the surface of the scaffolds was studied using ToF-SIMS. Lastly, the effects of varying the glycine spacer length on peptide immobilization on the scaffolds were assessed.

As described previously in Chapter 3, Section 3.3.3, post-photocrosslinking was method chosen to obtain a scaffold made up of acrylate fibrils by employing UV radiation to initiate polymerization after electrospinning. In this chapter, the CGRGD and CGDGEA peptides were incorporated into the fibrous scaffold through a photoinitiated thiol-acrylate reaction with the thiol groups located on the cysteines. This reaction was previously described in [141]. The preparation of the acrylate scaffold was illustrated in Chapter 3 (Section 3.3.3) however in this chapter with the addition of cysteine-conjugated peptides. The conditions identified for the (90:10) mol% MA:DEGMA concentration was used for all the scaffolds in this chapter. The peptides were added at different concentrations (0.5, 1, 2 and 5 mol%) to the MA:DEGMA composition. These different concentrations were selected because of its biological relevance for many peptides.

5.4.1 Determination of the effect of varying peptide concentration on overall peptide incorporation

5.4.1.1 Measurement of peptide incorporation by measuring free primary amine

Both the amount of peptide presented to the cells and the degree of functionalization are essential parameters that influence the success of a system as a cell adhesive material [35]. The approximate final concentration of peptides in a scaffold can be regulated by the feed concentration [35]. In addition, the concentration of the peptide can be regulated by varying the ratio of peptide-containing thiol monomer with acrylate co-monomers during synthesis of the scaffold. Hence, the thiol-acrylate peptide functionalization was studied with varying cysteine-conjugated DGEA and RGD concentrations (Figure 5.3). This was performed by determining the amount of primary amine groups on the scaffolds, which was performed using the ninhydrin and o-phthalaldehyde (OPA) assays. The final amount of unreacted amine measured was compared to the concentration of free amine prior to UV crosslinking. The CGDGEA and CGRGD peptide sequences were utilized for this study. The glycine amino acid was chosen in the peptide sequence to study the reactivity of the thiol groups with the presence of glycine during the thiol-acrylate polymerization. Glycine was used as a spacer residue to increase bioactivity of the peptide sequence, this will be described further in Section 5.4.7 and in Chapter 7 (Section 6.4.3). Determination of the peptide incorporation into the scaffolds was attempted using ATR-FTIR but clear differences in IR-spectra were not detected and could not be analyzed quantitatively (data now shown).

Figure 5.3 shows that no significant differences in peptide incorporation were observed for both CGRGD and CGDGEA peptides between all peptide concentrations tested. The cysteine-conjugated peptides showed above 85% of peptides were incorporated into the scaffolds. The only exception was displayed for 0.5 mol% concentration of both CGRGD and CGDGEA peptides, which showed 82% and 78% conjugation, respectively. However, complete peptide incorporation (100%) could not be achieved. Both ninhydrin and OPA assays gave very small differences in amine concentrations but the ninhydrin assays showed slightly higher amine measurements. This could be due to difference in the sensitivity of the assay. A qualitative method, using ninhydrin spray was also used to successfully confirm peptide immobilization on the surface of the scaffold (results not shown). These results prove that a very large proportion of peptides were incorporated in all scaffolds and are present in the fibrous scaffolds and accessible to small molecule chemical reagents.

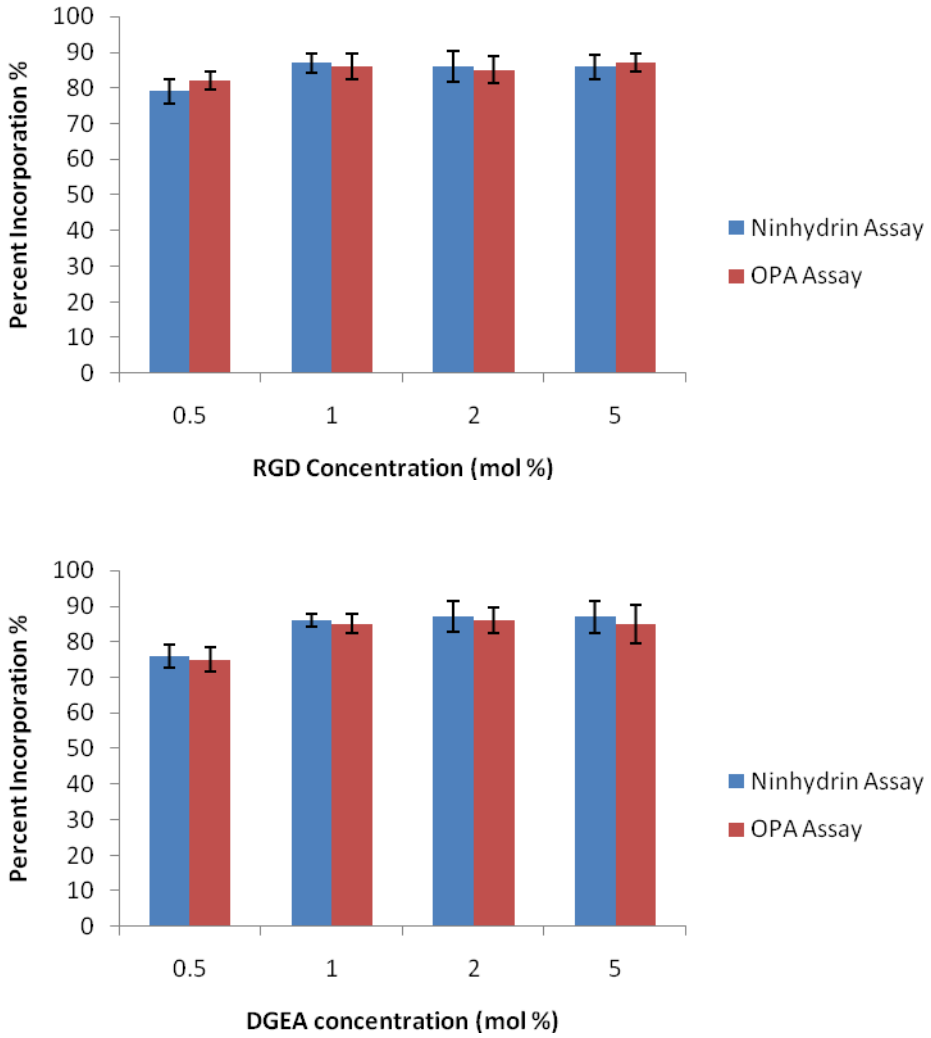

Figure 5.3 Variation of peptide incorporation of either CGRGD or CGDGEA with different concentrations of peptides (0.5, 1, 2 and 5 mol%) onto 90:10 MA:DEGMA scaffolds using ninhydrin and OPA assays. Mean ± SD, n = 3.

The measurement of peptide incorporation was further confirmed by quantifying the free sulfhydryl groups in solution using the Ellman's assay (Figure 5.4). The amount of thiol conversion measured was compared to the initial concentration of free thiol, prior to UV crosslinking. No significant differences in thiol conversion (around 85%) were observed between all peptide concentrations tested above 1 mol% for both CGRGD and CGDGEA peptides. Moreover, no significant differences were found between peptide incorporation of the CGDGEA and CGRGD peptides. A decrease in thiol conversion was however shown for the lowest peptide concentration tested (0.5 mol%) for both peptides, but was with no statistical significance. This may be due to the assay's sensitivity to low concentrations.

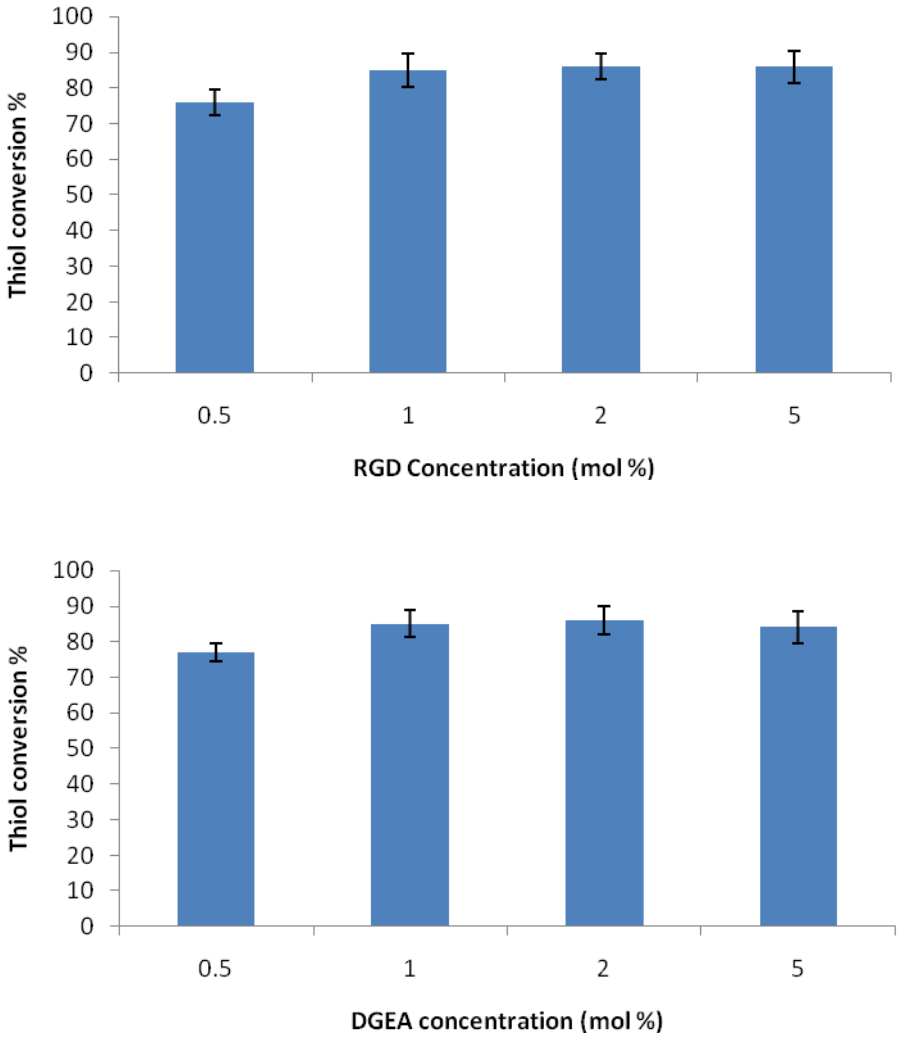

Figure 5.4 Determination of thiol conversion of peptides of either CGRGD or CGDGEA with different concentrations of peptides (0.5, 1, 2 and 5 mol%) onto 90:10 MA:DEGMA using Ellman's assay. Mean ± SD, n = 3.

The ninhydrin, OPA and Ellman's assay results herein demonstrated that both peptides, CGRGD and CGDGEA, could be efficiently conjugated into the fibrous acrylate scaffolds, for all different peptide concentrations, using a thiol-acrylate reaction. Complete peptide incorporation (100%) could not be achieved for any of the scaffolds. Salinas and co-workers reported a higher degree of peptide incorporation (~ 95%) using the thiol-acrylate conjugation to conjugate thiol-presenting peptides copolymerized with PEG diacrylate hydrogels [141]. In addition, Salinas and Anseth reported a final concentration of ~1mM of CGRGD peptides conjugated on a PEG-hydrogel system using a fluoraldeyde assay which is based on amine measurements similar to ninhydrin and OPA assay utilized in our study [135]. The higher degree of peptide incorporation in their studies may be due to the high concentration of thiol-peptides added into the hydrogel system, 20% overall thiol-peptide concentration in comparison to monomers in comparison to the studies investigated here

[141]. Nonetheless, the peptide incorporation displayed is comparable to other studies using other peptide immobilization chemistries. Using NHS chemistry, 80% of an RGD-containing peptide derivatised with acrylamidohexanoic acid was incorporated when copolymerized with acrylamide and bisacrylamide to form crosslinked gels [31]. Also, the incorporation of different peptides into a poly(ethylene glycol)-diacrylate (PEGDA) hydrogel was investigated by Hern and Hubbell, who found that acrylol-PEG-YGRGDS was incorporated with 84% efficiency [134]. However, these reactions are mechanistically different because these studies utilized vinyl monomers which are conjugated to peptide sequences which will affect the location (in the backbone of the polymer) and presentation of the peptides in the polymer network. Whereas in our study, the use of mono-thiol peptides was utilized, subsequently the peptides will always be incorporated at the chain start.

Several studies have utilized mixed-mode thiol-acrylate polymerization especially for the production of hydrogels. Rydholm and colleagues described the production of degradable thiol-acrylate networks in physiological conditions under exposure to UV light with or without presence of a photoinitiator [142, 143]. Also, work from the same group, by Reddy *et al*., reported the modelling results on the formation and degradation of the thiol-acrylate networks by copolymerization of the thiol monomer with PLA-b-PEG-PLA-based diacrylate macromers [261]. The conjugation of peptides through the mixed-mode thiol-acrylate photopolymerization for synthesis of PEG-peptide hydrogels was introduced by the same research group [135, 141]. Melkoumian and colleagues have demonstrated the synthesis of surfaces made of acrylates-conjugated to biologically active peptides for the culture of undifferentiated hESCs though levels of peptide immobilization were not reported [30]. Peptides derived from active domains of ECM proteins, such as bone sialoprotein, vitronectin, laminin and long or short fibronectin, were conjugated using EDC/NHS chemistry [30].

Alternatively, cysteine-conjugated peptides have been immobilized into hydrogels through Michael-type addition [262-264]. However, this reaction requires a careful balance and tuning of the thiol-acrylate ratio to allow controlled crosslinking and the reaction time is relatively slow compared to radical-mediated photopolymerization [141]. Herein we have utilized the thiol-acrylate polymerization in the UV-electrospinning system to produce RGD and DGEA peptide-functionalized fibrous acrylate scaffolds. This method provides a facile and robust way to incorporate peptides into electrospun scaffolds without the requirement to chemically modify the functional peptide motifs. Moreover, it allows for rapidly incorporating peptides into the fibrous scaffolds at relatively low quantities without the need for a second di-thiol to copolymerize. In addition, the mixed-mode thiol-acrylate approach has the advantage by introducing the peptide at the chain start to control the level of incorporation onto the scaffold.

It is important to note that there are many analytical methods and representations of the amount of peptide immobilized onto the scaffolds in the literature making quantitative comparisons between

the scaffolds developed here and other systems difficult. The nature of the scaffolds should have an impact on the level of quantification based on the same assay. Correspondingly, even if the same methodology for reporting quantification has been used, difference in degrees of swelling or bulk or surface modifications mean that actual ligand densities or concentrations can be different to those reported. For this reason, we have not compared the specific amount of peptides immobilised to many systems but chose the most similar to the scaffolds developed here and used peptide incorporation percentage to make comparisons discussed above.

5.4.2 Determination of the effect of peptide conjugation on fibre morphology

The morphology of the fibres was monitored after PEO extraction for both CGDGEA- and CGRGD-conjugated scaffolds with the varying concentration of peptides (Figure 5.5 and Figure 5.6). It was essential to analyze the fibre morphology as varying the peptides concentration could change the electrospinning parameters and affect fibre formation. Additionally, PEO extraction of the functionalized scaffolds was quantified by determining the mass loss and performing NMR analysis (methods described in detail in Chapter 3 (Section 3.3.8). The results obtained confirmed that PEO was extracted from the functionalized scaffold (results not shown).

It is clearly shown that thiol-acrylate conjugation of CGRGD peptides had no major effect on the overall morphology of the fibres as peptide concentration increased up to 1 mol% (Figure 5.5B and C). Similarly to unfunctionalized scaffolds (Figure 5.5A), upon hydration and after PEO elution out, fibres swelled but maintained the fibrous structure. The fibre diameter for the 0.5 mol% CGRGD concentration was approximately 938 ± 76nm, which was similar to the fibre diameter of the unfunctionalized scaffold (approximately 925 ± 60nm). However, increasing cysteine-conjugated peptides increased the fibre diameter to 1105 ± 67nm and 1204 ± 78nm, for 1 mol% and 2 mol% CGRGD concentrations, respectively. The highest concentration of CGRGD peptides (5 mol%) produced fibres with increased diameter and welding. It is possible that the welding is a result of fibres being brought together through attractive interactions between peptides. The peptides could aggregate during UV-polymerisation or peptides may have agglomerated during the PEO extraction process.

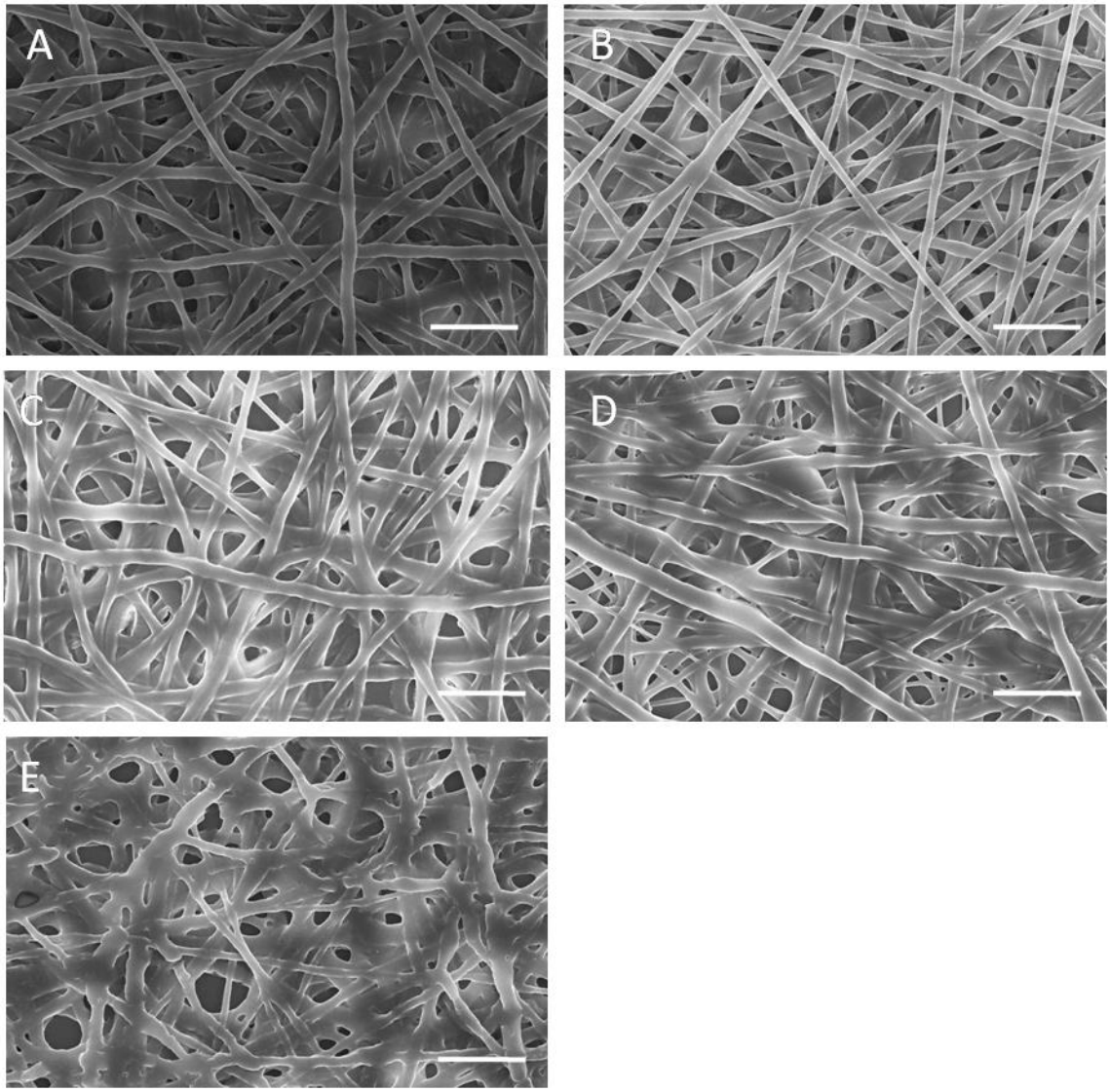

Figure 5.5 SEM micrographs of fibres with varying concentrations of CGRGD peptides after PEO extraction. After electrospinning, the fibres were immediately exposed to UV light for 10 minutes using a UVB (302nm) lamp in an oxygen free environment. After photocrosslinking, PEO from the scaffold is extracted from the scaffold by repeated washing with water for 5 days.CGRGD concentration: A) 0; B) 0.5; C) 1; D) 2 and E) 5 mol%. Scale bar: 5µm.

Similarly, thiol acrylate conjugation of CGDGEA peptides had no major effect on the overall morphology of the fibres as the peptide concentration increased up to 1 mol% (Figure 5.6B and C). Comparable to unfunctionalized scaffolds (Figure 5.6A), after PEO extraction, fibres swelled but maintained the fibrous structure. The fibre diameter for 0.5 and 1 mol% CGRGD was approximately 933 ± 86nm and 928 ± 80nm, respectively, which was similar to unfunctionalized scaffolds. However, increasing cysteine-conjugated peptides increased fibre diameter up to 1080 ± 96nm and 1154 ± 78nm, for 2 mol% and 5 mol% CGRGD concentrations, respectively. In contrast, incorporation of the CGDGEA peptide did not produce fibres with the high welding shown

for the CGRGD peptides. This may suggest that CGDGEA peptides aggregate less than that of CGRGD peptides causing less welding in fibre morphology.

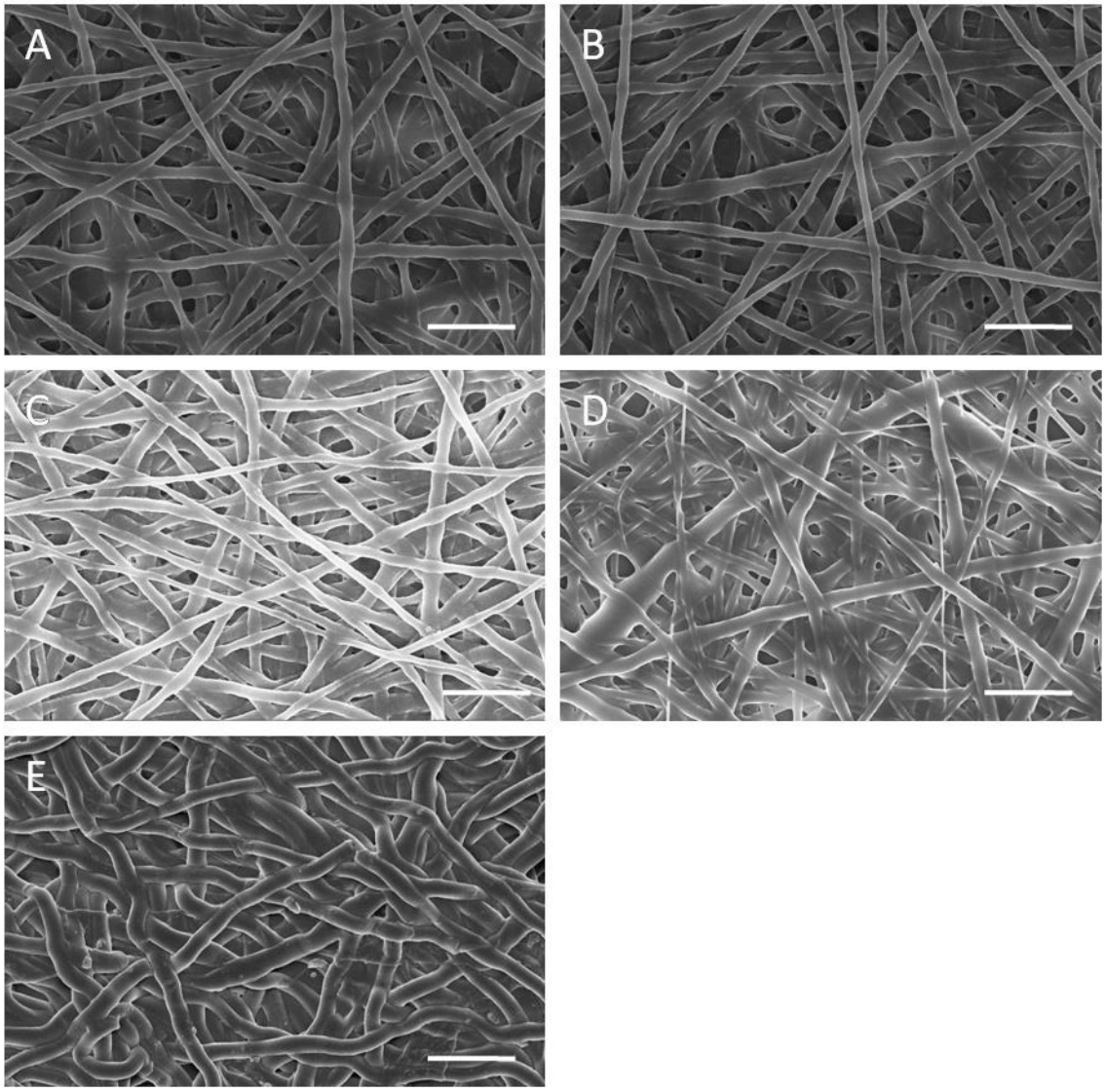

Figure 5.6 SEM micrographs of fibres with varying concentrations of CGDGEA peptides after extracting PEO. After electrospinning, the fibres were immediately exposed to UV light for 10 minutes using a UVB (302nm) lamp in an oxygen free environment. After photocrosslinking, PEO from the scaffold is extracted from the scaffold by repeated washing with water for 5 days. CGDGEA concentrations: A) 0; B) 0.5; C) 1; D) 2 and E) 5 mol%. Scale bar: 5µm.

Some research groups have reported the functionalization of peptides into fibres. RGD was successfully functionalized onto the surface of poly(D,L-lactic-co-glycolic acid) (PLGA) electrospun fibrous [137]. A solution of PLGA and PLGA-b-PEG-NH_2 was electrospun to develop a fibrous membrane with functional amine groups on the surface of the electrospun membrane and the RGD was immobilized onto the aminated surface under hydrated conditions [137]. However, this surface functionalization was limited to the surface of the scaffold and required a two-step process. Another group showed a different peptide immobilization technique by electrospinning a blend of poly(ε-caprolactone) (PCL) and self-assembling oligopeptides [265]. Self-assembled polymer nanofibres were formed due to alternating hydrophilic and hydrophobic side chain groups that was capable of generating extended ordered structures [265]. In addition, our group has recently reported on RGD functionalized-poly(γ-glutamic acid) (PGA) fibrous scaffolds [266]. The peptide was conjugated onto γ-PGA-benzyl via N,N'dicyclohexylcarbodiimide (DCC) and N,N-diisopropylethylamine (DIPEA) coupling reaction and the polymer was electrospun into a fibrous scaffold. These studies shown by Gentilini *et al.* have demonstrated that the functionalizing reactions to immobilize the peptides on the electrospun scaffolds did not affect the overall morphology of the fibres similarly shown to the studies presented here. Moreover, in the system investigated here, the peptides are introduced directly and without the need of additional chemicals which yielded similar desirable results in fibre scaffold morphology as post-conjugation.

5.4.3 Determination of the effect of increasing DGEA peptide concentration on the swelling properties of scaffolds

A unique characteristic of the fibrous scaffold was that swelling could be observed when the scaffold was immersed in water or media. This was discussed in detail in Chapter 3 (Section 3.4.6). The hydrated state of the scaffolds is also more physiologically relevant (i.e. *in vivo)* following incubation in water. To better understand the effect of functionalization of the scaffold with cysteine-conjugated peptides on the gel structure and swelling properties of the scaffold, a swelling study was conducted using a range of different concentrations of CGDGEA-conjugated acrylate scaffolds and compared to unconjugated scaffolds. CGRGD conjugated scaffolds showed similar swelling ratios compared to CGDGEA (results not shown). Systems with acrylate scaffolds were reacted with 0.5, 1, 2 and 5 mol% concentrations of CGDGEA (Figure 5.7). Similar to unfunctionalized fibrous scaffolds, all conjugated fibres with varying concentrations of CGDGEA showed similar swelling behaviour. An initial and short rapid swelling phase (10-30 min) was followed by a slow down of the penetrant uptakes (30-60 mins) and, eventually, the fibres become fully swollen. A trend of increased swelling as CGDGEA concentration increased was observed. The unconjugated scaffolds showed the lowest swelling of ~ 160% and, in contrast, the fibrous

scaffolds with the highest CGDGEA concentration presented swelling ratios significantly higher (~ 180%) than the scaffolds with lower concentrations of CGDGEA attached. Moreover, swelling was higher for peptide immobilized scaffolds despite larger diameter fibres shown in Figure 5.6. The peptide containing fibres seems to be more hydrophilic which consequently increases the overall swelling of the scaffolds. In addition, this illustrates the fact that the swelling ratio depends on the network crosslink density [141, 261]. Hence, as concentration of the peptide increases from 0.5 to 5 mol%, there is the increase in thiol content which alters the network structure, as a result of greater chain transfer, and subsequently the number of crosslinks per kinetic chain decreases, which increases the swelling rate.

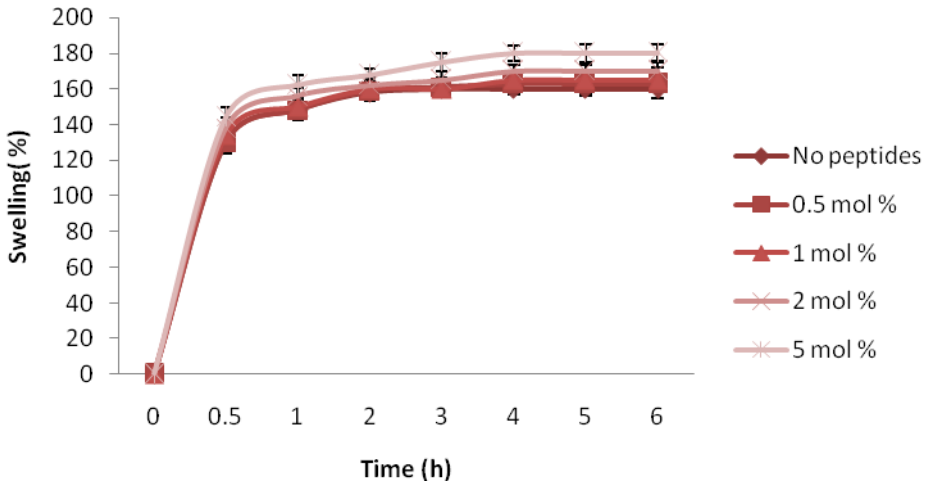

Figure 5.7 Swelling ratios of electrospun fibres for different concentrations of CGDGEA-functionalized scaffolds (0.5, 1, 2 and 5 mol%) and unfunctionalized acrylate scaffolds. Mean ± SD, n = 3.

5.4.4 Determining the effect of increasing DGEA peptide concentration on the mechanical properties of the fibres

Besides surface chemistry and topography, mechanical properties such as modulus are critical for the stability and support of implants/scaffolds in the body, and furthermore certain narrow ranges of stiffness have been shown to modulate cellular functions such as cell attachment, motility and differentiation [4, 204]. Hence, it is essential to characterize the mechanical properties of the fibrous acrylate scaffolds and investigate the effect of varying the peptide concentrations. The mechanical properties of the scaffolds functionalized with varying CGDGEA concentrations were determined in two different conditions: in dry and hydrated states (after PEO extraction), using the uniaxial tensile test to failure (Figure 5.8). The CGDGEA scaffolds were chosen to represent the peptide-conjugated scaffolds for this study however the CGRGD scaffolds needs to be tested.

Different CGDGEA concentrations exhibited no significant differences in the dry scaffolds except for a slight decrease of ~0.6 MPa in the tensile moduli of the functionalized scaffolds compared to unfunctionalized scaffolds. In order to investigate the mechanical properties under more physiological relevant conditions, the fibrous scaffolds were tested following incubation in water. Hydrated scaffolds displayed significantly decreased tensile moduli (~1.6 MPa) in comparison to the respective dry scaffolds. The variability between the dry and hydrated samples is due to water absorption and swelling, which reduces the tensile modulus values hence the scaffold becomes softer becoming more gel-like with increased hydration. However, a trend was displayed for hydrated scaffolds whereby increase in CGDGEA peptide concentration lead to a lower tensile moduli and the highest concentration of CGDGEA (5 mol%) displayed a significant decrease in tensile moduli when compared to the unfunctionalized scaffolds. This relates to the swelling ratios of the scaffolds shown in Figure 5.7.

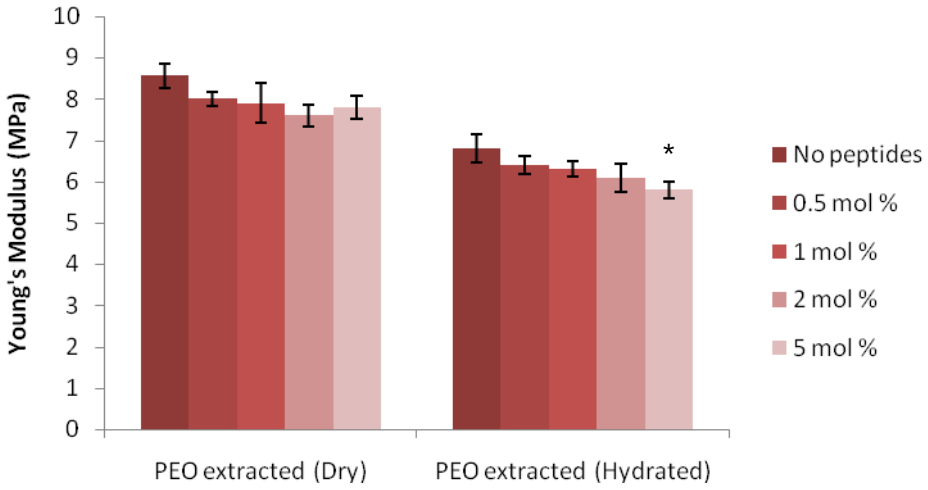

Figure 5.8 Fibres' mechanical properties: Young's modulus values of fibrous scaffolds after varying the CGDGEA peptide concentrations and unfunctionalized scaffolds. Mean ± SD, n = 3. (*) indicates that the difference between the marked bar and the unfunctionalized fibrous scaffold (90:10 MA:DEGMA) is statistically significant ($p<0.05$).

The major challenge in regenerating connective tissue for TE, particularly bone, is to present sufficient mechanical strength prior to cellular deposition of natural ECM [213]. This was discussed previously in Section 3.4.5. A tensile modulus of 6.5-7 MPa was measured for the DGEA peptide functionalized scaffolds. The tensile modulus is comparable to PCL scaffolds that have been reported to have tensile modulus from a range of 5-15 MPa. PCL is a commonly investigated polymer for electrospinning used for bone TE applications [206, 214]. This scaffold could potentially be suitable for regeneration of non-loading areas of bones such as craniomaxillofacial

bone defects. Work by Motherway and colleagues have shown that cranial human exhibiting average moduli of 150 MPa [215]. Though the acylate scaffold has much lower moduli, some studies suggests that the overall mechanical strength of a scaffold increases after cellular infiltration [213 181].

However, based on its mechanical properties, this fibrous scaffold may not be strong enough to support large defects of load-bearing bone. Studies have shown mineralized cortical and trabecular human bone exhibiting average moduli of 9905 and 365 MPa respectively [205].

5.4.5 Determining the *in vitro* degradation of scaffold

Central to the TE approach is the degradation of the scaffold over time, to become completely replaced by the natural ECM in the tissue. Hence, the objective is to implant the scaffold that will remain in a robust state in the site of injury for long enough to allow for the formation of native tissue, but which will in the end degrade and become replaced by newly synthesized matrix [29]. Hence it was critical to investigate the degradation of the fibrous scaffolds over time. 5 mol% CGDGEA and unfunctionalized fibrous scaffolds were used in this investigation to study the difference in degradation between peptide immobilized scaffolds and scaffolds without peptides. Figure 5.9 shows the degradation of both scaffolds after 4 months in NACl PBS. Both types of scaffolds demonstrated mass loss as early as the second week (~9%) and to four weeks (~14%). The peptide conjugated scaffolds showed higher mass loss after 8 weeks and reached a maximum of ~51% at 16 weeks. While, the unconjugated scaffolds showed a maximum degradation of ~45% at 16 weeks. This effect of higher degradation may be due to the peptide-network being more hydrophilic and also the thiol-conjugated peptides ability to act as a catalyst for degradation. The increase in overall mass loss by adding thiol groups in an acrylated PEG-PLA hydrogel network was demonstrated by Rydholm and colleagues [142]. However, they reported faster degradation rates as the PEG-PLA-diacrylate hydrogels achieved 90% mass loss after 7 weeks compared to ~51% after 16 weeks for the CGDGEA scaffolds. This difference is due to higher number of degradable units due to the presence of PEG-PLA segments which can be degraded quickly [142].

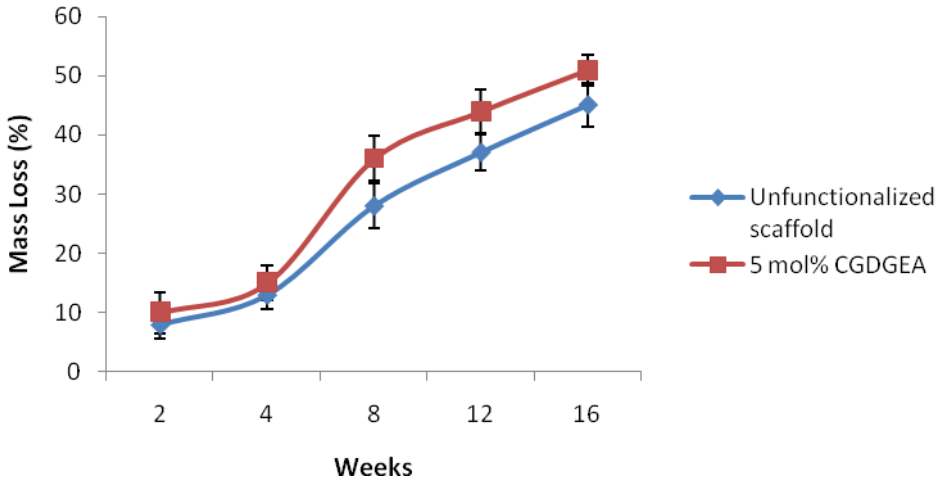

Figure 5.9 *In vitro* degradation of fibrous scaffolds with 5 mol% DGEA-peptide conjugation and without peptide conjugation on the fibrous scaffolds at 2, 4, 8, 12 and 16 weeks in 150mM NaCl PBS and placed on an orbital shaker at 37°C. Mean ± SD, n = 3.

The degradation rate of the acrylate scaffolds are comparable to the work of Ifkovits *et al.* that demonstrated ~ 33% degradation after 8 weeks for acrylated (poly-glycerol) scaffolds [212]. In addition, Atzet *et al*. showed lower mass loss compared to the acrylate fibrous scaffolds studied here, with ~ 30% mass loss after 12 weeks for poly(2-hydroxyethyl methacrylate)-co-polycaprolactone hydrogels [191]. This difference may be due to the hydrophobicity of PCL in the network. The fibrous scaffolds undergo bulk degradation mostly through hydrolysis of the ester bonds. In the presence of an aqueous environment, the hydrolytically degradable units are cleaved which results in the end products of the degradable units and kinetic chains formed during photocrosslinking (usually an alcohol and an oligomer polymer backbone). Hence when the hydrolytically degradable units are degraded, the poly-acrylic backbone, depending on its molecular weight, can be excreted through the glomerular filtration [175]. The molecular weight of the degraded poly-acrylic backbone is an important factor in the ultimate excretion.

Though the scaffolds did not reach 100% mass loss, it is predicted that at longer periods, the scaffolds would further degrade and *in vivo* the scaffold in the site of injury would become replaced by newly synthesized matrix. Some studies have shown that the degradation rates would increase *in vivo* due to a more dynamic surrounding because of fluid movement and exchange in the body to eliminate degradation products from the implant region compared to *in vitro* conditions [212].

While polyesters have been vigorously studied and considerable achievements made in their fabrication into TE scaffolds, a fundamental dilemma that is associated with their use is their bulk degradation. In general, polyester based scaffolds undergo bulk degradation with a non-linear degradation profile [189]. For example, after placement in media, the molecular weight of the

polymer begins to decrease on day one (PGA, PDLA) or after a few weeks (PLLA) [189, 267]. This is consequently followed by the mass loss of the scaffold when the molecular chains are reduced to a size which allows them to diffuse out of the polymer matrix [189, 268]. This phenomenon described and analyzed in detail by a number of research groups [269, 270], results in accelerated degradation (non-linear) and resorption kinetics until the physical integrity of polymer matrix is compromised [189]. Consequently, this phenomenon would decrease the overall mechanical properties of the scaffold drastically which is an important factor for bone TE applications. In addition, the mass loss is accompanied by a release gradient of acidic by-products which is detrimental to native tissues.

Bone is able to remodel *in vivo* under physiological loading [1]. It is a requirement that the degradation of the scaffold has to be in a controlled manner so that the scaffold maintains its physical properties for at least 6 months [189]. Subsequently, it will start decreasing its mechanical properties and should be degraded without a foreign body reaction after 12-18 months [189]. The fibrous acrylate scaffold showed an almost linear degradation profile which is suitable for bone TE applications. For example, ResorPin Systems (screws, nails, pins) and Leadfix Systems (screws, nails, pins) used in the area of craniomaxillofacial surgery observed similar degradation profiles [189, 271, 272]. Based on these degradation results, the fibrous scaffolds developed here are suitable for the use of TE applications which requires a scaffold to persist for long time periods to heal for example, bony defects in the craniomaxillofacial skeleton.

5.4.6 Surface characterization of peptide presentation on the scaffolds surfaces

The presentation and distribution of the peptides on the surface of the scaffolds were investigated using ToF-SIMS (performed and analyzed by Ms Nia Bell). There is a general assumption that the peptides are distributed uniformly over the surface of a scaffold however, the peptides could be distributed inside the scaffold or localized into clusters on the surface [35]. Consequently, it is important to study the presentation and distribution of peptides on the scaffolds surface. ToF-SIMS was chosen to characterise our system due to its ability to derive molecular information and its shallower information depth compared to XPS [273]. Additionally, we intended to exploit the imaging capabilities of modern ToF-SIMS instrumentation to investigate the distribution of the peptide on the scaffolds surface.

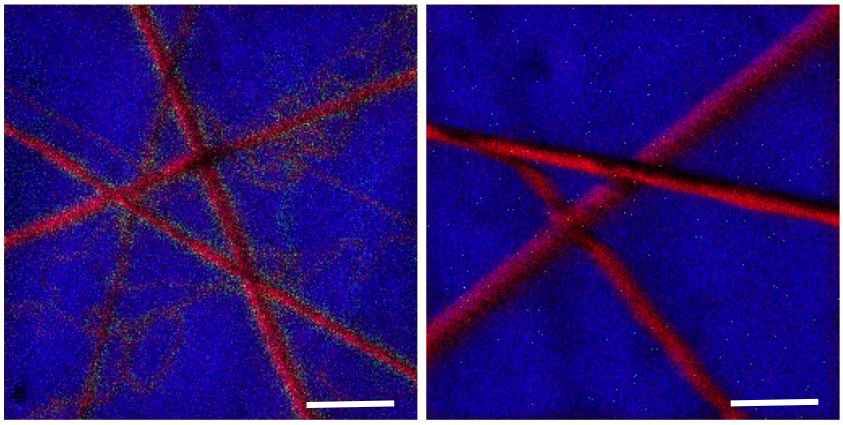

Figure 5.10 ToF-SIMS images (RGB mapping) showing the distribution of CRGD peptides on the surface of the fibres. A) scaffold with CRGD peptide, B) and scaffold without peptide (control). The substrate derived Al^+ ion (blue), the peptide fragment NH_4^+ (green) and the polymer derived $C_2H_5O^+$ ion (red) are mapped in RGB plots. Scale bar: 5µm.

All plot mapping were normalised to CHO^+, an intense polymer derived ion peak. Normalisation is known to reduce the occurrence and severity of spectral artefacts caused by differential sample charging and primary ion scattering from topographical surfaces [274]. The imaging are also normalised for the variable fibre coverage in each analysis area. The substrate derived Al^+ ion (blue), the peptide fragment NH_4^+ (green) and the polymer derived $C_2H_5O^+$ ion (red) are mapped in RGB plots. The images display the distribution and availability of the immobilized peptides on the surface of the fibres (Figure 5.10). There was clearly more NH_4^+ ion (green) detected in the scaffold sample incorporating the peptide when compared to the peptide free sample. Also, the NH_4^+ ion co-localised with the polymer derived ion $C_2H_5O^+$ (red) in the sample with peptide, as opposed to being scattered at a very low density across the whole sample of scaffold without peptide. The density of green spots in the sample of scaffold without peptide is indicative of the background signal due to the small H_2O^+ ion interference. Hence, the peptides represented in green were clearly present and distributed evenly on the surface of the fibres. This novel method of using ToF-SIMS to analyze peptide conjugation distribution was critical because the process of functionalization was performed in bulk throughout the whole scaffold and not specifically on the surface. It is important that the peptides are distributed on the surface of the fibres to ensure the peptide ligands are spatially accessible to the cell-surface integrins.

In the image of the peptide-containing scaffold, it appears that the number of counts from the peptide derived ion is higher at the edges of the fibres than on the top. This is an artefact which, in spite of the precautions taken, was caused by uneven charging of the polymer fibres, due to the sample holder geometry of the instrument. This artefact would have been reduced and higher ion intensities would have been recorded for the polymer and peptide-derived ion fragments if the

fibres had been aligned with the primary ion beam, as demonstrated by Van Royen *et al.* [273]. Nevertheless, the peptide-derived ions were detected in fibres of all diameters and at all orientations with respect to the primary ion source, which suggests a homogeneous distribution of the CRGD peptide on the scaffold's surface.

The surface availability of a target molecule was also demonstrated recently using ToF-SIMS on a hexyldimethylammonium (PCLhexaq) functionalised PCL electrospun scaffolds at varying concentrations [273]. Surface characterization of electrospun fibres has been investigated by some researchers to analyze bio-functional groups immobilized on the surface of fibres, usually quantified using the nitrogen content inferred from XPS [275]. However, ToF-SIMS was selected as the primary characterisation tool in this study due to superior surface sensitivity and ability of ToF-SIMS to detect lower concentrations of an analyte, compared to XPS [276].

5.4.7 Effect of the spacer arm length on peptide incorporation

It is well known that to enhance cell adhesion the peptide ligands must be spatially accessible to the cell-surface integrins [35]. Creating a distance between the peptide and the biomaterial can provide enhanced access required for integrin-ligand binding [135]. Thus, adding extra amino acids residues to act as a spacer arm between the peptide motif and the biomaterial surface provide mobility and reduces steric hindrance for the adhesive peptide to bind and interact with the cell surface integrin [32, 135]. However, the lengthening of a peptide can result in the formation of disulfide bonds or rearrangement of the peptides or sections of the peptide in a secondary structure (i.e folding) [141]. Glycine, an aliphatic amino acid, was chosen as spacer because it has been previously shown to have a nominal effect on the reactivity of the thiol groups since glycine is extremely inert [141]. Thus, we investigated the effect of varying the length of spacers (glycine) in the sequence on the peptide incorporation onto the scaffolds. The amount of glycines added was varied between 1, 3 and 6 amino acid residues.

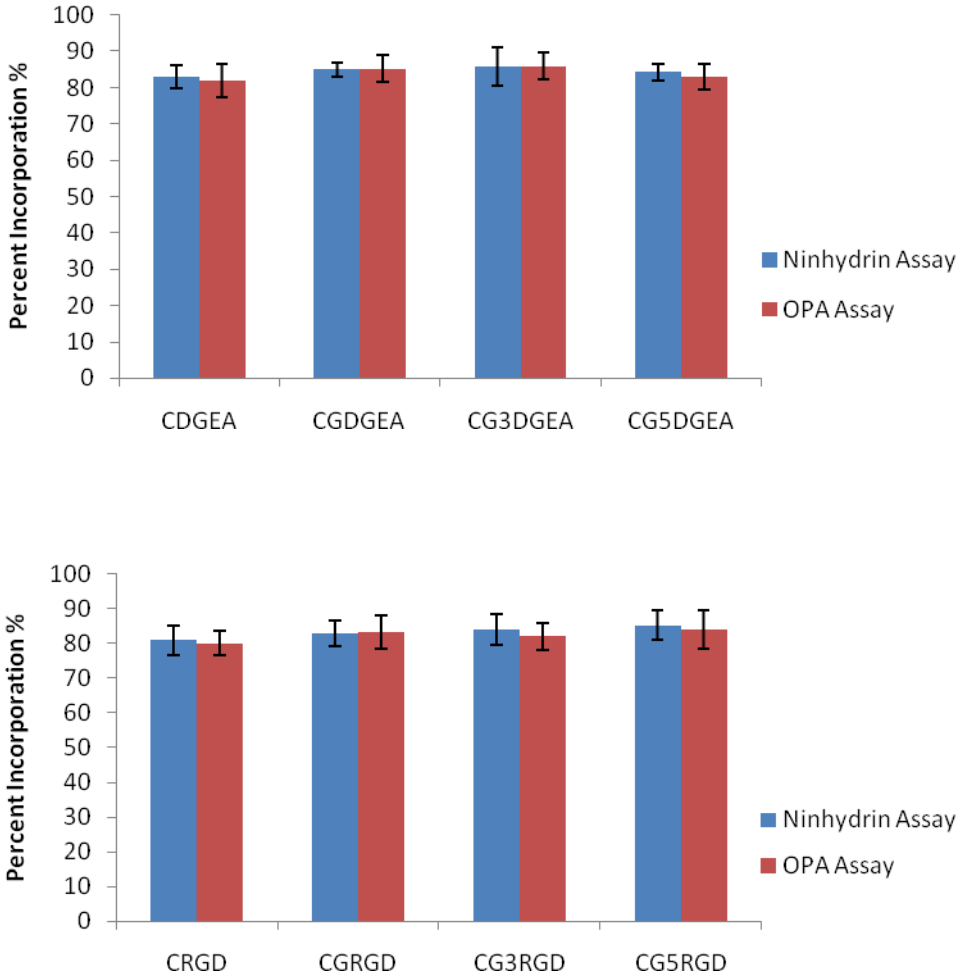

Figure 5.11 Effect of different number of spacer residues (glycine) on peptide incorporation either CGRGD or CGDGEA in acrylate scaffolds assessed using the Ninhydrin and OPA assays. Mean ± SD, n = 3.

The ninhydrin and OPA assays demonstrated that all different peptide sequences analysed were immobilized onto the fibrous scaffolds (Figure 5.11). Additionally, the ninhydrin and OPA assays showed no significant differences in the percentage of peptide incorporation onto the scaffolds amongst all peptides. For all peptide sequences, independently of the length of the spacer arm, the percentage of incorporation was approximately 80-86%. Both ninhydrin and OPA assays showed only very small non-significant differences in amine content.

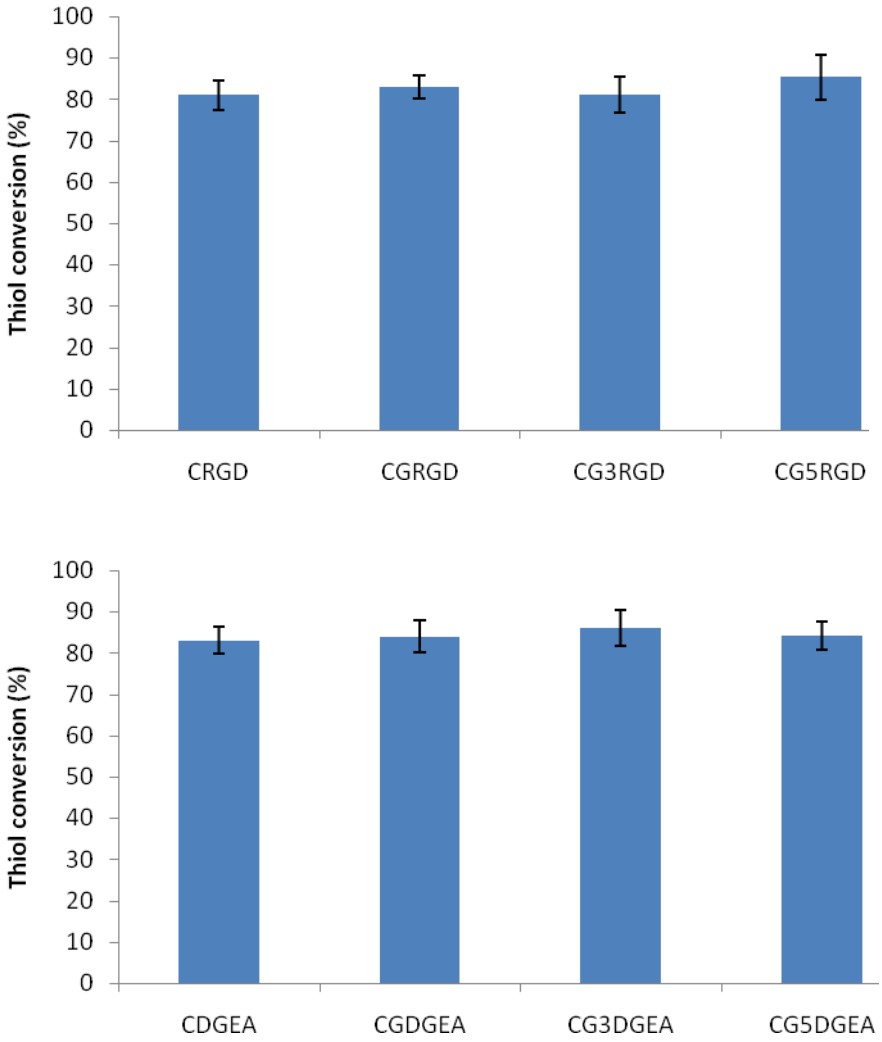

Figure 5.12 Effect of different number of spacer residues (glycine) on peptide incorporation either CGRGD or CGDGEA in fibrous acrylate scaffolds as assessed by Ellman's assay (thiol conversion of sulfydryl groups). Mean ± SD, n = 3.

The measurement of peptide incorporation was further confirmed by quantifying the free sulfhydryl groups in solution using the Ellman's assay (Figure 5.12). Similarly to the ninhydrin and OPA results, no significant differences were observed in thiol conversions between the RGD and DGEA sequences with different numbers of glycine spacers. For all the different peptides investigated, the percentage of thiol conversion was approximately 80-85%. Moreover, no difference was depicted between DGEA and RGD peptides. This gives evidence that all peptides were equally incorporated onto the scaffolds which is essential as the biological response of hMSCs to varying length of spacer arms was investigated and described in Chapter 6.

Glycine was selected as spacer because it has been previously demonstrated to have a nominal effect on the reactivity of the thiol groups [141]. Hence, it would have negligible effects on the thiol-

acrylate reaction during scaffold functionalization. This may explain the similar levels of peptide incorporation for the scaffolds with different glycine spacer lengths by not affecting the reactivity of the thiol groups during functionalization.

5.5 CONCLUSION

As described in Chapters 3 and 4, photocrosslinked fibres were successfully developed by electrospinning different MA and DEGMA compositions and post-UV crosslinking. However, the considerable increase in apoptosis of hMSCs for all fibrous scaffolds demonstrates a lower potential of the MA/DEGMA scaffold to support hMSCs attachment and viability. Thus, in this chapter, to increase the overall bioactivity of the scaffold, the functionalization of the previously developed acrylate UV-crosslinked fibrous scaffolds was investigated. Novel fibrous acrylate photo-crossslinked scaffolds were successfully developed introducing different amounts of cysteine-conjugated DGEA or RGD peptides onto the fibrous scaffolds. The synthesis of the functionalized scaffolds utilizes cysteine-functionalized RGD or DGEA peptide sequences in combination with the MA/DEGMA acrylates discussed in Chapter 3 and employs a photoinitiated mixed-mode thiol-acrylate polymerization mechanism. Cysteine-functionalized DGEA and RGD peptides were shown to be efficiently incorporated in the synthesized acrylate scaffolds with ~85% peptide incorporation. It was observed that immobilization of the peptides had no major effect on the overall morphology of the fibres, even as the peptide concentration was varied from 0.5 to 5 mol%. Except for the highest peptide concentration (5 mol%), all fibres conjugated with different concentrations of CGDGEA showed no significant differences for swelling behaviour and mechanical properties when compared to the unfunctionalized fibrous scaffolds. In addition, the degradation of the CGDGEA and unfunctionalized scaffolds were studied and both scaffolds degraded with mass loss of ~51% and ~45% at 16 weeks.

Most importantly, the peptides were accessible and homogeneously displayed on the surface of the scaffolds using ToF-SIMS for surface characterization. The efficiency of the peptides' conjugation using the thiol-acrylate reaction was similar, regardless of the length of the glycine spacer arms. For all peptide sequences, independently of the length of the arm spacer, the percentage of incorporation determined was approximately 80-86%.

Herein we have utilized the thiol-acrylate polymerization in the UV-electrospinning system to produce RGD and DGEA peptide-functionalized fibrous acrylate scaffolds. This method provides a facile and robust way to incorporate peptides into electrospun scaffolds without the need to chemically modify functional peptide motifs. The biological response of hMSCs to the functionalization with different peptide sequences and the use of different spacer arms on the DGEA and RGD peptides were investigated and will be described in Chapter 6.

CHAPTER 6

Assessment of effect of DGEA- and RGD-functionalized electrospun fibres on hMSC adhesion and differentiation

6.1 INTRODUCTION

A pivotal challenge in designing materials for TE is to provide critical cues that can direct cellular behaviour and promote tissue regeneration. Many attempts have been carried out to emulate the natural microenvironment using synthetic ECM-mimetic macromolecules that manipulate the ECM's biological, chemical and mechanical properties [116-119]. The ECM is primarily made of abundant nanometer-scale fibrous networks of proteins, glycoproteins and glycosaminogylcans including collagens, laminins, fibronectins, hyaluronic acids and growth factors [26]. These fibrous structures present cellular instructive cues to control cell-matrix interactions as they present biochemical ligands that interact exclusively with cellular integrins and activate cascading cellular signals [26]. Specifically, in addition to anchoring cells to mediate cell adhesion and presenting tissue organization, integrins convey intracellular signals that regulate cell migration, cycle progression and differentiation [88-90, 126].

Various ECM ligand peptide sequences have also been identified and demonstrated to regulate cellular functions. For example, RGD peptides from various ECM proteins, including fibronectin, laminin, collagen I, fibrinogen and vitronectin, have been demonstrated to enhance cell adhesion by inducing focal adhesion through integrin interaction [32]. Many integrins have been demonstrated to interact with ECM biomolecules in an RGD-dependent manner such as $\alpha_3\beta_1$, $\alpha_5\beta_1$, $\alpha_{IIb}\beta_3$, $\alpha_8\beta_1$, $\alpha_v\beta_1$, $\alpha_v\beta_3$, $\alpha_v\beta_5$, $\alpha_v\beta_6$, $\alpha_5\beta_8$ and $\alpha_4\beta_1$ [33]. Inspired by the bioactivity of the RGD sequence, many groups have worked on immobilizing the peptide to an extensive range of surfaces, scaffolds and hydrogels (reviewed in [33, 34] and [35]).

DGEA is a peptide sequence derived from collagen type 1 that has displayed a specific binding affinity for osteoblast via the $\alpha_2\beta_1$ integrin [42, 126]. In addition, DGEA has been shown to induce osteogenic differentiation [36-38]. Therefore, DGEA could serve as both a cell adhesion and differentiation factor. Nevertheless, collagen-derived peptides have been relatively less studied for their cellular response compared to other ECM peptides such as RGD [39-41]. However, it has been identified and demonstrated that collagen I binds to a different integrin receptor than fibronectin, and that the integrin-DGEA interaction is RGD-independent [42].

There are numerous approaches to present peptide sequences to cells with respect to the choice of peptide length, sequence arrangement as well as concentration [35]. These significantly affect the peptides' affinity for integrins as determined by the flanking residues, the conformation and/or the accessibility towards the integrins [35]. For instance, the binding specificity of the peptide to the cell surface integrin receptor can be enhanced by flanking residues and conformation [33, 132].

MSCs play an essential role in bone regeneration [75, 80]. These cells are recruited from the bone marrow and migrate into location of bone injury, differentiate into osteoblasts, and then produce an

osteoid matrix which is then mineralized and form new bone [76-80]. The potential for differentiation, and the relative simplicity with which they can be isolated and cultured *in vitro* without phenotypic alterations before specific differentiation, [76] make MSCs a suitable candidate for TE strategies [84]. The use of MSCs to induce tissue regeneration has then been extensively investigated [81-83]. These cells have been seeded into the scaffold and implanted into the body either directly or a few weeks later or after *in vitro* differentiation [81]. Relatively successful bone repair have been achieved but truly successful cartilage repair remains elusive [84]. Hence, studies aimed at defining the optimal scaffold environment to promote MSCs adhesion are needed.

Previously, we reported the successful development of novel fibrous acrylate photo-crossslinked scaffolds introducing different amounts of cysteine-conjugated DGEA or RGD peptides in the fibrous scaffolds. The synthesis of the functionalized scaffolds utilized cysteine-functionalized RGD or DGEA peptide sequences in combination with MA/DEGMA acrylates and employed a photoinitiated mixed-mode thiol-acrylate polymerization mechanism. In the present chapter, the biological response of hMSCs to the peptide-functionalized fibrous scaffold will be investigated.

6.2 MATERIALS

Roswell Park Memorial Institute 1640 medium (RPMI 1640), Fetal Bovine Serum (FBS), L-Glutamine, penicillin/streptomycin, Phosphate buffer saline (PBS) and trypsin/ethylenediamine tetra-acetic acid (trypsin/EDTA), alamarBlue® assay, Alexa-Fluor 568 Phallaoidin stain, Total DNA assay and the LIVE/DEAD® viability assay were purchased from Invitrogen GIBCO Corporation (UK). Caspase-glo®3/7 Assay was purchased from Promega (UK). Human mesenchymal stem cells (hMSCs) were purchased from Promocell (Germany) and hMSCs growth media and osteogenic media was purchased from Promocell (UK). BCA Protein assay kit was purchased from Thermo Fisher Scientific (UK). Alkaline Phosphatase Assay kit was purchased from BioAssay Systems (US) and the enzyme immunosorbent assay (EIA) from Takara Bio Inc (Japan). The antibodies anti-α_2, anti-β_3, and anti-hamster IgG were purchased from Abcam (UK).

6.3 METHODS

6.3.1 Cell culture

Low passage (p3-p6) human mesenchymal stem cells (hMSCs) were cultured using growth medium and supplements (Promocell). Initial culture of hMSCs was performed in 75 cm^2 flasks at 37°C, in a humidified atmosphere of 95% air with 5% CO_2, and supplied with fresh medium every 2-3 days. At 90% confluence, cells were detached using trypsin-EDTA and cell count was determined in a haemocytometer. Cells were resuspended in complete growth medium to achieve the appropriate concentration for seeding.

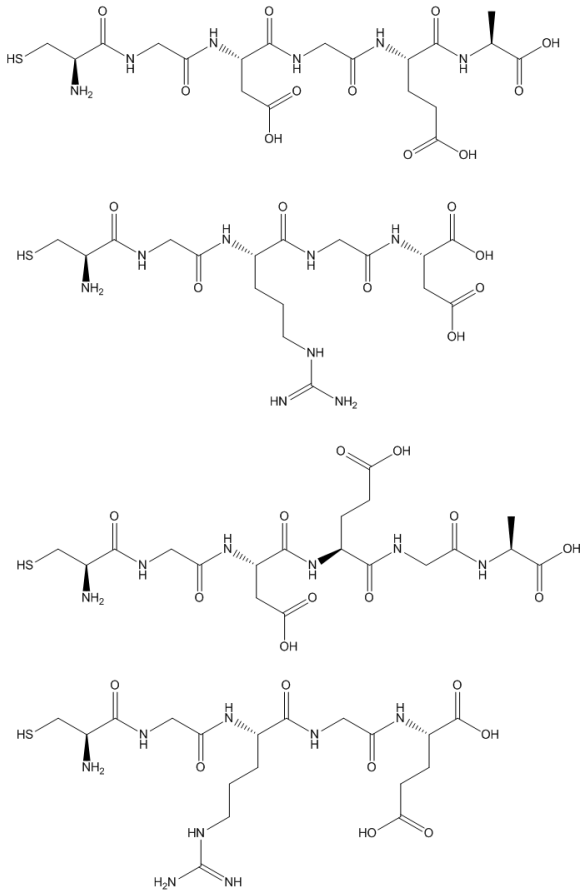

Figure 6.1 Sequences of the peptides used in this study. A) CGDGEA; B) CGRGD; C) CGDEGA and D) CGRGE

6.3.2 Preparation of peptide-conjugated electrospun fibres

The preparation of the peptide-functionalized scaffolds was described in Chapter 5 (Section 5.3.2). The schematic of the sequences of the peptides used in this study is illustrated in Figure 6.1. Briefly, the monomer mixtures were prepared by mixing (90:10) mol % of MA and DEGMA and varying concentrations of each peptide (0.5, 1, 2 and 5mol%) with the aid of PEO as a high molecular weight carrier polymer and ethanol as solvent. 2-hydroxy-4′-(2-hydroxyethoxy)-2-methylpropiophenone (Irgacure 2959) was added to the polymer solution as a photoinitiator and the solution was electrospun under conditions specified in Chapter 3 (Section 3.3.3) and (Table 3.2). After electrospinning, the fibres were immediately exposed to UV light for 10 minutes using a UVB (302nm) lamp in an oxygen free environment. Subsequently, 15mm diameter scaffolds were excised using a biopsy puncher and PEO was extracted from the fibres for five days in water. The scaffolds were air-dried overnight and the scaffolds were incubated in deionized water overnight before being placed in 24-well plates pre-coated with 1% (w/v) agarose gel (to prevent cell

adhesion at the bottom of the plate). Bovine type 1 collagen (1 mol% in PBS) was adsorbed overnight on TCP plates as controls.

For sterilization, samples in the 24-well plates were incubated with ethanol for one hour, soaked in PBS overnight and rinsed repeatedly with PBS and media before cell seeding. hMSCs were seeded on the electrospun fibres at a density of 1 x 10^4 cells/per cm^2 and incubated at 37°C overnight to allow cell adhesion. The cell culture medium was replaced every 2-3 days.

For the differentiation studies, hMSCs were seeded on the electrospun fibres at a density of 2 x 10^5 cells/per cm^2 and allowed to attach and grow for 7 days in order to reach confluency. After this period, growth media was changed to osteogenic media and the cells cultured for an additional 2 weeks. The osteogenic media was changed every 2 days. For experiments without osteogenic media, growth media was utilized throughout the three weeks.

6.3.3 AlamarBlue® assay

The alamarBlue® assay was performed to assess the viability of hMSCs on the fibrous scaffolds. The detection mechanism of this assay is the conversion of its active product, resazurin, into the fluorescent molecule, resorufin, by cells, which produces red fluorescence. Viable cells continuously convert resazurin into resorufin, due to their reduction potential. Hence, fluorescence can be used as a quantitative indicator of cell viability; the amount of fluorescence produced is then directly proportional to the number of living cells. The alamarBlue® assay was performed as specified by the manufacturer. Briefly, hMSCs were seeded in 24-well plates (1 x 10^4 cells/cm^2). At specific time points (1, 5, 10 days), cell-culture media was removed from the well plates and the wells were washed with 400 µL of PBS. 300µL of 10% (v/v) alamarBlue® in phenol red-free cell culture media were added per well (including one with no cells to be used as blank) and the well plates were incubated for 3 hours at 37°C. 100 µL of the reaction product were then transferred to a black 96-well plate and fluorescence was measured at an excitation wavelength of 540 nm and an emission wavelength of 590 nm using a microplate reader (SpectraMax M5, Molecular Devices).

6.3.4 MTS assay

In order to study the cell adhesion on the fibrous scaffolds, the number of viable cells was determined using the MTS assay. The mechanism behind this assay relies on the fact that metabolically active cells react with a tetrazolium salt (present in the MTS reagent) to produce a soluble formazan dye that can be detected at 490 nm. Firstly, stock MTS reagent was mixed with

media in a 1:5 ratio to make a working solution. The samples in the 24-well plates were rinsed with PBS and 600 µl of working solution were added to the wells. The samples were then incubated with the working solution for 3 hours at 37°C. Thereafter, 100µl from each well were aliquoted into a new 96-well plate. The 96-well plate was placed into a microplate reader (SpectraMax M5, Molecular Devices) and the absorbance of the content of each well was measured at 490 nm.

6.3.5 Caspase-glo®3/7 Assay

The Caspase-glo®3/7 assay is a luminescent apoptosis assay that measures the activity of caspases 3 and 7, two members of the cysteine aspartic acid-specific protease (caspase) family that play key effector roles in apoptosis in mammalian cells. The assay uses a luminogenic substrate DEVD sequence that has been shown to be specific to both caspase-3 and -7. The Caspase-glo®3/7 assay was performed as indicated by the manufacturer. Briefly, cell culture medium was removed and 300 µL of Caspase-glo®3/7 reagent were added to each well. The plates were gently mixed using a plate shaker for 30 seconds and then incubated at room temperature for 1 hour. Luminescence was measured using a microplate reader (SpectraMax M5, Molecular Devices). As a positive control for caspase activation cells exposed to 0.1% (w/v) staurosporine overnight, a known inducer of apoptosis, were used.

6.3.6 Actin immunostaining

The distribution/organization of the actin fibres were assessed by staining the cells with Alexa-Fluor Phalloidin 488/568. Nuclei were stained with Diamidino-2-phenylindole (DAPI). Firstly, the electrospun samples were washed twice with pre-warmed PBS and fixed with 4% (w/v) paraformaldehdye solution for 15 minutes at room temperature. After washing the samples twice with PBS, the cells were permeabilized with 0.1% (v/v) Triton X-100 solution for 5 minutes at room temperature. After further washing, the samples were incubated with Alexa-Fluor Phalloidin solution in 1% (w/v) BSA for 20 minutes at room temperature. The samples were then washed with BSA and PBS twice and, finally, Vectashield mounting medium with DAPI staining solution was added to samples and incubated for 5 minutes. Samples were rinsed with PBS twice and viewed with a fluorescence microscope (Olympus IX51 inverted microscope).

6.3.7 Cell adhesion assay

The cell adhesion assay protocol was performed as described in [42] but hMSCs adhesion to peptide-conjugated scaffolds was quantified using the MTS assay. The cells were seeded onto the scaffolds and allowed to adhere for specific time points (1, 2, 3 and 6 hours) with serum-free media. These time intervals were chosen because hMSCs are well spread between 1-6 hours and because at those time intervals, differences in cell spreading can be specifically attributed to the adhesion peptides immobilized on the scaffolds [42]. At later time intervals, cells produces their own adhesion molecules, which complicates the assessment of the peptides' effect [42]. After the specific binding time intervals, loosely bound cells were extracted by washing with PBS and the remaining cells were analyzed using the MTS assay. The cell adhesion experiments were performed with serum-free media.

6.3.8 Competitive cell adhesion assay

Human MSCs were pre-incubated in the presence of soluble CGDGEA, CGRGD and scrambled peptides with varying concentrations (0-5 mol%) in culture media for one hour. Then, the cells were seeded on the different peptide conjugated scaffolds as described above. After one hour, cell adhesion was analyzed using the MTS assay. The cell adhesion experiments were performed with serum-free media. For the integrin-blocking experiments, rather than pre-incubating the cells with soluble peptides, hMSCs were incubated with 1:200 dilution of three antibodies (anti-α_2, anti-β_3, or anti-hamster IgG) and cell adhesion was assessed using an MTS assay.

6.3.9 Alkaline Phosphatase assay

The Alkaline Phosphatase assay was used to detect/measure ALP activity. The assay utilizes p-nitrophenyl phosphate, which is hydrolyzed by ALP into a yellow product (maximal absorbance at 405nm). The reaction rate is directly proportional to the enzyme activity. For the differentiation studies, hMSCs were seeded on the electrospun fibres at a density of 2 x 10^5 cells/per cm^2 and allowed to attach and grow for 7 days in order to reach confluency. After this period, growth media was changed to osteogenic media and the cells cultured for an additional 2 weeks. The osteogenic media was changed every 2 days. For experiments without osteogenic media, growth media was utilized throughout the three weeks. Briefly, the ALP solution was prepared as follows: 5 mg 4-nitrophenyl phosphate disodium salt hexahydrate (PNP) tablet was thoroughly mixed in 5 ml of a solution containing 100 mM glycine, 0.1 mM $ZnCl_2$ and 0.1 mM $MgCl_2$ in dH_2O. The pH was adjusted to 10.4 at 37°C. At the indicated time points, cultures were lysed in dH_2O and 50 µl of

ALP solution were added per well. The samples were then placed on an orbital shaker, for 30 minutes, at room temperature, and the reaction was stopped with the addition of 100 µl of 1 M NaOH. Subsequently, absorbance was read at 405 nm in a microplate reader (SpectraMax M5, Molecular Devices).

6.3.10 Osteocalcin Production

The osteocalcin (OCN) production on the different peptide-conjugated scaffolds was determined using a enzyme immunosorbent assay (EIA) kit for intact OCN. The assay was performed according to the manufacturer's instructions, using the cell-culture supernatants. Briefly, 100 µl of each sample and carboxylated-type of osteocalcin (Gla-OCN) was added to the plate supplied by the manufacturer, which was previously coated with anti-Gla-OCN. The plate was then incubated for 2 hours, at room temperature, and the supernatant was aspirated. The plate was washed three times with 400 µl of PBS wash buffer. Next, 100 µl of horseradish peroxidase anti-OCN reagent were pipetted into all wells. The plate was mixed throughly by swirling and incubated at room temperature for 1 hour. Another wash was performed and 100 µl of substrate solution and hydrogen peroxide were added to each well and incubated, at room temperature, in the dark, for 15 min. The reaction was stopped by addition of 100 µl of stop solution (sulfuric acid) and absorbance was measured at 450 nm, using a microplate reader (SpectraMax M5, Molecular Devices). The amount of OCN in the culture medium was expressed as ng/ml and calculated using a standard curve constructed using a range of osteocalcin standards (0-16 ng/ml) provided in the kit and then normalised to total DNA content.

6.3.11 Total DNA assay

DNA concentration was measured using the Hoechst 33258 dye fluorescent assay. This assay is based on the enhanced fluorescence and shift in the emission wavelength of the fluorochrome Benzamide (Hoescht) when bound to DNA. Briefly, after 1, 5, and 10 days, cell-culture medium was removed from the well plates and cells were washed with PBS. 400 µL of water were added per well and cells were lysed by freeze-thaw cycles (30 minutes at -80°C and 20 min at 37°C, repeated 3 times). 50 µL of the cell lysates were added to 50 µL of Hoescht dye diluted to the working concentration (20 µg/mL) and allowed to react for 5 minutes before measurement. Fluorescence was measured using an excitation wavelength of 360 nm and an emission wavelength of 460 nm in a microplate reader (SpectraMax M5, Molecular Devices). DNA

concentrations were calculated using a standard curve prepared using calf thymus DNA at concentrations between 0-100 µg/mL.

6.3.12 Statistical analysis

All experimental data shown were expressed as mean ± SD and were obtained from experiments performed in triplicates, at least. All data analysis was performed in Excel. Statistical analysis was performed with one-way analysis of variance (ANOVA) using multiple comparisons (Bonferonni test) and significance was determined by $p<0.05$. This analysis was performed with Graphpad InStat (Prism) software.

6.4 RESULTS AND DISCUSSION

The study reported in Chapter 4 demonstrated that hMSCS cultured on the MA/DEGMA fibrous scaffolds presented increased apoptotic levels. Such increase suggested the MA/DEGMA scaffolds have a low potential to support hMSCs cell attachment and viability. Hence, in order to increase bioactivity of the acrylate scaffold, different amounts of cysteine-conjugated DGEA or RGD peptides were incorporated in the scaffolds. Chapter 5 described the functionalization of the referred scaffolds utilizing cysteine-functionalized RGD or DGEA peptide sequences in combination with MA/DEGMA monomers and employing a photoinitiated mixed-mode thiol-acrylate polymerization mechanism. Cysteine-functionalized DGEA and RGD peptides were demonstrated to be incorporated efficiently during the synthesis of the acrylate scaffolds. Subsequently, the investigation of the biological response of hMSCs to the peptide-immobilized fibrous scaffolds will be described in the present chapter. Initial hMSCs adhesion to the scaffolds, viability and osteogenic differentiation were evaluated.

Firstly, the effect of the presence of the CGDGEA and CGRGD peptides immobilized on the fibrous MA:DEGMA scaffolds at different concentrations, on hMSCs initial attachment was evaluated. Next, the difference of the effect of the two peptides (CGDGEA and CGRGD) on hMSCs adhesion and viability was assessed. Then, the effect of varying the length of spacer arms of DGEA and RGD on hMSCs adhesion and viability with glycine was analyzed. Next, the integrin specificity of hMSCs adhesion to the two peptides was evaluated using competitive adhesion assays. Finally, the ability of the peptide conjugated scaffolds to stimulate osteogenic hMSC differentiation was investigated.

6.4.1 Determination of the effect of CGDGEA and CGRGD peptide concentration on hMSCs adhesion

In order to further explore the biological potential of the peptide-immobilized fibrous scaffolds, their ability to sustain adhesion and viability of hMSCs was evaluated. Cell adhesion is critical for the assembly of individual cells into a scaffold, as most cells grown *in vitro* must adhere to the substrate to survive and proliferate [277]. Human MSCs are uncommitted, non hematopoietic progenitor cells that are characterized by their ability to differentiate in response to appropriate cues [82, 84]. The ease with which hMSCs can be isolated and cultured *in vitro* without phenotypic alterations before differentiation [76] make hMSCs a suitable candidate for TE purposes [84]. Thus, with the use of these cells, the effect of varying concentrations of CGDGEA and CGRGD ligands immobilized on the MA:DEGMA fibrous scaffolds on cell adhesion and viability was

evaluated. Firstly, the effect of varying CGDGEA concentrations on hMSCs adhesion on the fibrous scaffold was characterized using an MTS assay (Figure 6.2). The hMSCs were cultured directly on the peptide-conjugated scaffolds to evaluate the bioactivity of CGDGEA and CGDEGA peptides at different concentrations, unfunctionalized acrylate scaffolds, collagen 1 coated surfaces and TCP in serum free media were used as controls. Cells that adhere to the scaffold after specific binding time intervals were quantified using the MTS assay, which detects metabolically active cells as they react with a tetrazolium salt in the MTS reagent. The reaction produces a soluble formazan dye that can be measured by absorbance at 490nm. Cell adhesion to each scaffold was analyzed at 1 and 2 hours after cell seeding. The loosely attached cells were removed by washing with PBS and the adherent cells on the scaffolds were analyzed.

After one hour, a significant increase in adhesion of hMSCs to scaffolds conjugated with the CGDGEA peptide was observed in comparison to the non-functionalized scaffolds. A trend of enhancing cell adhesion as CGDGEA concentration increased was clearly shown, 5 mol% CGDGEA-conjugated scaffolds exhibited significantly enhanced attachment and the 2, 1 and 0.5 mol% CGDGEA concentration followed the trend in this specific order. In contrast, the presence of the CGDGEA scrambled peptide (CGDEGA), and unfunctionalized scaffolds showed significantly lower cell adhesion. The concentration-dependent trend continued to rise up to 2 hours in culture. The 5 mol% CGDGEA-containing fibres showed the highest level of cell adhesion, followed by the 2, 1 and 0.5 mol% CGDGEA–containing fibres. As expected, all different CGDGEA scaffolds with varying concentrations showed higher cell adhesion when compared to the scrambled peptides (CGDEGA), which presented attachment comparable to unfunctionalized scaffolds. This demonstrates the efficacy and bioactivity of the CGDGEA peptide in promoting cell adhesion, which is in agreement with studies previously performed by Culpepper and colleagues [80]. They have shown enhancement of cell adhesion for DGEA- and collagen 1-coated HA disks in comparison to uncoated HA disks [80]. Though, the experiments shown here reveal that CGDGEA ligands were not able to support attachment equivalently to collagen 1.

The hMSCs initial adhesion to the CGDGEA peptides conjugated fibrous scaffolds were demonstrated to be dose-dependent; increasing DGEA concentration on the scaffold further increased cell adhesion. Interestingly, the cell adhesion strength to the peptides immobilized on a substrate has been previously shown to correspond to the amount of integrin-ligand bonds [278-280]. Furthermore, Palacek *et al*. and Asthagiri *et al*. have revealed that a parameter, short term cell-substratum adhesion strength, can illustrate three critical factors: ligand surface density, receptor expression level and receptor-ligand binding affinity [278, 280, 281].

A few groups have suggested that collagen mimetic peptides, such as DGEA are attractive for the conjugation of biomaterials for a number of reasons [42, 80, 282]. Firstly, collagen 1 binds to

different integrin receptors from FN, VN and Fbg, and the integrin-collagen 1 interaction is believed to be RGD independent [42]. Consequently, DGEA may not compete with adsorbed FN, VN and Fbg for interaction with integrins [42, 282]. In addition, it is possible that collagen 1 would not adsorb to the surface of a scaffold in a high rate after implantation of the scaffold, because collagen 1 is not abundant in blood in comparison to fibronectin [42].

As 5 mol% of CGDGEA stimulated the highest cell binding for hMSCs after 2 hours when compared to other concentrations, it was chosen to be used in further experiments described in this chapter.

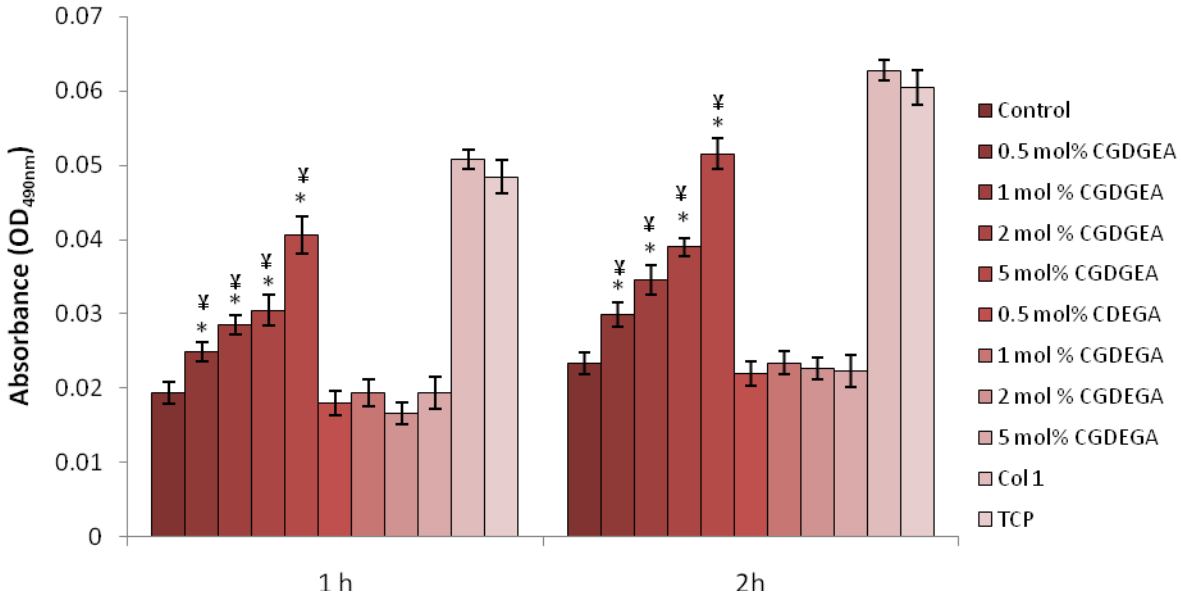

Figure 6.2 Effect of varying the concentration of CGDGEA peptides on the fibrous scaffolds on hMSC adhesion after 1 and 2 hr, determined using MTS assay. Mean ± SD, n = 3. (*) indicates that the difference between the marked bar and the control (unfunctionalized acrylate scaffold) of the same time period is statistically significant. (¥) indicates that the difference between the marked bar and scrambled peptide, (DEGA) of the same time period is statistically significant (p<0.05).

In addition, the effect of varying CGRGD concentration on hMSCs adhesion to the fibrous scaffolds was assessed (Figure 6.3). After one hour, scaffolds with 2 mol% CGRGD presented the highest cell adhesion, followed by 5 and 1 mol%. There was no significant difference between 0.5 mol% CGRGD and the unfunctionalized scaffolds or the scrambled peptide (CGRGE). After 2 hours, 2 mol% RGD peptides further enhanced cell attachment still followed by the 1 and 5 mol% scaffolds. The highest concentration of CGRGD peptides (5 mol%) was not able to stimulate cell adhesion above that of 2 mol%. The scrambled peptide, CGRGE immobilised onto scaffolds at different concentrations showed low cell adhesion levels, similar to the unfunctionalized scaffolds. This demonstrates the efficacy and bioactivity of CGRGD peptide in promoting cell adhesion.

The hMSCs adhesion rates to the CGRGD functionalized-scaffolds showed that an increase in peptide concentration for CGRGD does not always guarantee an increased cell adhesion. This was in agreement with Yang and colleagues, who demonstrated that the highest cell spreading of MSCs occurred at the minimum concentration investigated of 0.03 µM PLL-CRGDS coated onto PLA disks [35, 283]. The coating of PLL-GRGDS on PLA disks significantly enhanced cell spreading in concentrations of 0.3 and 0.03 µM but not at the higher concentrations of 3 and 30 µM [35, 284]. They suggested that the inhibitory effects of increased PLL concentrations dominated compared to the adhesive characteristic of the RGD peptide at high concentrations [35]. In contrast, Harbers and Healy have shown that with increasing RGD ligand density by grafting RGD on polystyrene surfaces, cell adhesion increased; this was characterized with the use of a centrifugal adhesion assay [280]. Hence, it is clear that the literature is controversial with regards to optimal concentrations for RGD-peptides immobilization on biomaterials.

Sawyer and colleagues also demonstrated that increasing RGD concentrations hinders cell attachment by immobilizing poly-glutamate E_7GRGDSPCA onto hydroxyapatite disks [285]. This decrease in cell adhesion as the peptide concentration increases was suggested to be due to the ligands being too closely packed at high concentrations and impeding the access to integrin receptors [35]. This could also explain the decrease in cell adhesion for the system investigated here. When CGRGD peptides concentration was increased up to 5 mol% cell attachment was reduced when compared to the intermediate concentration of 2 mol%, which showed optimal cell adhesion. It seems likely that the reduction in cell attachment is in fact due to lowered accessible ligand concentrations, even though this was not seen with the CGDGEA peptides. This distinction may be due to CGDGEA and CGRGD binding to different integrin receptors [42].

The amount of peptide presented to the cells and the degree of functionalization are evidently important factors affecting the potential of a biomaterial as a cell adhesive material [35]. It is important to note that there are many analytical methods and representations of the amount of peptide immobilized onto the scaffolds in the literature making quantitative comparisons between the scaffolds developed here and other systems complicated. The nature of the scaffolds should have an impact on the level of quantification based on the same quantitative methods. Correspondingly, even if the same methodology for reporting quantification has been used, difference in degrees of swelling or bulk or surface modifications mean that actual ligand densities or concentrations can be different to those reported. For this reason, we have not compared the specific amount of peptides immobilised and their specific cell response in the literature to our system.

In addition, there has been a lot of controversy about the use of RGD peptides on biomaterials. Some studies have shown inhibitory effects of RGD to cell growth on implants [286, 287]. The

inhibitory effects of RGD on cytocompatibility *in vivo* have not been indentified [42]. According to Hennessy *et al*., they suggest that synthetic RGD peptides on the biomaterial surface compete with adsorbed FN, VN and Fbg protein molecules which are abundant in blood for binding of cell surface integrins [42, 288-290]. These adhesion proteins interact with integrins through an RGD dependent mechanism [291-293]. Hence, this may imply that RGD peptides avert integrin receptors from binding and interacting with the adsorbed proteins, and consequently decreasing the overall effects of integrin signalling, as it is known that RGD peptides are weaker integrin ligands than the native full length adhesion proteins [132, 287, 294].

As 2 mol% CGRGD stimulated the highest cell binding after 2 hours in comparison to the other concentrations tested, it was chosen to be used in all further experiments reported in this chapter.

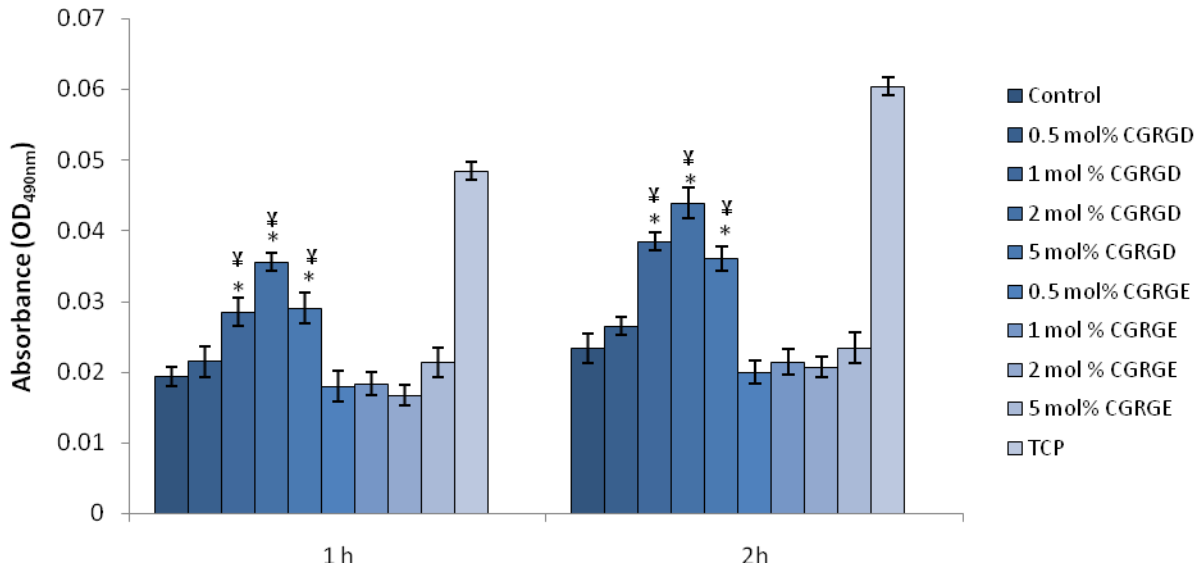

Figure 6.3 Effect of varying the CGRGD peptides concentration on the fibrous scaffolds on hMSC cell adhesion after 1 and 2 hr, determined using MTS assay. Mean ± SD, n = 3. (*) indicates the difference between the marked bar and the control (unfunctionalized acrylate scaffold) of the same time period is statistically significant. (¥) indicates that the difference between the marked bar and scrambled peptide (CGRGE) of the same time period is statistically significant (p<0.05).

6.4.2 Comparison of the effect of CGDGEA and CGRGD conjugation on hMSCs adhesion and viability

To further evaluate the cell adhesion at a longer time period and compare the efficacy of the CGDGEA and CGRGD ligands, the cell adhesion assay described above was repeated after longer time periods - 3, 6 and 9 hours (Figure 6.4). Based on results from previous adhesion experiments, the peptide concentrations used were 5 mol% for CGDGEA and 2 mol% for CGRGD.

After 3 hours, both DGEA and RGD peptides presented significantly higher cell adhesion in comparison to the control and the scrambled peptides. However, DGEA showed increased stimulation of adhesion when compared to RGD peptides. After 6 hours, similar results were depicted. This trend was more prominent after 9 hours, DGEA peptides supported higher levels of cell adhesion in comparison to RGD. Slight difference in cell adhesion was observed between CDEGA and RGE containing scaffolds with the control (unfunctionalized scaffold). However, even after 9 hours DGEA ligands were not able to support attachment equivalent to that of collagen 1.

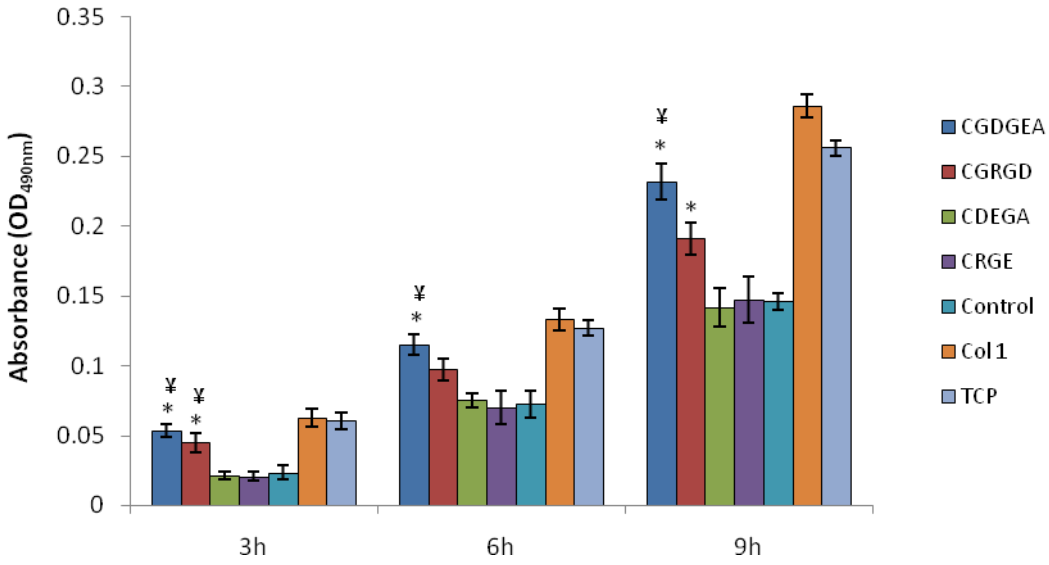

Figure 6.4 Effect of CGDGEA and CGRGD peptides immobilized on the fibrous scaffolds on hMSC cell adhesion after 3, 6 and 9 hours, determined using MTS assay. Mean ± SD, n = 3. The concentration for CGDGEA and CGRGD was 5 and 2 mol% respectively. (*) indicates the difference between the marked bar and the control (unfunctionalized scaffold) of the same time period is statistically significant. (¥) indicates that the difference between the marked bar and scrambled peptide with same peptide sequence of the same time period is statistically significant (p<0.05).

The reduced cell adhesion for RGD ligands in comparison to DGEA ligands is also in agreement with the investigation of Hennessy *et al.* [42]. They demonstrated the reduced potential of RGD in stimulating hMSCs adhesion to RGD-adsorbed hydroxyapatite disks when compared to DGEA.

Studies by Yoo *et al*. have also shown an enhanced adhesion of preosteoblast (MC3T3) on to DGEA peptides immobilized onto genetically engineered M13 phage tissue matrices in comparison to RGD peptides [38]. This is in contrast to other studies that showed that surfaces modified with a RGD containing peptide were found to exhibit greater cell attachment of hMSCs over short incubation periods [80, 295, 296]. These studies showed that DGEA peptides did not inhibit hMSCs adhesion but did not enhance cell adhesion either.

The binding of integrins with ligands induces a cascade of intracellular signals such as the activation of kinases, release of phosphatidylinositol by phospholipases and increased concentration of intracellular-free calcium [297, 298]. A study by Mineur has shown that the increase in intracellular Ca^{2+} occurs in an increasing number of cells as a function of the free DGEA and RGD peptide concentration [298]. In addition, they have demonstrated using blocking antibodies that free integrins and associated focal complexes generate Ca^{2+} signal due to interaction with DGEA and RGD by different cellular pathways [298]. Most importantly, one critical issue that was addressed in these adhesion experiments was that the overall bioactivity of the peptides, which was not altered after electrospinning and photocrosslinking.

To evaluate cell morphology and spreading, hMSCs were seeded onto different scaffolds, CGDGEA- and CGRGD-immobilized scaffolds and unconjugated scaffolds (control), as well as collagen 1 adsorbed surfaces and TCP. Following a 6 hours attachment interval, cells were stained with Alexa-phalloidin-488 and DAPI to visualize the actin filaments and nuclei, respectively. Figure 6.5 demonstrates the increase of hMSCs spreading with overall area for both peptide-conjugated scaffolds in comparison to the unconjugated scaffolds (control). hMSCs seeded on the CGDGEA-immobilized scaffolds had a well-spread morphology comparable to collagen 1 and TCP. This suggests that the DGEA peptides interacted with integrin receptors and generated enough integrin activation to induce the reconstruction of the actin cytoskeleton. In contrast, the CGRGD-immobilized scaffolds showed reduced cell number and less spreading compared to the CGDGEA-immobilized scaffolds, which confirms the results from the previous cell adhesion assays shown in Figure 6.3 and Figure 6.4.

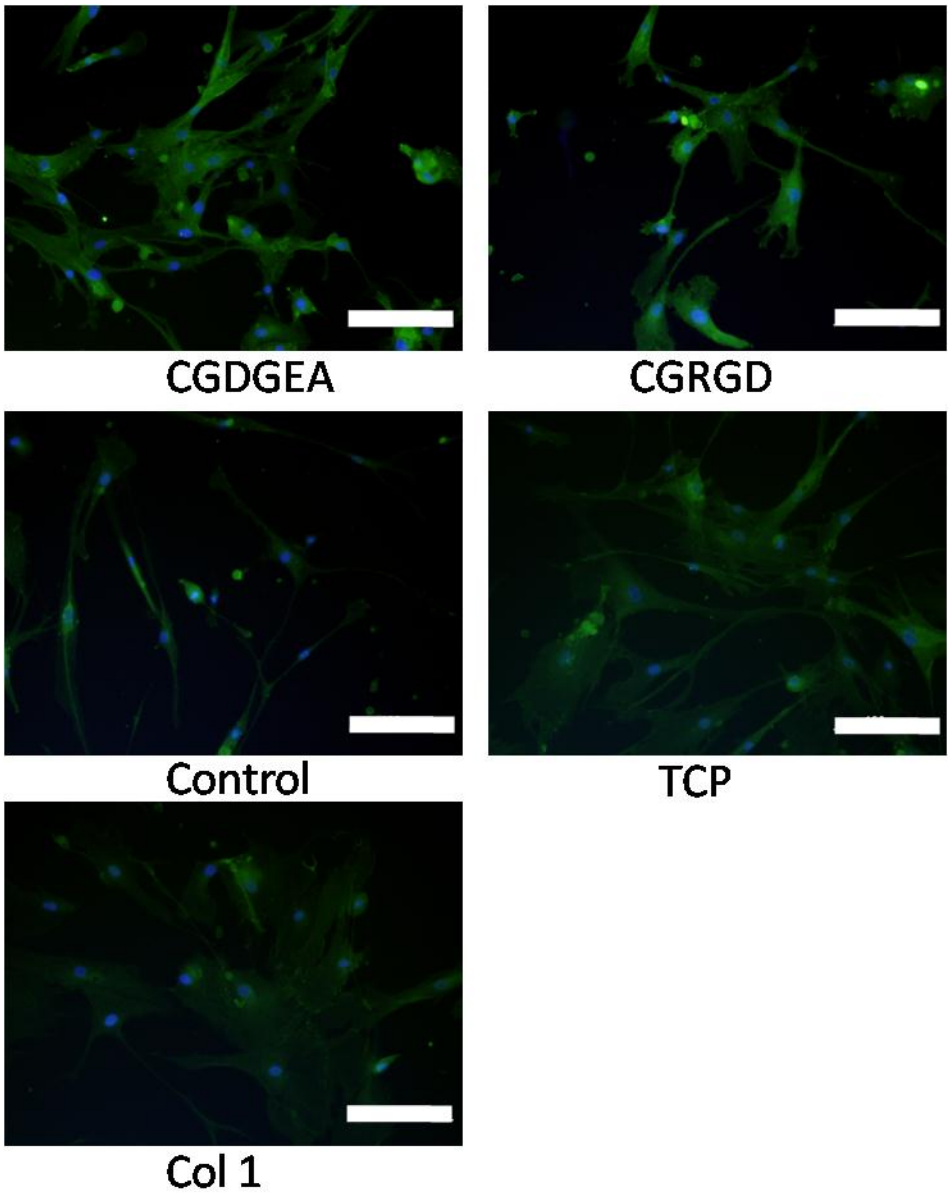

Figure 6.5 Actin and nuclei (DAPI) immunostaining of hMSCs seeded on fibrous scaffolds with CGDGEA and CGRGD peptides, control, TCP and collagen 1 after 6 hours. The concentration for CGDGEA and CGRGD was 5 and 2 mol%, respectively. Actin filaments were labelled with Alexa-phalloidin 488, appearing in green. Nuclei were labelled with DAPI, appearing in blue. Scale bar: 100μm.

Human MSCs viability on the peptide-conjugated photocrosslinked fibres was evaluated at days 1, 5 and 10, using the AlamarBlue® assay (Figure 6.6), an assay that measures enzymatic activity by assessing the cytoplasmic reduction potential of metabolically active cells. During the first 24 hours, the CGDGEA-functionalized scaffolds showed significant increase in hMSCs viability in comparison to the unconjugated and CGDEGA-functionalized scaffolds. The cell viability results were comparable to collagen 1-adsorbed surface and TCP. However, CGRGD-functionalized

scaffolds showed lower cell viability when compared to unconjugated scaffolds, but no statistical significance was shown. This result was also depicted on day 5. On day 10, CGDGEA-functionalized scaffolds showed the highest increase in cell viability, followed by the CGRGD-functionalized scaffolds. The scaffolds conjugated with both peptides showed significant enhancement of hMSCs cellular activity in comparison to the other scaffolds. Significant increase of cell viability on the CGRGD-conjugated scaffolds was only shown at day 10.

Scaffolds functionalized with both peptides CGRGD and CGDGEA were able to enhance hMSCs viability. As shown in studies performed by Yoo *et al*., MC3T3 cells grown on DGEA-phage matrices showed the highest metabolic activities which were similar to RGD-phage matrices after 10 days [38]. It is important to note that once cells cover the surface with their own matrix, the original surface, in this case of the peptide-conjugated scaffold, is no longer seen by cell integrins and becomes irrelevant to their continued adhesion and viability. ECM proteins production by cells adhered to a surface indicates that the cells are healthy, allowing them to maintain long-term attachment. However, initial cell adhesion is critical because most cells grown *in vitro* must initially adhere to the substrate to assemble and survive, and then grow and proliferate at later time points [277]. This can be evidently observed on the low viability of hMSC seeded on the unconjugated scaffolds and scrambled peptides.

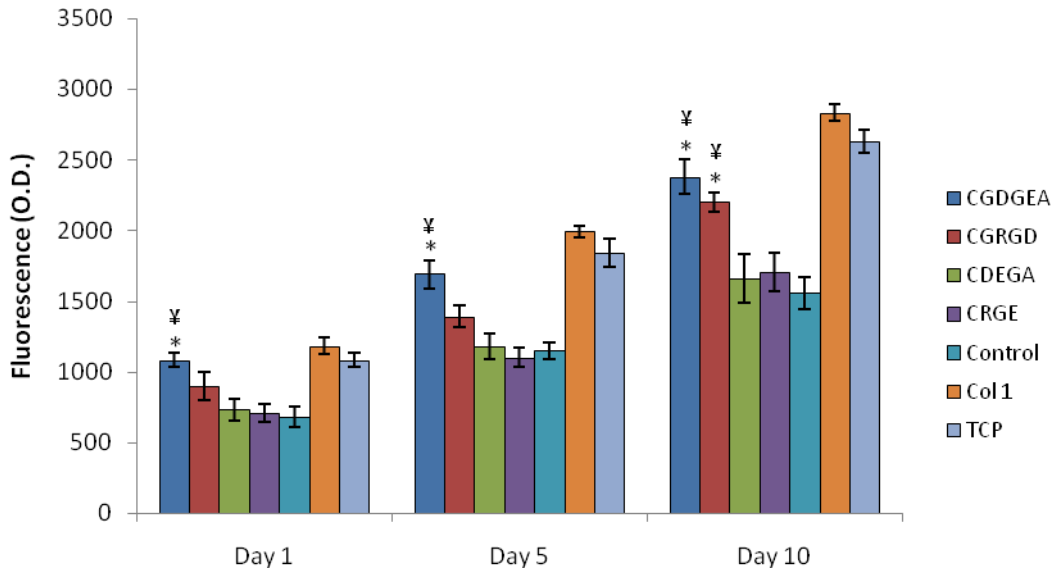

Figure 6.6 Effect of the peptide-functionalization of the photocrosslinked fibrous scaffolds on hMSC cell viability, determined using AlamarBlue® assay. Comparison of the effect of the difference peptides CGDGEA and CGRGD and controls (scrambled peptides). The concentration for CGDGEA and CGRGD used was 5 and 2 mol%, respectively. Mean ± SD, n = 3. (*) indicates the difference between the marked bar and the control (unfunctionalized) of the same time period is statistically significant. (¥) indicates that the difference between the marked bar and scrambled peptide with same peptide sequence of the same time period is statistically significant (p<0.05)

To determine whether the CGDGEA- and CGRGD-conjugated scaffolds affect hMSCs death, the hMSCs apoptosis levels was evaluated using the Caspase-glo® assay that measures the activity of caspases 3 and 7 (Figure 6.7). Confirming the results obtained with the AlamarBlue® assay discussed previously, a significant decrease in the apoptotic level was observed for hMSCs cultured in the CGDGEA fibrous scaffolds when compared to the unfunctionalized scaffold and DEGA. Decreased levels of apoptosis were also observed for cells cultured on CGRGD scaffolds, but no significance was shown. The scrambled peptides, CGDEGA and CGRGE showed levels of cell death similar to the unconjugated scaffolds. The effect of bioactive peptides on cell viability was most evident at day 10; apoptosis was significantly reduced for CGDGEA and CGRGD scaffolds.

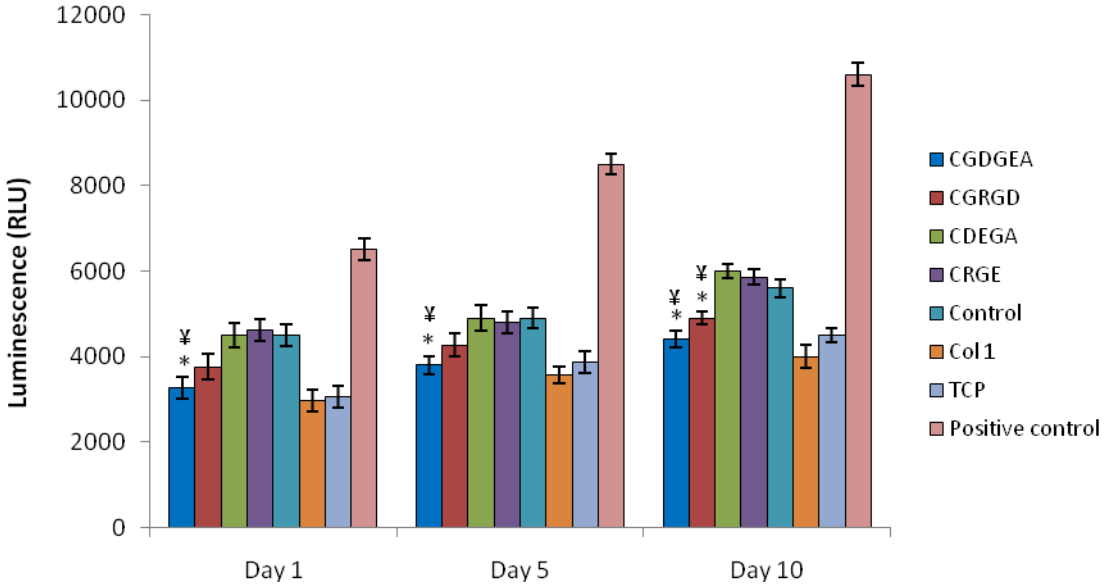

Figure 6.7 Effect of the peptide-functionalized photocrosslinked fibrous scaffolds on hMSC apoptosis, determined using Caspase glo® assay. Comparison of hMSCs cultured on MA-DEGMA photocrosslinked fibrous scaffolds, flat surfaces and TCP. The concentrations for CGDGEA and CGRGD used were 5 and 2 mol%, respectively. Cells treated with Staurosporine for 6 hours were used as positive control. The effect of the difference peptides CGDGEA and CGRGD and controls (scrambled peptides) were compared. Mean ± SD, n = 3. (*) indicates the difference between the marked bar and the control (unfunctionalized) of the same time period is statistically significant. (¥) indicates that the difference between the marked bar and scrambled peptide with same peptide sequence of the same time period is statistically significant (p<0.05).

6.4.3 Determination of the effect of varying glycine spacers on DGEA and RGD peptides on hMSCs adhesion and viability

It is well known that to enhance cell adhesion ligands must be spatially accessible to the cell-surface integrins [35]. Varying the length of the spacer arms is essential for or cell-ligand interactions as it has been shown to regulate adhesion and spreading of certain cell types [133]. Thus, we investigated the effect of varying the length of the peptide sequences' spacers (glycine) on cell adhesion (peptide sequences illustrated in Figure 6.8 and Figure 6.9). The amount of glycine added to the peptides varied between 1, 3 and 6 amino acid residues. Glycine, an aliphatic amino amino, was chosen as the spacer because it has been shown to have a nominal effect on the reactivity of the thiol group, as it is extremely inert [141].

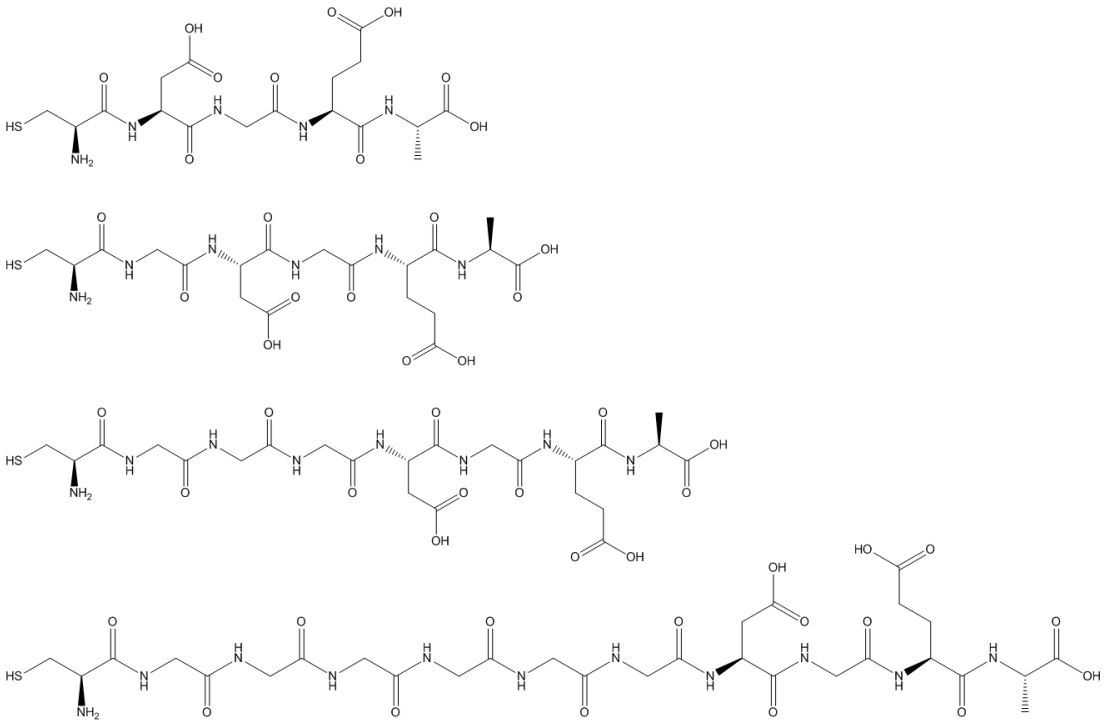

Figure 6.8 DGEA sequences used in the study of varying amount of the glycine spacer. A) CDGEA; B) CGDGEA; C) CGGGDGEA; D) CGGGGGGDGEA

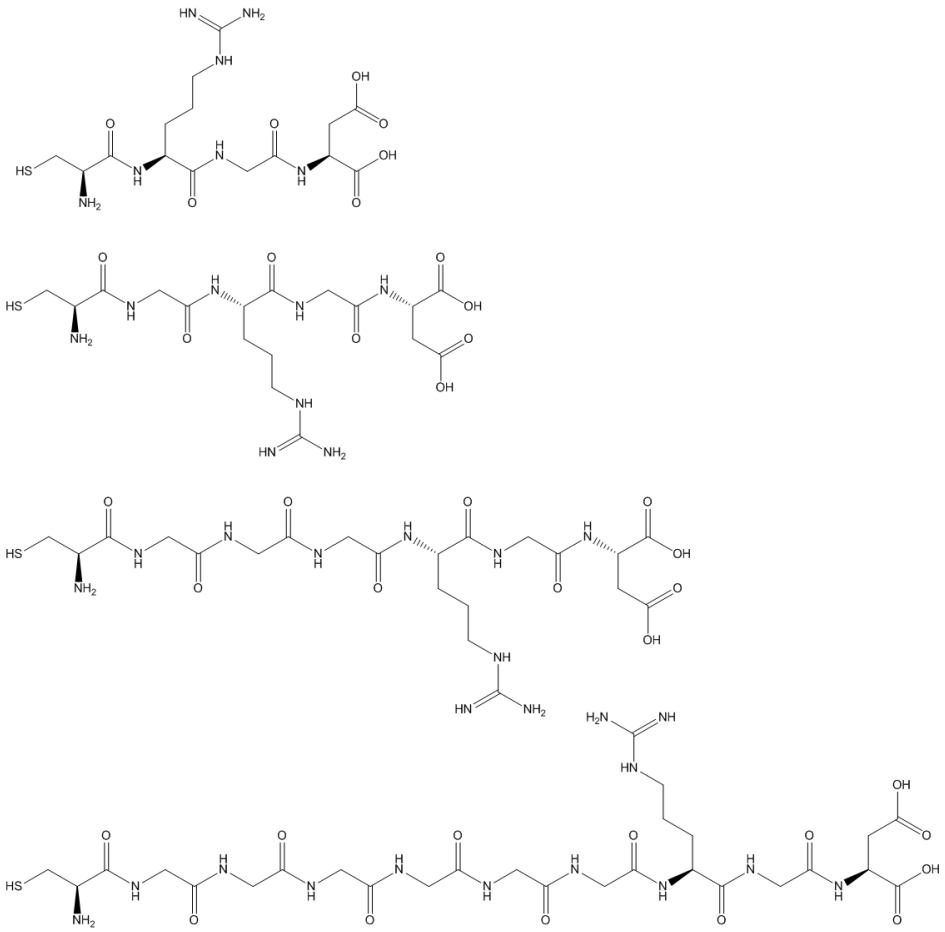

Figure 6.9 RGD peptide sequences used in the study of varying amount of the glycine spacers. A) CRGD; B) CGRGD; C) CGGGRGD; D) CGGGGGGGRGD.

After 3 hours, a significant increase in cell attachment was shown for DGEA-conjugated scaffolds with at least one glycine (Figure 6.10). Scaffolds functionalized with CDGEA supported the lowest cell adhesion for all time-points with cell metabolic activity levels comparable to the unconjugated scaffolds. The trend of increasing cellular adhesion with increasing number of glycines in the peptide sequence was observed after 9 hours. The effect of adding at least one glycine in the peptide sequence was most prominent after 9 hours. Additionally, the scaffolds functionalized with CG_6DGEA ligands demonstrated the highest cell adhesion levels.

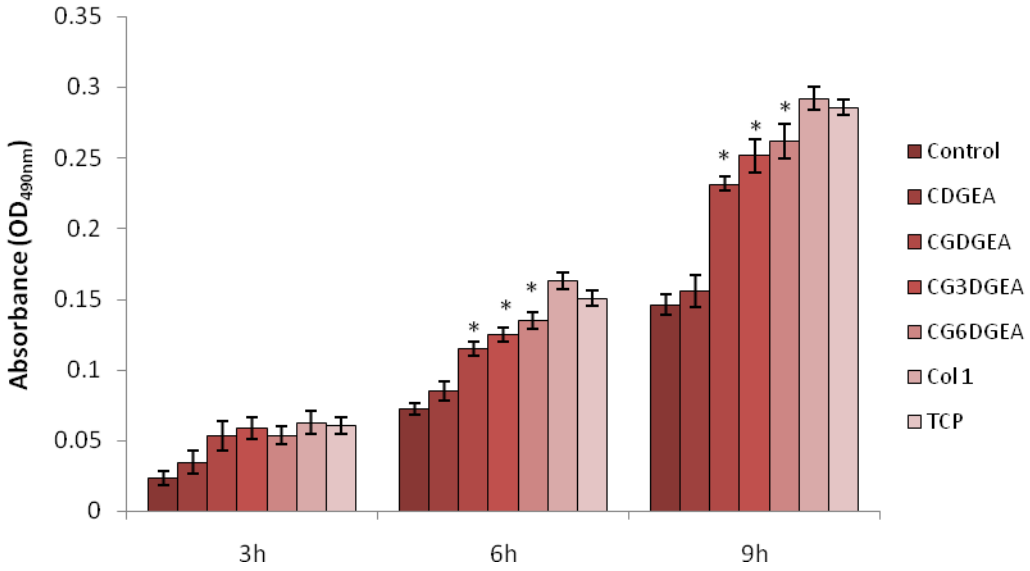

Figure 6.10 Effect of different number of spacer residues (glycine) to the DGEA peptides conjugated onto the fibrous scaffolds on hMSC cell adhesion after 3, 6 and 9 hours, determined using MTS assay. Mean ± SD, n = 3. The concentration for DGEA peptides used was 5 mol%. (*) indicates the difference between the marked bar and the control (unfunctionalized scaffold) of the same time period is statistically significant (p<0.05).

Similar experiments were repeated for RGD ligands with different numbers of glycine amino acids as spacer residues (Figure 6.11). After 3 hours, the CGRGD peptide-conjugated scaffolds supported higher cell adhesion in comparison to the other peptides-functionalized scaffolds and the control surfaces. The effect of adding more than one glycine spacer was only observed after 6 hours; CGRGD, CG_3RGD and CG_6RGD showed a significant increase in cell adhesion. After 9 hours, the CG_6RGD-conjugated scaffolds demonstrated the highest cell adhesion level. These results clearly indicate that introduction of spacer residues (glycine) to an adhesion peptide is important in regulating the attachment of cells adherence, and at least one glycine unit is needed for hMSCs attachment onto the scaffold system we studied.

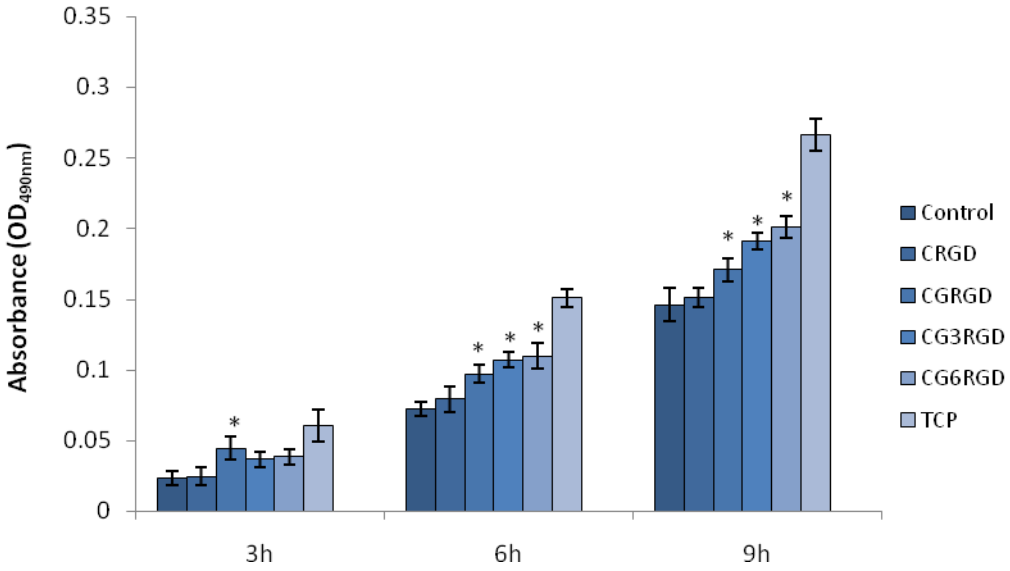

Figure 6.11 Effect of different number of spacer residues (glycine) on RGD peptides-conjugated onto the fibrous scaffolds on hMSC cell adhesion after 3, 6 and 9 hours, determined using MTS assay. Mean ± SD, n = 3. The concentration for RGD was 2 mol%. (*) indicates the difference between the marked bar and the control (unfunctionalized scaffold) of the same time period is statistically significant (p<0.05).

In addition, hMSCs viability on the DGEA scaffolds containing varying number of glycine residues was evaluated using the AlamarBlue® assay (Figure 6.12). On day 1, scaffolds functionalized with DGEA peptides with at least one glycine showed a significant increase in cell viability in comparison to the unconjugated scaffolds (control). All three peptides with glycines, CGDGEA and CG_3DGEA and CG_6DGEA revealed similar cellular activity. Similarly, this trend was observed at days 5 and 10. A higher viability was observed for all DGEA peptides with a glycine spacer arm. Similar values of cell viability were shown for the scaffolds functionalized with all the three DGEA peptides containing the different amount of glycine spacers. Hence, the incorporation of an increasing number of glycine residues significantly increased the overall bioactivity of DGEA, independently of the number of glycine residues used.

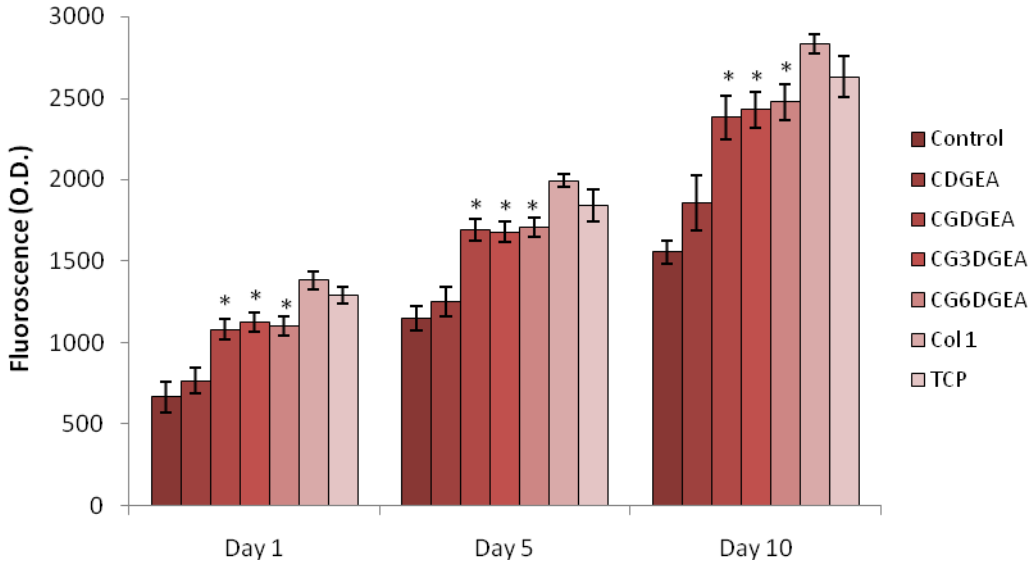

Figure 6.12 Effect of the different number glycine spacer residues on DGEA peptides on the functionalized photocrosslinked fibrous scaffolds on hMSC cell viability, determined using AlamarBlue® assay. The concentration for DGEA used was 5 mol%. Comparison of the effect of the different peptides of DGEA, collagen 1 adsorbed scaffold and unfunctionalized scaffold. Mean ± SD, n = 3. (*) indicates the difference between the marked bar and the control (TCP) of the same time period is statistically significant (p<0.05).

In addition, hMSCs viability was also evaluated on the scaffolds containing the RGD sequence with varying number of glycine residues using the AlamarBlue® assay (Figure 6.13). On day 1, scaffolds with all three RGD peptides with different number of glycine residues were observed to significantly increase cell viability in comparison to the control (unconjugated scaffold). On day 5, scaffolds functionalized with CGRGD and CG_3RGD peptides showed enhanced cell viability, similar to that observed for the CG_6RGD functionalized scaffolds. The same trend was observed at day 10, with scaffolds functionalized with CGRGD, CG_3RGD and CG_6RGD demonstrating enhanced cellular viability. Hence, similar to what was observed for the DGEA peptide-conjugated scaffolds, the data presented here demonstrates that the presence of a glycine residues significantly increased the overall bioactivity of RGD, independently of the number of glycine residues added.

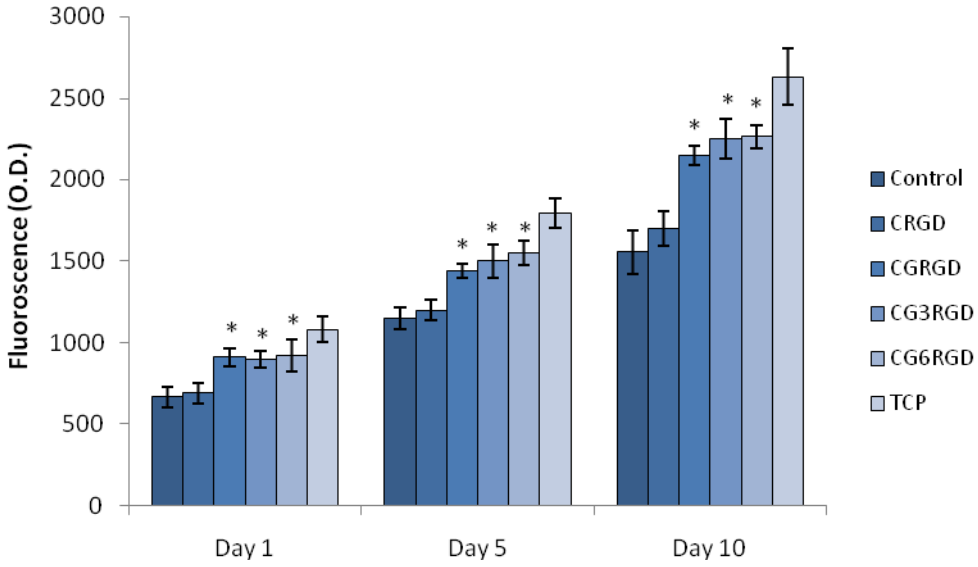

Figure 6.13 Effect of different number of spacer residues (glycine) for the RGD peptides conjugated to the photocrosslinked fibrous scaffolds on hMSC cell viability, determined using AlamarBlue® assay. The concentration of RGD used was 2 mol%. Comparison of the effect of the different peptides of RGD and unfunctionalized scaffolds. Mean ± SD, n = 3. (*) indicates the difference between the marked bar and the control (TCP) of the same time period is statistically significant (p<0.05).

The results presented above for both DGEA and RGD ligands have demonstrated the importance of using glycine residues as a spacer arm. Studies conducted by Lee *et al*. also showed the influence of glycine spacer arms on RGD sequences immobilized on alginate gels on cell adhesion and viability [133]. However, they found that a minimum number of four glycines was essential for enhancement of cell adhesion and viability.

A few groups have shown that PEG-diacrylate (PEG-DA) based hydrogels synthesized require a peptide with a long spacer arm between the scaffold and the ligand to enhance cell adhesion [18, 134, 135]. This is because PEG-DA hydrogels have two acylate groups and form a highly cross-linked network of long chains extending from the backbone [35, 135]. They suggested that the peptide conjugated into the backbone would be buried inside the bulk of the network unless it was attached to a spacer arm [35]. Specifically, work reported by Salinas and Anseth has demonstrated that incorporating RGD peptides with 8 glycines as a spacer arm in a PEG hydrogel system enhanced hMSCs viability up to ~ 88%, whereas short tethering of the RGD as pendant group without a spacer enhanced cell survival up to ~ 80% [135]. The short RGD sequence system reported slightly increased levels of cell viability and integrin up-regulation, while the RGD with a spacer arm sequence showed the highest level of cell survival and $\alpha_v\beta_3$ production [135]. Although, the level of cell viability and $\alpha_v\beta_3$ production observed when cells were cultured in the

hydrogel functionalized with the RGD sequence containing the spacer arm was not statistically significantly different from the short tethered RGD sequence [135]. Another group demonstrated that, by polymerizing a coating of acrylate-containing RGD, a system that utilized residual double bonds, the shortest spacer arm did not affectively promote cell adhesion. It only had an effect at high peptide concentrations [299]. The longer spacer arms were all equally effective at promoting cell attachment.

Beer and colleagues developed G_n-RGDF peptides with 1 to 19 glycine spacers and functionalized these peptides onto polyacrylonitrile beads [35, 300]. The agglutination of platelets was evaluated and Beer *et al.,* demonstrated that, as the length of the spacer arm increased to 9 glycine residues, the overall agglutination increased. On the other hand, as the spacer was further increased, agglutination declined. The decrease in agglutination with the longer spacer arm lengths was suggested to be due to the increased conformational entropy associated with the flexibility of spacer [35]. Based on the crystal structure of $\alpha_v\beta_3$ integrin and the binding site for RGD [301, 302], it was found that the RGD binding site is located very close to the surface of the integrin and that a long spacer was required to access it [35, 300]. The spacer arm is thought to prevent steric hindrance and electrostatic effects between the integrin and the scaffold [35]. Thus, this further explains why the length of the spacer is substrate specific. The results obtained from our study verified this conclusion, by which cells adhesion increases if RGD is spaced away from the scaffold.

6.4.4 Determination of the integrin specificity in hMSCs adhesion in competitive adhesion assays

Firstly, to further confirm the specificity of the peptides conjugated onto the scaffolds, effects on cell spreading were investigated using a soluble DGEA and RGD competitive assay (Figure 6.14 and Figure 6.15A). This was performed by determining the specificity of cell adhesion utilising soluble peptides that block the integrin binding sites and hence prevent cell adhesion by peptide-integrin specific routes. hMSCs were pre-incubated with different concentrations of soluble peptides of either DGEA, RGD or their controls DEGA or RGE, respectively, prior to seeding on the peptide-conjugated scaffolds. hMSCs were then cultured for one hour with serum-free media and cell attachment was analyzed using the MTS assay.

In Figure 6.14A, it is clear that as the concentration of soluble CGDGEA peptide increases, cell adhesion of the hMSCs significantly declines. Without the competing peptide treatment, hMSCs exhibited increased adhesion. The DGEA pre-treatment caused the decreased of hMSCs adhesion, which is caused by the competition of the DGEA soluble ligands. However, with the

CGRGD peptide treatment, only a slight decrease was observed in cell adhesion, as most of the cells maintained cell attachment. Cross-talk involving RGD and DGEA binding to integrins can be assessed by observing the effect of the soluble RGD peptide on cell binding to DGEA-conjugated scaffold. This observation shows that initial cell adhesion (after one hour) of hMSCs was mainly dependent on the presence of the DGEA motif. The control peptide CGDEGA did not block cell binding to the DGEA-conjugated scaffolds. The same observation was made by Yoo *et al*. when assessing adhesion of MC3T3 cells after pre-incubation with soluble DGEA and RGD peptides on DGEA-phages [38]. In addition, they have shown that after 24 hours, RGD-peptide cultures recovered full cell adhesion and viability [38]. This was due to higher dependency of cell adhesion on the DGEA ligands compared to the RGD ones.

Additionally, antibody-blocking studies were conducted to establish which integrins the DGEA and RGD peptides recognize. Various integrin receptors such as α1, α2, α3, α4, α5, αv, β1, β3 and β4 are known to be expressed on hMSCs [303]. The DGEA sequence has been shown to be specific to the α2β1 integrin [36, 37], whereas the RGD sequence binds to both αvβ3 and α5β1 [287]. For the integrin-blocking studies, instead of pre-incubating the cells with soluble peptides, hMSCs were pre-incubated with a 1:200 dilution of one of the following three antibodies: anti-α_2, anti-β_3, or anti-hamster IgG. Figure 6.14B clearly shows that the anti-α_2-antibody inhibited most cell attachment to the DGEA-conjugated scaffold but the same effect was not observed with the anti-β_3 antibody. The control IgG antibody showed no effect on cell binding to the peptide-conjugated scaffold.

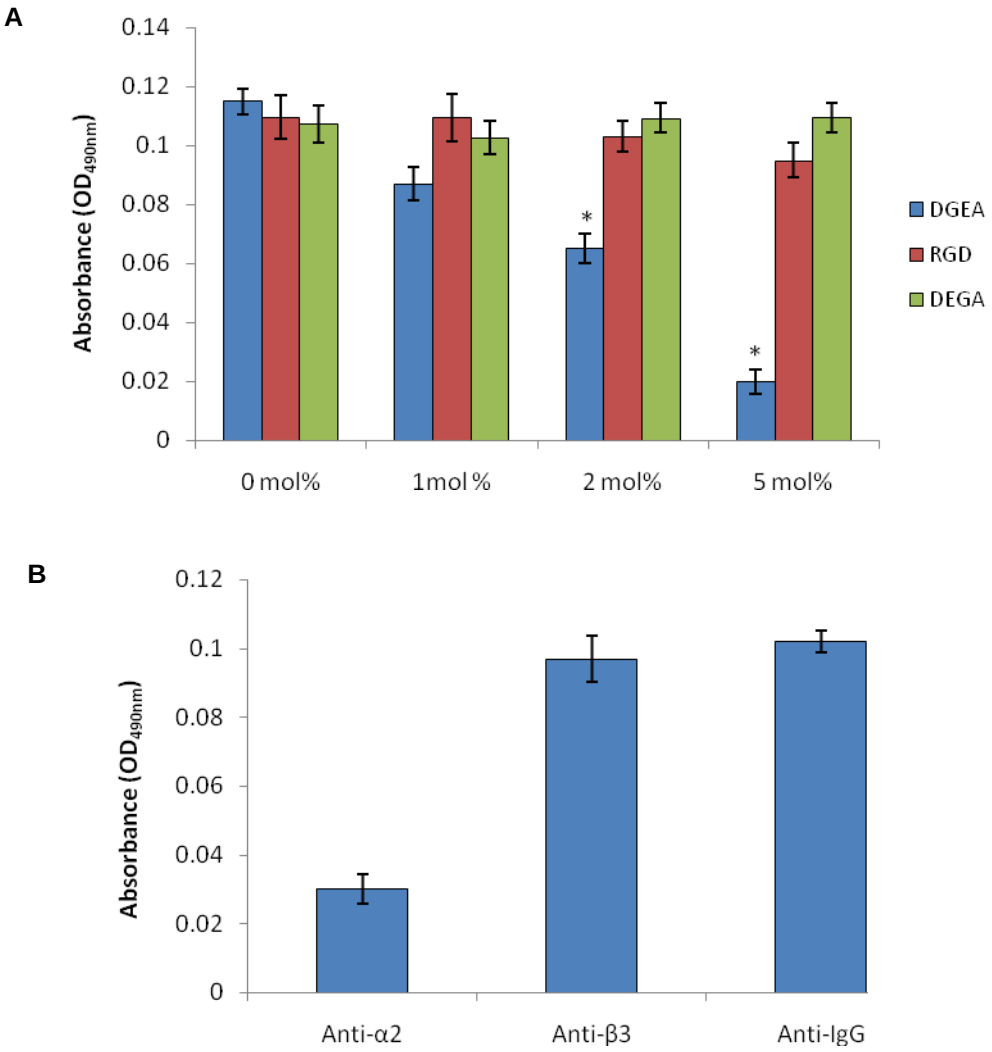

Figure 6.14 A) Competitive binding assay using CGDGEA, CGRGD and CGDEGA peptides against DGEA-functionalized fibrous scaffolds, analyzed using MTS assay. hMSCs were seeded on the DGEA-immobilized scaffolds after being pre-treated with soluble CGDGEA, CGRGD, CGDEGA peptides at different concentrations for one hour. Mean ± SD, n = 3. (*) indicates the difference between the marked bar and the control (0 mol% peptide concentration) of the same time period is statistically significant (p<0.05). B) Competitive binding assay using blocking antibodies against DGEA-immobilized fibrous scaffolds, analyzed using MTS assay. hMSCs were seeded on the DGEA-immobilized scaffolds after being pre-treated with soluble anti-α2, anti-β3 or anti-IgG for one hour.

In Figure 6.15A, as the concentration of soluble CGRGD peptide increases, cell adhesion decreases. Without the competing soluble peptide treatment, hMSCs revealed increased adhesion on the peptide functionalized scaffolds. Similarly, the soluble RGD pre-treatment of the cells caused a decreased in adhesion of hMSCs, which was caused by the competition of blocking of the receptors provided by the RGD soluble ligands. However, only a slight decrease in cell

adhesion was observed with the CGDGEA peptide pre-treatment; most of the cells still maintained cell attachment. Cross-talk of the RGD and DGEA binding integrins could be extrapolated by examining the effect of the soluble DGEA peptide on cell binding to the DGEA-conjugated scaffolds. The control peptide CGRGE did not inhibit cell binding to the DGEA-conjugated scaffolds. In Figure 6.15B, no decrease in cell attachment was observed when hMSCs were pre-treated with anti-α2 but the anti-β3- antibody blocked about half of the overall hMSCs attachment to the RGD-conjugated scaffolds. This was not observed for DGEA-conjugated scaffolds (Figure 6.14B). The incomplete blocking of the β3-antibody could be observed and the incomplete inihibition could be due to conjugated RGD engagement of the α5β1. The control IgG antibody had no effect on cell binding to the peptide-conjugated scaffolds.

Similar observations of integrin blocking using antibodies were shown using MC3T3-E1 cells on RGD- and DGEA-conjugated hydroxyapatite binding domains [304]. The authors further demonstrated that both peptides could engage in an integrin-specific signalling pathways by showing the ability of both peptides' to induce FAK phosphorylation, but only DGEA was able to initiate ERK1/2 phosphorylation [304]. The specificity of another collagen mimic peptide, GFOGER was assessed in a competitive assay of anti-α_2 antibody HT1080 cells, which have been shown to adhere to type 1 collagen by a single mechanism involving $\alpha_2\beta_1$ integrin, were incubated with an anti-α_2 antibody, which completely blocked all adhesion through $\alpha_2\beta_1$ integrin [282]. As shown in our study with the DGEA soluble peptides, they demonstrated low cell adhesion with an anti-α_2 antibody, which reflects on the specificity for the $\alpha_2\beta_1$ integrin.

Incorporating DGEA, a collagen type 1 mimetic peptide, in the scaffold offers an attractive approach for improving cell-material interactions and inducing cell adhesion, as was demonstrated in this section. However, RGD peptides are recognized by a number of integrins, including $\alpha_5\beta_1$, $\alpha_v\beta_3$ and $\alpha_{IIb}\beta_3$ [126, 292]. Hence, the lack of specificity of the RGD peptide causes minimal control over cellular responses.

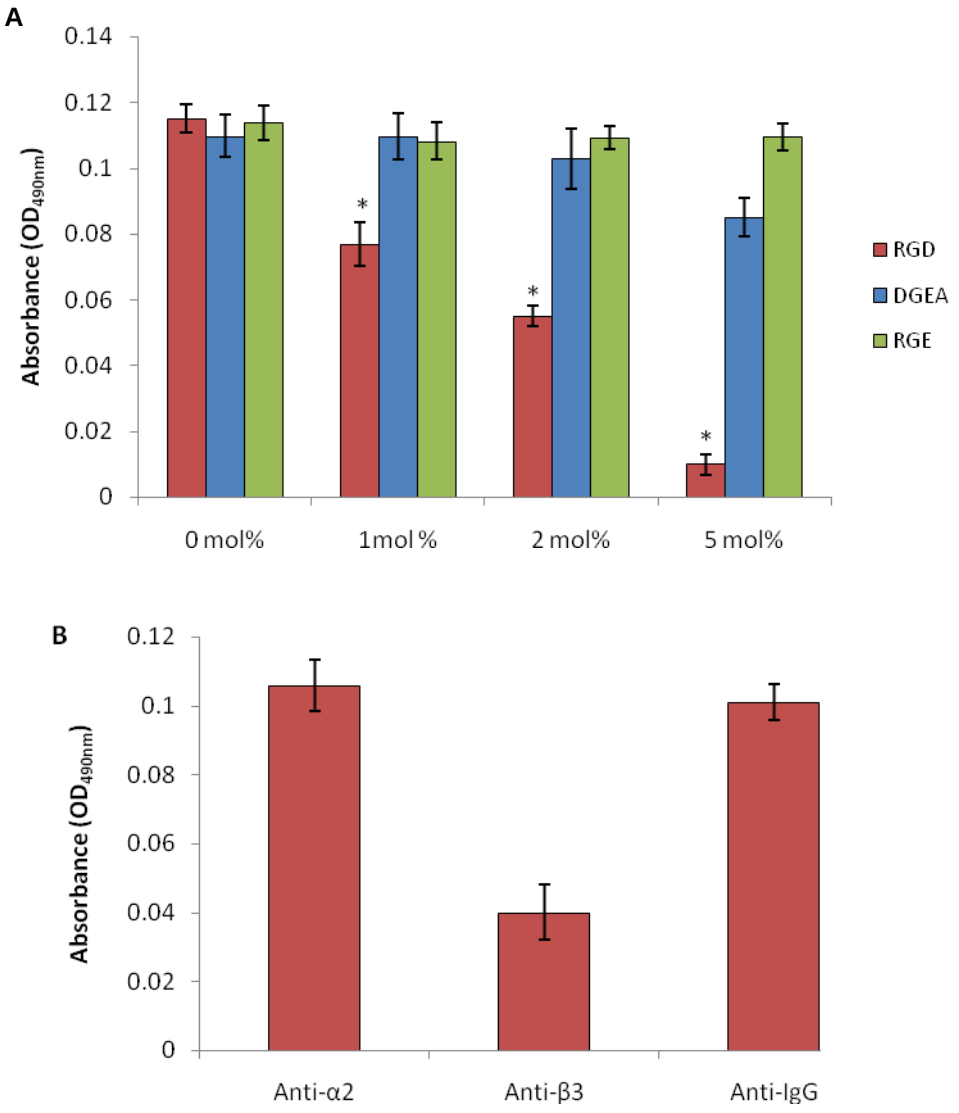

Figure 6.15 A) Competitive binding assay with CGDGEA, CGRGD and CRGE peptides against RGD-immobilized fibrous scaffold, analyzed using MTS assay. hMSCs were seeded on the RGD-immobilized scaffolds after being pre-treated with soluble CGDGEA, CGRGD and CRGE peptides at different concentrations for one hour. Mean ± SD, n = 3. (*) indicates the difference between the marked bar and the control (0 mol% peptide concentration) of the same time period is statistically significant (p<0.05) B) Competitive binding assay with blocking antibodies against RGD-immobilized fibrous scaffold, analyzed using MTS assay. hMSCs were seeded on the RGD-immobilized scaffolds after being pre-treated with soluble anti-α2, anti-β3 and anti-IgG for one hour. Mean ± SD, n = 3.

6.4.5 Assessment of ALP activity and OCN secretion on CGDGEA- and CGRGD-functionalized scaffolds

Based on our previous observations, CGDGEA-functionalized scaffolds demonstrated higher cellular adhesion and viability of hMSCs. In addition, many reports have been published describing activation of a collagen-selective integrin, $\alpha_2\beta_1$ integrin [42]. It induces osteoblast differentiation mediated by collagen- $\alpha_2\beta_1$ integrin interaction [36, 38, 42]. In addition, few studies have already reported the potential of RGD peptides to enhance osteogenic differentiation [234, 295, 296]. Accordingly, further investigation on CGDGEA and CGRGD peptides serving as differentiation factors for hMSCs was conducted. To evaluate this hypothesis, hMSCs were cultured on CGDGEA- and CGRGD-conjugated scaffolds for 14 days with or without osteogenic media and assessed for ALP activity and OCN secretion, as osteoblastic differentiation of hMSCs can be characterized by the activation of both ALP activity and OCN production as an early and late markers, respectively [126]. Specifically, ALP is an enzyme that induces phosphate precipitation and is an early marker of osteoblastic differentiation [126, 305]. OCN is a protein that is frequently utilized as an indicator of a mature osteogenic phenotype [126, 306].

As shown in Figure 6.16, CGDGEA-conjugated scaffolds showed higher levels of ALP activation than other scaffolds, signifying increased levels of osteogenic differentiation. As a negative control, hMSCs were cultured on TCP in osteogenic media. Type 1 collagen-coated surfaces also revealed high levels of ALP activation. All other CGRGD, CRGE or CGDEGA peptide-conjugated scaffolds, showed lower degrees of ALP activity when compared to TCP. These observations suggest that the collagen mimetic peptide CGDGEA, might be able to induce bone matrix mineralization, as also observed to type 1 collagen.

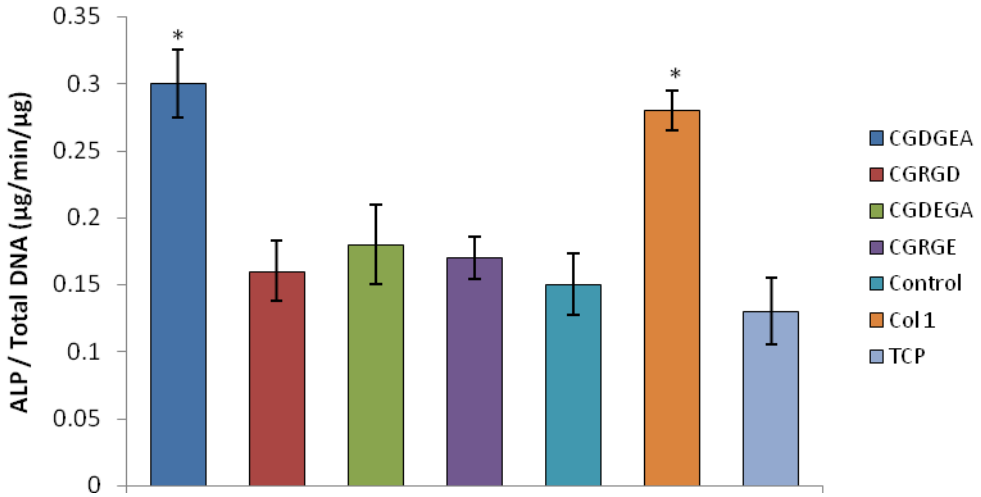

Figure 6.16 Effect of peptide-functionalized photocrosslinked fibrous scaffolds on alkaline phosphatase activity, determined using Alkaline Phosphatase assay. hMSCs were seeded on CGDGEA-conjugated scaffolds for 21 days, with osteogenic media. The concentration of CGDGEA and CGRGD used was 5 and 2 mol%, respectively. Comparison of the effect of the different peptides-containing scaffolds: CDGEA, RGD, and unfunctionalized. Mean ± SD, n = 3. (*) indicates the difference between the marked bar and the control (unfunctionalized scaffold) of the same time period is statistically significant (p<0.05).

To confirm the CGDGEA stimulation of hMSCs osteoblastic differentiation, a measurement of secreted OCN was evaluated using an enzyme immunosorbent assay (EIA) assay (Figure 6.17). The cells adherent to CGDGEA-functionalized scaffolds secreted significantly more OCN than the cell adherent to the other scaffolds when cultured in the presence of osteogenic media. Furthermore, CGDGEA-functionalized scaffolds stimulated OCN levels that were comparable to those measured on hMSCs cultured on the type 1 collagen-coated surfaces. These observations, together with the results obtained from the ALP activity assay, suggest that CGDGEA is able to induce hMSCs osteoblastic differentiation.

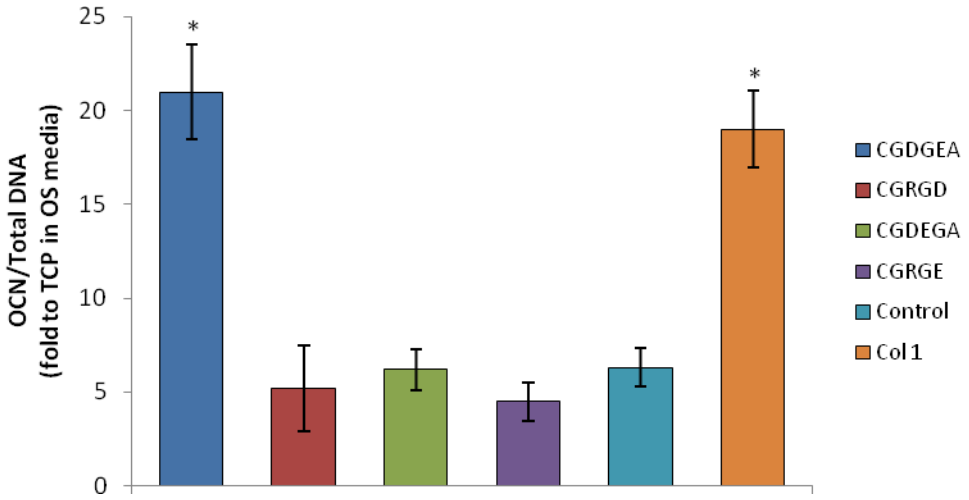

Figure 6.17 Effect of peptide-functionalized photocrosslinked fibrous scaffolds on osteocalcin secretion, determined using an enzyme immunosorbent assay (EIA) assay. hMSCs were seeded on CGDGEA-conjugated scaffolds for 21 days with osteogenic media. The concentration of CGDGEA and CGRGD used was 5 and 2 mol%, respectively. Comparison of the effect of the different peptide-conjugated scaffolds: CDGEA, RGD and unfunctionalized. Mean ± SD, n = 3. (*) indicates the difference between the marked bar and the control (unfunctionalized scaffold) of the same time period is statistically significant (p<0.05).

Results shown in Figure 6.16 and Figure 6.17 indicated that DGEA was capable of inducing osteoblastic differentiation on hMSCs cultured with osteogenic media. Nevertheless, previous investigations have shown that activation of $\alpha_2\beta_1$ could induce osteogenic differentiation even without differentiation inducers [42, 295]. Thus, a study was performed to investigate whether DGEA was able to stimulate osteoblastic differentiation without osteogenic media. To achieve this, hMSCs on peptide-conjugated scaffolds were cultured in growth media for three weeks and the ALP and OCN levels were evaluated.

Though levels of ALP activity and OCN secretion were much lower compared to the presence of osteogenic media, the cells grown on the DGEA-conjugated and type 1 collagen scaffolds showed higher ALP activity and OCN production than the cells grown on the other scaffolds (Figure 6.18 and Figure 6.19). These results suggest that the presence of DGEA is capable of activating collagen-binding integrins and stimulate osteogenic differentiation to a certain degree without the presence of the standard differentiation factors.

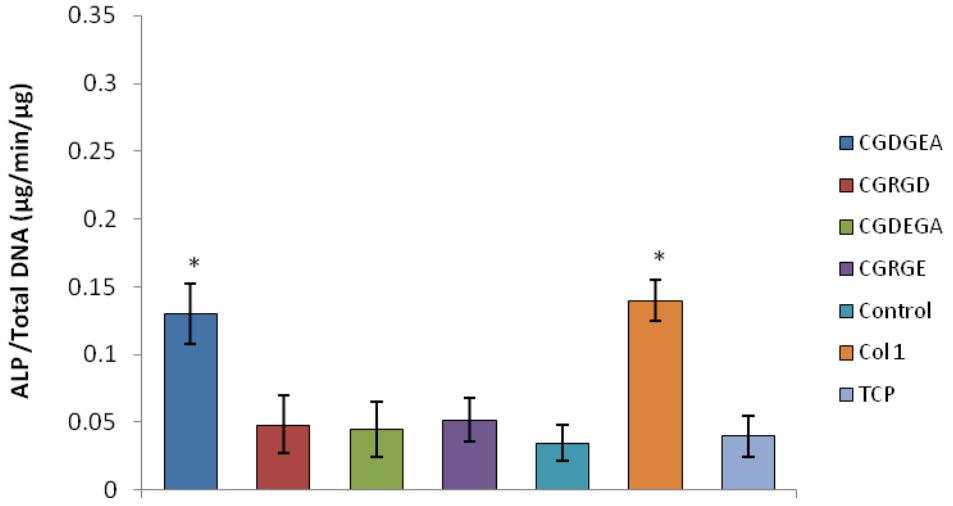

Figure 6.18 Effect of peptide-functionalized photocrosslinked fibrous scaffolds on alkaline phosphatase activity, determined using Alkaline Phosphatase assay. hMSCs were seeded on CGDGEA-conjugated scaffolds for 21 days without osteogenic media. The concentration of CGDGEA and CGRGD used was 5 and 2 mol%, respectively. Comparison of the effect of the different peptide-conjugated scaffolds: CDGEA, RGD and unfunctionalized. Mean ± SD, n = 3. (*) indicates the difference between the marked bar and the control (unfunctionalized scaffold) of the same time period is statistically significant *(p*<0.05).

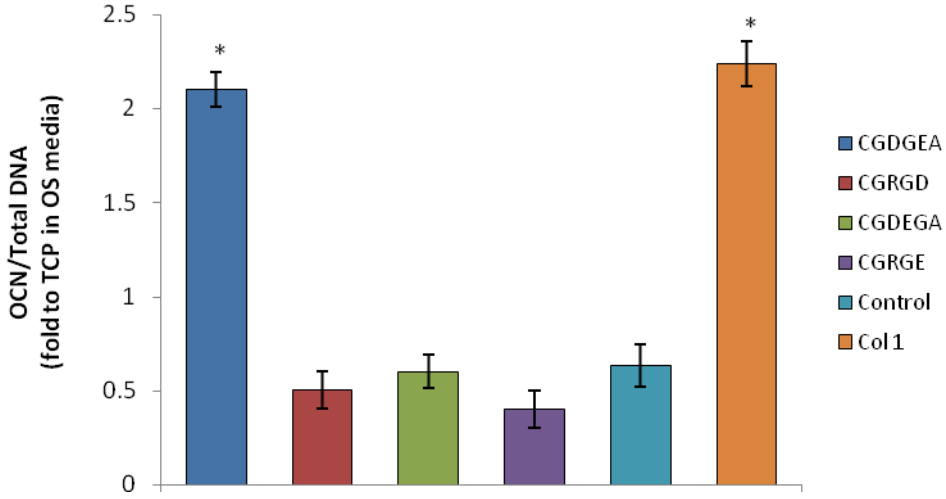

Figure 6.19 Effect of peptide-functionalized photocrosslinked fibrous scaffolds on osteocalcin secretion, determined using enzyme immunosorbent assay (EIA) assay. hMSCs were seeded on CGDGEA-conjugated scaffolds for 21 days without osteogenic media. The concentration of CGDGEA and CGRGD used was 5 and 2 mol%, respectively. Comparison of the effect of the different peptide-conjugated scaffolds: CDGEA, RGD and unfunctionalized. Mean ± SD, n = 3. (*) indicates the difference between the marked bar and the control (unfunctionalized scaffold) of the same time period is statistically significant (*p*<0.05).

These observations strongly suggest that the presentation of DGEA peptides to cells may serve as an osteogenic differentiation factor. The enhancement of osteoblastic differentiation was exhibited both in the presence and in the absence of osteogenic media, suggesting that DGEA can induce osteogenic differentiation even without osteogenic factors. This was also demonstrated in an investigation conducted by Hennessy *et al*. on hydroxyapatite surfaces [42, 80]. The authors have also demonstrated further that DGEA-coated HA disks implanted into rat tibiae improved bone ingrowth and induced increased levels of bone-implant direct contact than unmodified the HA disks [42]. Additionally, Yoo *et al*. have also shown early osteogenic differentiation on mouse preosteoblast cells stimulated by DGEA ligands on nanofibrous phage tissue matrices [38]. They further demonstrated osteogenic protein expression through mRNA quantification and bone cell protein marker expression induced by DGEA-engineered phage matrices. Moreover, the authors have also shown the higher potential of DGEA to induce osteogenic differentiation in comparison with RGD.

Other studies have demonstrated that RGD-modified surfaces are also able to promote osteogenic differentiation [234, 295, 296]. For example, PEG-DA hydrogels containing varying concentrations of RGD were synthesized to encapsulate MSCs and the expression of bone-related markers was examined [234]. The expression of alkaline phosphatase and osteocalcin were induced in the presence of RGD and a concentration-dependent trend was revealed with the increase in RGD concentration. In addition, investigations performed by Anderson *et al*. have shown that RGD has higher potential to stimulate osteogenesis compared to DGEA [295, 296]. But there studies were performed on self-assembled peptide amphiphiles, which may have caused differences in osteogenic response.

Integrins are focal transducers of ECM signals that influence osteoblast commitment and differentiation [126]. The $\alpha_1\beta_1$ and $\alpha_2\beta_1$ integrins are the main collagen-binding integrins, with $\alpha_1\beta_1$ possessing an increased affinity for type IV collagen while $\alpha_2\beta_1$ possessing an increased affinity for the fibrillar type 1 collagen [126, 307, 308]. Moreover, $\alpha_2\beta_1$ is substantially expressed in osteoblast-like cells and it is one of the major adhesion receptors used by these cells to attach to the collagen matrix [309].

Several investigations have indicated that the $\alpha_2\beta_1$ integrin interaction with type 1 collagen is a pivotal signal for the regulation of osteoblastic differentiation and matrix mineralization [36, 37, 120, 126, 128, 310]. Engagement of the $\alpha_2\beta_1$ integrin is related to the activation of osteoblast-specific factor (Runx-2 or Cbfa-1), a transcription factor that mediates osteogenic differentiation, specifically into the osteoblast phenotype, and is needed for the osteoblast-specific expression of the osteoblast-specific protein OCN [107, 110, 112, 126, 127, 280]. Moreover, the collagen type 1-$\alpha_2\beta_1$ integrin binding has been demonstrated to stimulate the osteogenic phenotype in MSCs [36,

37, 126]. This stimulation of osteoblastic phenotype in cells is due to the interaction of $\alpha_2\beta_1$ integrin to collagen type 1 which induces tyrosine phosphorylation of FAK and, consequently, the activation of ERK and MAPK which has been shown to influence osteoblast-specific gene expression and matrix mineralization [109, 111, 126, 128, 129]. Studies have reported that disrupting the $\alpha_2\beta_1$ interaction with type 1 collagen, by utilizing function-blocking antibodies, inhibits the expression of osteoblast specific genes, such as OCN and prevents the formation of mineralized matrix [36, 111, 126, 310].

A different collagen type-1 binding peptide, GFOGER (glycine-phenylalanine-hydroxyproline-glycine-glutamate-arginine) with a triple helical-like structure can also engage with the $\alpha_2\beta_1$ integrin receptor [311, 312] and has been shown to support cell adhesion and osteogenic differentiation comparable to collagen type 1 [282]. In addition, the authors demonstrated that $\alpha_2\beta_1$ integrin-specific GFOGER peptide induces FAK and ALP activation in MC3T3-E1 preosteoblast cells [126].

6.5 CONCLUSION

In the present chapter, the effects of DGEA- and RGD-conjugation of the MA/DEGMA fibrous scaffolds on hMSCs adhesion, morphology, viability and osteogenic differentiation were investigated. The results presented here strongly demonstrated the potential of DGEA- and RGD-conjugated fibrous scaffolds to support hMSCs adhesion and viability. Through cell adhesion and soluble peptide/antibody blocking competition assays, the bioactivity and specificity of each peptide-conjugated scaffolds were confirmed. hMSCs adhesion to DGEA peptides-conjugated scaffolds was found to be peptide concentration-dependent, whereby increasing DGEA concentration on the scaffolds further increased cell adhesion. In contrast, for the RGD-conjugated scaffold we found that increasing the peptide concentration (RGD) is not always guaranteed to enhance cell adhesion. Importantly, both DGEA and RGD peptides presented significantly higher cell adhesion levels in comparison to the control and the scrambled peptides. However, DGEA showed increased stimulation of adhesion compared to RGD peptides.

In addition, the effect of varying spacer glycine residue numbers for the DGEA and RGD peptide sequences on hMSCs adhesion and viability was also investigated. The results indicate that the introduction of spacer glycine residues to an adhesion peptide is vital in controlling the attachment of adherent cells. In the system studied, at least one glycine unit was shown to be beneficial for hMSCs adhesion onto the scaffold. Furthermore, increasing the number of glycine residues added to the peptides, significantly increased the adhesion and viability of hMSCs grown on the conjugated scaffold.

Lastly, hMSCs cultured on the DGEA-conjugated scaffolds were proven to activate osteogenic differentiation. Osteogenic differentiation markers, as ALP and OCN, were shown to be enhanced when hMSCs were grown on the DGEA-conjugated scaffolds for 14-21 days. Importantly, the enhanced osteoblastic activity was demonstrated both with and without osteogenic media, suggesting that the DGEA peptide is capable of stimulating osteogenic differentiation even in the absence of osteogenic factors.

Hence, the results here give evidence the high potential of DGEA-conjugated fibrous scaffolds for TE applications since these scaffolds were shown to significantly enhance cell viability and osteoblastic differentiation of hMSCs.

CHAPTER 7

Conclusions

The feasibility of electrospinning photocrosslinkable and low molecular weight acrylate monomers was investigated in this thesis. MA and DEGMA were the monomer and crosslinker of choice respectively with the aid of PEO as a polymer carrier and viscosity modifier. In Chapter 3, the ability to produce topologically and mechanically diverse fibrous scaffold materials was demonstrated. Photocrosslinked fibres were successfully developed by electrospinning different MA and DEGMA compositions and post-UV crosslinking. The effects of various processing parameters of electrospinning were investigated, including carrier polymer concentration, accelerating voltage, rate of delivery and monomer/carrier polymer ratios. With the use of high molecular weight PEO, all parameters were observed to have a profound effect on the electrospun fibres morphology. The analysis of this study lead to the determination of the optimal range of parameters required to produce uniform and bead-free electrospun MA/DEGMA fibrous scaffolds. When exposed to ultraviolet light in the presence of a photoinitiator, the crosslinked network was formed by converting the double bonds and a corresponding increase in mechanical strength was observed. PEO was extracted with thorough washing with water, and scaffolds swelled after incubation in water. Most importantly, varying MA and DEGMA composition affected overall fibre morphology, swelling and mechanics of the fibrous scaffold. A unique characteristic of the fibrous scaffold was that swelling could be observed when the scaffold is immersed in water or media. Swelling significantly increases with decreasing crosslinker concentration, the 90:10 ratio scaffolds displayed the highest degree of swelling, followed by 70:30 and 50:50 percentage MA:DEGMA compositions. Whereas, an increase in DEGMA (crosslinker) concentration lead to higher tensile modulus, which suggests an increase of crosslinking of acrylate within the network.

An assessment of biological activity of the acrylate fibrous scaffold was performed and described in Chapter 4. These studies were intended to evaluate the effect of varying ratios of MA:DEGMA of the fibrous scaffold on the viability of two different cell types, Saos-2 and hMSCs. Additionally, the effect of surface morphology on cellular activity was assessed by comparing the fibrous scaffolds to flat surfaces with equivalent chemical compositions. Lastly, the response of protein adsorption to all fibrous scaffolds and flat surfaces was evaluated.

The results presented in Chapter 4 strongly demonstrated the potential of MA/DEGMA fibrous scaffolds to support Saos-2 cell viability and proliferation. In agreement with literature, the MA:DEGMA photocrosslinked fibres increased the viability of Saos-2 cells in comparison to flat surfaces with similar chemistry. However, the considerable increase in apoptosis of hMSCS grown in all fibrous scaffolds and flat samples demonstrated the lower potential of the MA/DEGMA scaffold to support hMSCs attachment and viability. This was also evident in the cell activity assays, which showed decreased hMSCs metabolic activity assessed by alamarblue® assay in comparison to the negative control, TCP. On the other hand, in order to further explore the biological potential of the fibrous scaffolds, investigation of their ability to sustain cell viability over a

longer period of time was conducted. From day 15 onwards, a significant increase in cell viability was observed for hMSCs cultured on the 90:10 (MA:DEGMA) fibres. Such a result was not observed for the other scaffold compositions. Hence, this gives evidence that the 90:10 (MA:DEGMA) fibrous scaffolds could potentially support hMSCs viability better than the other scaffolds produced.

Furthermore, amongst the fibrous scaffolds and flat surfaces, the 90:10 (MA:DEGMA) fibres presented the highest cellular activity for both Saos-2 and hMSCs, which could be correlated to displaying of the best fibrous morphology from all the scaffold (shown in Chapter 3). Hence, as it has showed the highest cell response, best fibrous morphology and capability of maintaining mechanical integrity, the 90:10 (MA:DEGMA) composition was chosen as the best fibrous scaffold for bone tissue engineering purposes among the different compositions analysed. For this reason, the studies described in the following chapters were performed using this specific MA:DEGMA composition. Lastly, the response of protein adsorption to all fibrous scaffolds and flat surfaces was evaluated. Both fibrous scaffolds and flat surfaces displayed significantly lower protein adsorption compared to TCP. However, the fibrous scaffolds adsorbed higher amounts of serum proteins than the flat surfaces. Furthermore, this was most evident for the 90:10 (MA:DEGMA) ratio constructs, whereby the protein adsorption of the flat surface decreased to half when compared to the fibrous scaffold. This interesting result gives evidence that the fibrous architecture can alter protein adsorption.

The development of electrospun acrylate scaffolds conjugated with biological active peptides, RGD and DGEA were described in Chapter 5. The synthesis of the functionalized scaffold utilizes cysteine-functionalized RGD or DGEA peptide sequences in combination with MA/DEGMA monomers and employs a photoinitiated mixed-mode thiol-acrylate polymerization mechanism. Firstly, immobilization of DGEA and RGD peptides on the acrylate fibrous scaffold was analyzed by varying cysteine-conjugated DGEA and RGD concentrations. Measurement of peptide incorporation was determined by measuring free primary amine. The amount of free amine measured was compared to the initial concentration of free amine prior to UV crosslinking. The measurement of peptide incorporation was further confirmed by quantifying free sulfhydryl groups in solution. Cysteine-functionalized DGEA and RGD peptides were shown to be efficiently incorporated in the synthesized acrylate scaffolds with ~ 85% peptide incorporation. It was observed that immobilization of the peptides had no major effect on the overall morphology of the fibres, even as the peptide concentration was varied from 0.5 to 5 mol%. Except for the highest peptide concentration (5 mol%), all fibres conjugated with different concentrations of CGDGEA showed no significant differences for swelling behaviour and mechanical properties to when compared to the unfunctionalized fibrous scaffolds. In addition, the degradation of the CGDGEA

and unfunctionalized scaffolds were studied and both scaffolds degraded with mass loss of ~51% and ~45% at 16 weeks.

Most importantly, the presentation and distribution of the peptides on the surface of the scaffolds were investigated using ToF-SIMS. The ToF-SIMS results demonstrated the distribution of the immobilized peptides on the surface of the fibres. The peptides were clearly present and distributed evenly on the surface of the fibres. This novel method of using ToF-SIMS to analyze peptide conjugation distribution was critical because the process of functionalization was done in bulk throughout the whole scaffold and not only on the surface. It is important for the peptides to be distributed on the surface of the fibres to ensure that the peptide ligands are spatially accessible to the cell-surface integrins.

The efficiency of conjugation of peptides using thiol-acrylate reaction regardless of the number of glycine spacer arm length was also investigated. Glycine, an aliphatic amino amino was chosen as the spacer because it has been shown to have nominal effect on the reactivity of the thiol group as it is extremely inert [141]. Hence, it would have negligible effects on the thiol-acrylate reaction during functionalization of the scaffold. Varying the amount of spacer arms is essential for cell-scaffold interactions as it has been shown to influence the adhesion and spreading of certain cell types [35, 133]. The efficiency of the peptides conjugation using the thiol-acrylate reaction was similar, regardless of the length of the glycine spacer arms. For all peptide sequences, independently of the length of the arm spacer, the percentage of incorporation determined was approximately 80-86%.

The effect of DGEA- and RGD-conjugated fibrous scaffolds on hMSCs adhesion, morphology, viability and osteogenic differentiation were investigated in Chapter 6. The results presented demonstrated the potential of DGEA- and RGD-conjugated fibrous scaffolds to support hMSCs adhesion and viability. Through cell adhesion and soluble peptide/antibody blocking competition assays, the bioactivity and specificity of each peptide conjugated to the scaffolds were confirmed. The hMSCs adhesion to DGEA peptides have demonstrated to be concentration dependent, whereby increasing DGEA concentration on the scaffold further increased cell adhesion. In contrast, RGD-conjugated scaffolds have shown that an increase in peptide concentration for RGD is not always guaranteed to increase cell adhesion. Both DGEA and RGD peptides presented significantly higher cell adhesion in comparison to control and scrambled peptides. However, DGEA showed increased stimulation of adhesion compared to RGD peptides.

In addition, the effect of varying spacer arms (glycine) for the peptide sequence of DGEA and RGD ligands on hMSCs adhesion and viability was investigated. The results indicate that introduction of a spacer arm (glycine) to an adhesion peptide is vital in controlling the attachment

of adherent cells, and at least one glycine unit is required for hMSCs adhesion on the scaffold. Furthermore, increasing the amount of glycine increased the adhesion and viability of hMSCs.

Lastly, hMSCs cultured on DGEA conjugated scaffolds exhibited the activation of osteogenic differentiation markers, ALP and OCN. This enhanced osteoblastic activity was observed both in the presence and the absence of osteogenic media, indicating that DGEA can stimulate osteoblastic differentiation even in the absence of osteogenic media. Nevertheless, further studies are required to better comprehend the effect of the differentiation of the hMSCs. Further gene expression studies of Runx-2/Cbfa and other differentiation transcription factors should be assessed. In addition, the assessment of the differentiation effect of the peptide-conjugated scaffolds *in vivo* would be of interest, as it is acknowledged that results obtained *in vitro* cannot be directly translated to *in vivo* conditions.

Moreover, further improvements could be studied for the fibrous scaffold, especially to improve the limitation of cell infiltration of the scaffold. Though this was not investigated in the studies here, cell infiltration into these fibres is slow. To address this issue, by utilizing the UV system and the use of a UV mask on top of the scaffold during photocrosslinking could be investigated to increase porosity of the scaffold. Subsequently, uncrosslinked monomers could be leached out during washing and this could produce pores to improve infiltration throughout the fibrous scaffold. Alternatively, pores could be introduced by introducing salt particles which can then be leached out.

The mechanical properties of the scaffold could also be improved by aligning the fibres and varying fibre size. In addition, tri-laminar electrospun scaffolds could also be developed by using this UV system by sequential electrospinning in a continuous construct and UV patterning to create scaffolds that offers zone specific structural organization for the tissue function.

Furthermore, the concept of immobilizing synthetic peptides onto a scaffold in a facile and inexpensive manner was presented in this thesis thus this may form a platform for advanced development of the scaffold by adding different types of peptides with other functions such as growth factor or protein activation to modulate cellular functions. This would increase the overall functions and complexity of the scaffold.

As mentioned previously, further studies are required to better understand and control the cellular response to the fibrous acrylate scaffolds. In addition, further structural and functional improvements could be made to improve the scaffold for TE applications. However, our studies have clearly demonstrated the feasibility of producing fibrous scaffold materials using electrospinning photocrosslinkable and low molecular weight acrylate monomers, MA and DEGMA and post-UV crosslinking. Furthermore, cysteine-functionalized DGEA and RGD peptides were efficiently incorporated in the synthesized acrylate scaffolds by employing a photoinitiated mixed-

mode thiol-acrylate polymerization mechanism. The peptide-conjugated fibrous scaffolds showed increased hMSCs adhesion and viability, and additionally hMSCs cultured on DGEA-conjugated scaffolds showed the activation of osteogenic differentiation markers, ALP and OCN. This thesis has therefore been able to illustrate the great potential of these scaffolds for bone TE applications, specifically for non-loading bone such as in the craniomaxillofacial skeleton.

APPENDIX

Glycine Standard Curve for Ninhydrin Assay and Fluoraldehyde (OPA) assay

1. A gradient of concentrations was serial diluted from 10ml of 0.1M glycine with 50% (v/v) ethanol.

2. 0.5 ml of each concentration was placed in a 2 ml glass vial.

3. 100µL of 1M Ninhydrin (Section 5.3.3 and 5.3.4) was added to each vial. Immediate colour change was observed.

4. The vials were then incubated at room temperature for 4 hours, placed on an orbital shaker, to ensure the reaction between ninhydrin and the amine groups on all samples.

5. The samples were then removed and the absorbance of the solution was measured at 570nm, on a microplate reader (Spectramax M5, Molecular devices).

6. The optical densities (570nm) were plotted against the concentration of glycine which is represented by amine concentration.

Cysteine Standard Curve for Ellman's Assay

1. Cysteine hydrochloride monohydrate was dissolved with reaction buffer (0.1 M of sodium phosphate) to attain a set of cysteine standards of specific serial concentrations.

2. A set of 5 ml vials containing 250 µl of Ellman's reagent solution (DNTB) and 2.5ml of reaction buffer was prepared.

3. 250µL of each standard or unknown samples (Section 5.3.5) was added to each test tube prepared in step 2.

4. All standards and samples was mixed and incubated for 3 hours in 5 ml glass vials, at room temperature and placed on an orbital shaker.

5. Absorbance was measured at 412nm using a microplate reader (Spectramax M5, Molecular devices).

6. The values obtained for the standards were plotted with concentration of cysteine to generate a standard curve.

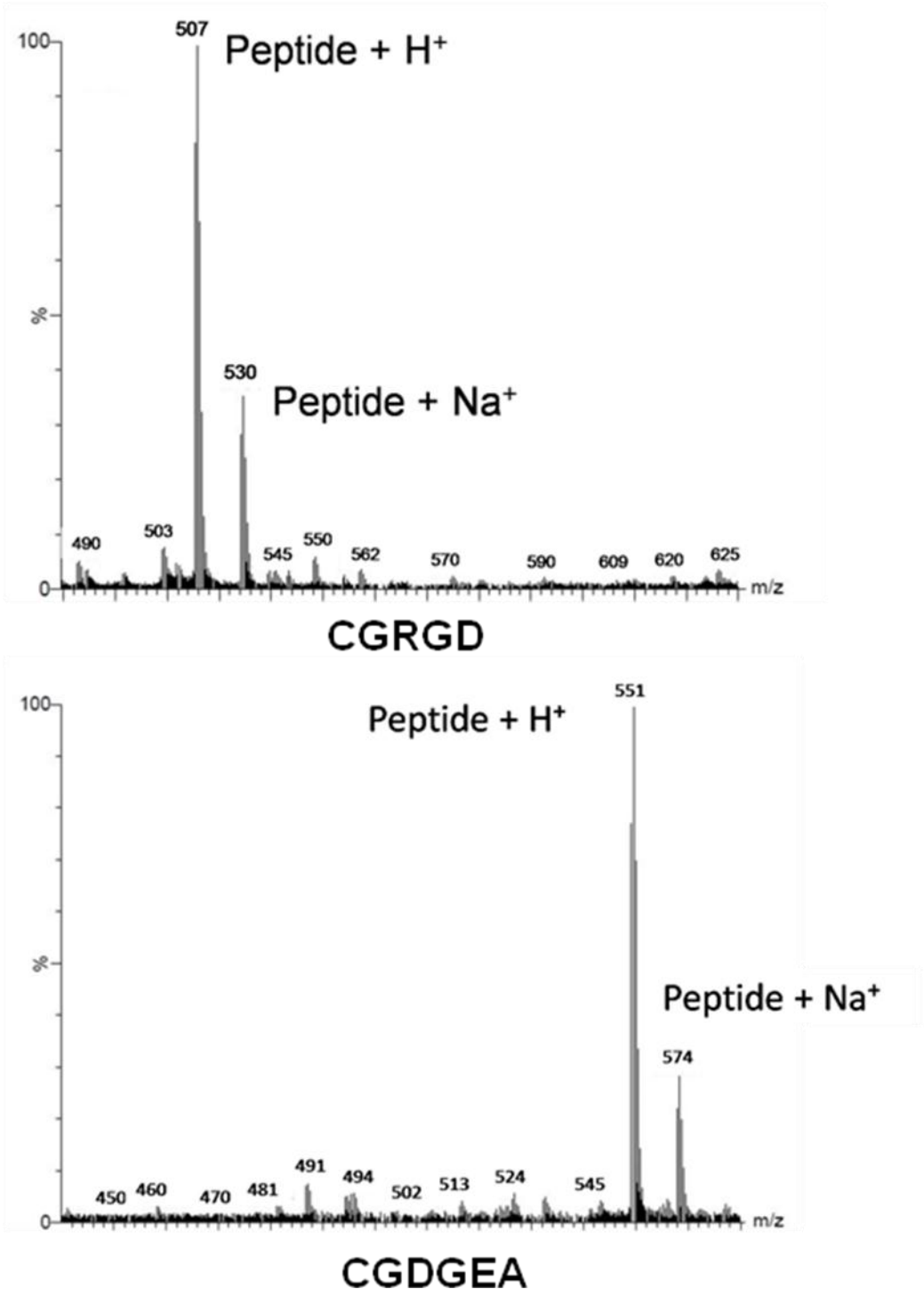

MALDI mass spectral analysis of peptides. MALDI mass spectrum for CGRGD and CGDGEA peptides, with the labelled ionisation peaks (Peptide + H^+/Na^+) representing peptide molecular weight of 506 (CGRGD) and 550 (CGDGEA).

REFERENCES

1. Stevens MM. Biomaterials for bone tissue engineering. Materials Today. 2008;11(5):18-25.
2. Kneser U, Schaefer DJ, Munder B, Klemt C, Andree C, Stark GB. Tissue engineering of bone. Minimally Invasive Therapy & Allied Technologies. 2002;11(3):107-16.
3. Langer R, Vacanti J. Tissue engineering. Science. 1993;260(5110):920-6.
4. Discher DE, Mooney DJ, Zandstra PW. Growth factors, matrices, and forces combine and control stem cells. Science. 2009;324(5935):1673-7.
5. Spradling A, Drummond-Barbosa D, Kai T. Stem cells find their niche. Nature. 2001;414(6859):98-104.
6. Streuli C. Extracellular matrix remodelling and cellular differentiation. Current Opinion in Cell Biology. 1999;11(5):634-40.
7. Place ES, Evans ND, Stevens MM. Complexity in biomaterials for tissue engineering. Nature Materials. 2009;8(6):457-70.
8. Lanza RP, Langer RS, Vacanti J. Principles of tissue engineering: Academic Press; 2007.
9. Anderson DG, Levenberg S, Langer R. Nanoliter-scale synthesis of arrayed biomaterials and application to human embryonic stem cells. Nature Biotechnology. 2004;22(7):863-6.
10. Tan AR, Ifkovits JL, Baker BM, Brey DM, Mauck RL, Burdick JA. Electrospinning of photocrosslinked and degradable fibrous scaffolds. Journal of Biomedical Materials Research Part A. 2008;87A(4):1034-43.
11. Ji Y, Ghosh K, Shu XZ, Li B, Sokolov JC, Prestwich GD, et al. Electrospun three-dimensional hyaluronic acid nanofibrous scaffolds. Biomaterials. 2006;27(20):3782-92.
12. Stitzel J, Liu J, Lee SJ, Komura M, Berry J, Soker S, et al. Controlled fabrication of a biological vascular substitute. Biomaterials. 2006;27(7):1088-94.
13. H Reneker D, Chun I. Nanometre diameter fibres of polymer, produced by electrospinning. Nanotechnology. 1996;7(3):216.

14. Li D, Xia Y. Electrospinning of nanofibers: Reinventing the wheel? Advanced Materials. 2004;16(14):1151-70.

15. Sell S, Barnes C, Smith M, McClure M, Madurantakam P, Grant J, et al. Extracellular matrix regenerated: tissue engineering via electrospun biomimetic nanofibers. Polymer International. 2007;56(11):1349-60.

16. Ifkovits JL, Burdick JA. Review: photopolymerizable and degradable biomaterials for tissue engineering applications. Tissue Engineering. 2007;13(10):2369-85.

17. Fisher JP, Dean D, Engel PS, Mikos AG. Photoinitiated polymerization of biomaterials. Annual Review of Materials Research. 2001;31:171-81.

18. Shin H, Jo S, Mikos AG. Modulation of marrow stromal osteoblast adhesion on biomimetic oligo[poly(ethylene glycol) fumarate] hydrogels modified with Arg-Gly-Asp peptides and a poly(ethylene glycol) spacer. Journal of Biomedical Materials Research. 2002;61(2):169-79.

19. Cruise GM, Scharp DS, Hubbell JA. Characterization of permeability and network structure of interfacially photopolymerized poly(ethylene glycol) diacrylate hydrogels. Biomaterials. 1998;19(14):1287-94.

20. Wang D-A, Williams CG, Li Q, Sharma B, Elisseeff JH. Synthesis and characterization of a novel degradable phosphate-containing hydrogel. Biomaterials. 2003;24(22):3969-80.

21. Kloxin AM, Kasko AM, Salinas CN, Anseth KS. Photodegradable hydrogels for dynamic tuning of physical and chemical properties. Science. 2009;324(5923):59-63.

22. Strang R, Cummings A, Stephen KW. Laboratory studies of visible-light cured fissure sealants: setting times and depth of polymerization. Journal of Oral Rehabilitation. 1986;13(4):305-10.

23. Venhoven BAM, de Gee AJ, Davidson CL. Light initiation of dental resins: dynamics of the polymerization. Biomaterials. 1996;17(24):2313-8.

24. Anseth K, Newman S, Bowman C. Polymeric dental composites: Properties and reaction behavior of multimethacrylate dental restorations

Biopolymers II. In: Peppas N, Langer R, editors.: Springer Berlin / Heidelberg; 1995. p. 177-217.

25. Nijst CLE, Bruggeman JP, Karp JM, Ferreira L, Zumbuehl A, Bettinger CJ, et al. Synthesis and characterization of photocurable elastomers from poly(glycerol-co-sebacate). Biomacromolecules. 2007;8(10):3067-73.

26. Rozario T, DeSimone DW. The extracellular matrix in development and morphogenesis: A dynamic view. Developmental Biology. 2010;341(1):126-40.

27. Giancotti FG. Complexity and specificity of integrin signalling. Nature Cell Biology. 2000;2(1):E13-4.

28. Harburger DS, Calderwood DA. Integrin signalling at a glance. Journal of Cell Science. 2009;122(2):159-63.

29. Place ES, George JH, Williams CK, Stevens MM. Synthetic polymer scaffolds for tissue engineering. Chemical Society Reviews. 2009;38(4):1139-51.

30. Melkoumian Z, Weber JL, Weber DM, Fadeev AG, Zhou Y, Dolley-Sonneville P, et al. Synthetic peptide-acrylate surfaces for long-term self-renewal and cardiomyocyte differentiation of human embryonic stem cells. Nature Biotechnology. 2010;28(6):606-10.

31. Brandley BK, Schnaar RL. Covalent attachment of an Arg-Gly-Asp sequence peptide to derivatizable polyacrylamide surfaces: Support of fibroblast adhesion and long-term growth. Analytical Biochemistry. 1988;172(1):270-8.

32. Pierschbacher MD, Ruoslahti E. Cell attachment activity of fibronectin can be duplicated by small synthetic fragments of the molecule. Nature. 1984;309(5963):30-3.

33. Hersel U, Dahmen C, Kessler H. RGD modified polymers: biomaterials for stimulated cell adhesion and beyond. Biomaterials. 2003;24(24):4385-415.

34. Schaffner P, Dard MM. Structure and function of RGD peptides involved in bone biology. Cellular and Molecular Life Sciences. 2003;60(1):119-32.

35. Perlin L, MacNeil S, Rimmer S. Production and performance of biomaterials containing RGD peptides. Soft Matter. 2008;4(12):2331-49.

36. Mizuno M, Fujisawa R, Kuboki Y. Type I collagen-induced osteoblastic differentiation of bone-marrow cells mediated by collagen-α2β1 integrin interaction. Journal of Cellular Physiology. 2000;184(2):207-13.

37. Mizuno M, Kuboki Y. Osteoblast-related gene expression of bone marrow cells during the osteoblastic differentiation induced by type I collagen. Journal of Biochemistry. 2001;129(1):133-8.

38. Yoo SY, Kobayashi M, Lee PP, Lee S-W. Early osteogenic differentiation of mouse preosteoblasts induced by collagen-derived DGEA-peptide on nanofibrous phage tissue matrices. Biomacromolecules. 2011;12(4):987-96.

39. Murphy CM, Haugh MG, O'Brien FJ. The effect of mean pore size on cell attachment, proliferation and migration in collagen–glycosaminoglycan scaffolds for bone tissue engineering. Biomaterials. 2010;31(3):461-6.

40. Sawyer AA, Song SJ, Susanto E, Chuan P, Lam CXF, Woodruff MA, et al. The stimulation of healing within a rat calvarial defect by mPCL–TCP/collagen scaffolds loaded with rhBMP-2. Biomaterials. 2009;30(13):2479-88.

41. Schneider RK, Puellen A, Kramann R, Raupach K, Bornemann J, Knuechel R, et al. The osteogenic differentiation of adult bone marrow and perinatal umbilical mesenchymal stem cells and matrix remodelling in three-dimensional collagen scaffolds. Biomaterials. 2010;31(3):467-80.

42. Hennessy KM, Pollot BE, Clem WC, Phipps MC, Sawyer AA, Culpepper BK, et al. The effect of collagen I mimetic peptides on mesenchymal stem cell adhesion and differentiation, and on bone formation at hydroxyapatite surfaces. Biomaterials. 2009;30(10):1898-909.

43. Lysaght MJ, Jaklenec A, Deweerd E. Great expectations: Private sector activity in tissue engineering, regenerative medicine, and stem cell therapeutics. Tissue Engineering Part A. 2008;14(2):305-15. Epub 2008/03/13.

44. Viola J, Lal B, Grad O. The emergence of tissue engineering as a research field. 2003 August 2010.

45. Marklein RA, Burdick JA. Controlling stem cell fate with material design. Advanced materials. 2010;22(2):175-89.

46. Michalopoulos GK, DeFrances MC. Liver regeneration. Science. 1997;276(5309):60-6.

47. Thomson JA, Itskovitz-Eldor J, Shapiro SS, Waknitz MA, Swiergiel JJ, Marshall VS, et al. Embryonic stem cell lines derived from human blastocysts. Science. 1998;282(5391):1145-7.

48. Stevens MM, Marini RP, Schaefer D, Aronson J, Langer R, Shastri VP. In vivo engineering of organs: The bone bioreactor. Proceedings of the National Academy of Sciences of the United States of America. 2005;102(32):11450-5.

49. Bouchie A. Tissue engineering firms go under. Nature Biotechnology. 2002;20(12):1178-9.

50. Johnson PC, Mikos AG, Fisher JP, Jansen JA. Strategic directions in tissue engineering. Tissue Engineering. 2007;13(12):2827-37.

51. Julian G. Tissue engineering applications. UK Society for Biomaterials Conference 2006.

52. Hollander AP, Dickinson SC, Sims TJ, Brun P, Cortivo R, Kon E, et al. Maturation of tissue engineered cartilage implanted in injured and osteoarthritic human knees. Tissue Engineering. 2006;12(7):1787-98.

53. Rubbens MP, Mol A, Boerboom RA, Bank RA, Baaijens FP, Bouten CV. Intermittent straining accelerates the development of tissue properties in engineered heart valve tissue. Tissue Engineering Part A. 2009;15(5):999-1008.

54. Lutolf MP, Weber FE, Schmoekel HG, Schense JC, Kohler T, Müller R, et al. Repair of bone defects using synthetic mimetics of collagenous extracellular matrices. Nature Biotechnology. 2003;21(5):513-8.

55. Chung EH, Gilbert M, Virdi AS, Sena K, Sumner DR, Healy KE. Biomimetic artificial ECMs stimulate bone regeneration. Journal of Biomedical Materials Research Part A. 2006;79A(4):815-26.

56. Bauer TW, Muschler GF. Bone graft materials: An overview of the basic science. Clinical Orthopaedics and Related Research. 2000;371:10-27.

57. Garrison KR, Shemilt I, Donell S, Ryder JJ, Mugford M, Harvey I, et al. Bone morphogenetic protein (BMP) for fracture healing in adults. Cochrane Database of Systematic Reviews (Online). 2010(6):CD006950.

58. Szpalski C, Barr J, Wetterau M, Saadeh PB, Warren SM. Cranial bone defects: current and future strategies. Neurosurgical Focus. 2010;29(6):8.

59. Schneider OD, Weber F, Brunner TJ, Loher S, Ehrbar M, Schmidlin PR, et al. In vivo and in vitro evaluation of flexible, cottonwool-like nanocomposites as bone substitute material for complex defects. Acta Biomaterialia. 2009;5(5):1775-84.

60. Elsalanty ME, Por Y-C, Genecov DG, Salyer KE, Wang Q, Barcelo CR, et al. Recombinant human BMP-2 enhances the effects of materials used for reconstruction of large cranial defects. Journal of Oral and Maxillofacial Surgery. 2008;66(2):277-85.

61. Pham QP, Sharma U, Mikos AG. Electrospinning of polymeric nanofibers for tissue engineering applications: a review. Tissue engineering. 2006;12(5):1197-211.

62. Murugan R, Ramakrishna S. Design strategies of tissue engineering scaffolds with controlled fiber orientation. Tissue Engineering. 2007;13(8):1845-66.

63. Kim J, Kim IS, Cho TH, Lee KB, Hwang SJ, Tae G, et al. Bone regeneration using hyaluronic acid-based hydrogel with bone morphogenic protein-2 and human mesenchymal stem cells. Biomaterials. 2007;28(10):1830-7.

64. Lee KY, Mooney DJ. Hydrogels for tissue engineering. Chemical Reviews. 2001;101(7):1869-79.

65. Hollister SJ. Porous scaffold design for tissue engineering. Nature Materials. 2005;4(7):518-24.

66. Jones JR, Poologasundarampillai G, Atwood RC, Bernard D, Lee PD. Non-destructive quantitative 3D analysis for the optimisation of tissue scaffolds. Biomaterials. 2007;28(7):1404-13.

67. Zhang R, Ma PX. Synthetic nano-fibrillar extracellular matrices with predesigned macroporous architectures. Journal of Biomedical Materials Research. 2000;52(2):430-8.

68. Park GE, Pattison MA, Park K, Webster TJ. Accelerated chondrocyte functions on NaOH-treated PLGA scaffolds. Biomaterials. 2005;26(16):3075-82.

69. Sokolsky-Papkov M, Agashi K, Olaye A, Shakesheff K, Domb AJ. Polymer carriers for drug delivery in tissue engineering. Advanced Drug Delivery Reviews. 2007;59(4–5):187-206.

70. Li W-J, Laurencin CT, Caterson EJ, Tuan RS, Ko FK. Electrospun nanofibrous structure: A novel scaffold for tissue engineering. Journal of Biomedical Materials Research. 2002;60(4):613-21.

71. Leong KF, Cheah CM, Chua CK. Solid freeform fabrication of three-dimensional scaffolds for engineering replacement tissues and organs. Biomaterials. 2003;24(13):2363-78.

72. Ahn S, Kim Y, Lee H, Kim G. A new hybrid scaffold constructed of solid freeform-fabricated PCL struts and collagen struts for bone tissue regeneration: fabrication, mechanical properties, and cellular activity. Journal of Materials Chemistry. 2012;22(31):15901-9.

73. Weigel T, Schinkel G, Lendlein A. Design and preparation of polymeric scaffolds for tissue engineering. Expert Review of Medical Devices. 2006;3(6):835-51.

74. Stein GS, Lian JB, Owen TA. Relationship of cell growth to the regulation of tissue-specific gene expression during osteoblast differentiation. The FASEB Journal. 1990;4(13):3111-23.

75. Gentleman E, Swain RJ, Evans ND, Boonrungsiman S, Jell G, Ball MD, et al. Comparative materials differences revealed in engineered bone as a function of cell-specific differentiation. Nature Materials. 2009;8(9):763-70.

76. Pittenger MF, Mackay AM, Beck SC, Jaiswal RK, Douglas R, Mosca JD, et al. Multilineage potential of adult human mesenchymal stem cells. Science. 1999;284(5411):143-7.

77. Bruder SP, Jaiswal N, Ricalton NS, Mosca JD, Kraus KH, Kadiyala S. Mesenchymal stem cells in osteobiology and applied bone regeneration. Clinical Orthopaedics and Related Research. 1998;355:S247-S56.

78. Conget PA, Minguell JJ. Phenotypical and functional properties of human bone marrow mesenchymal progenitor cells. Journal of Cellular Physiology. 1999;181(1):67-73.

79. Anselme K. Osteoblast adhesion on biomaterials. Biomaterials. 2000;21(7):667-81.

80. Culpepper BK, Phipps MC, Bonvallet PP, Bellis SL. Enhancement of peptide coupling to hydroxyapatite and implant osseointegration through collagen mimetic peptide modified with a polyglutamate domain. Biomaterials. 2010;31(36):9586-94.

81. Caplan AI. Adult mesenchymal stem cells for tissue engineering versus regenerative medicine. Journal of Cellular Physiology. 2007;213(2):341-7.

82. Tuan RS, Boland G, Tuli R. Adult mesenchymal stem cells and cell-based tissue engineering. Arthritis Research & Therapy. 2003;5(1):32-45.

83. Abdallah BM, Kassem M. The use of mesenchymal (skeletal) stem cells for treatment of degenerative diseases: Current status and future perspectives. Journal of Cellular Physiology. 2009;218(1):9-12.

84. Chen FH, Rousche KT, Tuan RS. Technology Insight: adult stem cells in cartilage regeneration and tissue engineering. Nature Clinical Practice Rheumatology. 2006;2(7):373-82.

85. Halstead L, Scott M, Rifas L, Avioli L. Characterization of osteoblast-like cells from normal adult rat femoral trabecular bone. Calcified Tissue International. 1992;50(1):93-5.

86. Malekzadeh R, Hollinger JO, Buck D, Adams DF, McAllister BS. Isolation of human osteoblast-like cells and in vitro amplification for tissue engineering. Journal of Periodontology. 1998;69(11):1256-62.

87. Rodan SB, Imai Y, Thiede MA, Wesolowski G, Thompson D, Bar-Shavit Z, et al. Characterization of a human osteosarcoma cell line (Saos-2) with osteoblastic properties. Cancer Research. 1987;47(18):4961-6.

88. Roskelley CD, Desprez PY, Bissell MJ. Extracellular matrix-dependent tissue-specific gene expression in mammary epithelial cells requires both physical and biochemical signal transduction. Proceedings of the National Academy of Sciences of the United States of America. 1994;91(26):12378-82.

89. Clark E, Brugge J. Integrins and signal transduction pathways: the road taken. Science. 1995;268(5208):233-9.

90. Miyamoto S, Teramoto H, Coso OA, Gutkind JS, Burbelo PD, Akiyama SK, et al. Integrin function: molecular hierarchies of cytoskeletal and signaling molecules. The Journal of Cell Biology. 1995;131(3):791-805.

91. Shoulders MD, Raines RT. Collagen structure and stability. Annual Review of Biochemistry. 2009;78:929-58.

92. Yu SM, Li Y, Kim D. Collagen mimetic peptides: progress towards functional applications. Soft Matter. 2011;7(18):7927-38.

93. Gordon MK, Hahn RA. Collagens. Cell and Tissue Research. 2010;339(1):247-57.

94. Ratner B, TA H. The role of adsorbed proteins in tissue response to biomaterials. Biomaterial Science- An introduction in materials in medicine. 2 ed. San Diego, CA: Elsevier; 2004. p. 225-36.

95. Singh P, Carraher C, Schwarzbauer JE. Assembly of fibronectin extracellular matrix. Annual Review of Cell and Developmental Biology. 2010;26:397-419.

96. Barczyk M, Carracedo S, Gullberg D. Integrins. Cell and Tissue Research. 2010;339(1):269-80.

97. Hynes RO. The emergence of integrins: a personal and historical perspective. Matrix Biology : Journal of the International Society for Matrix Biology. 2004;23(6):333-40.

98. Mao X, Peng H, Ling J, Friis T, Whittaker AK, Crawford R, et al. Enhanced human bone marrow stromal cell affinity for modified poly(l-lactide) surfaces by the upregulation of adhesion molecular genes. Biomaterials. 2009;30(36):6903-11.

99. Siebers MC, ter Brugge PJ, Walboomers XF, Jansen JA. Integrins as linker proteins between osteoblasts and bone replacing materials. A critical review. Biomaterials. 2005;26(2):137-46.

100. Takada Y, Ye X, Simon S. The integrins. Genome Biology. 2007;8(5):215.

101. Petit V, Thiery J-P. Focal adhesions: Structure and dynamics. Biology of the Cell. 2000;92(7):477-94.

102. O'Toole TE. Integrin signaling: Building connections beyond the focal contact? Matrix Biology. 1997;16(4):165-71.

103. Cowles EA, Brailey LL, Gronowicz GA. Integrin-mediated signaling regulates AP-1 transcription factors and proliferation in osteoblasts. Journal of Biomedical Materials Research. 2000;52(4):725-37.

104. Giancotti FG, Ruoslahti E. Integrin signaling. Science. 1999;285(5430):1028-33.

105. Hynes RO. Integrins: bidirectional, allosteric signaling machines. Cell. 2002;110(6):673-87.

106. Coppolino MG, Dedhar S. Bi-directional signal transduction by integrin receptors. The International Journal of Biochemistry & Cell Biology. 2000;32(2):171-88.

107. Carvalho RS, Kostenuik PJ, Salih E, Bumann A, Gerstenfeld LC. Selective adhesion of osteoblastic cells to different integrin ligands induces osteopontin gene expression. Matrix Biology. 2003;22(3):241-9.

108. Gordon JA, Hunter GK, Goldberg HA. Activation of the mitogen-activated protein kinase pathway by bone sialoprotein regulates osteoblast differentiation. Cells Tissues Organs. 2009;189(1-4):138-43.

109. Takeuchi Y, Suzawa M, Kikuchi T, Nishida E, Fujita T, Matsumoto T. Differentiation and transforming growth factor-beta receptor down-regulation by collagen-alpha2beta1 integrin interaction is mediated by focal adhesion kinase and its downstream signals in murine osteoblastic cells. The Journal of biological chemistry. 1997;272(46):29309-16.

110. Xiao G, Wang D, Benson MD, Karsenty G, Franceschi RT. Role of the alpha2-integrin in osteoblast-specific gene expression and activation of the Osf2 transcription factor. The Journal of biological chemistry. 1998;273(49):32988-94.

111. Xiao G, Jiang D, Thomas P, Benson MD, Guan K, Karsenty G, et al. MAPK pathways activate and phosphorylate the osteoblast-specific transcription factor, Cbfa1. The Journal of biological chemistry. 2000;275(6):4453-9.

112. Franceschi RT, Xiao G, Jiang D, Gopalakrishnan R, Yang S, Reith E. Multiple signaling pathways converge on the Cbfa1/Runx2 transcription factor to regulate osteoblast differentiation. Connective Tissue Research. 2003;44 Suppl 1:109-16.

113. Salasznyk RM, Klees RF, Williams WA, Boskey A, Plopper GE. Focal adhesion kinase signaling pathways regulate the osteogenic differentiation of human mesenchymal stem cells. Experimental Cell Research. 2007;313(1):22-37.

114. Komori T, Yagi H, Nomura S, Yamaguchi A, Sasaki K, Deguchi K, et al. Targeted disruption of Cbfa1 results in a complete lack of bone formation owing to maturational arrest of osteoblasts. Cell. 1997;89(5):755-64.

115. Schaller MD. Biochemical signals and biological responses elicited by the focal adhesion kinase. Biochimica et Biophysica Acta (BBA) - Molecular Cell Research. 2001;1540(1):1-21.

116. Weber LM, Hayda KN, Haskins K, Anseth KS. The effects of cell–matrix interactions on encapsulated β-cell function within hydrogels functionalized with matrix-derived adhesive peptides. Biomaterials. 2007;28(19):3004-11.

117. Zhu Y, Gao C, Liu X, He T, Shen J. Immobilization of biomacromolecules onto aminolyzed poly(L-lactic acid) toward acceleration of endothelium regeneration. Tissue Engineering. 2004;10(1-2):53-61.

118. Steele JG, Dalton BA, Johnson G, Underwood PA. Adsorption of fibronectin and vitronectin onto Primaria™ and tissue culture polystyrene and relationship to the mechanism of initial attachment of human vein endothelial cells and BHK-21 fibroblasts. Biomaterials. 1995;16(14):1057-67.

119. Ma PX. Biomimetic materials for tissue engineering. Advanced Drug Delivery Reviews. 2008;60(2):184-98.

120. Salasznyk RM, Williams WA, Boskey A, Batorsky A, Plopper GE. Adhesion to vitronectin and collagen I promotes osteogenic differentiation of human mesenchymal stem cells. Journal of Biomedicine & Biotechnology. 2004;2004(1):24-34.

121. Venugopal J, Ramakrishna S. Biocompatible nanofiber matrices for the engineering of a dermal substitute for skin regeneration. Tissue Engineering. 2005;11(5-6):847-54.

122. Eichler J. Peptides as protein binding site mimetics. Current Opinion in Chemical Biology. 2008;12(6):707-13.

123. LeBaron RG, Athanasiou KA. Extracellular matrix cell adhesion peptides: functional applications in orthopedic materials. Tissue Engineering. 2000;6(2):85-103.

124. Salber J, Gräter S, Harwardt M, Hofmann M, Klee D, Dujic J, et al. Influence of different ECM mimetic peptide sequences embedded in a nonfouling environment

on the specific adhesion of human-skin keratinocytes and fibroblasts on deformable substrates. Small. 2007;3(6):1023-31.

125. Sreejalekshmi KG, Nair PD. Biomimeticity in tissue engineering scaffolds through synthetic peptide modifications—Altering chemistry for enhanced biological response. Journal of Biomedical Materials Research Part A. 2011;96A(2):477-91.

126. Reyes CD, García AJ. α2β1 integrin-specific collagen-mimetic surfaces supporting osteoblastic differentiation. Journal of Biomedical Materials Research Part A. 2004;69A(4):591-600.

127. Xiao G, Gopalakrishnan R, Jiang D, Reith E, Benson MD, Franceschi RT. Bone morphogenetic proteins, extracellular matrix, and mitogen-activated protein kinase signaling pathways are required for osteoblast-specific gene expression and differentiation in MC3T3-E1 cells. Journal of Bone and Mineral Research. 2002;17(1):101-10.

128. Suzawa M, Tamura Y, Fukumoto S, Miyazono K, Fujita T, Kato S, et al. Stimulation of Smad1 transcriptional activity by Ras-extracellular signal-regulated kinase pathway: A possible mechanism for collagen-dependent osteoblastic differentiation. Journal of Bone and Mineral Research. 2002;17(2):240-8.

129. Tamura Y, Takeuchi Y, Suzawa M, Fukumoto S, Kato M, Miyazono K, et al. Focal adhesion kinase activity is required for bone morphogenetic protein—Smad1 signaling and osteoblastic differentiation in murine MC3T3-E1 cells. Journal of Bone and Mineral Research. 2001;16(10):1772-9.

130. Gobin AS, West JL. Cell migration through defined, synthetic ECM analogs. The FASEB Journal. 2002;16(7):751-3.

131. Massia SP, Hubbell JA. An RGD spacing of 440 nm is sufficient for integrin alpha V beta 3-mediated fibroblast spreading and 140 nm for focal contact and stress fiber formation. The Journal of Cell Biology. 1991;114(5):1089-100.

132. Pierschbacher M, Hayman EG, Ruoslahti E. Synthetic peptide with cell attachment activity of fibronectin. Proceedings of the National Academy of Sciences. 1983;80(5):1224-7.

133. Lee JW, Park YJ, Lee SJ, Lee SK, Lee KY. The effect of spacer arm length of an adhesion ligand coupled to an alginate gel on the control of fibroblast phenotype. Biomaterials. 2010;31(21):5545-51.

134. Hern DL, Hubbell JA. Incorporation of adhesion peptides into nonadhesive hydrogels useful for tissue resurfacing. Journal of Biomedical Materials Research. 1998;39(2):266-76.

135. Salinas CN, Anseth KS. The influence of the RGD peptide motif and its contextual presentation in PEG gels on human mesenchymal stem cell viability. Journal of Tissue Engineering and Regenerative Medicine. 2008;2(5):296-304.

136. Kim TG, Shin H, Lim DW. Biomimetic scaffolds for tissue engineering. Advanced Functional Materials. 2012;22(12):2446-68.

137. Kim TG, Park TG. Biomimicking extracellular matrix: cell adhesive RGD peptide modified electrospun poly(D,L-lactic-co-glycolic acid) nanofiber mesh. Tissue Engineering. 2006;12(2):221-33.

138. Chen J-P, Su C-H. Surface modification of electrospun PLLA nanofibers by plasma treatment and cationized gelatin immobilization for cartilage tissue engineering. Acta Biomaterialia. 2011;7(1):234-43.

139. Ma Z, Mao Z, Gao C. Surface modification and property analysis of biomedical polymers used for tissue engineering. Colloids and Surfaces B: Biointerfaces. 2007;60(2):137-57.

140. Cramer NB, Bowman CN. Kinetics of thiol–ene and thiol–acrylate photopolymerizations with real-time fourier transform infrared. Journal of Polymer Science Part A: Polymer Chemistry. 2001;39(19):3311-9.

141. Salinas CN, Anseth KS. Mixed mode thiol−acrylate photopolymerizations for the synthesis of PEG−peptide hydrogels. Macromolecules. 2008;41(16):6019-26.

142. Rydholm AE, Bowman CN, Anseth KS. Degradable thiol-acrylate photopolymers: polymerization and degradation behavior of an in situ forming biomaterial. Biomaterials. 2005;26(22):4495-506.

143. Rydholm AE, Reddy SK, Anseth KS, Bowman CN. Controlling network structure in degradable thiol−acrylate biomaterials to tune mass loss behavior. Biomacromolecules. 2006;7(10):2827-36.

144. Teo WE, Ramakrishna S. A review on electrospinning design and nanofibre assemblies. Nanotechnology. 2006;17(14):R89-R106.

145. Schiffman JD, Schauer CL. A review: Electrospinning of biopolymer nanofibers and their applications. Polymer Reviews. 2008;48(2):317-52.

146. Agarwal S, Wendorff JH, Greiner A. Use of electrospinning technique for biomedical applications. Polymer. 2008;49(26):5603-21.

147. Formhals A, inventor; Process and apparatus for preparing artificial threads. United States1934.

148. Doshi J, Reneker DH. Electrospinning process and applications of electrospun fibers. Journal of Electrostatics. 1995;35(2–3):151-60.

149. Greiner A, Wendorff JH. Electrospinning: A fascinating method for the preparation of ultrathin fibers. Angewandte Chemie International Edition. 2007;46(30):5670-703.

150. Shin YM, Hohman MM, Brenner MP, Rutledge GC. Experimental characterization of electrospinning: the electrically forced jet and instabilities. Polymer. 2001;42(25):09955-67.

151. Shin YM. Electrospinning: A whipping fluid jet generates submicron polymer fibers. Applied Physics Letters. 2001;78:1149.

152. Sill TJ, von Recum HA. Electrospinning: Applications in drug delivery and tissue engineering. Biomaterials. 2008;29(13):1989-2006.

153. Deitzel JM, Kleinmeyer J, Harris D, Beck Tan NC. The effect of processing variables on the morphology of electrospun nanofibers and textiles. Polymer. 2001;42(1):261-72.

154. Meechaisue C, Dubin R, Supaphol P, Hoven VP, Kohn J. Electrospun mat of tyrosine-derived polycarbonate fibers for potential use as tissue scaffolding material. Journal of Biomaterials Science Polymer Edition. 2006;17(9):1039.

155. Megelski S, Stephens JS, Chase DB, Rabolt JF. Micro- and nanostructured surface morphology on electrospun polymer fibers. Macromolecules. 2002;35(22):8456-66.

156. Zuo W, Zhu M, Yang W, Yu H, Chen Y, Zhang Y. Experimental study on relationship between jet instability and formation of beaded fibers during electrospinning. Polymer Engineering & Science. 2005;45(5):704-9.

157. Wannatong L, Sirivat A, Supaphol P. Effects of solvents on electrospun polymeric fibers: preliminary study on polystyrene. Polymer International. 2004;53(11):1851-9.

158. Erh-Hsuin L. Biofunctionalized electrospun scaffolds for cartilage tissue engineering. London: Imperial College; 2010.

159. Zhang C, Yuan X, Wu L, Han Y, Sheng J. Study on morphology of electrospun poly(vinyl alcohol) mats. European Polymer Journal. 2005;41(3):423-32.

160. Jin H-J, Fridrikh SV, Rutledge GC, Kaplan DL. Electrospinning bombyx mori silk with poly(ethylene oxide). Biomacromolecules. 2002;3(6):1233-9.

161. Chen F, Li X, Mo X, He C, Wang H, Ikada Y. Electrospun chitosan-P(LLA-CL) nanofibers for biomimetic extracellular matrix. Journal of Biomaterials Science Polymer Edition. 2008;19(5):677-91. Epub 2008/04/19.

162. Bhattarai N, Li Z, Edmondson D, Zhang M. Alginate-Based Nanofibrous Scaffolds: Structural, Mechanical, and Biological Properties. Advanced Materials. 2006;18(11):1463-7.

163. Thomas V, Jose MV, Chowdhury S, Sullivan JF, Dean DR, Vohra YK. Mechano-morphological studies of aligned nanofibrous scaffolds of polycaprolactone fabricated by electrospinning. Journal of Biomaterials Science, Polymer Edition. 2006;17(9):969-84.

164. Sui G, Yang X, Mei F, Hu X, Chen G, Deng X, et al. Poly-L-lactic acid/hydroxyapatite hybrid membrane for bone tissue regeneration. Journal of Biomedical Materials Research Part A. 2007;82A(2):445-54.

165. Mohammadi Y, Soleimani M, Fallahi-Sichani M, Gazme A, Haddadi-Asl V, Arefian E, et al. Nanofibrous poly(epsilon-caprolactone)/poly(vinyl alcohol)/chitosan hybrid scaffolds for bone tissue engineering using mesenchymal stem cells. The International Journal of Artificial Organs. 2007;30(3):204-11.

166. Li W-J, Danielson KG, Alexander PG, Tuan RS. Biological response of chondrocytes cultured in three-dimensional nanofibrous poly(ϵ-caprolactone) scaffolds. Journal of Biomedical Materials Research Part A. 2003;67A(4):1105-14.

167. Yoshimoto H, Shin YM, Terai H, Vacanti JP. A biodegradable nanofiber scaffold by electrospinning and its potential for bone tissue engineering. Biomaterials. 2003;24(12):2077-82.

168. Shin M, Yoshimoto H, Vacanti JP. In vivo bone tissue engineering using mesenchymal stem cells on a novel electrospun nanofibrous scaffold. Tissue Engineering. 2004;10(1-2):33-41.

169. Cai YZ, Wang LL, Cai HX, Qi YY, Zou XH, Ouyang HW. Electrospun nanofibrous matrix improves the regeneration of dense cortical bone. Journal of Biomedical Materials Research Part A. 2010;95A(1):49-57.

170. Holzwarth JM, Ma PX. 3D nanofibrous scaffolds for tissue engineering. Journal of Materials Chemistry. 2011;21(28):10243-51.

171. Anderson DG, Tweedie CA, Hossain N, Navarro SM, Brey DM, Van Vliet KJ, et al. A combinatorial library of photocrosslinkable and degradable materials. Advanced Materials. 2006;18(19):2614-8.

172. Wayne R. Principles and applications of photochemistry: Oxford University Press; 1988.

173. Andrzejewska E. Photopolymerization kinetics of multifunctional monomers. Progress in Polymer Science. 2001;26(4):605-65.

174. Rabek JF. Photodegradation of polymers1996.

175. Baroli B. Photopolymerization of biomaterials: issues and potentialities in drug delivery, tissue engineering, and cell encapsulation applications. Journal of Chemical Technology & Biotechnology. 2006;81(4):491-9.

176. Burdick JA, Ward M, Liang E, Young MJ, Langer R. Stimulation of neurite outgrowth by neurotrophins delivered from degradable hydrogels. Biomaterials. 2006;27(3):452-9.

177. Ifkovits JL, Devlin JJ, Eng G, Martens TP, Vunjak-Novakovic G, Burdick JA. Biodegradable fibrous scaffolds with tunable properties formed from photo-cross-linkable poly(glycerol sebacate). ACS Applied Materials & Interfaces. 2009;1(9):1878-86.

178. Davis KA, Burdick JA, Anseth KS. Photoinitiated crosslinked degradable copolymer networks for tissue engineering applications. Biomaterials. 2003;24(14):2485-95.

179. Anseth KS, Metters AT, Bryant SJ, Martens PJ, Elisseeff JH, Bowman CN. In situ forming degradable networks and their application in tissue engineering and drug delivery. Journal of Controlled Release. 2002;78(1–3):199-209.

180. Sawhney AS, Pathak CP, Hubbell JA. Bioerodible hydrogels based on photopolymerized poly(ethylene glycol)-co-poly(.alpha.-hydroxy acid) diacrylate macromers. Macromolecules. 1993;26(4):581-7.

181. Lutolf MP, Lauer-Fields JL, Schmoekel HG, Metters AT, Weber FE, Fields GB, et al. Synthetic matrix metalloproteinase-sensitive hydrogels for the conduction of tissue regeneration: Engineering cell-invasion characteristics. Proceedings of the National Academy of Sciences. 2003;100(9):5413-8.

182. Burkoth AK, Anseth KS. A review of photocrosslinked polyanhydrides: in situ forming degradable networks. Biomaterials. 2000;21(23):2395-404.

183. Moan J, Berg K, Kvam E, Western A, Malik Z, Rück A, et al. Intracellular localization of photosensitizers. Ciba Foundation Symposium 146 - Photosensitizing Compounds: Their Chemistry, Biology and Clinical Use: John Wiley & Sons, Ltd.; 2007. p. 95-111.

184. Terakado M, Yamazaki M, Tsujimoto Y, Kawashima T, Nagashima K, Ogawa J, et al. Lipid peroxidation as a possible cause of benzoyl peroxide toxicity in rabbit dental pulp--a microsomal lipid peroxidation in vitro. Journal of Dental Research. 1984;63(6):901-5.

185. Atsumi T, Murata J, Kamiyanagi I, Fujisawa S, Ueha T. Cytotoxicity of photosensitizers camphorquinone and 9-fluorenone with visible light irradiation on a human submandibular-duct cell line in vitro. Archives of Oral Biology. 1998;43(1):73-81.

186. Kim SH, Kim S-H, Nair S, Moore E. Reactive electrospinning of cross-linked poly(2-hydroxyethyl methacrylate) nanofibers and elastic properties of individual hydrogel nanofibers in aqueous solutions. Macromolecules. 2005;38(9):3719-23.

187. Sundararaghavan HG, Metter RB, Burdick JA. Electrospun fibrous scaffolds with multiscale and photopatterned Porosity. Macromolecular Bioscience. 2010;10(3):265-70.

188. Gunatillake PA, Adhikari R. Biodegradable synthetic polymers for tissue engineering. European Cells and Materials. 2003;5:1-16; discussion

189. Hutmacher DW. Scafolds in tissue engineering bone and cartilage. Biomaterials. 2000;21(2529):2543.

190. Hutcheon GA, Messiou C, Wyre RM, Davies MC, Downes S. Water absorption and surface properties of novel poly(ethylmethacrylate) polymer systems for use in bone and cartilage repair. Biomaterials. 2001;22(7):667-76.

191. Atzet S, Curtin S, Trinh P, Bryant S, Ratner B. Degradable poly(2-hydroxyethyl methacrylate)-co-polycaprolactone hydrogels for tissue engineering scaffolds. Biomacromolecules. 2008;9(12):3370-7.

192. Choi SS, Hong JP, Seo YS, Chung SM, Nah C. Fabrication and characterization of electrospun polybutadiene fibers crosslinked by UV irradiation. Journal of Applied Polymer Science. 2006;101(4):2333-7.

193. Liu Y, Bolger B, Cahill PA, McGuinness GB. Water resistance of photocrosslinked polyvinyl alcohol based fibers. Materials Letters. 2009;63(3–4):419-21.

194. Wang H, Feng Y, An B, Zhang W, Sun M, Fang Z, et al. Fabrication of PU/PEGMA crosslinked hybrid scaffolds by in situ UV photopolymerization favoring human endothelial cells growth for vascular tissue engineering. Journal of Materials Science: Materials in Medicine. 2012;23(6):1499-510.

195. Li W-J, Cooper Jr JA, Mauck RL, Tuan RS. Fabrication and characterization of six electrospun poly(α-hydroxy ester)-based fibrous scaffolds for tissue engineering applications. Acta Biomaterialia. 2006;2(4):377-85.

196. Son WK, Youk JH, Lee TS, Park WH. The effects of solution properties and polyelectrolyte on electrospinning of ultrafine poly(ethylene oxide) fibers. Polymer. 2004;45(9):2959-66.

197. Fong H, Chun I, Reneker DH. Beaded nanofibers formed during electrospinning. Polymer. 1999;40(16):4585-92.

198. Shenoy SL, Bates WD, Frisch HL, Wnek GE. Role of chain entanglements on fiber formation during electrospinning of polymer solutions: good solvent, non-specific polymer–polymer interaction limit. Polymer. 2005;46(10):3372-84.

199. Tan SH, Inai R, Kotaki M, Ramakrishna S. Systematic parameter study for ultra-fine fiber fabrication via electrospinning process. Polymer. 2005;46(16):6128-34.

200. Ramakrishna S, Fujihara K, Teo W-E, Ma Z. An introduction to electrospinning and nanofibers. Singapore: World Scientific; 2005.

201. Zong X, Kim K, Fang D, Ran S, Hsiao BS, Chu B. Structure and process relationship of electrospun bioabsorbable nanofiber membranes. Polymer. 2002;43(16):4403-12.

202. Demir MM, Yilgor I, Yilgor E, Erman B. Electrospinning of polyurethane fibers. Polymer. 2002;43(11):3303-9.

203. Williams CG, Malik AN, Kim TK, Manson PN, Elisseeff JH. Variable cytocompatibility of six cell lines with photoinitiators used for polymerizing hydrogels and cell encapsulation. Biomaterials. 2005;26(11):1211-8.

204. Engler AJ, Sen S, Sweeney HL, Discher DE. Matrix elasticity directs stem cell ineage specification. Cell. 2006;126(4):677-89.

205. Smith KE, Hyzy SL, Sunwoo M, Gall KA, Schwartz Z, Boyan BD. The dependence of MG63 osteoblast responses to (meth)acrylate-based networks on chemical structure and stiffness. Biomaterials. 2010;31(24):6131-41.

206. Baker BM, Gee AO, Metter RB, Nathan AS, Marklein RA, Burdick JA, et al. The potential to improve cell infiltration in composite fiber-aligned electrospun scaffolds by the selective removal of sacrificial fibers. Biomaterials. 2008;29(15):2348-58.

207. Simon GP, Allen PEM, Williams DRG. Properties of dimethacrylate copolymers of varying crosslink density. Polymer. 1991;32(14):2577-87.

208. Anseth KS, Bowman CN, Brannon-Peppas L. Mechanical properties of hydrogels and their experimental determination. Biomaterials. 1996;17(17):1647-57.

209. Nielsen LE. Cross-linking–effect on physical properties of polymers. Journal of Macromolecular Science Part C, Reviews in Macromolecular Chemistry and Physics. 1969;3(1):69.

210. Elliott JE, Macdonald M, Nie J, Bowman CN. Structure and swelling of poly(acrylic acid) hydrogels: effect of pH, ionic strength, and dilution on the crosslinked polymer structure. Polymer. 2004;45(5):1503-10.

211. Khetan S, Burdick JA. Patterning network structure to spatially control cellular remodeling and stem cell fate within 3-dimensional hydrogels. Biomaterials. 2010;31(32):8228-34.

212. Ifkovits JL, Padera RF, Burdick JA. Biodegradable and radically polymerized elastomers with enhanced processing capabilities. Biomedical Materials. 2008;3(3):034104. Epub 2008/08/12.

213. McCullen SD, Ramaswamy S, Clarke LI, Gorga RE. Nanofibrous composites for tissue engineering applications. Wiley Interdisciplinary Reviews: Nanomedicine and Nanobiotechnology. 2009;1(4):369-90.

214. Zhang Y, Ouyang H, Lim CT, Ramakrishna S, Huang Z-M. Electrospinning of gelatin fibers and gelatin/PCL composite fibrous scaffolds. Journal of Biomedical Materials Research Part B: Applied Biomaterials. 2005;72B(1):156-65.

215. Motherway JA, Verschueren P, Van der Perre G, Vander Sloten J, Gilchrist MD. The mechanical properties of cranial bone: The effect of loading rate and cranial sampling position. Journal of Biomechanics. 2009;42(13):2129-35.

216. Lee JH, Bucknall DG. Swelling behavior and network structure of hydrogels synthesized using controlled UV-initiated free radical polymerization. Journal of Polymer Science Part B: Polymer Physics. 2008;46(14):1450-62.

217. Buyanov AL, LG Rs, LG K. Elastic bahaviour of equilibrium-swollen polyelectrolyte hydrogels based on acrylamide and sodium acrylate Russian Journal of Applied Chemistry. 1992;65(1):150.

218. Vohra S, Hennessy K, Sawyer A, Zhuo Y, Bellis S. Comparison of mesenchymal stem cell and osteosarcoma cell adhesion to hydroxyapatite. Journal of Materials Science: Materials in Medicine. 2008;19(12):3567-74.

219. McQuillan DJ, Richardson MD, Bateman JF. Matrix deposition by a calcifying human osteogenic sarcoma cell line (SAOS-2). Bone. 1995;16(4):415-26.

220. Pautke C, Schicke M. Characterization of osteosarcoma cell lines MG-63, Saos-2 and U-2 OS in comparison to human osteoblasts. Anticancer Research. 2004;24(6):3743-8.

221. Shapira L, Halabi A. Behavior of two osteoblast-like cell lines cultured on machined or rough titanium surfaces. Clinical oral implants research. 2009;20(1):50-5.

222. Badami AS, Kreke MR, Thompson MS, Riffle JS, Goldstein AS. Effect of fiber diameter on spreading, proliferation, and differentiation of osteoblastic cells on electrospun poly(lactic acid) substrates. Biomaterials. 2006;27(4):596-606.

223. Filmon R, Basle MF, Atmani H, Chappard D. Adherence of osteoblast-like cells on calcospherites developed on a biomaterial combining poly(2-hydroxyethyl) methacrylate and alkaline phosphatase. Bone. 2002;30(1):152-8. Epub 2002/01/17.

224. Engel E, Martínez E, Mills CA, Funes M, Planell JA, Samitier J. Mesenchymal stem cell differentiation on microstructured poly (methyl methacrylate) substrates. Annals of Anatomy - Anatomischer Anzeiger. 2009;191(1):136-44.

225. Tao S, Young C, Redenti S, Zhang Y, Klassen H, Desai T, et al. Survival, migration and differentiation of retinal progenitor cells transplanted on micro-machined poly(methyl methacrylate) scaffolds to the subretinal space. Lab on a Chip. 2007;7(6):695-701.

226. Kojima N, Yamada M, Paranjpe A, Tsukimura N, Kubo K, Jewett A, et al. Restored viability and function of dental pulp cells on poly-methylmethacrylate (PMMA)-based dental resin supplemented with N-acetyl cysteine (NAC). Dental Materials. 2008;24(12):1686-93.

227. Nocca G, Martorana GE, De Sole P, De Palma F, Callà C, Corsale P, et al. Effects of 1,4-butanediol dimethacrylate and urethane dimethacrylate on HL-60 cell metabolism. European Journal of Oral Sciences. 2009;117(2):175-81.

228. Chang H-H, Guo M-K, Kasten FH, Chang M-C, Huang G-F, Wang Y-L, et al. Stimulation of glutathione depletion, ROS production and cell cycle arrest of dental pulp cells and gingival epithelial cells by HEMA. Biomaterials. 2005;26(7):745-53.

229. Yoshii E. Cytotoxic effects of acrylates and methacrylates: Relationships of monomer structures and cytotoxicity. Journal of Biomedical Materials Research. 1997;37(4):517-24.

230. About I, Camps J, Mitsiadis TA, Bottero M-J, Butler W, Franquin J-C. Influence of resinous monomers on the differentiation in vitro of human pulp cells into odontoblasts. Journal of Biomedical Materials Research. 2002;63(4):418-23.

231. About I, Camps J, Burger A-S, Mitsiadis TA, Butler WT, Franquin J-C. Polymerized bonding agents and the differentiation in vitro of human pulp cells into odontoblast-like cells. Dental Materials. 2005;21(2):156-63.

232. Imazato S, Horikawa D, Nishida M, Ebisu S. Effects of monomers eluted from dental resin restoratives on osteoblast-like cells. Journal of Biomedical Materials Research Part B: Applied Biomaterials. 2009;88B(2):378-86.

233. Bryant SJ, Nuttelman CR, Anseth KS. Cytocompatibility of UV and visible light photoinitiating systems on cultured NIH/3T3 fibroblasts in vitro. Journal of Biomaterials Science, Polymer Edition. 2000;11(5):439-57.

234. Yang F, Williams CG, Wang D-a, Lee H, Manson PN, Elisseeff J. The effect of incorporating RGD adhesive peptide in polyethylene glycol diacrylate hydrogel on osteogenesis of bone marrow stromal cells. Biomaterials. 2005;26(30):5991-8.

235. Kilpadi KL, Sawyer AA, Prince CW, Chang P-L, Bellis SL. Primary human marrow stromal cells and Saos-2 osteosarcoma cells use different mechanisms to adhere to hydroxylapatite. Journal of Biomedical Materials Research Part A. 2004;68A(2):273-85.

236. Duan X, Jia S-F, Zhou Z, Langley RR, Bolontrade MF, Kleinerman ES. Association of αVβ3; integrin expression with the metastatic potential and migratory and chemotactic ability of human osteosarcoma cells. Clinical and Experimental Metastasis. 2005;21(8):747-53.

237. Clover J, Gowen M. Are MG-63 and HOS TE85 human osteosarcoma cell lines representative models of the osteoblastic phenotype? Bone. 1994;15(6):585-91.

238. Marco RAW, Díaz-Montero CM, Wygant JN, Kleinerman ES, McIntyre BW. α4 integrin increases anoikis of human osteosarcoma cells. Journal of Cellular Biochemistry. 2003;88(5):1038-47.

239. Curtis A, Wilkinson C. Topographical control of cells. Biomaterials. 1997;18(24):1573-83.

240. Stevens MM, George JH. Exploring and engineering the cell surface interface. Science. 2005;310(5751):1135-8.

241. Bettinger CJ, Langer R, Borenstein JT. Engineering substrate topography at the micro- and nanoscale to control cell function. Angewandte Chemie International Edition. 2009;48(30):5406-15.

242. Martínez E, Engel E, Planell JA, Samitier J. Effects of artificial micro- and nano-structured surfaces on cell behaviour. Annals of Anatomy - Anatomischer Anzeiger. 2009;191(1):126-35.

243. Zinger O, Zhao G, Schwartz Z, Simpson J, Wieland M, Landolt D, et al. Differential regulation of osteoblasts by substrate microstructural features. Biomaterials. 2005;26(14):1837-47.

244. Boyan BD, Bonewald LF, Paschalis EP, Lohmann CH, Rosser J, Cochran DL, et al. Osteoblast-mediated mineral deposition in culture is dependent on surface microtopography. Calcified Tissue International. 2002;71(6):519-29.

245. Metter RB, Ifkovits JL, Hou K, Vincent L, Hsu B, Wang L, et al. Biodegradable fibrous scaffolds with diverse properties by electrospinning candidates from a combinatorial macromer library. Acta Biomaterialia. 2010;6(4):1219-26.

246. Allen LT, Tosetto M, Miller IS, O'Connor DP, Penney SC, Lynch I, et al. Surface-induced changes in protein adsorption and implications for cellular phenotypic responses to surface interaction. Biomaterials. 2006;27(16):3096-108.

247. Wang YX, Robertson JL, Spillman WB, Jr., Claus RO. Effects of the chemical structure and the surface properties of polymeric biomaterials on their biocompatibility. Pharmaceutical Research. 2004;21(8):1362-73.

248. Andrade J, Hlady V. Protein adsorption and materials biocompatibility: A tutorial review and suggested hypotheses

Biopolymers/Non-Exclusion HPLC. Springer Berlin / Heidelberg; 1986. p. 1-63.

249. Jager M, Zilkens C, Zanger K, Krauspe R. Significance of nano- and microtopography for cell-surface interactions in orthopaedic implants. Journal of Biomedicine and Biotechnology. 2007;2007(8):69036.

250. Iuliano DJ, Saavedra SS, Truskey GA. Effect of the conformation and orientation of adsorbed fibronectin on endothelial cell spreading and the strength of adhesion. Journal of Biomedical Materials Research. 1993;27(8):1103-13.

251. Håkansson M, Linse S. Protein reconstitution and 3D domain swapping. Current Protein & Peptide Science. 2002;3(6):629-42.

252. Grafahrend D, Calvet JL, Klinkhammer K, Salber J, Dalton PD, Möller M, et al. Control of protein adsorption on functionalized electrospun fibers. Biotechnology and Bioengineering. 2008;101(3):609-21.

253. Woo KM, Chen VJ, Ma PX. Nano-fibrous scaffolding architecture selectively enhances protein adsorption contributing to cell attachment. Journal of Biomedical Materials Research Part A. 2003;67A(2):531-7.

254. Haubner R, Gratias R, Diefenbach B, Goodman SL, Jonczyk A, Kessler H. Structural and functional aspects of RGD-containing cyclic pentapeptides as highly potent and selective integrin αVβ3 antagonists. Journal of the American Chemical Society. 1996;118(32):7461-72.

255. Lecamp L, Houllier F, Youssef B, Bunel C. Photoinitiated cross-linking of a thiol–methacrylate system. Polymer. 2001;42(7):2727-36.

256. Merrifield RB. Solid phase peptide synthesis. I. The synthesis of a tetrapeptide. Journal of the American Chemical Society. 1963;85(14):2149-54.

257. Zhu Y, Gao C, Liu X, Shen J. Surface modification of polycaprolactone membrane via aminolysis and biomacromolecule immobilization for promoting cytocompatibility of human endothelial cells. Biomacromolecules. 2002;3(6):1312-9.

258. Ogden G, Foldi P. Amino acid analysis: an overview of current methods. Chromatography Online. 1987;5(1):28.

259. Benson JR, Hare PE. O-phthalaldehyde: fluorogenic detection of primary amines in the picomole range. Comparison with fluorescamine and ninhydrin. Proceedings of the National Academy of Sciences. 1975;72(2):619-22.

260. Ellman GL. Tissue sulfhydryl groups. Archives of Biochemistry and Biophysics. 1959;82(1):70.

261. Reddy SK, Anseth KS, Bowman CN. Modeling of network degradation in mixed step-chain growth polymerizations. Polymer. 2005;46(12):4212-22.

262. Mann BK, Tsai AT, Scott-Burden T, West JL. Modification of surfaces with cell adhesion peptides alters extracellular matrix deposition. Biomaterials. 1999;20(23–24):2281-6.

263. Rowley JA, Madlambayan G, Mooney DJ. Alginate hydrogels as synthetic extracellular matrix materials. Biomaterials. 1999;20(1):45-53.

264. Lutolf MP, Hubbell JA. Synthesis and physicochemical characterization of end-linked poly(ethylene glycol)-co-peptide hydrogels formed by michael-type addition. Biomacromolecules. 2003;4(3):713-22.

265. Iucci G, Ghezzo F, Danesin R, Modesti M, Dettin M. Biomimetic peptide-enriched electrospun polymers: A photoelectron and infrared spectroscopy study. Journal of Applied Polymer Science. 2011;122(6):3574-82.

266. Gentilini C, Dong Y, May JR, Goldoni S, Clarke DE, Lee B-H, et al. Functionalized poly(γ-glutamic acid) fibrous scaffolds for tissue engineering. Advanced Healthcare Materials. 2012;1(3):308-15.

267. Wong WH, Mooney DJ. Synthesis and properties of biodegradable polymers used as synthetic matrices for tissue engineering. Synthetic Biodegradable Polymer Scaffolds Atala A, Mooney D, eds Burkhäuser, Boston. 1997:51-84.

268. Kronenthal RL. Biodegradable polymers in medicine and surgery. Polymer Science Technology. 1975;8:119-37.

269. Göpferich A. Mechanisms of polymer degradation and erosion. Biomaterials. 1996;17(2):103-14.

270. Vert M, Mauduit J, Li S. Biodegradation of PLA/GA polymers: increasing complexity. Biomaterials. 1994;15(15):1209-13.

271. Rehm K, Claes L, Helling H, Hutmacher D. Application of a polylactide pin. An open clinical prospective study. Biodegradable implants in fracture" fixation Hong Kong: World Scientic. 1994:54.

272. Hutmacher DW, Kirsch A, Ackermann KL, Hürzeler MB. A tissue engineered cell-occlusive device for hard tissue regeneration--a preliminary report. The International Journal of Periodontics & Restorative Dentistry. 2001;21(1):49.

273. Van Royen P, Boschmans B, dos Santos A, Schacht E, Dubruel P, Cornelissen R, et al. Static secondary ion mass spectrometry for the surface characterisation of individual nanofibres of polycaprolactone functionalised with an antibacterial additive. Analytical and Bioanalytical Chemistry. 2011;399(3):1163-72.

274. Lee JLS, Gilmore IS, Seah MP. Quantification and methodology issues in multivariate analysis of ToF-SIMS data for mixed organic systems. Surface and Interface Analysis. 2008;40(1):1-14.

275. Gentsch R, Pippig F, Schmidt S, Cernoch P, Polleux J, Börner HG. Single-step electrospinning to bioactive polymer nanofibers. Macromolecules. 2011;44(3):453-61.

276. Kingshott P, McArthur S, Thissen H, Castner DG, Griesser HJ. Ultrasensitive probing of the protein resistance of PEG surfaces by secondary ion mass spectrometry. Biomaterials. 2002;23(24):4775-85.

277. Khew ST, Tong YW. The specific recognition of a cell binding sequence derived from type I collagen by Hep3B and L929 cells. Biomacromolecules. 2007;8(10):3153-61.

278. Asthagiri AR, Nelson CM, Horwitz AF, Lauffenburger DA. Quantitative relationship among integrin-ligand binding, adhesion, and signaling via focal adhesion kinase and extracellular signal-regulated kinase 2. The Journal of biological chemistry. 1999;274(38):27119-27.

279. Garcia AJ, Huber F, Boettiger D. Force required to break α5β1 integrin-fibronectin bonds in intact adherent cells is sensitive to integrin activation state. The Journal of biological chemistry. 1998;273(18):10988-93.

280. Harbers GM, Healy KE. The effect of ligand type and density on osteoblast adhesion, proliferation, and matrix mineralization. Journal of Biomedical Materials Research Part A. 2005;75A(4):855-69.

281. Palecek SP, Loftus JC, Ginsberg MH, Lauffenburger DA, Horwitz AF. Integrin-ligand binding properties govern cell migration speed through cell-substratum adhesiveness. Nature. 1997;385(6616):537-40.

282. Reyes CD, García AJ. Engineering integrin-specific surfaces with a triple-helical collagen-mimetic peptide. Journal of Biomedical Materials Research Part A. 2003;65A(4):511-23.

283. Yang XB, Roach HI, Clarke NMP, Howdle SM, Quirk R, Shakesheff KM, et al. Human osteoprogenitor growth and differentiation on synthetic biodegradable structures after surface modification. Bone. 2001;29(6):523-31.

284. Quirk RA, Chan WC, Davies MC, Tendler SJB, Shakesheff KM. Poly(l-lysine)–GRGDS as a biomimetic surface modifier for poly(lactic acid). Biomaterials. 2001;22(8):865-72.

285. Sawyer AA, Weeks DM, Kelpke SS, McCracken MS, Bellis SL. The effect of the addition of a polyglutamate motif to RGD on peptide tethering to hydroxyapatite and the promotion of mesenchymal stem cell adhesion. Biomaterials. 2005;26(34):7046-56.

286. Williams DF. The role of short synthetic adhesion peptides in regenerative medicine; The debate. Biomaterials. 2011;32(18):4195-7.

287. Bellis SL. Advantages of RGD peptides for directing cell association with biomaterials. Biomaterials. 2011;32(18):4205-10.

288. Preissner KT. Structure and biological role of vitronectin. Annual Review of Cell and Developmental Biology. 1991;7(1):275.

289. Dahlbäck B. Blood coagulation. The Lancet. 2000;355(9215):1627-32.

290. Mosher DF. Physiology of fibronectin. Annual Review of Medicine. 1984;35:561-75.

291. Wilson CJ, Clegg RE, Leavesley DI, Pearcy MJ. Mediation of biomaterial-cell interactions by adsorbed proteins: a review. Tissue Engineering. 2005;11(1-2):1-18.

292. Ruoslahti E. RGD and other recognition sequences for integrins. Annual Review of Cell and Developmental Biology. 1996;12:697-715.

293. Ruoslahti E. The RGD story: a personal account. Matrix Biology. 2003;22(6):459-65.

294. Hautanen A, Gailit J, Mann DM, Ruoslahti E. Effects of modifications of the RGD sequence and its context on recognition by the fibronectin receptor. The Journal of biological chemistry. 1989;264(3):1437-42.

295. Anderson JM, Kushwaha M, Tambralli A, Bellis SL, Camata RP, Jun H-W. Osteogenic differentiation of human mesenchymal stem cells directed by extracellular matrix-mimicking ligands in a biomimetic self-assembled peptide amphiphile nanomatrix. Biomacromolecules. 2009;10(10):2935-44.

296. Anderson JM, Vines JB, Patterson JL, Chen H, Javed A, Jun H-W. Osteogenic differentiation of human mesenchymal stem cells synergistically enhanced by biomimetic peptide amphiphiles combined with conditioned medium. Acta Biomaterialia. 2011;7(2):675-82.

297. Schwartz MA. Spreading of human endothelial cells on fibronectin or vitronectin triggers elevation of intracellular free calcium. The Journal of Cell Biology. 1993;120(4):1003-10.

298. Mineur P, Guignandon A, Lambert CA, Amblard M, Lapière CM, Nusgens BV. RGDS and DGEA-induced [Ca2+]i signalling in human dermal fibroblasts. Biochimica et Biophysica Acta (BBA) - Molecular Cell Research. 2005;1746(1):28-37.

299. Kantlehner M, Finsinger D, Meyer J, Schaffner P, Jonczyk A, Diefenbach B, et al. Selective RGD-mediated adhesion of osteoblasts at surfaces of implants. Angewandte Chemie International Edition. 1999;38(4):560-2.

300. Beer JH, Springer KT, Coller BS. Immobilized Arg-Gly-Asp (RGD) peptides of varying lengths as structural probes of the platelet glycoprotein IIb/IIIa receptor. Blood. 1992;79(1):117-28.

301. Xiong J-P, Stehle T, Diefenbach B, Zhang R, Dunker R, Scott DL, et al. Crystal structure of the extracellular segment of integrin αVβ3. Science. 2001;294(5541):339-45.

302. Smith JW, Cheresh DA. Integrin (alpha v beta 3)-ligand interaction. Identification of a heterodimeric RGD binding site on the vitronectin receptor. The Journal of biological chemistry. 1990;265(4):2168-72.

303. Chamberlain G, Fox J, Ashton B, Middleton J. Concise review: mesenchymal stem cells: Their phenotype, differentiation capacity, immunological features, and potential for homing. Stem Cells. 2007;25(11):2739-49.

304. Gilbert M, Giachelli CM, Stayton PS. Biomimetic peptides that engage specific integrin-dependent signaling pathways and bind to calcium phosphate surfaces. Journal of Biomedical Materials Research Part A. 2003;67A(1):69-77.

305. Aubin J E. Mesenchymal stem cells and osteoblast differentiation. Principles of bone biology. 2002:59-81.

306. Weinreb M, Shinar D, Rodan GA. Different pattern of alkaline phosphatase, osteopontin, and osteocalcin expression in developing rat bone visualized by in situ hybridization. Journal of Bone and Mineral Research. 1990;5(8):831-42.

307. Kapyla J, Ivaska J, Riikonen R, Nykvist P, Pentikainen O, Johnson M, et al. Integrin α2 domain recognizes type I and type IV collagens by different mechanisms. The Journal of biological chemistry. 2000;275(5):3348-54.

308. Heino J. The collagen receptor integrins have distinct ligand recognition and signaling functions. Matrix Biology. 2000;19(4):319-23.

309. Gronthos S, Stewart K, Graves SE, Hay S, Simmons PJ. Integrin expression and function on human osteoblast-like cells. Journal of Bone and Mineral Research. 1997;12(8):1189-97.

310. Jikko A, Harris SE, Chen D, Mendrick DL, Damsky CH. Collagen integrin receptors regulate early osteoblast differentiation Induced by BMP-2. Journal of Bone and Mineral Research. 1999;14(7):1075-83.

311. Knight CG, Morton LF, Onley DJ, Peachey AR, Messent AJ, Smethurst PA, et al. Identification in collagen type I of an integrin alpha2 beta1-binding site containing an essential GER sequence. The Journal of biological chemistry. 1998;273(50):33287-94.

312. Knight CG, Morton LF, Peachey AR, Tuckwell DS, Farndale RW, Barnes MJ. The collagen-binding A-domains of integrins alpha(1)beta(1) and alpha(2)beta(1) recognize the same specific amino acid sequence, GFOGER, in native (triple-helical) collagens. The Journal of biological chemistry. 2000;275(1):35-40.